NOTICE

The quality of this microfiche is heavily dependent upon the quality of the original thesis submitted for microfilming. Every effort has been made to ensure the highest quality of reproduction possible.

If pages are missing, contact the university which granted the degree.

Some pages may have indistinct print especially if the original pages were typed with a poor typewriter ribbon or if the university sent us a poor photocopy.

Previously copyrighted materials (journal articles, published tests, etc.) are not filmed.

Reproduction in full or in part of this film is governed by the Canadian Copyright Act, R.S.C. 1970, c. C-30. Please read the authorization forms which accompany this thesis.

THIS DISSERTATION
HAS BEEN MICROFILMED
EXACTLY AS RECEIVED

AVIS

La qualité de cette microfiche dépend grandement de la qualité de la thèse soumise au microfilmage. Nous avons tout fait pour assurer une qualité supérieure de reproduction.

S'il manque des pages, veuillez communiquer avec l'université qui a conféré le grade.

La qualité d'impression de certaines pages peut laisser à désirer, surtout si les pages originales ont été dactylographiées à l'aide d'un ruban usé ou si l'université nous a fait parvenir une photocopie de mauvaise qualité.

Les documents qui font déjà l'objet d'un droit d'auteur (articles de revue, examens publiés, etc.) ne sont pas microfilmés.

La reproduction, même partielle, de ce microfilm est soumise à la Loi canadienne sur le droit d'auteur, SRC 1970, c. C-30. Veuillez prendre connaissance des formules d'autorisation qui accompagnent cette thèse.

LA THÈSE A ÉTÉ
MICROFILMÉE TELLE QUE
NOUS L'AVONS REÇUE

PREFACE

One of the problems of great fundamental interest to electrochemists and surface scientists interested in gas/solid interfaces has been the manner in which the first monolayer of surface oxide or other films develops on a metal substrate. For electrochemists this problem is relevant to continuing efforts to understand electrocatalysis, especially in anodic processes, at metals, and the phenomenon of passivation. The first layer of electrodeposited oxide species is intimately connected with the deposition processes involved in the formation of second or third layers before bulk-phase oxide formation sets in. A better understanding of monolayer deposition is necessary in order to enable the transition to bulk-phase from monolayer deposition to be understood.

The sensitive technique of cyclic voltammetry has been used in the present work and is specially suited to the investigation of the kinetics and phenomenology of electrodeposition and reduction of surface oxide films on noble metals. Following a brief introductory review, and description of experimental procedures, the thesis is divided into 6 further chapters which cover various aspects of phenomenology of the results and specific discussion of mechanisms of monolayer oxide deposition, growth with time, and reduction.

Some of the work presented in this thesis has been published in the first two papers listed below, and a number of additional papers are in preparation.

1. The Role of Ion Adsorption in Surface Oxide Formation and Reduction at Noble Metals: General Features of the Surface Process. H. Angerstein-Kozlowska, B.E. Conway, B. Barnett and J. Mozota; J. Electroanal.Chem. 100 (1979) 417

2. The Use of a Minicomputer for Data Collection and Treatment in the Study of Electrochemical Surface Processes. J. Mozota, B. Barnett,

D. Tessier, B.E. Conway and H. Angerstein-Kozlowska; Analytica Chimica Acta, 1981, Accepted for publication

3. Kinetics of Transitional Growth in Submonolayer to Multilayer Oxide Film Formation at Au, in preparation

4. Kinetics of Distinguishable Stages in Oxide Film Reduction at Au, in preparation

5. Application of the Direct Logarithmic Law to Surface Oxide Deposition at Constant Potential, in preparation.

ACKNOWLEDGEMENTS

The author wishes to express sincere gratitude to Professor B.E. Conway for invaluable discussions and advice throughout this work and especially during the writing of the thesis. Many thoughtful and stimulating discussions with Professor Conway have been of great influence and are gratefully acknowledged.

Special thanks are due to Dr. H. Angerstein-Kozlowska for expert advice about experimentation and for many contributions and discussions throughout evaluation of the results.

Special thanks are offered to Master Glassblower, Mr. Egon Kristof for construction of electrochemical glassware, to Ms. Eva Szabo and Mr. Pierre Langevin for assistance in preparation of diagrams and to many friends and colleagues for support and discussions throughout this work.

The author acknowledges the award of scholarships from the Association of Professors of the University of Ottawa and the Noranda Research Center (the Noranda Research Scholarship).

In addition, special thanks are extended to the author's sister-in-law, June, for her patient typing of the thesis. She didn't know what she was getting into.

Above all, the author wishes to thank his wife, Pat, for her patience, encouragement and most of all her self-sacrifice throughout this work.

TABLE OF CONTENTS

LIST OF FIGURES

Page No.

Page No.

LIST OF TABLES

ABSTRACT

Linear potential sweeps and the sensitive experimental technique of cyclic-voltammetry have been used to investigate the kinetics and phenomenology of electrodeposition and reduction of surface oxide films on gold electrodes in monolayer and submonolayer quantities from acid and alkaline solutions. Special experimental procedures were implemented in order to attain the conditions of high purity shown to be required, but not previously appreciated, in order to study surface oxidation processes on gold at very low coverages.

A series of experiments were performed in order to establish if the main electrodeposited species at Au is OH or O in the initial monolayer. Kinetic analyses of the results in several ways indicated that a 2 e^- electrodeposition and reduction of O species is involved so that the principal species covering the electrode is O.

Even in submonolayer quantities, oxide, as O species, is deposited and reduced in several energy states; information concerning the nature and significance of these states has enabled important conclusions regarding the mechanism of monolayer oxide formation and reduction to be made. The role of ions of the electrolyte, especially anions, in determining the early stages and energies thereof in oxide deposition was found to be surprisingly important. In acid solutions, strong specific adsorption of anions significantly inhibits the onset of oxide deposition. It was shown that blocking effects of anions which are more strongly adsorbed than the ions of the supporting electrolyte used in the experiments are important at concentrations as low as 10^{-7} to 10^{-8} M.

Moreover, it was found that these anions play an important role in surface oxide deposition processes in (a) establishing energies of an initial, reversibly deposited O species; (b) promoting place-exchange processes at low fractional coverages (< 0.3) and (c) controlling the rate of deposition of O species at intermediate coverages (0.1 ~ 0.5). Deposition of O species up to and beyond monolayer coverages is controlled by non-ion-assisted place-exchange processes.

The transition from submonolayer, through monolayer to multilayer anodic oxide film growth was studied as a function of time ($10^{-4} \leq t < 100$ s) and potential, V, in several solutions. Electrochemically controlled growth (with Tafel slope of ca 60 mV/decade) can be distinguished at low V and t, and is represented by linear log (1-Θ) vs t kinetics. Slower growth in two stages is observed at larger V and t, and proceeds with linear Θ vs log t kinetics (the so-called direct logarithmic growth law) exhibiting clearly distinguishable slopes for the two stages. The growth process appears to be continuous in nature from submonolayer, through monolayer to multilayer oxide film formation.

The kinetics of reduction of the three main distinguishable states of surface oxide that are developed at Au are evaluated using several different techniques. These states differ on account of the extent to which adsorbed anions are bound adjacent to electrodeposited O species and because some species are in a place-exchanged state. Partial reduction of anodically characterized oxide films to appropriate potentials in a cathodic sweep, followed by continued reduction at constant potential, revealed that the reduction proceeds, surprisingly, by an irreversible, electrochemically controlled process for which log Θ is linearly dependent on reduction time, t. A Tafel slope of 60 mV/decade was obtained for this process.

Transfer coefficients for the distinguishable surface processes are evaluated from information on the dependence of peak potentials on log [sweep rate, s] derived from linear potential-sweep experiments. The reduction processes are too irreversible for the reversibility parameter, s_o, to be evaluated.

Mechanistic examination of the results indicates that a quasi-chemical step, such as reverse place-exchange of O/Au, does not control the reduction kinetics nor does reduction involve hole growth following nucleation of holes. The role of a quasi-chemical step is required to account for the growth and aging effects observed, and the observed hysteresis between oxide formation and reduction.

CHAPTER 1

GENERAL INTRODUCTION

1. The Formation and Reduction of Thin Oxide Films at Noble Metal Electrodes

The work described in this thesis involves a comprehensive study of the electrochemical formation and reduction of monolayers and submonolayers of oxide at Au in particular and at noble metals in general.

Previously, the processes of formation and reduction of submonolayer coverages of oxide at noble metals through to thicker multilayer films, have been studied by various workers, mainly at Pt and to some extent at Au. In the present work, attention is directed largely to the study of Au for several reasons to be discussed below.

1) At Au, the stages of growth and reduction of oxide films up to monolayer coverage can be better resolved than at Pt[1-3], especially by means of linear potential sweep amperometry.

2) The surface oxide formation and reduction processes at Au are more sensitive to anion effects than those at Pt[2,3] or other noble metals, so that work on Au provides a better system for investigation of these effects.

3) Also, on Au, it is possible to follow the transition from monolayer to thicker oxide film growth and hence the relation between these types of processes.

4) Au, amongst the other noble metals, provides a good example for evaluation of the general features of the current (i) vs potential (V) profiles for surface oxidation, especially the hysteresis between oxide film formation and reduction processes[4,5].

Anodic polarization of Au in acidic solution leads at first to

development of a monolayer of surface oxide and, with longer polarization and/or higher potentials, eventually to multilayer formation of bulk-phase Au_2O_3[3,6-9]. Various electrochemical and spectroscopic methods have been employed in this work. Extensive reviews have become available recently[3,6,8,9]. Some of the significant results will be discussed in section 3. Generally there is little agreement between various workers, even in the phenomenological behavior of i vs V profiles in cyclic-voltammetry[10-16]. These divergences of the results probably arise from inadequate control of the history of the electrode, the type of anions in the solution, etc. The lack of agreement between various workers with respect to their results and interpretations of the behavior observed provided one of the main motivations for the present work. The others were the opportunity which Au offers for a sensitive study of anion effects in oxide film formation and for following the transition from monolayer to multilayer film growth.

2. Background on Oxidation of Pt and Other Noble Metals

The stages of formation and reduction of surface oxide films on Pt have been the subject of many original papers[4,17-22] and reviews[3,6,7,23]. Some of the main features of the behavior observed at Pt will be summarized here in so far as they have a bearing on similar processes found at Au. All the noble metals show a potential region, prior to evolution of O_2, over which surface oxidation occurs and a more cathodic region over which reduction takes place. Large differences arise, however, (a) in the potential range for onset of surface oxidation (0.25 V for Ru, 0.35 V for Ir, 0.75 V for Pt and 1.35 V for Au, depending on the anion of the electrolyte and pH) and (b) in the degree of reversibility with which some fraction of the monolayer is initially deposited and reduced. Particular details follow.

(a) Stages in Monolayer Oxide Formation

Between the thermodynamic limits of potential for decomposition of water to H_2 or O_2, there can arise at Pt or Au Faradaic surface processes leading to deposition or desorption of H (in the case of Pt) or oxygen species (in the case of Pt or Au and other noble metals). In the formation of the film oxygen species, one of the most interesting features is the appearance of several distinguishable states below monolayer coverage which are resolvable in cyclic-voltammetry experiments, as will be described in Chapter 2. The importance of use of ultra-clean solutions in studies of this kind has been stressed in recent work from this laboratory, e.g. using specially prepared pyrodistilled water[3]. The significance of the observed stages of electrodeposition of oxide monolayers at Pt or Au has been the subject of a number of papers in recent years[24-32].

In particular, stages of monolayer oxidation corresponding to formation of successive overlay lattices have been identified and the extents of reversible, in relation to irreversible, formation of surface oxide have been distinguished quantitatively[3,20-22]. For example, at Pt, almost reversible formation and reduction of OH species occurs up to 0.9 V, E_H*, depending on the anion of the electrolyte, and up to 1.05 V in alkaline solution. Greater irreversibility sets in when the films have been slowly grown at a controlled potential[19-22] or if they have been formed at potentials > 0.9 V, E_H.

Initially, it has been suggested, OH species are deposited at Pt in arrays on the surface[20] but at higher coverages and potentials, or after longer times, the submonolayer of OH or O species (depending on

---

* Throughout this thesis, potentials of electrodes are expressed in volts on the scale of the hydrogen reference electrode in the same solution and denoted for convenience by "V, E_H".

coverage) becomes reconstructed by a place-exchange mechanism[20,22] leading to irreversibility in the formation and reduction processes.

In the initial stages of oxide formation at Pt up to ca 210 $\mu C \cdot cm^{-2}$ of anodic charge passed, the electrodeposited species are OH; these are polar with respect to the underlying Pt atoms so that lateral dipole-dipole repulsions arise across the surface. These can be relieved by a field-assisted place-exchange of OH groups with immediately underlying atoms of the Pt substrate to which they are bound. Such a process (discussed in more detail below) results in a more stable, ionically bonded, two-dimensional surface oxide phase. At higher degrees of oxidation of the surface, these place-exchanged species become converted to O species ("OHPt $\longrightarrow$ "OPt" + H^+ + e) and some growth of a second layer begins. This reconstruction of the deposited oxide relieves the dipole-dipole repulsions and facilitates film growth by stabilizing the oxide network.

b) Induced vs Intrinsic Heterogeneity

The development of successive overlay lattices below monolayer coverage is believed to be associated with the successive current peaks observed in the i vs V oxidation profiles. Successive ordered structures have characteristic free energies which change as coverage increases. Superimposed on this effect are changes of state of the oxygen layer resulting from place-exchange.

This interpretation of the origin of multiple states of chemisorption of OH or O species is to be contrasted with other interpretations in which it is considered that a range of site energies for H_2O discharge and chemisorption of oxygen species exists at a metal electrode surface.

This intrinsic heterogeneity of a substrate surface is due to a distribution of different crystal faces and (especially for the higher index planes) the existence of kink and step sites.

Accordingly, attempts to test this interpretation have involved studies of gas-phase dissociative chemisorption of O_2 or electrochemical deposition of O species on various characterized principal index planes of single-crystals of Pt[33-38] and Au[10,14-16]. The results obtained by electrochemical studies have been contradictory (cf refs 10 and 14-16) both in terms of the experimental results found and the interpretations proposed. This has been, in part, due to the use of inadequately rigorous conditions of solution purification.

Hubbard recently reported[36] LEED experiments on Pt indicating that an initial surface reconstruction takes place immediately on exposure of the surface to H_2O but no further changes arise on exposure to electrolyte ions, e.g. H^+, ClO_4^-. Thus, the pristine state of a single-crystal surface characterized in the gas (vacuum) phase is difficult to maintain.

Additionally, Hubbard[38] found that successions of dilute overlay lattices, e.g. of I, are generated on single-crystal planes and Somorjai[39] demonstrated that heats of chemisorption of small molecules on single-crystal planes of transition metals may differ by up to 85 kJ mol^{-1} from one plane to another. This observation of chemisorption in multiple states of binding indicates that even a single-crystal plane is heterogeneous when viewed by the adsorbed species. Thus, it is not possible to assign a unique value for the heat of chemisorption of an adsorbate on a given transition metal.

c) Hysteresis in Reduction of Oxide Films

When formation and reduction of surface oxide is not reversible,

either "kinetic irreversibility" or "hysteresis" is involved. Kinetic irreversibility implies that the reduction process is chemically the reverse of the forward process but that its rate constant is much smaller than that of the forward process so that, to achieve significant reduction rates, a substantial overpotential is required. In contrast, "hysteresis" implies that a different pathway is involved in reduction compared with oxidation, arising because of an irreversible change of state of the oxide film. Place-exchange is a frequently cited process corresponding to such a change of state involved in the electrochemical formation and reduction of oxide monolayers on noble metals.

d) The Place-Exchange Process

A process termed "place-exchange", in which adsorbed oxygen atoms change places with underlying metal atoms and are incorporated into the substrate, was suggested by Lanyon and Trapnell[40] to account for the initial gas phase oxidation of metals. The process reduces the total energy of adsorbed dipoles (by dipole reversal) and is confirmed by the observation of changes of work function during adsorption[41-45] which depend on aging and temperature. Place-exchange is supported by the work function measurements of Quinn and Roberts[41], and Roberts[46], and studies of this phenomenon were extended to multilayer film growth by Eley and Wilkinson[47], and applied to the initial stages of metal oxidation by several other authors[48-52]. Klemperer has reviewed much of this work[44].

The role of place-exchange processes in gas phase oxygen adsorption on metals is therefore quite well established. On the basis of these results, it would appear that such processes are also likely to play an important role in anodic oxide film growth, where they are generally less well established, but strongly indicated.

The hysteresis observed in i vs V profiles for formation and reduction of O monolayers on Au electrode surfaces, and the logarithmic decay of anodic currents with time after an anodic sweep is interrupted[3,53,54], suggest that post-electrochemical reconstruction processes (place-exchange) are occurring, as proposed by several authors in work on electrochemical oxidation of Pt[20,21,55,56] and Au[57-59].

As in gas phase oxidation, strong polar bonding forces in oxygen monolayer films at electrodes establish surface metal-oxygen dipoles whose mutual interactions may be changed from repulsive to attractive ones by the place-exchange process. On account of the changed state of the deposited O layer, which arises when place-exchange in oxygen monolayer films occurs, continued deposition of OH or O species can take place in excess of what would be thermodynamically determined by the electrosorption isotherm for OH or O species at that potential. Several authors have argued[10,59-66] that a physical rearrangement of this type would be field-assisted. Thus, place-exchange will be assisted not only locally by the repulsive forces between the metal-oxygen surface dipoles, but also by the double-layer field at the electrode interface and local fields of adsorbed anions.

The place-exchange process will be activation-controlled, so its rate is expected to increase with temperature, at constant potential. At a given temperature and potential, this rate should depend on the zero-field free energy of activation for the process. Although such a quantity is difficult to evaluate, it should depend on the lattice energy of the particular metal, in addition to electronegativity differences affecting the magnitude of the metal-oxygen surface dipole.

Au is a "soft" metal with a much smaller lattice energy than that of Pt. Thus[67], the boiling point of Au is 3080 K, considerably lower than that of Pt, 4100 ± 100 K, and the heat of vaporization of Au (310 kJ mol^{-1}) is similarly much lower than that of Pt (510 kJ mol^{-1}); this indicates that place-exchange processes will be kinetically easier at Au than at Pt and should become significant at lower oxygen coverages on Au than on Pt. A number of the results obtained in the present work show this to be the case.

e) Growth Laws Observed for Thin Anodic Oxide Films (Transition to thicker film growth)

All metals, except gold, are unstable at room temperature in contact with O_2, and thermodynamically tend to form an oxide film[71]. At sufficiently positive electrode potentials and in appropriate solutions, anodic oxide films form at most noble metals unless other oxidation reactions, such as anodic dissolution, supersede[68].

Depending on the metal and the conditions employed for formation or growth of oxide, films of less than a monolayer or up to a few thousand layers of oxide may result, having various physical properties, e.g. good or bad conductivity. It has been found that several types of kinetic laws may describe the growth of oxide (in quantity as formation charge q, coverage Θ, or thickness, x) as a function of time, with conformation to one of these laws usually enabling one or other mechanism of oxide growth to be assigned, but not always unambiguously.

Various types of growth laws have been extensively reviewed in the literature[48,68-75]. Here only two need be examined in detail. It should be emphasized, however, that the kinetics of formation of a chemisorbed oxide monolayer are usually difficult to distinguish from those for

second or third layer formation.

Growth of thin anodic oxide films usually proceeds according to (a) the "direct" logarithmic law or (b) the "inverse" logarithmic law of growth. Damjanovic[76] (and others[77]) has extensively reviewed the mechanisms of oxide film growth and the experimental support for each of these laws.

i) The Direct Logarithmic Rate Law

When an (anodic) oxide is highly conducting (as at the noble metals Pt, Ir, Pd and Au[68,78]), oxide growth exhibits direct logarithmic kinetics in time[68]. In such cases, oxide growth is believed to proceed through the place-exchange mechanism described earlier. This mechanism has been used as a basis for a model of thick film growth[79-81].

Direct logarithmic kinetics, originally treated by Tammann[82], arise whenever it is postulated that the free energy of activation, $\Delta G^{\ddagger}$, for the oxide growth process increases linearly with oxide thickness, x, i.e.

$$\Delta G^{\ddagger} = \Delta G_o^{\ddagger} + bx \qquad (1\text{-}1)$$

where b is a constant.

Since the rate of oxide growth is proportional to the exponential of $\Delta G^{\ddagger}$, an integrated rate law of the direct logarithmic form

$$x = k \ln t + k' \qquad (1\text{-}2)$$

results, for which k and k' are constants and t is time. Although a rate law of this form is usually attributed to a mechanism of place-exchange, any process for which the free energy of activation increases linearly with oxide thickness, or coverage, produces a relation such as eqn.(1-2). For coverages below a monolayer, electrosorption with a linear decrease of adsorption energy with coverage, due to repulsive interactions giving

a term in exp [-gθ] in the oxidation rate equation, also gives direct logarithmic kinetics, as observed by various workers experimentally at Pt[30,31,56,65,66,83] and at Au[10,59,62,64,84,85]. Gilroy[83] used measurements of the quantity of oxide potentiostatically formed at Pt electrodes, as measured by cathodic galvanostatic reduction and current integration, to develop an oxide growth model based on rate-determining nucleation (and growth).

At present, no single model of oxide formation kinetics has emerged to account successively for logarithmic growth, although a number of analyses are available (see reviews cited above).

While thin film oxidation kinetics rarely follow a single, simple logarithmic rate law over extended periods of time, they frequently conform to a two-stage logarithmic law. The interpretation is controversial, however: compare the work of refs. 48,86-90 with that of refs. 91, 92. Young and Dignam[93] conclude that no theory of general applicability yet exists which explains direct logarithmic kinetics often observed at many metals at low temperatures.

ii) The Inverse Logarithmic Law

A different kind of growth law was treated by Mott[94-96] and by Cabrera and Mott[97] for development of thin films formed both by anodic and atmospheric oxidation.

According to these authors[97], oxide films grow at a metal surface by atoms being injected, as ions, from the surface across an energy barrier first into interstitial positions in the growing oxide phase, and are then transported through the oxide layer under the influence of that part of the overall metal/solution field which resides across the oxide layer. This situation usually implies that the oxide

film is more or less an insulator so that high-field conditions obtain. It is difficult to see how this mechanism applies to mono-, or submonolayer films at Pt or Au where the potential difference is mainly due to metal/oxygen surface dipoles and adsorbed anions. Although "monolayer oxide" can hardly be an insulator in the conventional solid-state sense, the Mott-Cabrera "high-field" mechanism of oxide film growth was applied to Pt oxidation by Ord and Ho[61] and by Damjanovic in some of his work[98-102] but, in the latter case, thicker films more extensive than a monolayer were involved up to x = ca 1 nm.

The high-field growth law usually applies to development of oxide films at the valve metals, Al, Ta, Nb, Ti etc., where thick insulating oxide films are formed.

The high-field growth law, in integrated form is*

$$\frac{1}{x} = k' - k \ln t \qquad (1\text{-}3)$$

Experimentally it is not easy to distinguish the applicability of this law to experimental results from that of the "direct" law, unless accurate measurements are available over 4 ~ 5 decades of time.

The applicability of the "inverse" vs the "direct" logarithmic law to growth of thin anodic oxide films formed on noble metals is, in fact, a matter of continuing controversy[76,77,100]. Several authors; for example, Vetter and Schultze, and Ord and Ho, have reported an inverse logarithmic law of growth for very thin oxide films (< 1.5 nm) on Pt[61,65,66,99,100] and Au[59].

---

* Recently, Ghez[103] has shown that this form of the Mott-Cabrera law is not a strictly accurate solution to the problem; a more correct test of the high-field growth mechanism is by means of a plot of $\frac{1}{x}$ vs $\ln [t/x^2]$. Other general cases have been considered as well[104].

Much of this controversy, as noted by several authors[53,105-107], arises because an unambiguous distinction between the "direct" and "inverse" logarithmic growth laws cannot be made on the basis of 1/x or x dependencies on log t unless the range of t is very long. Thus, Damjanovic[76] has stated that in order to distinguish between these two laws, oxide growth measurements should be extended over as much as four decades of time, preferably for oxide thicknesses initially as low as possible in order to measure larger relative thickness changes.

In the study of the deposition of the first few (1 ~ 3) layers of oxide, the concept of "film thickness" in the sense used in "high-field" theories is questionable. It is difficult, as well, to postulate a potential drop across a film for film thicknesses less than a monolayer, in a theory in which that potential drop determines the rate of growth through an activated ion transport process across a macroscopic lattice film.

Furthermore, interpretations of oxide growth such as that in the theory of Vetter and Schultze[59,65,66] do not allow for the fact that more than one process can give rise to the transients they measure, including the quite different processes (which they acknowledge are occurring) of initial deposition of O (or OH) species and growth of oxide at higher coverages involving the place-exchange mechanism. i vs V profiles for O deposition at Au indicate, for example, 3 or 4 distinguishable states as peaks already below monolayer coverage.

The confusion seems also to extend to the treatment of experimental results. For example, in Vetter and Schultze's work[65] referred to above, it is claimed that, for potentiostatic formation of the oxide film at Pt up to 3 layers of O in extent, the "direct" log growth law

[eqn.(1-2)] applies over the whole range of growth times (5 decades of t).

However, they use these experimental data to derive an electrochemical theory of oxygen deposition at Pt[65,66] and Au[59]. Current densities, i_+, of oxide formation determined from integral charge vs log t plots, were used to establish the variation of current density with potential of oxide formation at constant coverage (Tafel lines), and thence to evaluate Tafel slopes for the surface oxidation process. The Tafel equation derived in this manner is written as

$$\frac{dV}{d \log i_+} = b_+ = \frac{2.3\ RT}{\alpha F}(1 + a\Theta) = b_+^{\circ}(1 + a\Theta) \qquad (1\text{-}4)$$

where the Tafel factor, b_+, is a function of oxide coverage, Θ, as shown in eqn. (1-4). However, the reaction rate expression based on eqn. (1-4) of Vetter and Schultze does not give the required linear relation (direct logarithmic) between x and log t to which their experimental data conform for growth of oxide on Pt[65,66] and on Au[59] at various growth potentials over 4-5 decades of growth time. Their derived expression (eqn. 1-4) corresponds, in fact, to an inverse logarithmic relation, since an oxide thickness term is in the denominator of an exponential expression of rate.

From all these comments, it seems necessary to conclude that the formation of submonolayers of oxide should be considered in a quite different way from that for formation of thicker oxide films ($\Theta > 1$), although, experimentally, the direct growth line of quantity Q of oxide vs log t usually passes through the limit $Q \equiv 1$ monolayer without inflection, e.g. as found at Pt[65,83]. For example, for OH or O film formation up to the monolayer limit of coverage, approaches and models developed in modern surface science should be applied, e.g. concepts of overlay lattices and reconstruction of the metal surface. This approach will be taken in the interpretation of a number of the original results to be reported

in later chapters of this thesis.

Damjanovic et al employed galvanostatic transients[98,99] to study the mechanism of thin anodic oxide film growth at Pt in acid and alkaline solutions[101,102]. They concluded that the thin film growth kinetics (< 1.0 nm but > ca 1 monolayer) followed the Mott-Cabrera formalism of high-field assisted formation of ions and subsequent migration of these ions through the oxide phase. Between one and three monolayers of oxide, the same law for growth of oxide was found to apply[100] regardless of the mode of film growth (viz. under potentiodynamic, galvanostatic and hybrid galvano-potentiostatic conditions). The rate of growth of the oxide film, expressed as a current density i, up to an average of ca 1:0 nm thickness is expected to follow[98,99,101] the equation

$$i = i_o \exp \frac{\alpha (V - V_o)}{x} \qquad (1\text{-}5)$$

where x and i_o are constants independent of pH, V_o is a parameter that changes with pH and x is again the film thickness. $(V - V_o)/x$ is, of course, the field across the oxide.

3. Previous Work on Oxidation of Au

In recent years, work on the formation and reduction of oxide monolayers on Au has been reported in various papers. Work in earlier periods was sporadic. The early (pre-1940) work has been reviewed by Deborin and Ershler[108], and was mainly concerned with formation of thick oxide films.

Here we shall restrict the discussion to results of some of the more important, recent work. Several reviews of the literature concerning Au and its oxidation have become recently available[3,6-9] and illustrate the discrepant views on the subject which exist at the present time.

Renewed interest in the anodic oxidation of Au began about the

time of Laitinen and Chao's work[109] published in 1961. They found one chronopotentiometric arrest at about 1.35 V in 1 M $HClO_4$, and proposed a step-wise oxidation to form $Au\text{-}OH_{ads}$, $Au\text{-}O_{ads}$ and eventually Au-O-OH.

In a series of papers, Brummer and Makrides[110] and Brummer[54] and Makrides[85,111] studied the kinetics of surface oxide formation in molar $HClO_4$ solutions by potentiostatic anodization in the range 1.2 - 1.85 V (E_H). The quantities of oxide deposited in these experiments (corresponding to less than 2 monolayers as O species) were evaluated from subsequent galvanostatic reduction transients[110]. The chronopotentiograms showed that the reduction of oxide occurred over a small potential range, depending on the cathodic current density. The anodic (deposition) charge increased linearly* with potential, at constant formation time, over the range 1.45 - 1.8 V. These results, and those of Laitinen and Chao[109], were interpreted, due to the absence of multiple arrests, as evidence against the formation of stoichiometric Au (I) or Au (II) intermediates.

Cathodic chronopotentiograms were used to construct log i vs V curves which followed a Tafel relation for oxide reduction with a slope of 41 mV. This slope was independent of the potential of oxide formation and pH in the range studied.

To account for these observations, Brummer and Makrides proposed a mechanism for reduction in which it was assumed that reduction of an Au (II) intermediate is the slow step, and for which a Tafel slope (dV/d log i) of 39 mV, for $\alpha = 0.5$, is predicted.

Brummer[54] also investigated oxide growth kinetics in experiments he referred to as "aging". Oxide was formed potentiostatically at a

---

* This is an artefact due to lack of sensitivity of the galvanostatic method which is essentially an integral technique as it measures V as a function of $\int$ idt = charge passed.

series of potentials (1.45 - 1.85 V) for various growth times (aging, in his terms) and its quantity determined in a galvanostatic reduction. It was found that oxide continues to grow slowly, even at long times of formation; the range of potentials over which reduction occurs becomes less positive for longer growth times indicating stabilization of the film. A logarithmic oxide growth law was reported (oxide coverage less than 2 monolayers as O species throughout these measurements) having a slope [dQ/d log t] increasing as the potential of oxide formation was increased.

More recently, Gruneberg[112] used potentiodynamic sweeps and was the first to observe two reduction peaks in the cathodic sweep. The i vs V reduction profile was later resolved by Gol'dshtein et al[1,2] into three distinct peaks. An initial reversible region was noted at low coverage ($\Theta < 0.1$). These authors investigated the kinetics of oxygen deposition[113] and derived a Tafel slope of 50 ± 2 mV for the oxidation.

Vetter and Berndt[114], using the galvanostatic method, found that the amount of charge involved in monolayer formation was independent of pH in the range 0 - 12, and that the charging curves shifted by ca 59 mV per pH unit.

Schultze and Vetter[59] investigated time effects in galvanostatic experiments at Au in 0.5 M H_2SO_4 and found that the state of oxygen chemisorbed on the surface depends not only on coverage, but also on the conditions under which it was formed. At very low coverages (< 0.1), chemisorbed oxygen "ions" were considered to be in equilibrium with the electrolyte. At higher coverages, a field-assisted place-exchange process was considered to become rate-determining. These authors (most of whose data corresponds to oxide films less than 1.5 - 2 monolayers as O species)

also believe that oxide formation advances uniformly over the whole surface (since they observed no inflections in the charging curves) so that oxide grows continuously with increasing time or potential. The cathodic reduction of oxide[59] was assumed to proceed only at the edges of oxide islands as supposed by various other workers[115-117]. Schultze and Vetter[59] also derived coverage-dependent Tafel slopes, linearly dependent upon θ, with initial values of 25 mV (decade)$^{-1}$ for oxide deposition and 38 mV (decade)$^{-1}$ for reduction of gold surface oxide. The treatment was similar to that discussed earlier (section 2e) for Pt[65,66] in connection with oxide growth laws.

In potentiodynamic formation and reduction of oxide monolayers on (111) and (100) planes of gold single-crystals, Dickertmann, Schultze and Vetter[10] postulated that the role of crystal faces on the kinetic parameters may be important for the growth of thin epataxial oxide layers.

They observed distinct, separate peaks for oxide deposition in i vs V profiles on the different single-crystals, although a polycrystalline surface showed a more monotonic curve. In spite of the significant differences in the anodic regions, all curves coincided in the cathodic region. This indicates that the state of the oxide at the end potential of the anodic sweep is essentially the same, regardless of the orientation of the surface used. The i vs V profiles presented by these authors for a polycrystalline electrode (in 1 M $HClO_4$) did not exhibit any oxide deposition currents until potentials of 1.5 V or more are attained in the anodic sweep. (The normal potential for onset of oxidation in this solution is 1.35 V E_H.) This inhibition of oxide deposition by ca 0.15 V (cf the work of Sharp[3], Sotto[14-16] or Arvia[11-13,118,119] must be attributed to substantial contamination of the solution by impurities. In addition, the

absence of fine structure in the i vs V profiles confirms this supposition. Desorption of impurities in the first few potential cycles was acknowledged by these authors as an experimental requirement.

The requirments for very "clean" experimental conditions must be stressed, especially with regard to investigations at single-crystal electrodes. Results presented earlier (p. 5) on vacuum/gas phase studies indicate that surface reconstruction may be important at low levels of H_2O adsorption from the gas phase. Also, the results of Rand and Woods[120] indicate that the charge associated with corrosion of Au in aq. medium in each cycle taken to 1.54 V (later stepped to 1.8 V) is of the order of 4 $\mu C\ cm^{-2}$ or ca 1% of a monolayer (as O species). Thus an electrode pretreatment involving strong anodic polarization or multiple potential-cycling can seriously affect the integrity of a single-crystal substrate surface. That such pretreatments have been employed and were required by most workers because of insufficiently pure solutions, emphasizes the difficulties in using single-crystals and explains the discrepancies between various workers' results. In the present study, it is believed that the application of ultra-high-purity conditions (described below) eliminates or greatly reduces the need for electrode surface pretreatment.

Sotto[14-16,121-123] also investigated monolayer surface oxide formation and reduction at single-crystal Au electrodes. Cycling pretreatments were used in her work also in order to obtain i vs V profiles which did not change with continued cycling. It is difficult to imagine that sustained polarization at potentials ca 1.9 V (r.h.e.) employed in the pretreatment programs would have no damaging effects on single-crystal planes of the Au electrodes used.

Sotto found, however, that depending on pH, temperature and

sweep rate, between one and three cathodic current peaks could be observed on each single-crystal plane studied. These current peaks were attributed[15, 16,122,123] to the reduction of three successive oxide states at gold, all existing simultaneously on the electrode surface. These states were supposed to be 3-dimensional nuclei of Au (III) (as $Au_2O_3.n\ H_2O$), Au (II) as AuO or $Au(OH)_2$ and Au (I) as Au_2O or AuOH. The latter two states were said to be strictly localized on the surface (but not the phase oxide, Au_2O_3) and to be involved in a stepwise mechanism of oxidation.

The stage of reversible deposition of oxide observed at low coverages and with moderate to high sweep rates by Gol'dshtein et al[1,2] and by Arvia et al[12,13,124] (and also in the present work) was not discussed by Sotto. Her experimental results were interpreted in terms of an "energetic heterogeneity" of the electrode surface, even for single-crystal electrodes, with the above species being successively formed.

It might be expected that a stepwise reduction of oxide, such as proposed by Sotto, would result in some stoichiometric relationship between the charges associated with the three current peaks. This, however, was not proposed or observed.

Although the experimental conditions employed by Sotto were not ideal (especially for the single-crystals employed), a careful analysis of the stages of reduction of the oxide film at Au was made in terms of the distinguishable current peaks of the i vs V profile at different temperatures and on different crystal faces. Experiments were performed in which an oxide monolayer was partially reduced in a cathodic sweep, followed by reduction at controlled potential within the range of potentials of the reduction peaks, then further by completion of reduction in a continuated cathodic sweep. This type of experiment made it possible to observe and resolve the sequence of reduction stages and the interdependence of the behavior of the

three (according to Sotto) reduction peaks. Such an approach is particularly valuable when employed under conditions of very high solution purity, as was the case in the present work.

A detailed investigation of the formation and reduction of Au surface oxide using cyclic voltammetry was undertaken by Arvia and co-workers[11-13,118,119,124-127] using a variety of conditions.

In early work[11,12], these authors resolved the monolayer oxide formation profile into three regions and showed the various conditions (e.g. changes of sweep rate) required in order to observe three separate current peaks for reduction of monolayer levels of oxide. Also, experiments at different temperatures[11] led to dramatic changes in the reduction profiles. Thus, the cathodic reduction of oxide appears as a single, very narrow peak at 343 K but at 262 K two peaks are clearly observed, but this effect was not explained. Some chemical dissolution or corrosion of the oxide[11] on open circuit was also noted. It was also observed[12] that the shapes of the i vs V profiles depended strongly on the nature of the anions of the solution, e.g. with ClO_4^- and SO_4^{2-}.

In subsequent work[13,118], the influence of open-circuit aging of the oxide, including chemical dissolution effects, was examined. Stepwise oxidation mechanisms were proposed (leading to phase oxide Au_2O_3 formation, even for a monolayer of oxide) and one feature of the several mechanisms advanced was the action of a "chemical" step in stabilizing the oxide film. It was suggested that such a step could be a disproportionation reaction (without net electron transfer) in which Au_2O_3 is formed from less highly oxidized material and Au metal is regenerated. For the monolayer processes involved, it is difficult to accept this type of disporportionation mechanism. It was concluded that aging effects (involving time-

dependent, non-electrochemical processes) determine most of the features of i vs V profiles for oxidation and reduction.

A type of dynamic aging of oxide[119], achieved by rapid cycling of potential within a restricted region of the usual range of potentials in the V vs t sweep, has been used by Arvia in a series of papers to evaluate the kinetics of the aging process or the non-electrochemical processes (probably the same as "aging") which have been considered for Pt[128] and Au[119]. It was concluded that surface reconstruction may account for the formation of a stabilized (i.e. more difficultly reducible) oxide film after a period of aging. It is important to note that aging effects were attributed by Arvia (especially see refs. 13,118) to stepwise oxidation stages involving stoichiometric species and their interconversion by disproportionation (cf above), rather than lattice rearrangement processes.

In more recent work[124], the multiplicity of peaks observed in i vs V profiles at Au in alkaline solution was examined. An increased structure in the i vs V profiles is observed under these conditions and the appearance of reversible currents for apparent oxide deposition and reduction over a wide potential range was cited (cf. ref 129).

The lack of structure in most of the i vs V profiles presented by Arvia et al, combined with the observation of agitation-sensitive current peaks at potentials for which no reactions are expected, strongly indicates contamination by impurities in their work. Mechanical and electropolishing (in a CN^- containing bath) procedures were used in their work. Specific mechanisms for the surface oxide formation and reduction processes were not elucidated by means of diagnostic parameters[130-133] (see Chapter 3, p. 56) for i vs V profiles for surface processes.

4. Previous Work on Oxidation of Au: Relation to Ion Effects

A number of workers[1-3,12] have observed that the anions of

supporting electrolytes have important effects in determining the energies of the early stages of oxide deposition, both at Pt and Au, as resolved in an anodic potential sweep. These effects are undoubtedly determined by the varying strengths of specific adsorption of anions and the electrostatic effects associated with the relation of the potential ranges for oxide deposition (in acid solution) to the potential of zero charge[134,135] for the solution being investigated. In acid solutions, the effect of adsorption of cations on Au can generally be neglected[136,137] because the potential of zero charge (p.z.c.) is (arquably) at about 0.2 V[138] to 0.3 V[139] E_H, or higher in the usual acid solutions employed to investigate oxide monolayer deposition. For example, Bockris and co-workers[140] found a value of 0.17 V for the p.z.c. of Au in dilute perchloric acid solutions. Such a value for the p.z.c. indicates that at potentials near those for onset of surface oxidation, strong electrostatic attraction operates between the metal electrode surface and anions of the electrolyte; oxide deposition begins at ca 1.0 ± 0.1 V positive to these values of the p.z.c.

It may therefore be expected that specifically adsorbed anions will have a major influence on the deposition of O-species. It has been found[137] that the specific adsorption of anions at Au decreases in the order $I^- > Br^- > OH^- > Cl^- > SO_4^{2-} > ClO_4^- > F^-$. Thus it is found that O species begin to deposit on Au at potentials about 100 mV more anodic in H_2SO_4 solution than in $HClO_4$ solution[1,2] apparently because of the difficulty of displacing the more strongly adsorbed SO_4^{2-} ion from the electrode surface.

The exact value of the p.z.c. for Au is somewhat controversial. In any case it depends on solution composition and temperature. Also, of great importance, its value depends very much on the crystal face of the substrate metal that is available for adsorption[141-147], as might be

expected by the known variation of work function of a metal with crystal plane.

The p.z.c. of Au has been evaluated by a number of workers by several methods. An excellent review[9] has recently become available in which the major studies are critically examined. A table summarizing the results and methods of numerous studies is given. In acid solutions, the p.z.c. values vary from 0.10 to 0.30 V.

More recently, Clavilier and van Huong[138] have studied a large range of concentrations of the electrolytes $KClO_4$ and $HClO_4$; and determined the potential of zero charge by means of differential capacity vs potential curves. They found that the value of the p.z.c. was, surprisingly, independent of concentration and pH, and was -0.040 V (s.c.e.). The actual value of the p.z.c. is found to be difficult to establish, but the potentials where the net charge on the electrode becomes positive is in the range 0.1 up to 0.40 V (r.h.e.). Thus, anion effects are expected to be important at the relatively high anodic potentials required to deposit oxide at Au.

A related topic is the question of solvent orientation at electrode surfaces discussed by Trasatti[148-150] in relation to the energies of specific adsorption of anions. It is proposed that the relative orientation of water dipoles at a given metal electrode surface may be evaluated from a knowledge of the p.z.c., the work function and the electronegativity of the metal. It is argued that no preferential orientation of water is expected at Au, thus conferring a type of "hydrophobicity" on the electrode surface. The concept of hydrophobicity is somewhat controversial however. Gardner and Woods[151] have recently stated that Au and Pt are in fact hydrophilic metals, contradicting other published interpretations. If Au exhibits "hydrophobicity", it is expected that the effects of anion adsorption on deposition of O species will be more important than at metals

where the solvent (H_2O) is more strongly bound to the electrode. This is part of the motivation for undertaking a study of the influence of anion adsorption on the processes of surface oxide deposition and reduction on Au in the present work.

5. Aims of the Present Work

As was described in earlier sections of this chapter, the formation of surface oxide on Au electrodes has been studied by a number of workers, but it is obvious that a clear understanding of the system has by no means yet been achieved. This may be attributed in part to the restricted types of experiments performed by most workers and to the failure of a number of workers to appreciate the requirements for use of extremely "clean" solutions etc. Even amongst workers using the same experimental techniques, it is clear that there exists considerable disagreement not only with regard to interpretation of experimental results but also over the results themselves. In the present work, a main aim is to develop experimental techniques which result in substantial improvements in the cleanliness of test solutions and may help clarify these difficulties.

The exact nature of the monolayer oxide film is not at all well established (e.g. AuOH, AuO). The application of several experimental approaches enabling determination of Tafel slopes for oxide deposition provides insight into the chemical nature of the film and, as well, suggests plausible mechanistic sequences for oxide deposition and growth processes. The existence and the importance of any place-exchange processes is still not agreed upon, neither is the sequence of steps and their relative rates in an overall mechanism of oxide growth and reduction.

In the light of previous work, the aims of the present study are therefore:

a) mainly to determine the processes of formation of the first monolayer of oxide prior to thicker film formation. This includes attempting to evaluate the chemical nature of the film, the sequence of consecutive discharge steps in relation to non-electrochemical rearrangement steps, coupled with discharge or reduction, and the rates of the steps involved in an overall mechanism including processes involved in film formation leading to expressions for an oxide growth law. The appropriateness of a mechanism of nucleation and growth for monolayer surface oxide formation and reduction will also be evaluated critically.

b) to evaluate the influence of co-adsorption of anions on the processes involved in formation and reduction of monolayers and submonolayers of oxide. Because of the importance of such effects, a number of ions of different adsorbability have been employed.

An investigation of these problems which integrates a variety of measurements and also experimental approaches employed in some cases by other workers, combined with the use of theoretical information available as diagnostic parameters of i vs V profiles derived earlier in this laboratory (see Chapter 3, p. 56) enables a clear understanding of monolayer surface oxide deposition and reduction to emerge. In addition, the uniform application of high purity conditions (described in Chapter 2) in all these measurements should not only eliminate some of the contradictions in results of earlier investigations but should also permit much more sensitive and reliable measurements to be made.

CHAPTER 2

EXPERIMENTAL

1. General Choice of Methods

In the present work, the kinetics of surface oxidation of noble metals, principally Au, have been studied. Because surface processes are involved, in which virtually non-continuous currents pass, it was necessary to employ non-steady-state methods in the experiments in the usual way.

The preferred techniques were cyclic and linear potential sweep voltammetry, conducted at various sweep rates with complex potential-time programs when necessary. Kinetics of electrolytic growth or reduction of oxide films for various periods of time were also studied by application of linear potential sweeps at various rates after the controlled periods of growth or reduction at a fixed potential. These techniques provide a very sensitive and accurate way of following non-steady-state electrode processes at metal surfaces in terms of:

a) currents generated for production of surface films in various states;

b) distinction, in terms of electrochemical free energy, of the various stages of development of surface films, e.g. distinguishable adsorption states; and

c) evaluation of the kinetics and extent of reversibility of electrolytic surface processes.

The method is specially suited to the study of surface processes where small, time dependent current densities are involved.

A key point in this work was the perceived necessity of adopting special techniques for water purification, cell and glassware treatment, and an efficient experimental technique in which contact of all materials with the air during, and in preparation for, experiments was minimized. The degree of experimental "cleanliness" required in order to achieve "clean" cyclic voltammetric profiles, unaffected by traces of foreign ions and molecules, is much greater, at least for Au, than was previously thought. Accordingly, new procedures were developed and incorporated into the general experimental technique; they resulted in substantial improvements in the cleanliness of test solutions and the reliability and reproducibility of the resulting i vs V profiles that were obtained. In addition, use of these procedures helped to clarify some of the discrepant results in the literature of this field, and will be shown to be essential if satisfactory results are to be obtained.

In the potentiodynamic sweep method [4,152] a potentiostat, controlled by an electronic function generator, sweeps the potential of a working electrode through a pre-arranged, time-dependent program and the resulting time - (and hence potential-) dependent currents are followed as a function of potential on an X - Y recorder or an oscilloscope, or are stored digitally in a mini-computer[153].

The form in which potentiodynamic data are obtained is illustrated in Figure 2-1, which represents the current-potential (i vs V) profile for a Au electrode cycled between 0.40 and 1.69 V in 0.1 M $HClO_4$ at a sweep rate of 0.020 V s^{-1}. The currents observed

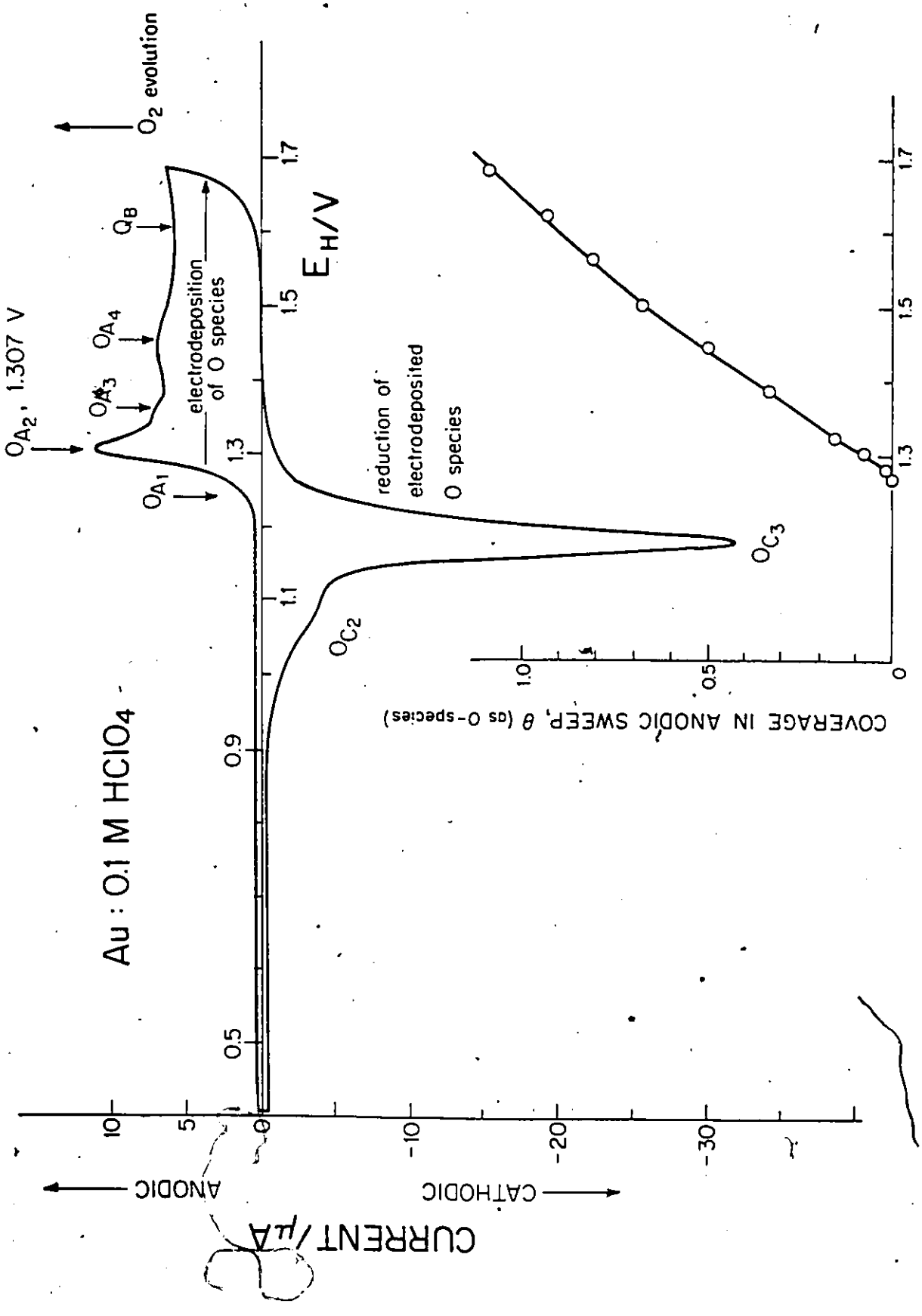

Figure 2-1 Typical potentiodynamic current-potential profile at Au in 0.1 M $HClO_4$ at s = 0.020 V s^{-1}, T = 298 K.

are the sum of components due to the Faradaic electrodeposition or dissolution of surface species (self-stifling reactions in this system) and the non-Faradaic double-layer charging currents which correspond to redistribution of ions and molecules (including water dipoles) in the interphase adjacent to the electrode surface so as to achieve an electrostatic equilibrium at the potential concerned.

The range of potential over which the current response is almost independant of potential in the anodic-going sweep, commencing at 0.4 V, is a potential region in which only double-layer charging currents arise. Their values are useful in the subsequent treatment of the i vs V profiles for surface oxidation. At more positive potentials, proceeding in the anodic direction of the sweep, electrodeposition of O-containing species takes place in a series of distinguishable stages at corresponding energies (potentials), followed, at potentials greater than 1.7 V, by the evolution of O_2. The electrodeposited O species are all reduced in the subsequent cathodic sweep in what appears to be (mainly) a single bound state. The charges represented in this diagram are of the order, e.g. for O-deposition, of 400 $\mu C\ cm^{-2}$. This is a very small, but accurately measurable quantity of charge, corresponding to a monolayer of electrodeposited O species, and illustrates the sensitivity of these measurements. Currents due to the evolution of H_2 may be observed when the potential of the cathodic sweep is less than ca 0.0 V (not shown in Figure 2-1). The adsorption of H species is not observed

on Au prior to H_2 evolution[154,155].

The existence of multiple states of adsorption, such as those shown in Figure 2-1, is now established in many stystems. While early studies of this type were frequently irreproducible and conflicting, the consistent application of high purity experimental conditions has produced major advances in this field, especially in terms of quantitative evaluation of multiple state adsorption in monolayers[3].

The method also has the important advantage that it generates directly a differential record of the adsorption behavior arising in electrodepositon or electrochemical removal of a monolayer at a metal surface since currents (i) generated in a sweep at a rate $\frac{dV}{dt}$ are proportional to the adsorption capacitance C, i.e.

$$i = C\frac{dV}{dt}$$

and C is the differential coefficient of the electrochemical isotherm relating coverage Θ of some electrodeposited species, e.g. metal atoms or, in oxidation, OH and O species, to the potential, i.e.

$$C = Q\frac{d\Theta}{dV}$$

where Q is the charge required to deposit (or remove) a monolayer of the electrodeposited chemisorbed species. Hence an electrochemical "spectrum" of electro-generated adsorbed species in terms of the potentials at which they are deposited or removed from the surface is directly recorded in the potential sweep method.

The sweep rate dependence of the potentials at which various current peaks arise gives a measure of the reversibility of the reactions. Also, if the electrochemical process occurs uniformly over an electrode surface, the amount of charge passed under a given set of conditions gives a measure of the surface coverage by the species deposited or removed from the surface.

The relative merits of potentiostatic and galvanostatic methods in the study of surface reactions have been widely discussed[156,157].

The special advantage of use of the potentiostatic method is that it permits a selective study of individual surface reactions according either to their reversible potentials or to the overpotentials required for the passage of significant currents (10^{-5}-10^{-3}A cm^{-2}). Furthermore it can be used dynamically to give information about reaction kinetics[158] by means of studies based on measurements of relaxation times of the processes involved.

i) Information Available from Potentiodynamic Current vs Potential (i vs V) Profiles

The number, size and shape of the peaks generated in current vs potential profiles obtained from potentiodynamic sweeps provide (amongst other factors) important information concerning the nature of the adsorption-desorption reactions occurring at the electrode surface. When the availability of reactants at the electrode is diffusion-limited, the associated peak current varies with the square-root of the sweep rate. When

there is no diffusional limitation, the resulting peak currents will be directly proportional to the sweep rate. It is this linear relationship which identifies Faradaic surface reactions, since no mass-transport over any significant distance is involved in such processes.

A number of authors have conducted theoretical work on the behavior of various electrochemical surface processes under conditions of potential-sweep and potential-step modulation. The generalized forms of the current-potential profiles which arise in simple reversible and irreversible surface reactions have been calculated and the effects of several different thermodynamic parameters in these systems have been investigated in a number of papers.[55,130-133,159-166]

Most of the results obtained hitherto have been concerned with theoretical analyses of single-electron discharge processes leading to the formation (and subsequently the removal) of a single monolayer of adsorbed species at the electrode.

The electrochemical surface reactions of particular interest in the present work, although studied at monolayer and submonolayer coverages, generally exhibit several peaks in the i vs V profiles. These peaks usually overlap too much to enable accurate deconvolution into component simple peaks to be achieved, thence permitting an evaluation of the corresponding individual isotherms to be made.

Under optimal conditions, it is sometimes possible to separate a current-potential profile into a sequence of electro-

chemical adsorption (or desorption) capacitance components and thence the contributing adsorption isotherms.

When component peaks can be resolved, a) their symmetry gives information on the reversibility of the process(es), while b) their breadth gives a measure of the extent of lateral interaction amongst the adsorbed species in the monolayer in terms of the half-widths (width at half-height) of the peaks[130-132,159].

Electrical Circuitry

The basic electrical circuit used in this work is well known and is shown in Figure 2-2. The potential of the working electrode was controlled by a high output voltage Wenking potentiostat according to a program set by an electronic function generator. Servomex LF 141, Tacussel GSTP2 and (principally) Tacussel GSATP function generators were used interchangeably for this purpose, according to the complexity of the cyclic program required (see Chapter 2, section 6).

The potential of the working electrode was measured with reference to a Pt/H_2 reference electrode in the same solution through a Tektronix Type O operational amplifier acting as a very high impedance 1:1 amplifier (cathode follower). Currents passed between the working electrode and the counter electrode were measured as potentials across a Leeds and Northrup 4755 high quality decade resistance box (ohmic transducer) inserted in series with the counter electrode. Experimental current-potential (i vs V) profiles were recorded on a Hewlett-Packard Moseley Model 7001 AM X-Y recorder, or were monitored on a

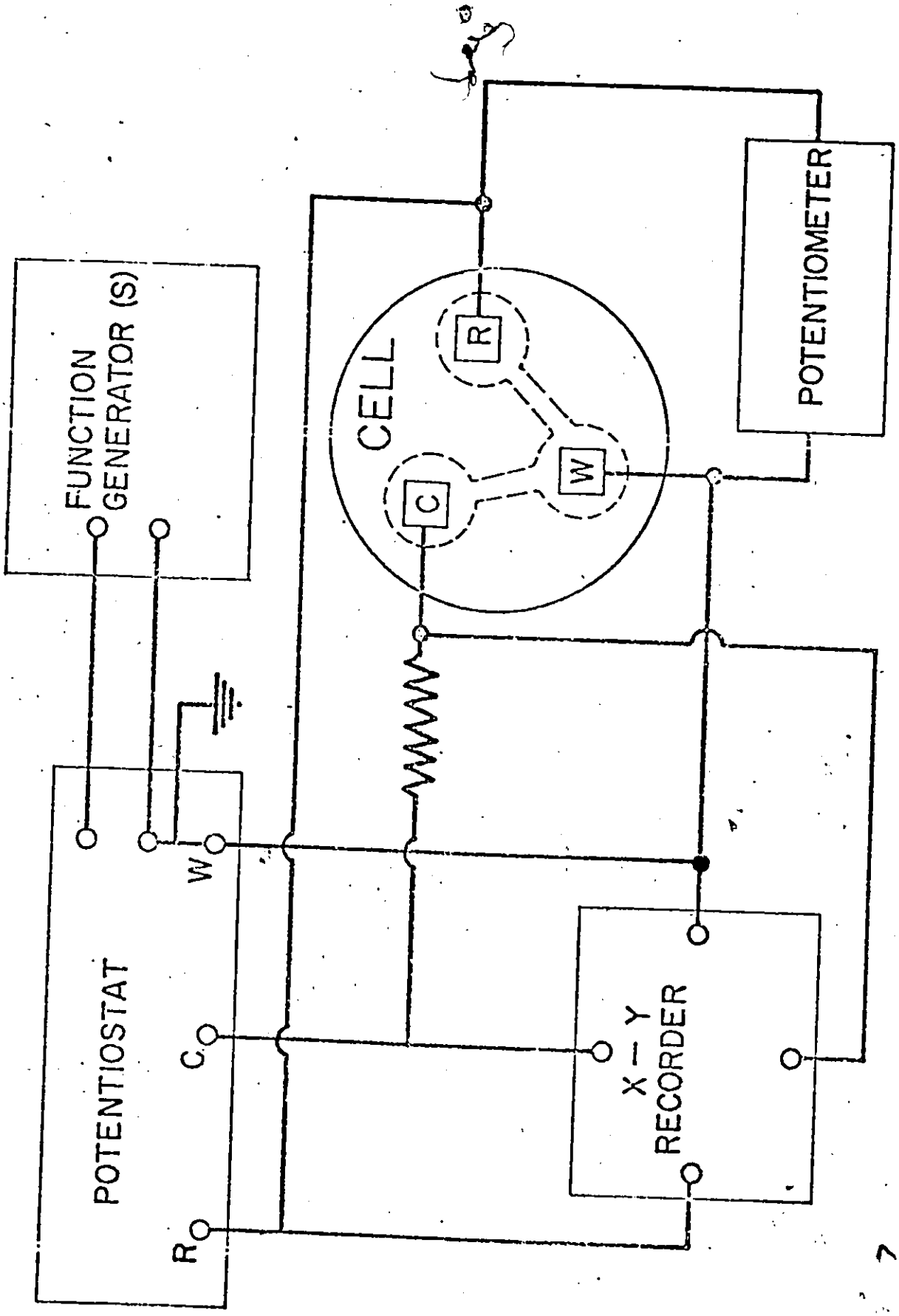

Figure 2-2 Electrical circuitry employed in potentiodynamic sweep studies

Tektronix 564B or 5115 storage oscilloscope from which they could be recorded using a Polaroid camera provided with high speed (type 47, 3000 ASA) Polaroid film. Continuous readout of the working electrode potential was available on a digital multimeter. The circuit was grounded from a single point (the working electrode) directly to an incoming fire hydrant.

2) Choice of Conditions

The study of surface oxide formation and reduction on Au electrodes in acid and alkaline solutions was conducted under rather specialized conditions in order to minimize, avoid or eliminate interfering influences (to be discussed in detail later) which otherwise vitiate the study of electrode surface processes at monolayer levels of coverage.

Surface processes at Au were investigated over ranges of potential where no continuous Faradaic reactions occur. Under these conditions, any adventitious diffusion-controlled currents (which are identified by their sensitivity to stirring of the solution) may normally be attributed to the reaction of solution impurities at the electrode surface. Also, in order to study adsorption processes at electrodes, it is necessary to maintain the concentration of reactant at levels sufficiently high that complications from diffusion-controlled reaction rates are avoided. In the present work, this presented no problem since the solutions were either acid or alkaline in which the reactant for surface oxidation is either H_2O or OH^-, respectively. However, other adsorption processes, e.g. involving ions at

trace concentrations, may be diffusion limited.

3. The Purity Problem

i) Water

In the early seventies, it was found in this laboratory that solutions made from distilled city water, re-distilled from alkaline $KMnO_4$, began to give impurity currents at Pt, with selective blocking of the surface processes associated with deposition of O and H species. Problems connected with water purity also began to appear at about this time in a number of other laboratories in the Ottawa area. Although the nature of the new impurity(ies) could not be established, a new method[167] was developed to remove impurities by catalytic pyrodistillation.

The type of apparatus now used routinely in this laboratory for all surface studies, and employed throughout this work, is shown in Figure 2-3. Details concerning the construction and development of this apparatus are fully described elsewhere[3,167,168]

This pyrodistillation process, in which water is distilled over Pt/Rh catalyst at high temperatues in an oxygen-rich environment, is based on the destructive oxidation of impurities to gaseous oxidation products (e.g. CO_2, NO_2). It is thought to be superior to other purification methods recently used elsewhere and based on the adsorption of impurities on activated charcoal[169] or on platinized Pt sponge potentiostatted at 0.005 - 0.350 V[170]

Adsorption methods involve the difficulty of preparing and maintaining the adsorbent material in an ultrapure condition (difficult with charcoal), and the assumption that new impurities

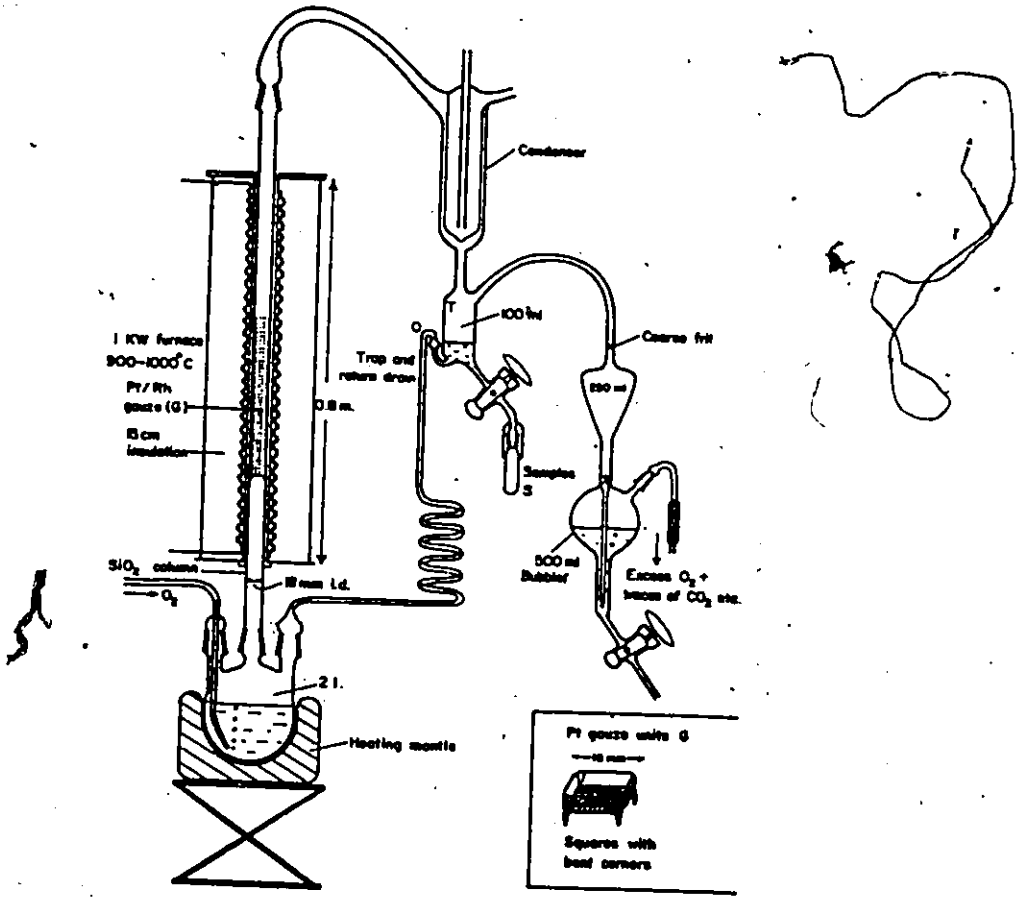

Figure 2-3 Apparatus for the pyrodistillation of water

appearing in the water supply will still be removed by the same adsorbent.

The use of catalytically pyrodistilled water and AristaR grade acid eliminates the need for potentiodynamic pre-electrolysis involving high anodic potentials (see Pre-treatment) in order to obtain "clean" i vs V profiles for Pt and Au. "Clean" i vs V profiles, unchanging and independent of agitation, are normally obtained at Pt in this laboratory within ca 10 anodic/cathodic cycles over a potential range 0.07 to 1.32 V E_H in a fresh solution; under optimum conditions, they can be obtained on the second cycle after the electrode had been left on open-circuit for many hours in a deaerated solution[171]. This important result eliminates the objection that the structure of the current-potential profile for Pt (and for Au) in aqueous solution is an artefact arising from multiple cycling.

On Au electrodes, the use of pyrodistilled water and AristaR grade acid, combined with the special cleaning procedures to be described below, have made it possible to achieve "clean" i vs V profiles for Au under optimal conditions in 5 cycles or less.

Following years of earlier experiences in this laboratory with surface processes at Pt electrodes in clean and impure solutions[3], the series of solution purity criteria and general principles for diagnosing the cause of impurity effects, which were developed for electrochemical surface studies on Pt, have been updated and improved for application to the study of surface

oxidation of Au. This was necessary because it was observed that, in many respects, Au is more sensitive to impurity effects than is Pt. These important effects and conclusions have been summerized in Table 2-1.

Concurrently, the development of several criteria for cleanliness which are required to establish the purity of a Au electrode-solution system over and above the ionic effects (e.g. of SO_4^{-2}) to be discussed later are summarized in column three of Table 2-1.

ii) Pre-treatment of Electrodes

Most workers investigating the formation and reduction of oxide species on gold have found it necessary to subject the working electrode under study to a variety of pre-treatments, some of which are very elaborate and/or quite severe. For example, they may involve harsh chemical[109], electrochemical[14, 59,113,117,172-174] or mechanical[12,13,118] procedures, or some combination thereof[110,115,116,175]. Many authors have stated that this pre-treatment is necessary in order to "activate"[14] the electrode or to obtain reproducible results[10,59], even when their investigations have been concerned with single-crystal electrodes[10,14,16].

The results of the present study have clearly indicated that "clean", reproducible i vs V profiles can be obtained using pyrodistilled water[167] and the fairly extensive cleaning procedures described below. An important conclusion regarding the experimental procedures used here is that the need for potentially disruptive pre-treatments of electrodes has been eliminated,

TABLE 2-1

EXPERIMENTAL PHENOMENON	SOURCE OF PROBLEM	CRITERION FOR CLEANLINESS
i) agitation spoils or worsens i vs V profile	diffusion control of impurities	absence of any stirring effects
ii) agitation improves i vs V profile	leaking electrode (impurities leak thru poor metal/ glass seal)	on the i vs V profile
iii) i vs V profile is "dirty" but unaffected by agitation	impurities adsorbed on electrode	maintenance of resolution of multiple states and peaks in profile, esp. peaks for onset of oxide deposition, down to sweep rates as low as 0.005 V s^{-1}.
iv) as in iii) but improves with potentiodynamic cycling	oxidizable or reducible impurities	equality of anodic and cathodic charges for oxide deposition and reduction
v) overall slant or shift in baseline of i vs V profile	severely leaking electrode or electronic artefact	absence of any slant in profile's zero-current baseline

allowing the study of the surface processes at Au electrodes to be made without the involvement of interfering influences from solution impurities or of corrosive attack on the Au surfaces.

iii) Cleaning Procedures

All glass apparatus used for the first time was soaked (inside and out) overnight in fresh concentrated CrO_3-H_2SO_4 solution. This was thoroughly rinsed away with doubly distilled water and replaced with fresh concentrated H_2SO_4 (Baker analyzed reagent grade).

When starting an experiment, the H_2SO_4 was poured away and the cell was immediately rinsed 10 - 12 times with pyrodistilled H_2O, filled with pyrodistilled water and then left to stand for approximately 20 minutes. After this, pyrodistilled water was boiled in the cell itself, often with several changes of pyrodistilled water. The cell was then rinsed thoroughly with the experimental solution and set up in a N_2 tent.

It was established early in the work that atmospheric exposure of the cell walls must be minimized. The electrodes received similar treatment, and were inserted in the cell for the pyrodistilled water steamings and were kept in the cell thereafter.

All volumetric glassware in which pyrodistilled water was collected and stored, and in which experimental

solutions were prepared, were subjected to similar pre-treatment, including multiple boilings of pyrodistilled water in situ. This was found to be necessary in order to leach adsorbed SO_4^{-2} from the walls of the glass, from which it is otherwise slowly desorbed building up concentration levels of SO_4^{-2} which are deleterious in some experiments, e.g. in pure aqueous $HClO_4$ solutions.

After an experiment, the solution was poured out and the cell immediately refilled with fresh concentrated H_2SO_4. The electrodes were removed and stored in fresh concentrated H_2SO_4, pyrodistilled water and the experimental solutions. In addition, the cleaning procedure was essential following each experiment, not only to maintain cleanliness, but also to eliminate the effects of extraneous anions.

Identical cleaning procedures were applied to the ancillary glassware used for preparing salts or solutions.

iv) Experimental Cells

After some experience was gained with cells of several different designs, it became apparent that a special cell would have to be fabricated which minimized the possibility of impurity effects. The cell and reference electrode system which was designed to achieve the ultimate experimental purity is shown in Figure 2-4, and was used subsequently in the bulk of the work.

The cumulative experience has been that substantially "cleaner" results can be obtained by simplifying the cell design as much as possible, so that glass surface area to solution volume ratio is minimized and contact between ground-glass joints and the

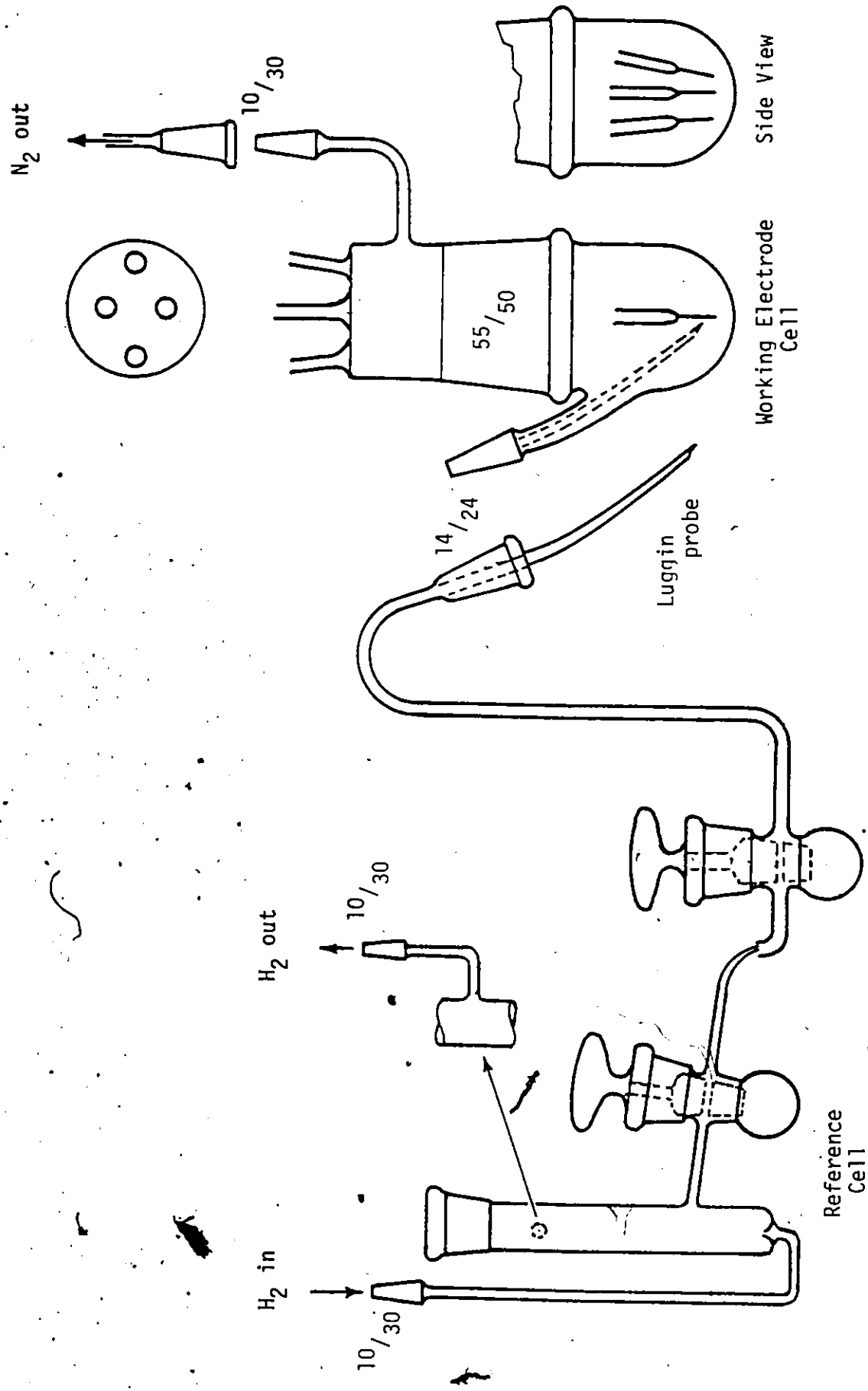

Figure 2-4 : Schematic designs and set-up of experimental cells

solution is avoided.

It was discovered at an early stage of this work that very low levels of SO_4^{-2}, which can still be leached from glass after previous cleaning of a cell with 98% H_2SO_4 even after multiple rinsing with pyrodistilled water, would lead to problems when oxide formation on Au in $HClO_4$ solutions was studied. The adsorption of the remaining traces of SO_4^{-2} ion was only eliminated by repetitive boiling of the cell and all other glassware in several changes of pyrodistilled water.

These procedures enabled it to be demonstrated that effects of SO_4^{-2} ions are important even at concentrations as low as 10^{-8}-10^{-7}M with regard to interference in oxide film deposition at Au from aqueous $HClO_4$ solutions.

Also, after the sensitivity of the system to all forms of impurities was appreciated, all work was conducted in a N_2—tent.

All solutions used were deoxygenated by bubbling a slow stream of purified N_2 (99.95% pure as supplied in cylinders) through them for 30 minutes. The N_2 gas was purified in a conventional gas train[176] which consisted of molecular sieves (BDH type 4A), dried $Mg(ClO_4)_2$ as desiccant, Cu turnings at 623K (periodically regenerated by heating in purified H_2) followed by three activated charcoal traps cooled by liquid N_2.

4. Solutions

The purest commercially available H_2SO_4 and $HClO_4$ (BDH AristaR grade) were employed, without further purification, to make up experimental solutions. The limits of impurities in

these acids are quoted as well below 1 ppm, and impurity effects in the solution were very rarely traced to the acid supply (note that the acid reagents are diluted by at least 50 times in making up experimental solutions).

The starting material for NaOH solutions was Fisher certified reagent grade electrolytic NaOH pellets (Na_2CO_3 = 0.42%). Alkaline solutions made up from NaOH, even after double recrystallizations from boiling saturated NaOH solutions, are difficult to obtain carbonate-free. $Ba(OH)_2$ (BDH AnalaR, analytical reagent as $Ba(OH)_2 \cdot 8H_2O$ with carbonate = 0.5%) rather than NaOH, was therefore used in order to depress the carbonate concentration, taking advantage of the low solubility product of $BaCO_3$ ($K_{sp}[BaCO_3] = 8.1 \times 10^{-9}$ at 298K). The $Ba(OH)_2$ was recrystallized twice from boiling, saturated pyrodistilled water under N_2 was stored under N_2. Test solutions were prepared under N_2 and were eventually boiled under N_2 before use.

Na_2CO_3 and $Na_2B_4O_7$, used in this work, were recrystallized twice from pyrodistilled water.

Temperature Control

The effects of solution temperature were studied by immersing the working compartment of the cell into a 10 liter water bath where the temperature was controlled to ± 0.5K by crushed ice or by a Haake E52 circulating water heater. The cell was arranged so that the reference electrode was inside the water bath, maintained at the same temperature as the working electrode. The form of i vs V profiles on Au is very sensitive to temperature,

probably due to temperature-dependence of anion adsorption.

5. Electrodes

Working, counter and internal reference electrodes were made from Au wires of 99.999% purity, using Johnson Matthey "Grade 1" Au. Appropriate lengths of these wires, of diameter 0.51 mm (0.020") were first degreased overnight in refluxing acetone in a Soxhlet extractor. After short lengths of Au were flame welded to much longer Ag electrical-contact wires, a droplet of (Pb-free) soft-glass was melted on to the Au wire and sealed into the end of a soft-glass tube, typically leaving 10 mm of Au wire protruding beyond the end of the tube. The Ag-Au contact was at least 2 cm above the glass seal. The soft glass had been previously cleaned in fresh concentrated chromic acid solution and rinsed thoroughly with pyrodistilled water. The degreased Au wires were handled only by means of cleaned platinum tipped forceps. The completed electrodes were washed and stored in fresh concentrated H_2SO_4.

Counter electrodes, and internal reference electrodes when required, were made of the same Au material also prepared in the manner described above for the test electrodes.

The use of large area Pt counter electrodes or Pt wire counter electrodes with Au working electrodes has been found[3] to cause contamination of the Au electrode with Pt[155,177], presumably because Pt is dissolved at the counter electrode and redeposited at the working electrode[120,178].

Reversible hydrogen electrodes (r.h.e.) were used as

reference electrodes throughout the work and all potentials are reported with respect to this electrode in the same solution and denoted by the scale "E_H". They consisted of tightly-folded layers of woven Pt gauze platinized according to the procedure of Feltham and Spiro[179]. Potentials were checked from time to time amongst several electrodes similarly prepared. Electrolytic H_2, further purified as described in refs. 55,176, was used for the H_2 reference electrodes.

Even though very small charges are associated with monolayer surface processes (typically 100 - 400 μC cm^{-2}), quite high currents can arise during potentiodynamic sweep experiments at sweep rates of the order of 0.5V s^{-1} and greater. This can introduce significant ohmic "iR" errors between the working electrode and the Luggin capillary of the Pt/H_2 reference electrode. In addition, the impedance associated with the reference electrode side tubing and stopcock are such that serious potential oscillations can result at elevated sweep rates. Errors associated with these effects at sweep rates > 0.2 V s^{-1} were avoided by using as a reference the potential of an "internal" Au electrode (in the cell) similar to the working electrode. This wire was placed as close to the working electrode as possible. The potential of this "floating" reference electrode remained constant to within ± 2 mV over periods of many minutes when a small amount of oxide (ca 1 - 1.5 monolayers) was first deposited on this electrode. The resulting "stable" potential occurs in the region of the natural rest potential (1.350 V) attributable to equilibria involving Au/Au_2O_3[7,180].

The potential scale for all current vs potential curves was calibrated from the sweep reversal potentials, (using the internal reference electrode potential) which were always measured against the external Pt/H_2 reference electrode.

6. Types of Potential Programs

Throughout this work, a variety of potential-time programs was employed. They were designed in response to an evolving understanding of the features of the oxide formation process, and what properties of these processes could be realistically measured and evaluated. Fortunately, the Tacussel function generator provides sufficient capability to construct complex programs enabling the surface processes to be studied at various sweep rates ranging from 0.0005 V s^{-1} to 1000 V s^{-1} within complex programs containing fixed potential holding periods ranging from 10^{-4}s to 10^{3}s or more.

The general types of potential-time programs used in this work, and how these programs permitted investigation of the different states of surface oxidation of Au after allowing them to be distinguished, are briefly summarized below. Additional information concerning individual experiments is presented with the relevant experimental data and discussions in chapters which follow.

a) The single or repetitive linear potentiodynamic sweep mode, Figure 2-5a, permits evaluation of the general features of the surface oxide formation and reduction processes in terms of resulting i vs V profiles which can be obtained over a wide range of sweep rates. The latter variation of conditions provides

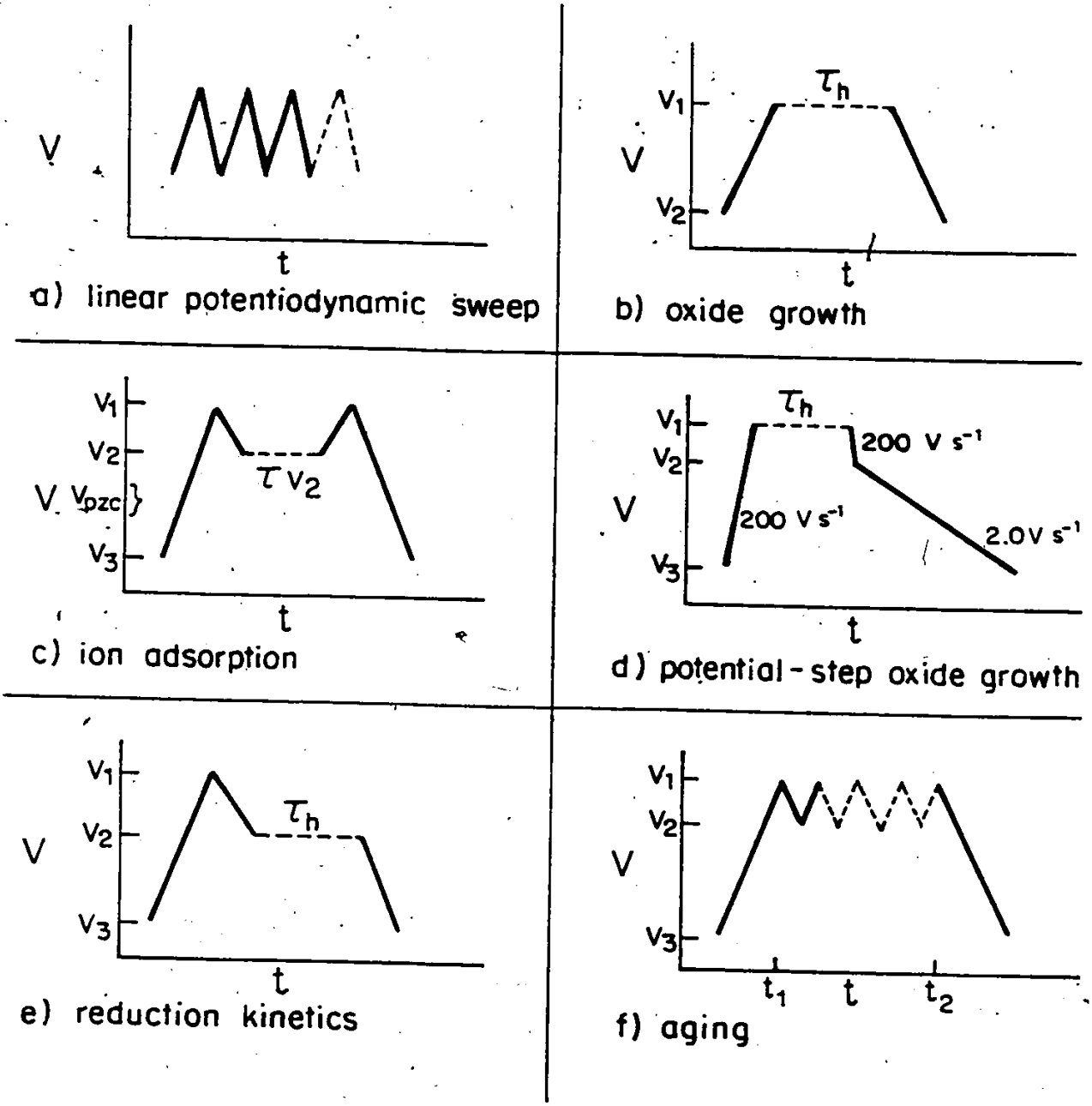

Figure 2-5 Potential-time programs employed in this work

information on the kinetics and reversibility of the processes involved.

b) The potential limit of a sweep (such as that shown in Figure 2-5a) may be maintained for controlled periods of time at suitable positive values in order to evaluate the kinetics and nature of oxide film growth at given fixed potentials as a function of time (Figure 2-5b). The charge associated with oxide growth during such "holding" experiments is determined from the subsequent cathodic sweep in which the oxide is reduced. The resulting information is used to construct isotherms and establish rate laws and kinetic equations which represent the experimental behavior.

c) The program of Figure 2-5c provides a means of following the effects of variable extents of adsorption of anions in the double-layer on the initial stages of surface oxidation of Au. By taking a cathodic sweep to various values V_2 and with various times (τ_{V_2}) of holding the potential constant at V_2 (where V_2 > potential of zero charge [p.z.c.] > V_3), the extent of anion adsorption can be varied and its effects in a subsequent anodic sweep taken to V_1 in the region where the initial stages of oxidation of the Au surface commence, can be sensitively followed. Thus, with or without a period of holding at the cathodic end-potential, V_2, the effect of not having crossed the p.z.c. during the cathodic sweep after oxide reduction during that sweep, and, thereby not having expelled anions from the double-layer in that cathodic sweep can be evaluated.

d) The potential-step type of "holding" program

(Figure 2-5d) was developed after the data of several experiments had been examined. Oxide growth is allowed to proceed for a controlled period of time at a suitable positive potential (V_1) and the charge associated with oxide growth under these conditons is measured in a relatively slow reduction sweep at 2.0 V s^{-1} over a potential range V_2 to V_3. The growth potential is approached very quickly in a rapid (200 V s^{-1}) initial anodic sweep in order to minimize the time spent during the sweep itself at oxidizing potentials, i.e. at potentials above that at which onset of oxide deposition occurs. Similarly, the initial section of the cathodic sweep is carried out very quickly (200 V s^{-1}) until potentials are reached at which the oxide begins to be reduced. This also minimizes any time spent in the cathodic sweep over a potential range where the oxide film can continue to grow before electrochemical reduction commences, viz. where the current signal crosses the zero current line.

e) The program of Figure 2-5e allows evaluation of the kinetics of oxide reduction (as opposed to those of oxide formation measured by 2-5d) through the use of a program which permits the formation of oxide at any appropriate sweep rate up to any appropriate anodic end potential, V_1. The oxide thus formed is reduced to varying degrees in a subsequent cathodic sweep taken up to some (variable) potential at which reduction of oxide becomes observable. Maintenance of such potentials (V_2) for controlled periods of time allows the kinetics of oxide reduction to be evaluated at constant potential as a function of that potential.

Under optimal conditions, the kinetics of changes of individual states of the oxide film corresponding to resolved peaks in the i vs V profile for the reduction of the film are resolvable.

f) The program of Figure 2-5f allows the effects of aging of the oxide to be evaluated. After the formation of the oxide film under suitable (variable but controlled) conditions at a potential V_1, partial reduction of some (variable) amount of that oxide occurs in the potential range V_1 to V_2, followed by re-oxidation from V_2 to V_1. This partial reduction and subsequent re-oxidation is allowed to take place a controlled number of times. Then when the total oxide is finally reduced (after t_2) a very different i vs V profile is obtained than would have resulted from reduction after t_1. Under these conditions, the growth of oxide is observed while some initial surface oxide already exists on the electrode and serves as a basis for continued oxide growth. It is found that under conditions in which the final i vs V reduction profile (after t_2) is different from the initial one (obtainable at t_1) a hysteresis effect is involved in which the first portion of oxide removed in reduction down to some residual oxide coverage Θ_2 is not identical with that oxide deposited in the return anodic sweep back to V_1. An aging of the oxide is induced, in which oxide growth and reduction proceed quite differently and apparently in a preferred manner.

7. Determination of Actual Surface Area of the Au Electrodes and Their Coverage by O Species

Owing to the variable surface roughness at most electrodes,

it is not practical to estimate real areas from geometric areas. Real areas of Pt electrodes are, however, easily calculated from the measurable accommodation for electrodeposited H[181,182] in a monolayer but this method is not applicable to Au.

The corresponding charge required to deposit a monovalent ion on every surface atom on a polycrystalline Au electrode (200 μC cm^{-2}) could be obtained by multiplying this figure by the ratio of the squares of the atomic radii of Au and Pt. Because of the absence of an "internal" standard for Au electrodes based on H accommodation, a means of evaluating electrode areas from the discharge of O species must be utilized.

The real areas of Au electrodes were determined according to the method of Michri, Pshchenichnikov and Burshtein[183] who found that the oxidation charge below the potential of the well-defined current minimum (designated Q_B) immediately preceding O_2 evolution in 0.5 M H_2SO_4 was 400 μC per real cm^2 which is assumed[183] to correspond to deposition of a monolayer of O species.

These authors obtained calibration data for the Au electrode areas by means of B.E.T. measurements. Their conclusion about the charge for monolayer oxidation by O species was shown to be valid over a wide range of temperatures and sweep rates, and has been verified by recent work in this laboratory[3]. Although this method was developed for use in aq. H_2SO_4, it appears to have general application to oxide formation on Au in various media where a current minimum, apparently corresponding to monolayer oxide coverage, is always observed immediately preceding the

potential at which O_2 evolution currents are observable.

Thus, oxide coverages and electrode areas can be calculated from graphical integration (weighing fine paper: accuracy ± 1%) of the i vs V profiles, setting Q_B = 400 μC cm^{-2} (corresponding to one monolayer of oxide counted as a 2-electron O species). Double-layer charging currents were subtracted on the basis that they would be approximately the same on the O-covered surface as on bare Au.

CHAPTER 3

RESULTS AND DISCUSSION

General Features of i vs V Profiles for Deposition and Reduction of O Species on Au

The stages of formation of an oxide monolayer on Au or other noble metals, which are distinguishable in potentiodynamic sweep experiments, vary considerably depending on the type of electrolyte in which the oxidation is carried out, especially when different anions are present. Both temperature and rates of potential change in a sweep experiment have dramatic effects on the i vs V profiles observed. Also, the value of the potential of zero charge usually has a smaller, though quite striking effect.

In a general way, the structure observed in the i vs V profiles for cathodic sweeps taken from polarization to a given anodic potential, V_A, giving rise to surface oxide reduction, provides an indication of the state(s) of oxidation of the surface achieved in the previous anodic sweep up to V_A. This relationship cannot be treated rigorously, however, due to the varying irreversibility of various states of oxidation of the surface that are observed.

From the kinetic and mechanistic point of view, the general form of i vs V profiles in cyclic-voltammetry of electrode surface processes such as monolayer oxidation of Au depends on a) whether 1 or 2 electrons per adsorbed particle are transferred; b) whether, in the resulting ad-layer, lateral repulsions or attractions in the 2-dimensional lattice are significant; c) whether the process, at a given sweep rate, behaves in a kinetically reversible way or not; d) whether the formation or reduction of a two-dimensional surface film proceeds by a mechanism of nucleation and growth (nucleation of holes in reduction) and e) whether 2 or more consecutive steps are involved in the surface process, e.g. deposition by electron transfer

coupled with a lattice rearrangement step; if so, then the rate constants of these steps, relative to one another and to s, determine the shapes of the i vs V profiles.

Diagnostic criteria for most of these effects were worked out quantitatively by computer simulation by Klinger[184] in a previous thesis from this laboratory. A summary of his findings is given in Literature Table 1 (see below) for such quantities as the half-width $\Delta V_{1/2}$, of i vs V profiles (giving the lateral interaction parameter, g, in a Frumkin-type isotherm[159]) the coverage, Θ_p, at the capacitance peak, C_p, and the change of C_p (measured as i/s) with sweep rate as the process changes from a condition of kinetic reversibility to irreversibility as $s > s_o$, the limiting maximum sweep rate for which the process just remains reversible.

Literature Table 1

Characteristic Quantities for Reaction M+A $\rightleftharpoons$ MB+e (g=o for The Adsorbed Layer of B) Under Potential-Sweep Conditions

Parameters	$C_p(=i_p/s)$ (Farad cm^{-2})	$\Delta V_{1/2}$ (V)	$\Theta_{B,P}$	$dV_p/d \log \frac{s}{k}$ (V)
Value for reversible conditions	2.14×10^{-3}	0.091	0.50	0
Value for irreversible conditions	1.57×10^{-3}	0.126	0.63	0.118

Simulated types of behavior of a le surface process coupled with a chemical (potential-independent step) were also derived; these calculations show how peak shapes and peak heights change with increasing s for a 2-step reaction in relation to the behavior of a 1 step reaction. These differences of behavior can be identified experimentally quite easily. Examples of the simulated behavior for the two main types of cases are shown in Literature

Figures 1 and 2.

In the present work, these results are important since a) lateral interactions (the g factor[159]) and b) 2-step chemical-electrochemical (or vice versa) reaction sequences are likely to be involved in surface oxidation of Au, e.g. where lattice rearrangement of deposited O species is coupled with the electron transfer and O atom deposition (or desorption) steps. The diagnostic criteria of various kinds will therefore be referred to in a number of places in the ensuing discussion in this and other chapters which follow.

1. Kinetic Irreversibility in the Experimental Behavior at Au

Usually the electrochemical surface reactions observed on noble metals in the oxidation direction of potentiodynamic sweeps are found to be rapid, i.e. the processes have large anodic rate constants or reversibility parameters, s_o[185]. However, a fundamental feature of the i vs V profiles for Au is their "kinetic irreversibility".

Figure 3-1 illustrates this feature of the behavior of Au electrodes in a saturated $Ba(OH)_2$ solution. The sweep rate has been steadily diminished from 0.050 V s^{-1} down to 0.0005 V s^{-1} (0.5 mV s^{-1}) which is approximately the lower limit of sweep rate at which i vs V profiles may be practically recorded.

Even in the best, practically attainable, clean solution, the two predominant features of kinetic irreversibility are apparent;

a) the peak potentials for both the oxidation and reduction are not independent of sweep rate, i.e. the oxide formation process (for example) is still occurring at a significant overvoltage (low s_o), and

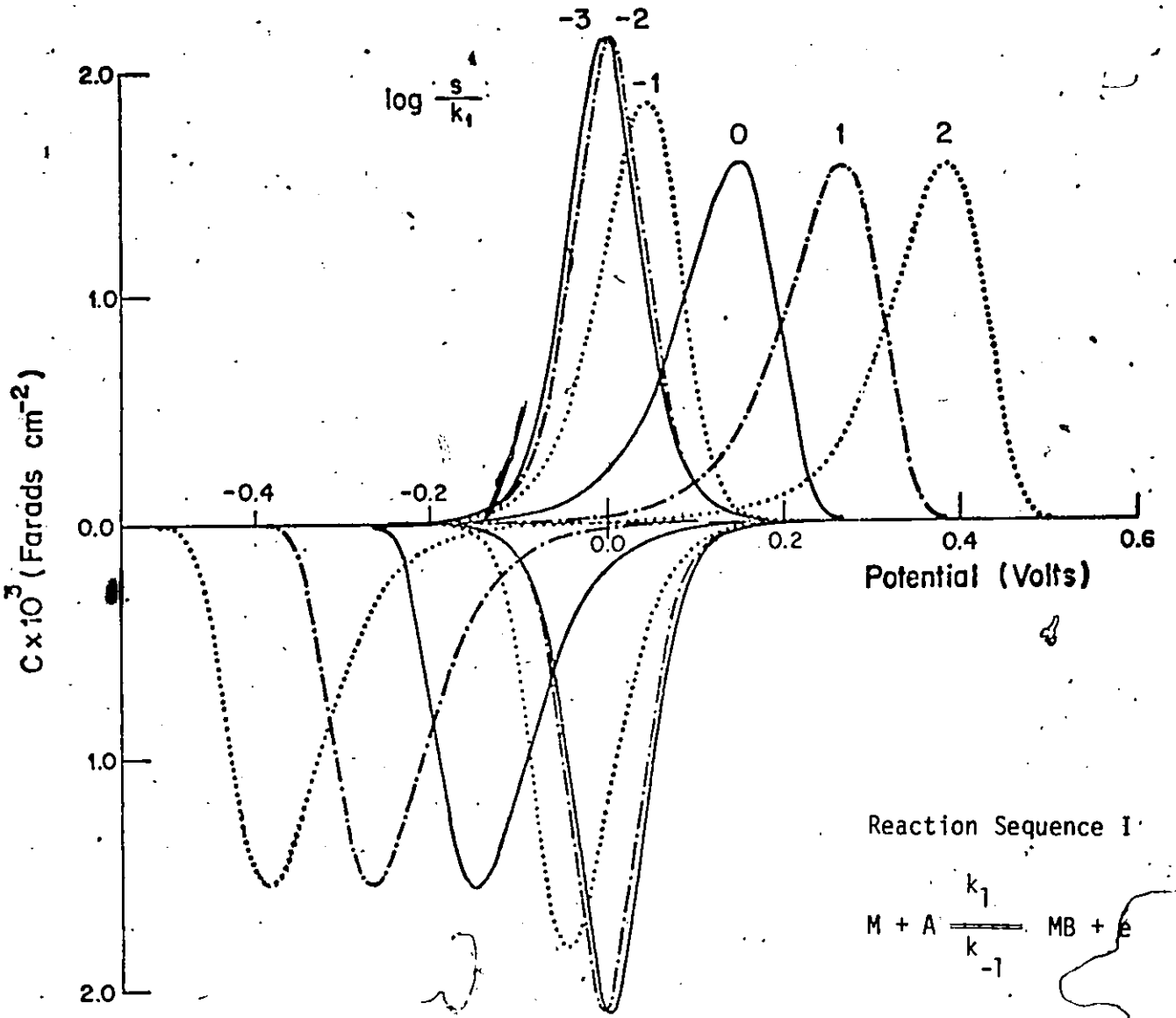

Reaction Sequence I

$$M + A \underset{k_{-1}}{\overset{k_1}{\rightleftharpoons}} MB + e$$

Literature Figure 1 Anodic and cathodic C-V profiles for the 1-e surface reaction (I) for various s/k_1 values showing progression from reversible to irreversible behaviour

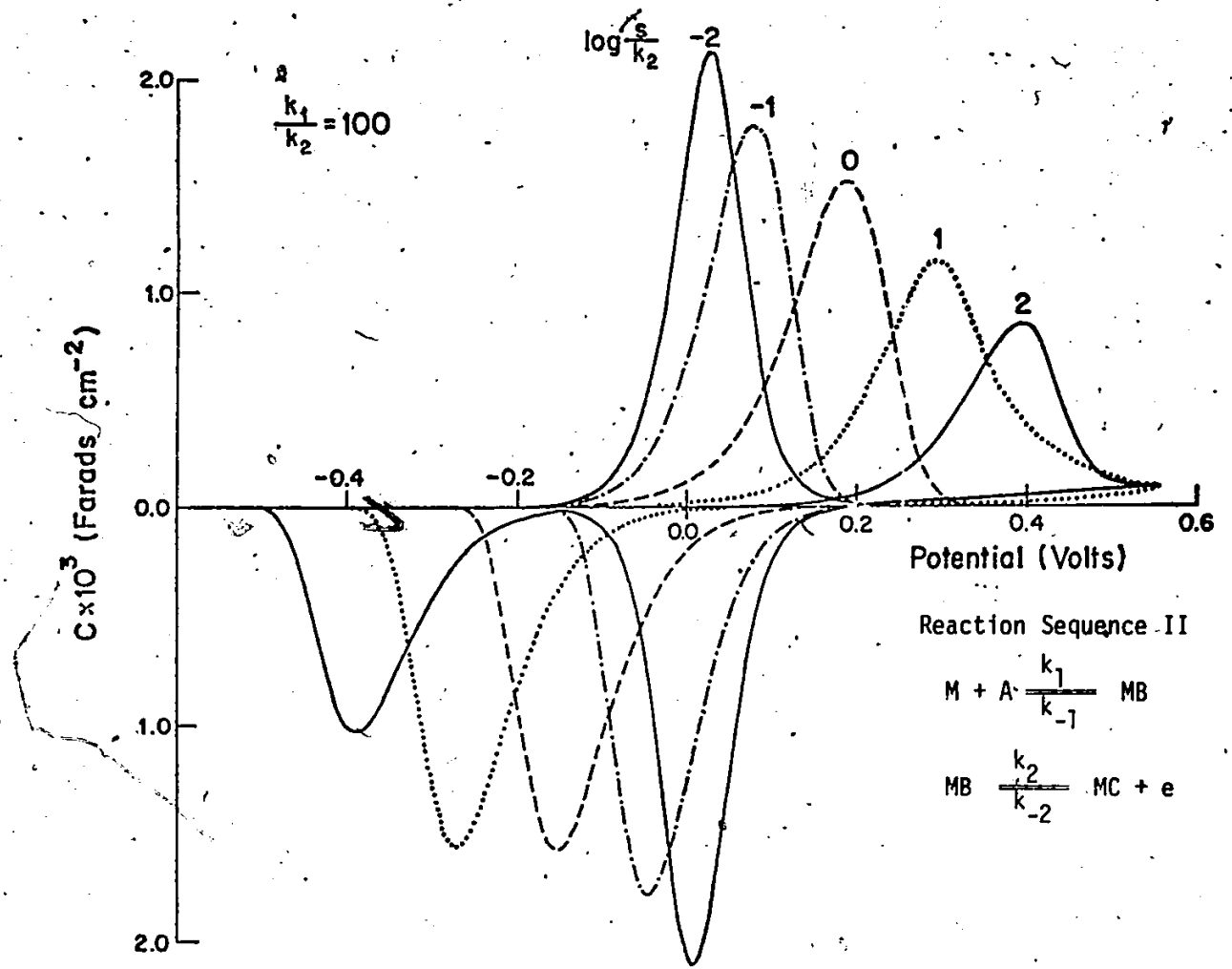

Literature Figure 2 Anodic and cathodic C vs V profiles for reaction sequence (II) for various s/k_2 values showing change from reversible to irreversible behavior of step [2] for k_1/k_2 ratios = 10^2

- 59 -

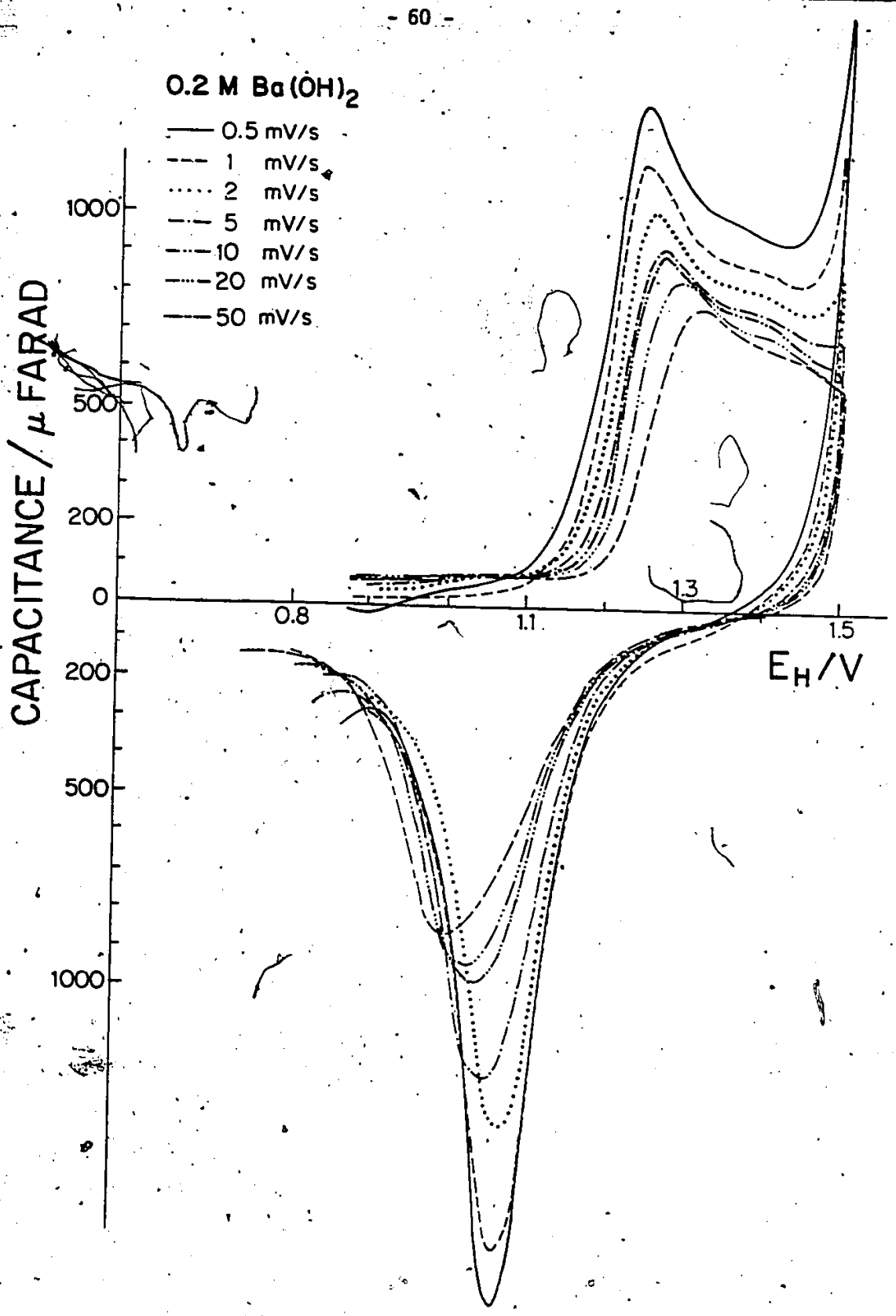

Figure 3-1 Potentiodynamic current-potential profiles at Au involving a series of sweep rates in 0.2 M $Ba(OH)_2$; T = 298 K.

b) even at the slowest sweep rates employed, the charge required for oxide film formation does not become independent of sweep rate.

Slow processes are therefore occurring as they do at Pt. Also

c) even at the slowest sweep rates that are practically usable, the anodic i vs V profile is not, and does not approach, a mirror image of the cathodic i vs V profile as would arise[130] if the processes were reversible. This is probably because the anodic and cathodic pathways of the reaction are not simply the reverse of one another and an irreversible change of state associated with place-exchange of the system occurs after the O species have been electrodeposited.

2. Features of i vs V Profiles for Au in Various Electrolytes

In order to discuss the effects of ion adsorption on surface oxidation processes at gold or other noble methods, and eventually to consider the kinetics and mechanisms of these surface processes, it will be necessary to illustrate a series of i vs V profiles recorded in several different media.

Regardless of the nature of the cations or anions of the electrolyte in which the surface oxide formation and reduction is carried out, some important general features of the resulting i vs V profiles are common; in particular, a number of distinct peaks corresponding to distinguishable states of the film are apparent in the oxide formation and especially in the subsequent reduction of the oxide films. These states are most easily observed when only submonolayer oxides are formed and reduced. Some similar features

arise in each medium and the behavior can be considered as generally representative of the initial stages of formation and reduction of oxide films on Au in all the media. The ions of different electrolytes exert, however, specific secondary effects, significantly shifting the potentials of the generally observed different states of oxidation according to the strength of adsorption of the ions.

It will be shown that the general features of i vs V profiles are determined by:

a) the competition between the onset of surface oxidation and potential-dependent anion adsorption;

b) the potential at which this commencement of surface oxidation occurs;

c) the specific adsorption tendency of the ions (which also depends on potential)

and, at a later stage in the oxidation process,

d) the influence of these ions on the kinetics of any post-electrochemical reactions, such as rearrangement of the O/Au sub-monolayer lattice or place exchange which occurs between Au atoms and deposited OH and O species, leading to their stabilization.

In what follows, stages of oxide monolayer formation and reduction which can be distinguished in several media (acid and alkaline), will be discussed. Special attention will be given to the effects of ion adsorption/desorption on

a) the onset of oxide film formation,

b) the influence of these ions and other conditions on the kinetics of any post-electrochemical surface reactions and on

the observed development of several distinguishable stages of reduction of the film and

c) on the hysteresis observed between oxide formation and reduction.

i) Effects of Traces of Sulfate Ion

In early experiments, the effects of anions were investigated in a series of $HClO_4$ solutions in which the ClO_4^- anion concentration was varied from 10^{-3}M up to 1M (10^{-3}M, 10^{-2}M, 0.1M, 1.0M). It was discovered that the initial oxidation peak could be made to appear at potentials approximately 50 mV less anodic than in early experiments in which the role of traces of SO_4^{-2} had not, at that time been appreciated (see below). The results of these experiments showed that even after the usual elaborate procedures of rinsing cell glasses prior to each experiment, traces of sulfate (from the H_2SO_4 cleaning solution) were evidently leached from the walls of the cell over periods of time of 24 hours or more. Furthermore, it was found that these traces of sulfate, which is more strongly adsorbed on Au than perchlorate[2], were sufficient to displace the initial stage of oxide deposition positively by 50 mV when present in concentrations as low as $10^{-7} \sim 10^{-8}$M.

Figure 3-2 shows the effects of traces of SO_4^{-2} on the i vs V profiles for formation and reduction of the oxide film on Au in 0.1 M $HClO_4$. The series of curves in this figure show the remarkable sensitivity of the Au electrode to effects of traces of SO_4^{-2} (or HSO_4^-) ion on the potential for onset of surface oxidation. The solid line curve of Figure 3-2 is obtained in $HClO_4$ solution whenever SO_4^{-2} is present in concentrations exceeding ca 10^{-8}M.

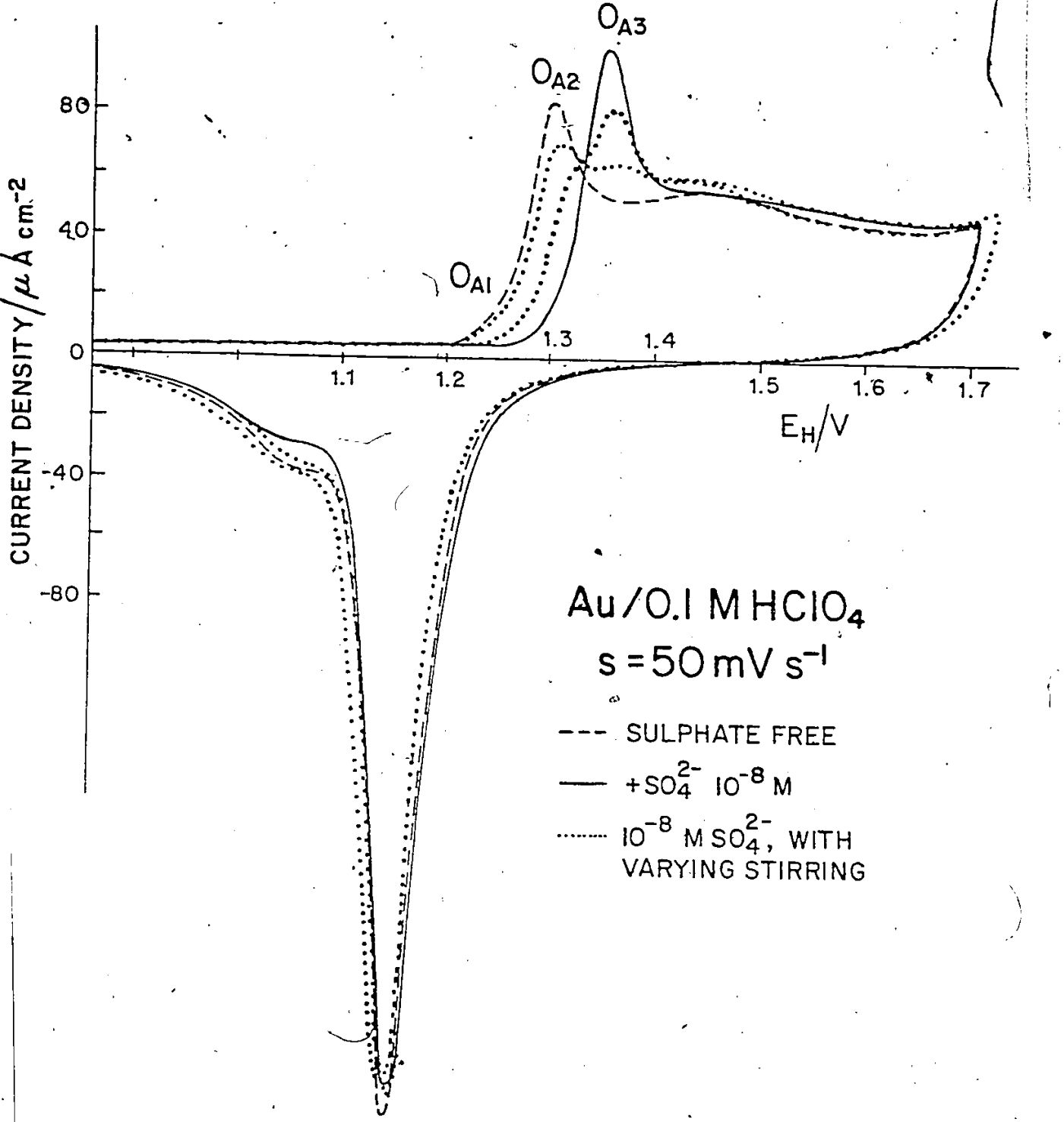

Figure 3-2 Potentiodynamic current-potential profiles for Au in 0.1 M $HClO_4$ at 0.050 V s^{-1} in sulfate-free solution and with traces of SO_4^{2-} ions present; T = 298 K

Under these conditions, the initial stage of depositon of O species has a peak potential of 1.350V E_H.

The dashed line profile shows the behavior observed when the special steps described in the experimental section are introduced in order to reduce the level of SO_4^{-2} remaining residually after acid cleaning treatment of the cell and solution containing vessels. Under these conditons the first stage of oxide deposition has a peak potential (O_{A2}) of 1.300 V vs H_2/Pt.

The dotted curves in Figure 3-2 represent characteristic transitional profiles which are observed when adventitious quantities of SO_4^{-2}, although still very small, are high enough to effect a partial blocking of oxide deposition, dependent on stirring conditions. In the presence of SO_4^{-2}, the almost reversible stage O_{A1} is suppressed.

An important observation was that profiles of this type could be transformed into profiles of the dashed-line type characteristic of a cleaner solution, when e.g. reduction of the agitation rate, use of boiling water procedures for cell cleaning, or replacement of the experimental solution with fresh stock solution after overnight soaking of the cell with the given experimental solution. The latter two procedures facilitate leaching and removal of SO_4^{-2} from the glassware.

Additions of H_2SO_4 in trace quantities to $HClO_4$ solutions of known purity produced profiles of the solid-line type (Fig. 3-2) and established the lower concentration level for the SO_4^{-2} effect as approximately 10^{-7} to 10^{-8}M.

The effects of traces of SO_4^{-2} at Au as shown in Figure 3-2 have a fundamental bearing on the significance of multiple-state deposition of oxygen species. It is seen in the figure that increasing concentration of sulfate species causes the first peak, O_{A2}, to be lowered but increases, by an equivalent quantity, the O species deposited in the next peak O_{A3}, but without a concomitant change in the respective peak potentials. Thus, there is not a progressive displacement of the peak to more positive potentials, as might be expected, but an apparent "interchange" of material between two states. Indeed, this is demonstrated by the appearance of an "isosbestic" (isopotential) point. Very similar behavior is found in the effects of small concentrations of halide ions[186] or in the presence of ClO_4^- anions, adsorbed or desorbed by a negative potential excursion, on the redistribution of H amongst the 4 or 5 chemisorption states observed[187,188] in clean dilute solutions at Pt.

This result emphasizes the importance of ions in determining the potentials at which the early stages of oxide deposition are observed. Thus, the rigorous experimental procedures used in this work and the resulting new levels of purity attained, allow study of these surface processes at solution purity levels not previously possible nor thought to be important for the complete understanding of the system. On the contrary, at Au, the present work shows that the presence of certain trace ionic impurities can give rise to seriously misleading behavior.

3. General Characteristics of the i vs V Profiles

The general features of the current-potential profiles

for electrodeposition of O-species (see Chapters 4, 5 and 8 for reasons why "O" rather than "OH" species are considered) on Au from 0.05 M H_2SO_4 and 0.1 M $HClO_4$, 0.1 M Na_2CO_3 & 0.024 M $Na_2B_4O_7$ are shown in Figures 3-3 and 3-4. In each of these diagrams, a family of i vs V profiles has been generated in which the end potential of the anodic sweep has been increased progressively to more positive values in successive sweeps. In this way, the evolution of the distribution of peaks (or states of surface oxidation) is followed as a function of coverage for the given experimental conditions of sweep rate and temperature.

The hysteresis between formation and reduction of oxide species is a familiar and striking feature of the behavior and is accentuated by the strong adsorption of anions. Equivalent quantities of oxide are reduced at only much less positive potentials than those at which the oxide is formed. In addition, it is evident from the coverage vs potential plot of Figure 3-3 and from the shape of the i vs V profile in Figure 3-4, that oxide coverage does not increase linearly with increasing potential even though oxide is formed over a relatively broad range of potentials, but rather several stages of oxide formation contribute charge over different distinct potential ranges.

Although the onset of oxidation in sulfuric acid solutions occurs at potentials ca 50 mV more positive than in perchloric acid solutions, and although potential changes depend systematically on sweep rates and temperatures employed, various surface bonding states of O-species on Au are easily recognized and resolved in the i vs V

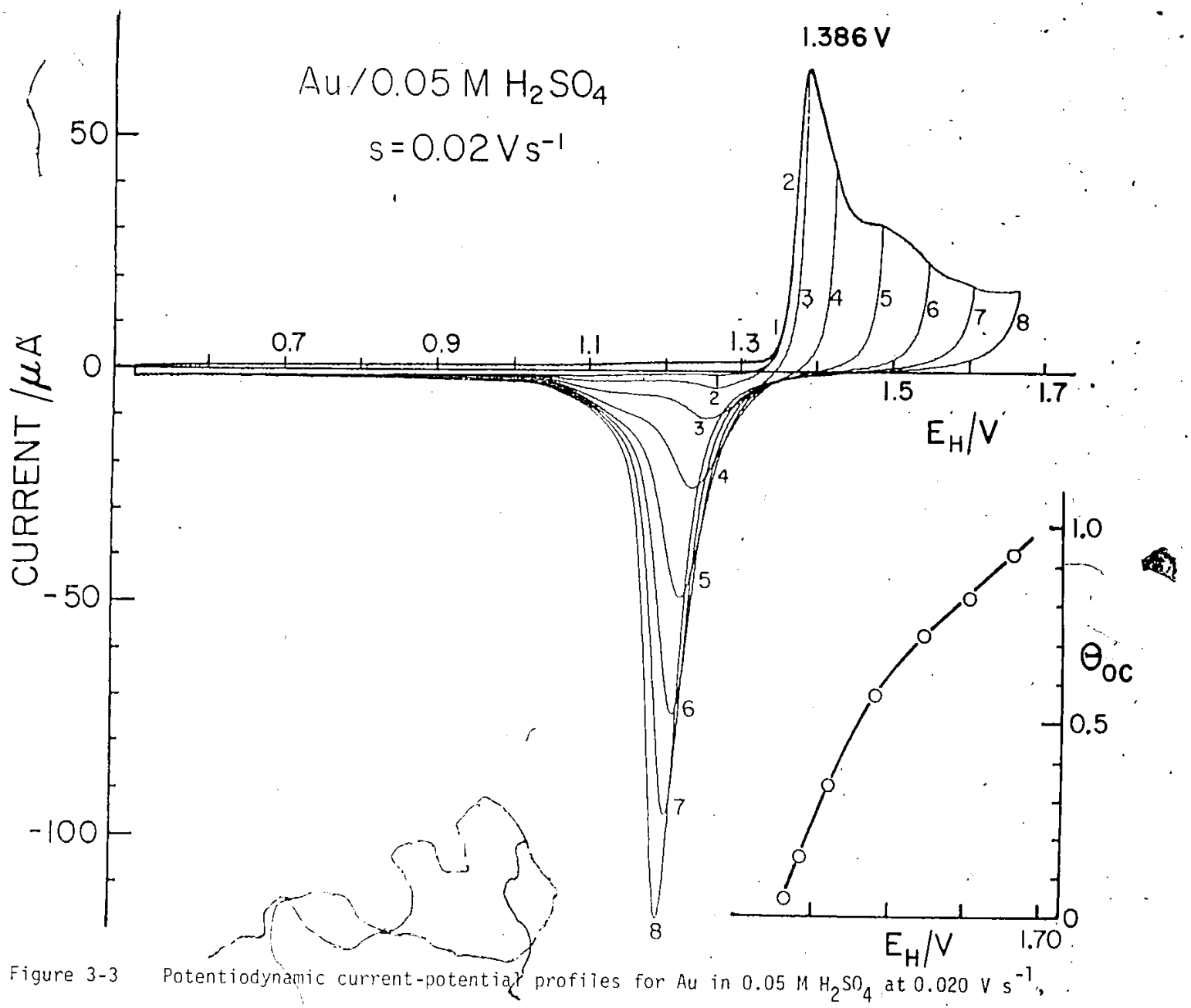

Figure 3-3 Potentiodynamic current-potential profiles for Au in 0.05 M H_2SO_4 at 0.020 V s^{-1}, 298 K taken to a series of anodic end potentials

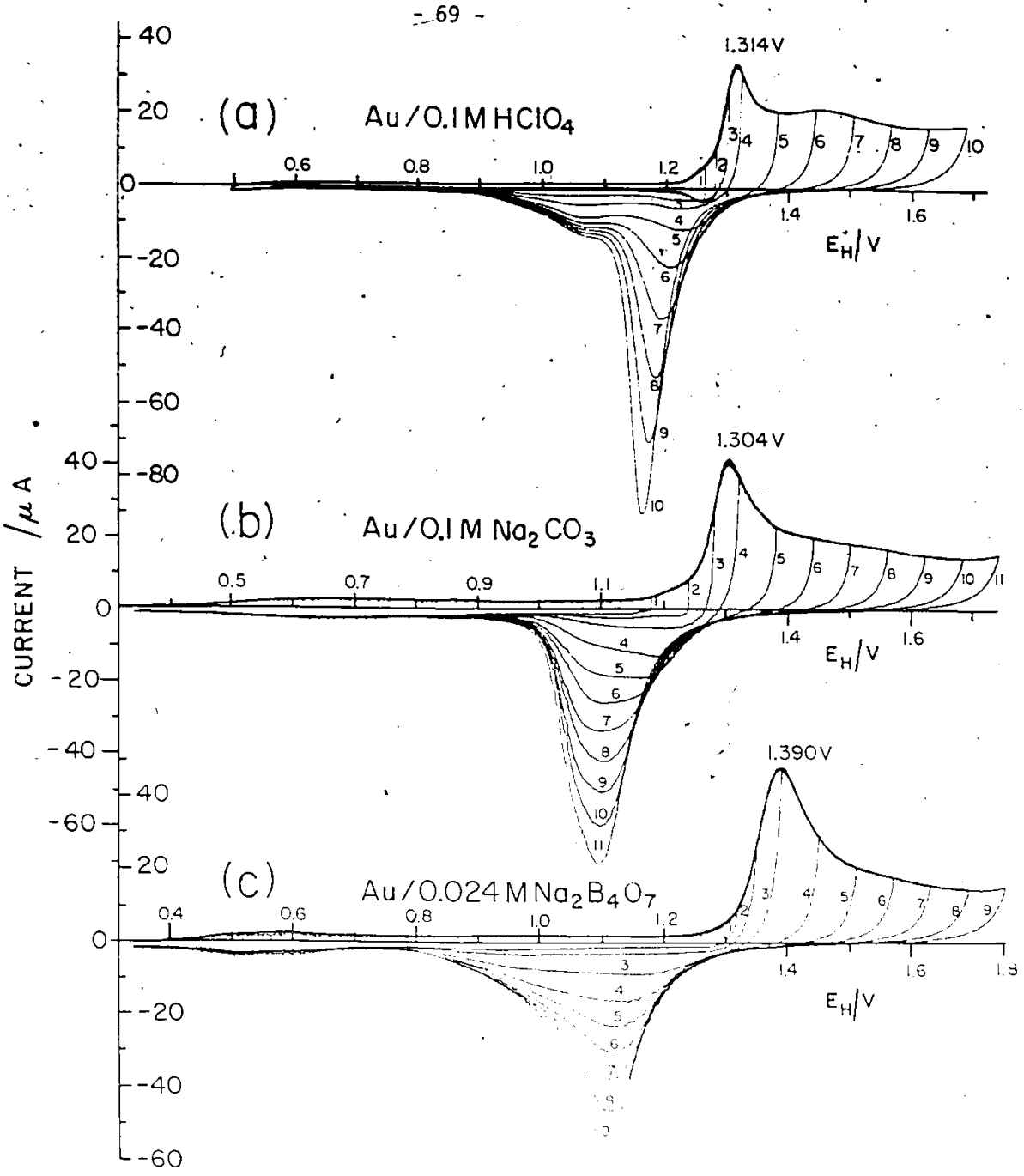

Figure 3-4 Potentiodynamic current-potential profiles for Au at 0.050 V s^{-1}, 298 K taken to a series of anodic end potentials in (a) 0.1 M $HClO_4$ (b) 0.1 M Na_2CO_3 and (c) 0.024 M $Na_2B_4O_7$

profiles for the various solutions studied.

For these reasons, and to simplify greatly discussions of these properties, simple designations for each of the distinct peaks observed will be introduced. The abbreviations O_{C1}, O_{C2}, O_{C2}', etc, designate states of deposited O-species resolved in terms of their reduction in the cathodic sweep. Similarly, O_{A1}, O_{A2}, etc., are used to designate the corresponding states which can be distinguished in the anodic sweep. The numeric subscript represents the order of appearance of these distinguishable states as the potential limit in the anodic sweep, and simultaneously the oxide coverage is increased. It is important to note that all these states which are resolved correspond to coverages of oxygen species (taken as O) less than a monolayer.

Much evidence indicates that the variety of stages of surface oxidation resolvable on Au is greater than on the other noble metals[129]. Figure 3-5 illustrates i vs V profiles which show good resolution of the submonolayer stages of oxide film growth referred to above. Comparison of these four profiles shows the electrochemical behavior of these states for quite different conditions of oxide coverage and relative contribution of the state in the overall deposit.

The successive distinguishable stages of oxide film growth are exemplified in Figure 3-5a-d:

i) (Figure 3-5a) States O_{C1}, O_{C1}', (and O_{A1}) appear first. The current peaks corresponding to these states refer to a first formed, reversible stage of surface oxidation; in 0.5 M H_2SO_4 and

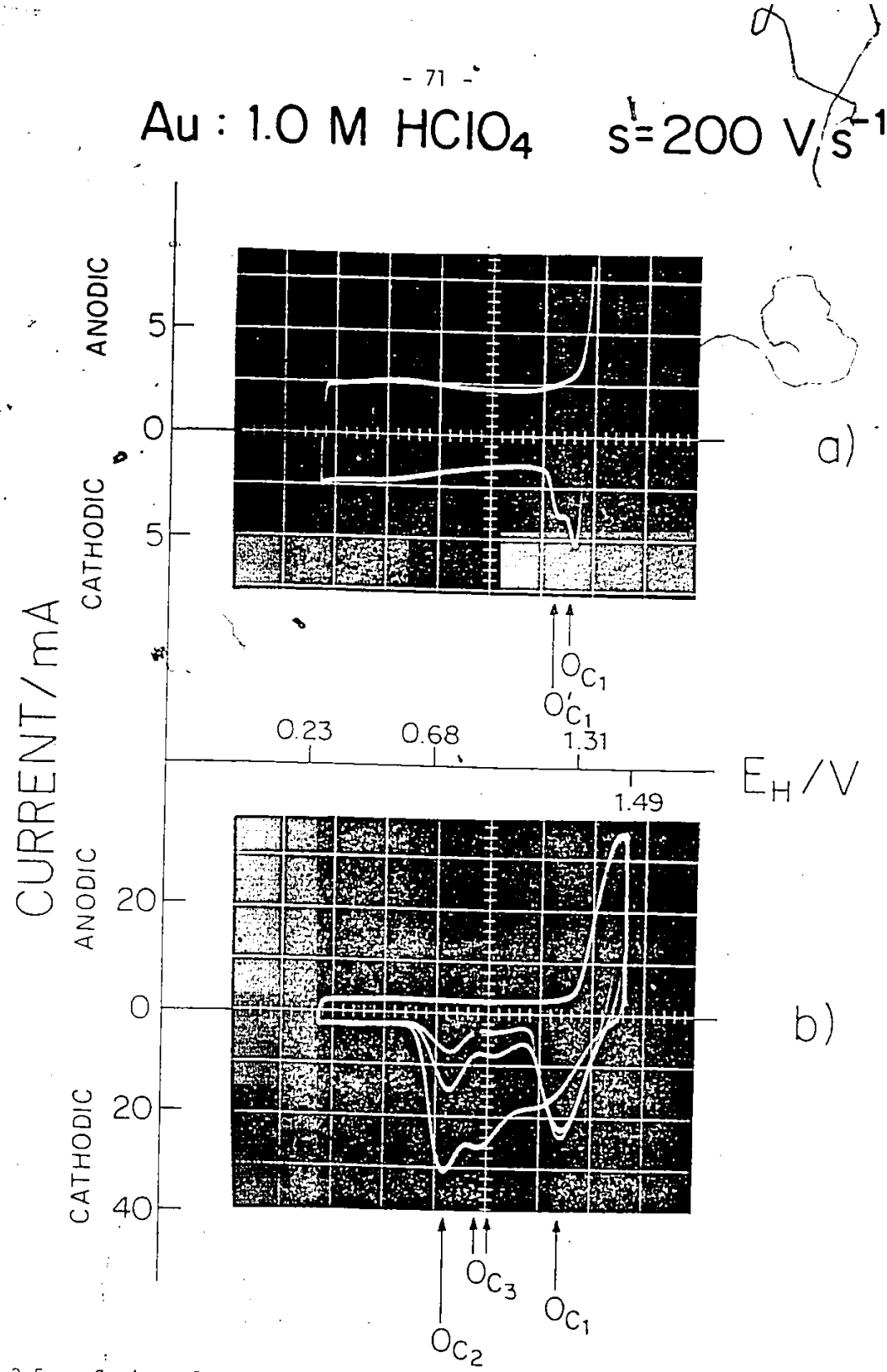

Figure 3-5 Series of potentiodynamic current-potential profiles for Au in 0.1 M $HClO_4$ showing development of several current peaks for reduction of submonolayer coverages of oxide; 293 K (a) reversible reduction in O_{C1} at 200 V s^{-1} (b) growth of oxide at constant potential of 1.49 V for 10^{-4}, 10^{-3}, 10^{-2} s; s = 200 V s^{-1}

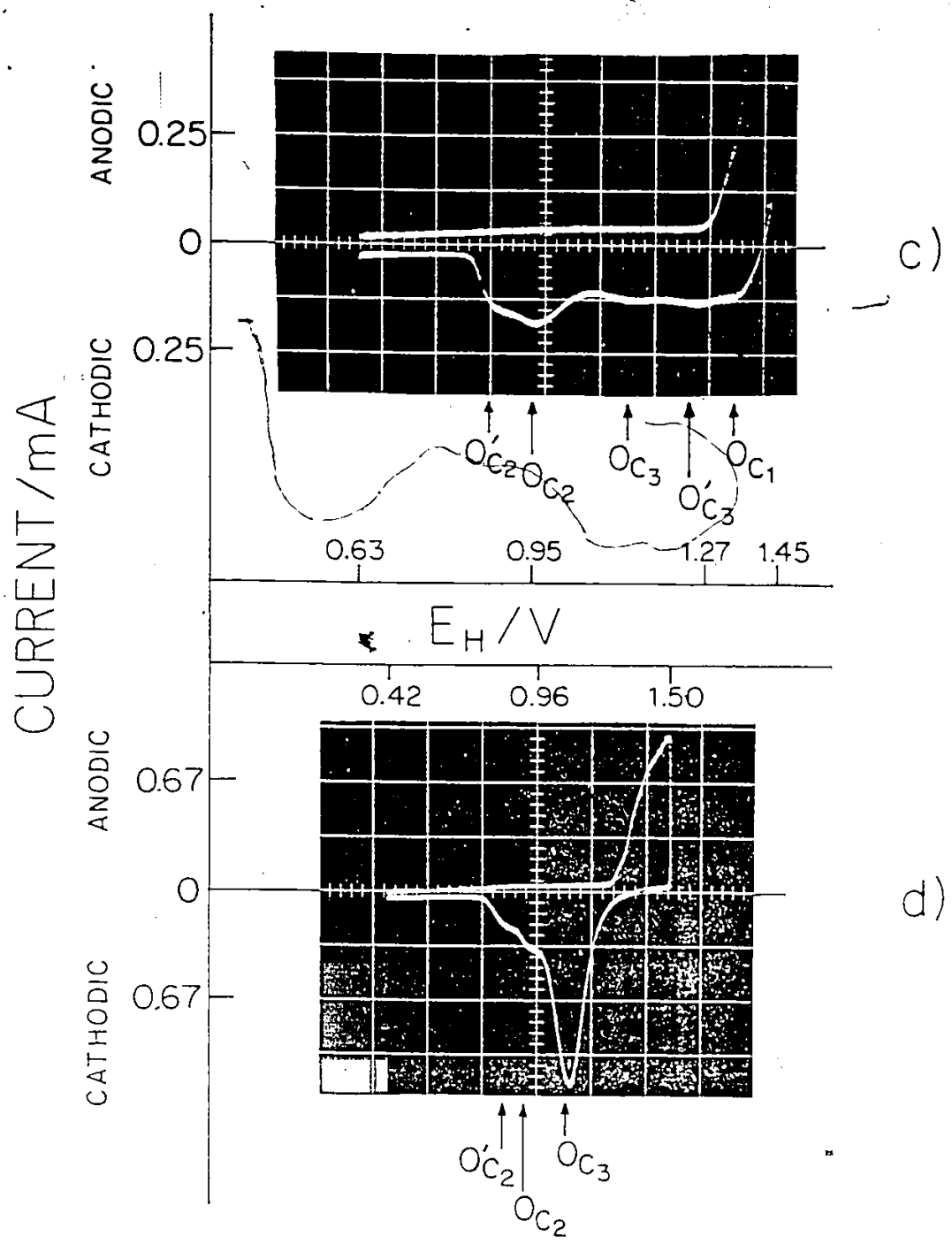

Figure 3-5 Series of potentiodynamic current-potential profiles for Au in 0.1 M $HClO_4$ showing development of several current peaks for reduction of submonolayer coverages of oxide; 293 K (c) s = 20 V s^{-1} (d) growth of oxide at constant potential of 1.50 V for 10 s, s = 2.0 V s^{-1}

1.0 M $HClO_4$ these states are distinguishable only at low coverages and high sweep rates.

In slow sweeps, the O_{A1}/O_{C1} state is only observed in solutions of relatively weakly adsorbed anions as e.g. in 0.1 M $HClO_4$ (Figure 3-4a) or in very dilute solutions of other salts. In H_2SO_4 solutions, the initial stage has a much smaller charge and can be resolved only in very fast sweeps (ca 10 V s^{-1}). This indicates that strongly adsorbed anions (e.g. SO_4^{-2}) increase the rate of the post-electrochemical process of place-exchange as suggested by the earlier (in terms of coverage) appearance of the peaks formed after O_{C1} (i.e. O_{C2}, O_{C3}, e.g. see Figure 3-5b).

Studies in more dilute solutions (10^{-2} M and 10^{-3} M $HClO_4$) have verified that these current peaks correspond to development of the surface oxide in states of low coverage, < 0.1 monolayer. However, in these dilute solutions, it is possible to observe these peaks at sweep rates that are orders of magnitude lower than those required for resolution of these states in the more concentrated solutions, for which it appears that these states are not observed or are prevented from being distinguished by the presence of anions adsorbed at the higher concentrations of electrolyte. Extremely high sweep rates are required to "catch" the O_{C1} process, i.e., for it to be manifested as a resolvable peak.

This is a result of anion adsorption effects in electrolytes at moderate concentrations. Such effects can be circumvented by use of electrolyte solutions several orders of magnitude more dilute. Then sweep rates correspondingly lower in magnitude can be used for examining the influence of the anions on the oxide formation and

reduction processes. In this way, O_{C1} peaks may be observed in these dilute solutions at sweep rates which are orders of magnitude lower than in the more concentrated solutions. In such dilute solutions, the total or saturation coverage of oxide species corresponding to O_{C1} is not changed by more than 20%, compared with its coverage in the stronger solutions. This fact must be taken, in conjunction with the sweep rate effect described above, as evidence that this state is not sensitive to the anion environment (i.e. concentration), but, rather, is affected by the rate (or more properly, the pseudo-equilibrium established) at which adsorotion of anions is re-established in the inner layer after they have been expelled in the previous cathodic sweep taken to potentials more negative than the p.z.c. (see section on Ion Effects).

The first cathodic peak observed, O_{C1}, corresponds to an almost reversible reduction of the first species formed anodically, O_{A1} (see Figure 3-5a). It is only observed, however, if the anodic sweep is allowed to generate only a small degree of surface oxidation (O_{A1} state) (Figure 3-4a, curves 1, 2) and if the experimental conditions (high sweep rate, low temperatures) are such as to render and "post-electrochemical" rearrangement steps or ion adsorption/desorption processes slow in the time-scale of the anodic and cathodic sweeps over this region of the potential range (cf. the similar situation with Pt[20]). As with Pt, this initial process involves deposition and reduction of electrodeposited O (and possibly some OH) species that remain in a chemisorbed state (unrearranged) on the metal surface in some array of minimum energy (cf. ref. 20) in the presence of co-adsorbed anions.

Depending on the environment of the electrodeposited species with respect to co-adsorbed anions, the potential of the redox process O_{A1}/O_{C1} on Au varies. It is about 150 mV more positive in 0.5 M H_2SO_4 than in 0.1 M Na_2CO_3. The charges of specifically adsorbed anions in the inner region of the double-layer make the very first stage of surface oxidation energetically more difficult due to repulsive interactions which such deposited OH or O species would experience with the adsorbed anions (Figure 3-6).

ii) (Figure 3-5b) An increase in the positive end-potential in the anodic sweep, or with anodic holding at potentials where only the O_{C1} peak (and its satellite - see below) is observed, causes the appearance of the O_{C2} and O_{C2}' peaks (Figure 3-5b). The experimental behavior shows that a critical saturation level exists for deposition of O-species into the O_{C1} and O_{C1}' (Figure 3-5a) states (which may be different at different potentials) following which, oxide formation charge is apparently increased through build-up of species in the O_{C2} (and O_{C2}') states. In 1M $HClO_4$ (Figure 3-5a-d), the development of species in state O_{C3} soon follows that in O_{C2}, as is observed for all acid solutions. Even in alkaline solution, where the behavior of these peaks may be quite different, the order of their appearance is conserved.

iii) (Figure 3-5c) (Expanded potential scale) If the overall degree of surface oxidation is driven to exceed the saturation limiting coverage by the O_{C1} species, the additionally deposited O-species are reduced in several different states at potentials less positive than that for O_{C1}. After reaching its characteristic saturation coverage, the coverage (as charge) associated with the O_{C1}

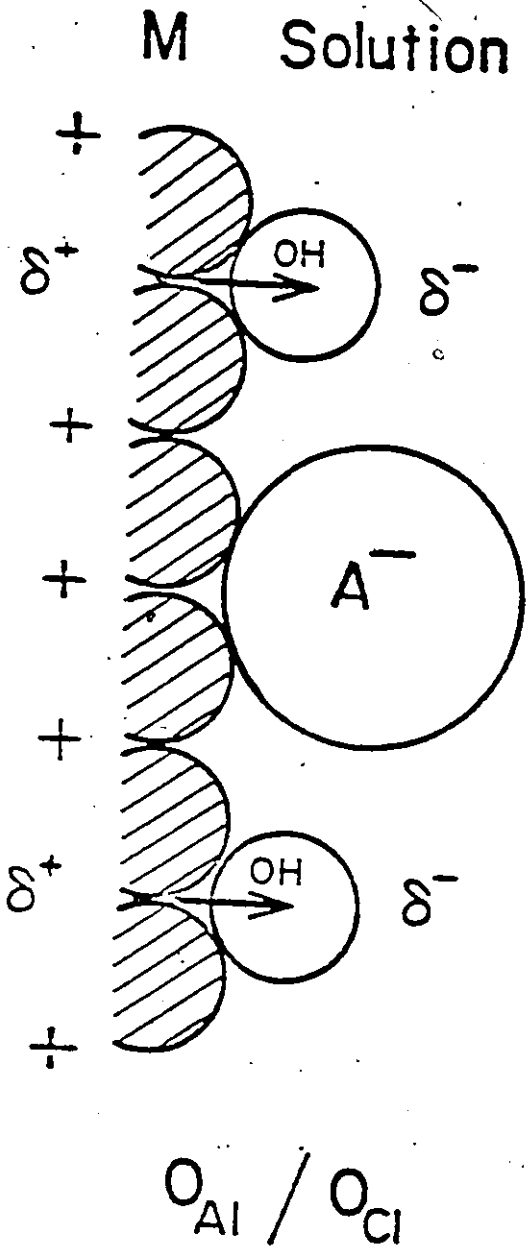

Figure 3-6 Model of anion interaction effects in initial stages of metal oxidation

state tends to decrease as overall oxide coverage is increased while simultaneously its peak potential moves sharply in the cathodic direction. This state appears to be unstable at these potentials (and coverages), and a new peak for a state O_{C3} (and O_{C3}') becomes significant.

iv) (Figure 3-5d) At higher overall coverage by O-species, the coverages associated with the O_{C2} and O_{C2}' peaks also reach saturation levels (in the solutions discussed thus far) with O_{C2}' coverage being just a fraction of that due to O_{C2}. Beyond this stage of surface oxidation, corresponding to approximately one-half a monolayer of deposited species (as O), additional growth of surface oxide occurs exclusively through the O_{C3} and O_{C3}' states, mainly the former. Thus O_{C3}, under most conditions, is identified as the reduction peak for the state in which the main growing film is reduced (or the main growth peak).

Peaks Designated by Primes

In all instances observed in this study, it appears that the "primed" peaks (example, Figure 3-5a-d) are simply satellite peaks of the unprimed states observed on the cathodic sweep; they exhibit similar behavior patterns. The species associated with primed peaks all reach saturation levels appreciably smaller than those for the corresponding main peaks, which (except for state O_{C3}), also have their own saturation levels. An obvious possible explanation is that there is more than one crystal face present on the electrode surfaces having its own characteristic ion adsorption behavior. This effect is hardly detected in solutions containing more strongly adsorbed anions. Rather particular conditions must generally be selected in

order to observe these peaks at all. In the material which follows, the main peaks are discussed without the need to consider the states represented by primes.

i) Ion Adsorption & General Features

Figure 3-7 shows a family of i vs V profiles for Au taken on different electrodes in aqueous $HClO_4$ down to the lowest practical concentration, 0.001 M, that can be studied. As the anion concentration is decreased, the peak for onset of oxide deposition appears at progressively smaller anodic potentials and there is a little more overlap between the anodic and cathodic profiles. This is due to smaller ClO_4^- adsorption in the 0.001 M solution than in the stronger solutions.

With increasing concentration of $HClO_4$ small but significant displacements of the O_{A2} and O_{A3} peaks arise; $(dE_p\ (O_{A3})/d \log C = 0.014$ V for H_2SO_4 and $(dE_p\ (O_{A2})/d \log C) = 0.006$ V for $HClO_4$.

Closer examination of the families of i vs V profiles in Figures 3-3 and 3-4 shows a common trend in the evolution of these profiles as oxide coverage is increased in successive profiles. In acid solutions, the double-layer charging current is remarkably constant on the scale of the oxidation currents observed and reflects a relatively constant and strong degree of anion adsorption. (On a very sensitive current scale, or in a.c. measurements[121], significant potential-dependent variation of double-layer capacitance is, however, observed.) Initial oxide deposition occurs in the O_{A1}/O_{C1} state but is not easily visualized for all these solutions at the low sweep rates of Figures 3-3 and 3-4. The first oxidation state is soon followed by deposition of oxide species in a state which is subsequently

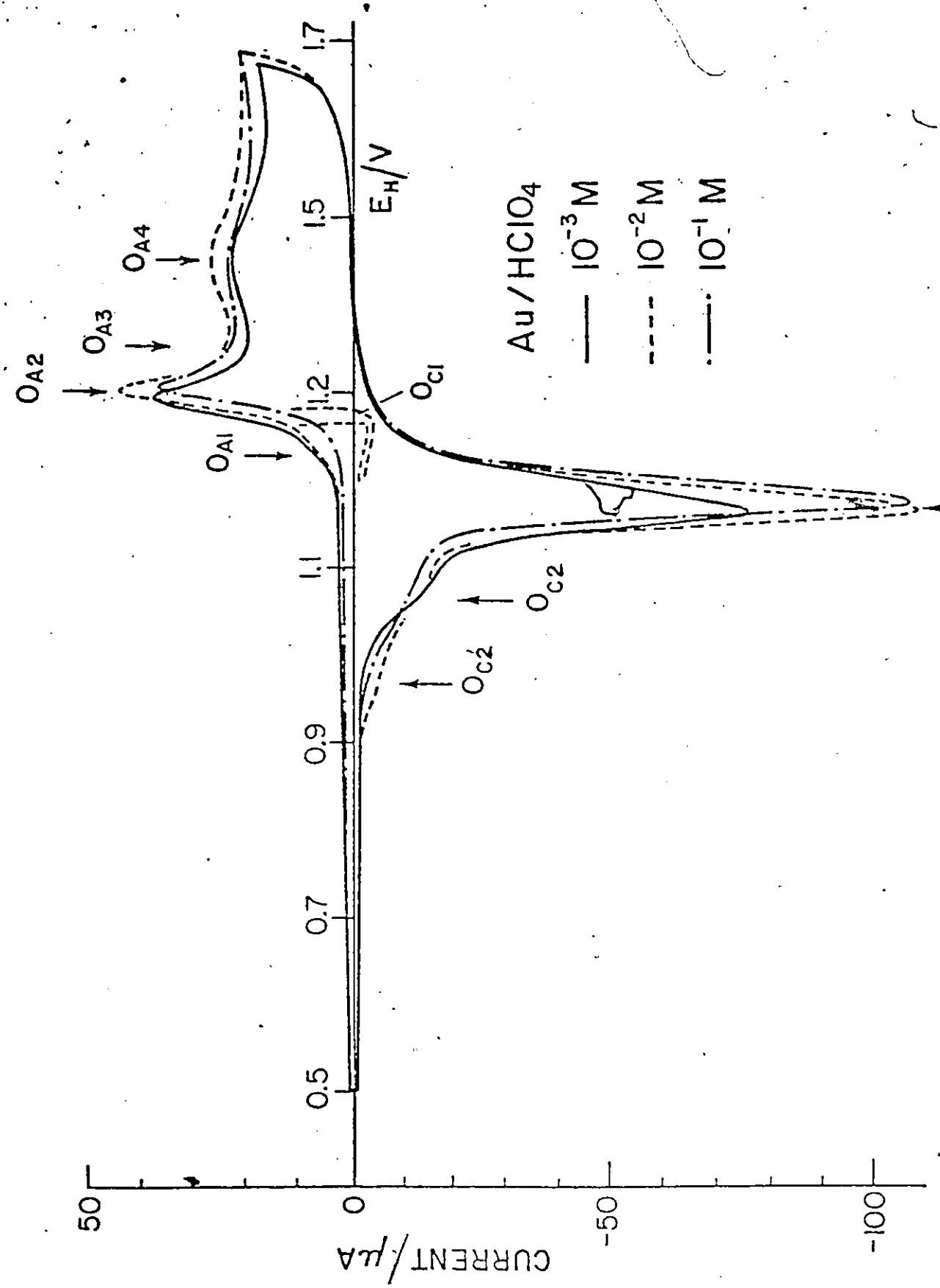

Figure 3-7 Potentiodynamic current-potential profiles for Au at 0.020 V s^{-1}, 298 K for several concentrations of $HClO_4$, showing designation of anodic and cathodic peaks

reduced in the O_{C2} and then in the O_{C3} states. The O_{C2} species attains a saturation coverage, the level of which varies somewhat with electrolyte. As oxide coverage increases, the O_{C3} peak corresponds to the principal state in which growth has occurred; that is, oxide at increasing extents of deposition (coverage) is reduced in a subsequent cathodic sweep in a single state but with proportionate increasing charge.

In alkaline solutions, with CO_3^{-2} and $B_4O_7^{-2}$ ions, several features of the i vs V profiles are to be noted especially in relation to the behavior in 0.1 M $HClO_4$, Figure 3-4a, and 0.05 M H_2SO_4, Figure 3-3. The anodic i vs V profile for 0.1 M Na_2CO_3 is less well resolved and the reversible process O_{A1}/O_{C1} less apparent, though the onset of oxidation is earlier. The potential of the first peak (1.304 V) indicates that the state O_{A2} is not blocked. In comparison, the anodic i vs V profile for 0.024 M $Na_2B_4O_7$ is even less well resolved and there is evidently a large effect associated with adsorption of $B_4O_7^{-2}$, presumably on account of the polymeric nature of this ion. Onset of surface oxidation in this electrolyte is displaced to 1.39 V, indicating that both the O_{A1} and the O_{A2} states are blocked. In addition, the extent of hysteresis between the oxide formation and reduction processes is much increased in comparison with that in CO_3^{-2} or ClO_4^- solutions. A loss of resolution in the cathodic oxide reduction profiles follows the same trend. It is apparent that anions of the electrolyte not only block the initial stage of oxidation (Fig. 3-2) and displace the potentials for onset of surface oxidation (Fig. 3-7), but they also have an important

influence on the state (revealed by the cathodic reduction behavior) of the oxide film that is generated in their presence during the cathodic sweep. This may be the result of a) the ion-dependent overall field in the inner-layer during the course of the oxide film growth, b) and/or the result of the local fields of ions adsorbed on the metal surface during oxide film growth ("discreteness of charge" effect) and c) anion adsorption in the completed oxide film. These points will be discussed in a later chapter.

At this stage it is possible to state an order of competitive adsorption of oxyanions with respect to the potentials at which electrodeposition of oxygen species at Au can commence by displacement of the adsorbed ions: $CO_3^{-2} < ClO_4^{-}$ (0.001 < 0.01 < 0.1 < 1.0 M) < SO_4^{-2} (0.001 < 0.1 < 1 M) < $B_4O_7^{-2}$ (0.024 M)

The reduction behavior may be interpreted in terms of the well known hysteresis between the process of formation and reduction of thin oxide films[17,55,56] due to the (physical) change of state of the film as it is laid down. This occurs through a quasi-chemical process of place-exchange considered as a "post-electrochemical" step in film formation and then as a "pre-electrochemical" step in reduction[22]. It is expected that anions will tend to increase the rate of the post-electrochemical process of place exchange to varying degrees through stabilization or destabilization of a transition state of the process. This will be explored in subsequent discussion after presentation of additional data.

4. Use of Alkaline Solutions

The logical extension of work on anion effects is to find a "reference" system in which anions are not involved in the

oxidation processes. The blocking effects of anions suggest that additional oxidation peaks at even lower anodic potentials might be present if there were no anion adsorption. Studies on this question can be made in either of two ways:

1. Effects of electrostatic adsorption of ions depend on the difference of potential between the point of zero charge (p.z.c.) and the potential for onset of surface oxidation. An attempt can be made to find a system in which the p.z.c. lies at more positive potentials than those for oxide deposition, then the initial stage of oxidation will be less affected by anion adsorption. Use of alkaline solutions shifts the H_2 and O_2 reversible potentials to values ca 0.8 V more negative so that the potential range for surface oxidation is effectively about 0.8 V less positive to the potential of zero charge than in 1.0 M acid solution. Thus, experiments in Na_2CO_3 or NaOH should enable surface oxidation to be studied at potentials substantially less positive than the p.z.c., so that anion adsorption should be diminished.

2. Experiments may be done in alkaline solution, e.g. NaOH, where the only anions present (OH^-) are those directly involved in the deposition process itself and which, at least at Pt or Hg, are regarded as not being strongly adsorbed.

This was the motivation for carrying out experiments in 1 M NaOH.

i) The Carbonate Problem

Unfortunately, the chemical NaOH cannot be obtained with less than about 0.5% carbonate present. The anion sensitivity of

the processes being studied is such that these levels of carbonate cannot be tolerated, particularly since carbonate appears (cf. Figs. 3-3 and 3-4) to be a strongly adsorbed anion which would then lead to i vs V profiles in which the effects of adsorbed carbonate dominate. Recrystallizations of NaOH were therefore required, though these could be only partially successful if done in open air due to rapid CO_2 adsorption by NaOH solutions. In general, elimination of carbonate from NaOH solutions poses one of the most difficult problems in chemistry. Attempts to purify NaOH early in the work were not satisfactory, though the general characteristics of sweeps on Au were recorded.

One method that was used to try to alleviate this problem was through the use of a nitrogen glove bag. In the recrystallization processes, saturated solutions at 373 K were placed directly in the N_2 bag to cool, in order to minimize CO_2 absorption.

In addition, amounts of $Ba(OH)_2$ were added to some solutions 1.0M in NaOH in order to depress carbonate concentration through the low solubility of $BaCO_3$ ($K_{sp} = 8.1 \times 10^{-9}$ at 298 K). The net effect of these experimental modifications, coupled with additional recrystallizations, was a gradual improvement from the point of view of CO_3^{-2} adsorption effects in the i vs V profiles obtained.

Finally, it was decided to use saturated solutions of doubly recrystallized $Ba(OH)_2$ itself, thus minimizing the effects of CO_2 absorption in a strongly alkaline environment. The solubility of $Ba(OH)_2$ at 288 K is approximately 0.2 M.

ii) Saturated $Ba(OH)_2$

Use of solutions saturated in $Ba(OH)_2$ provided valuable first information on the nature of oxide deposition at Au in alkaline solution, and resulted in several improvements in experimental technique early in the work. Experimental procedure evolved to the point where the cell was assembled completely under N_2, with all sweeps performed in the N_2 glove bag. The degree of cleanliness has been improved to the point where "clean" sweeps for $Ba(OH)_2$ solutions at Au may now be routinely obtained. Use of the nitrogen glove bag has proven invaluable from the point of view of not only improving the level of cleanliness attainable, but also of prolonging the lifetime of a clean solution before its ultimate contamination from the environment.

Figure 3-8 shows families of i vs V profiles for Au in saturated $Ba(OH)_2$ solutions taken at 0.050 V s^{-1}. Figure 3-8b shows a result for $Ba(OH)_2$ containing traces of CO_3^{-2}; it was profiles such as these that were obtained until special efforts were made to eliminate residual traces of carbonate. These procedures involve, in addition to all the previously described techniques, the in situ boiling of the solution in the experimental cell, the whole apparatus being maintained in the N_2 glove bag.

Sustained boiling of the solution under N_2 eliminates CO_2 and, after cooling, establishes a low-carbonate pseudo-equilibrium. When carbonate concentration has been depressed sufficiently, the i vs V profile of Figure 3-8a is obtained in the same solution and on the same electrode as that which earlier gave the behavior in Figure 3-8b.

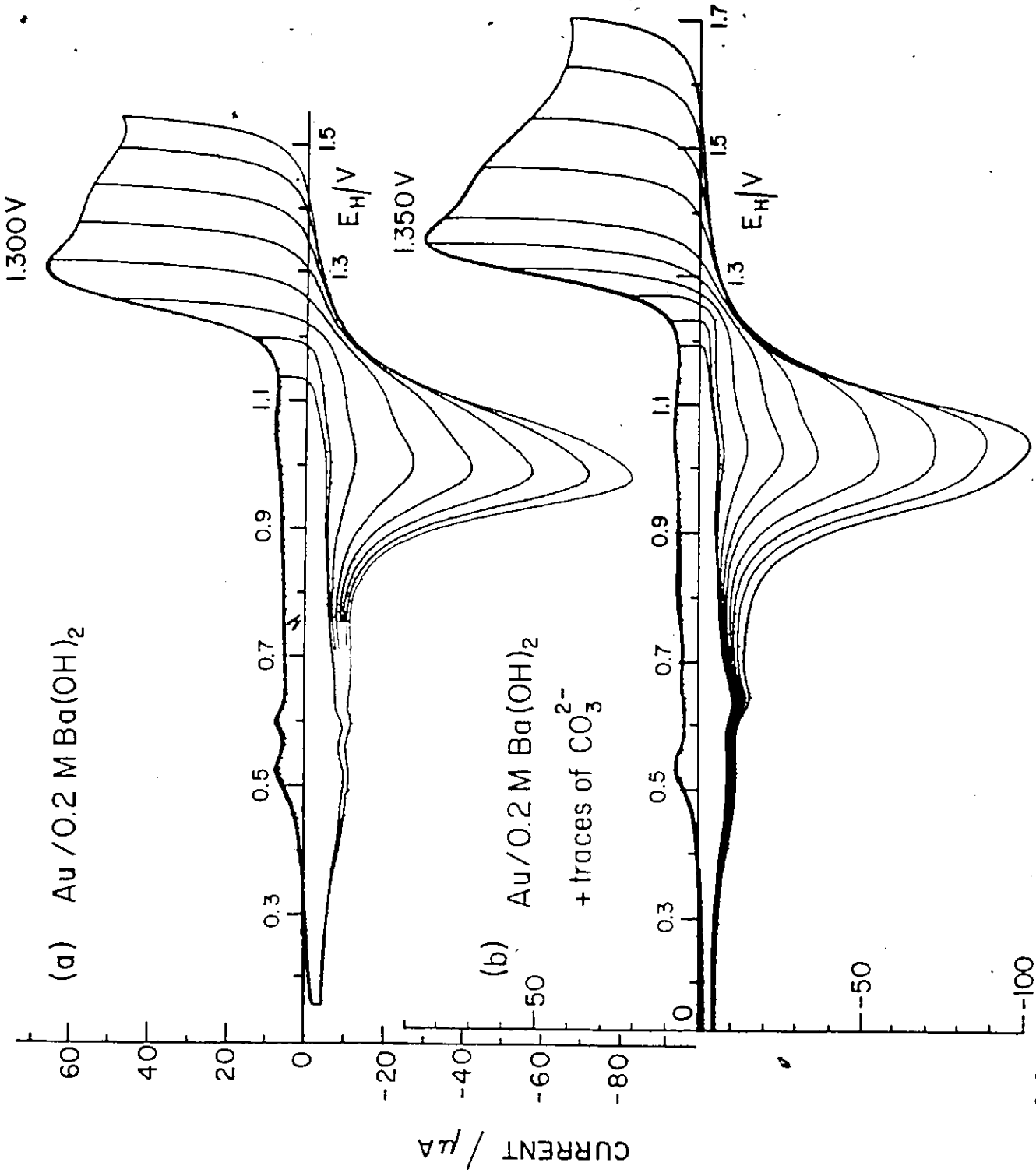

Figure 3-8 Potentiodynamic current-potential profiles for Au electrode in (a) 0.2 M $Ba(OH)_2$ and (b) 0.2 M $Ba(OH)_2$ + traces of CO_3^{2-} ion at 0.050 V s^{-1}, 298 K

Several features of these i vs V profiles should be noted, especially in evaluation of the effects of carbonate. Structure is observed in the i vs V profile in Figure 3-8a over the double-layer charging region between 0.5 and 0.6 V and again at 1.05 V, coupled with a general increase of currents over the double-layer region. The first large peak for oxide deposition now appears at approximately 1.300 V (compared with 1.350 V when traces of CO_3^{-2} are present) and the oxygen evolution reaction now commences measurably at potentials above 1.50 V (compared to ca 1.70 V).

The low, broad peak on the anodic sweep centered at approximately 1.05 V (prior to the main surface oxidation profile) is also observed conjugately on the cathodic i vs V profile when the potential limit of the anodic sweep is restricted to values below 1.20 V, i.e., the potential at which surface oxidation commences. This peak depends very much on solution purity and consequently may represent an initial reversible process, e.g. random deposition of nuclei, which would be easily blocked by foreign ions.

Special attention was given to the development of the various current peaks as a function of oxide coverage for the two solutions referred to in Figure 3-8. The families of i vs V profiles shown here enables it to be seen that, in the presence of carbonate (Figure 3-8b), oxide growth proceeds giving rise to species reducible in states O_{C2} and O_{C3}. However, O_{C2} appears to attain a saturation level and further overall deposition beyond this limit gives rise to species which are reduced in the O_{C3} peak, i.e. O_{C3} corresponds to the state in which the main growing film is reduced. This is just the

situation observed earlier in Figures 3-3 and 3-4 for acid solutions. However, in carbonate-free solution, a different growth mechanism is apparently involved. Figure 3-8a shows that it is apparently O_{C2} that is the main, or "growth" peak, and that it is O_{C3} that reaches some saturation level at fairly low total oxide coverages. This is totally different from the growth behavior previously observed in this work under other conditions.

Figure 3-9 shows how the quantities of species distinguished in the O_{C1}, O_{C2} and $O_{C3\&4}$ regions depend on E_A; the attainment of a limiting coverage (calculated as O-species) by species in the O_{C2} state is to be noted, as is also the decrease of O_{C1} as O_{C3} increases.

In contrast to the behavior in $HClO_4$, in Na_2CO_3 (Fig. 3-4b) the peaks O_{C2} and O_{C3} continue to increase to comparable extents with increasing E_A, though it appears that O_{C3} ultimately predominates. With $Na_2B_4O_7$ solution, intermediate behavior is seen (Fig. 3-4c) in the cathodic i vs V profile: it is mainly peak O_{C3}, which increases but O_{C2} shows some progressive enhancement; the component O_{C2}' is also present.

The observed limiting extent of generation of the state corresponding, in reduction, to O_{C2} in Figure 3-4a cannot be attributed to the presence of a certain fraction of the surface in a different plane of orientation from the remainder since the quantity of surface oxide associated with the O_{C2} state can become greater when $HClO_4$ is replaced by Na_2CO_3 or $Na_2B_4O_7$ (Fig. 3-4b,c) or $Ba(OH)_2$ (Fig. 3-8) at the same electrode. However, crystal plane effects could account for their behavior if it is recognized that a given exposed plane

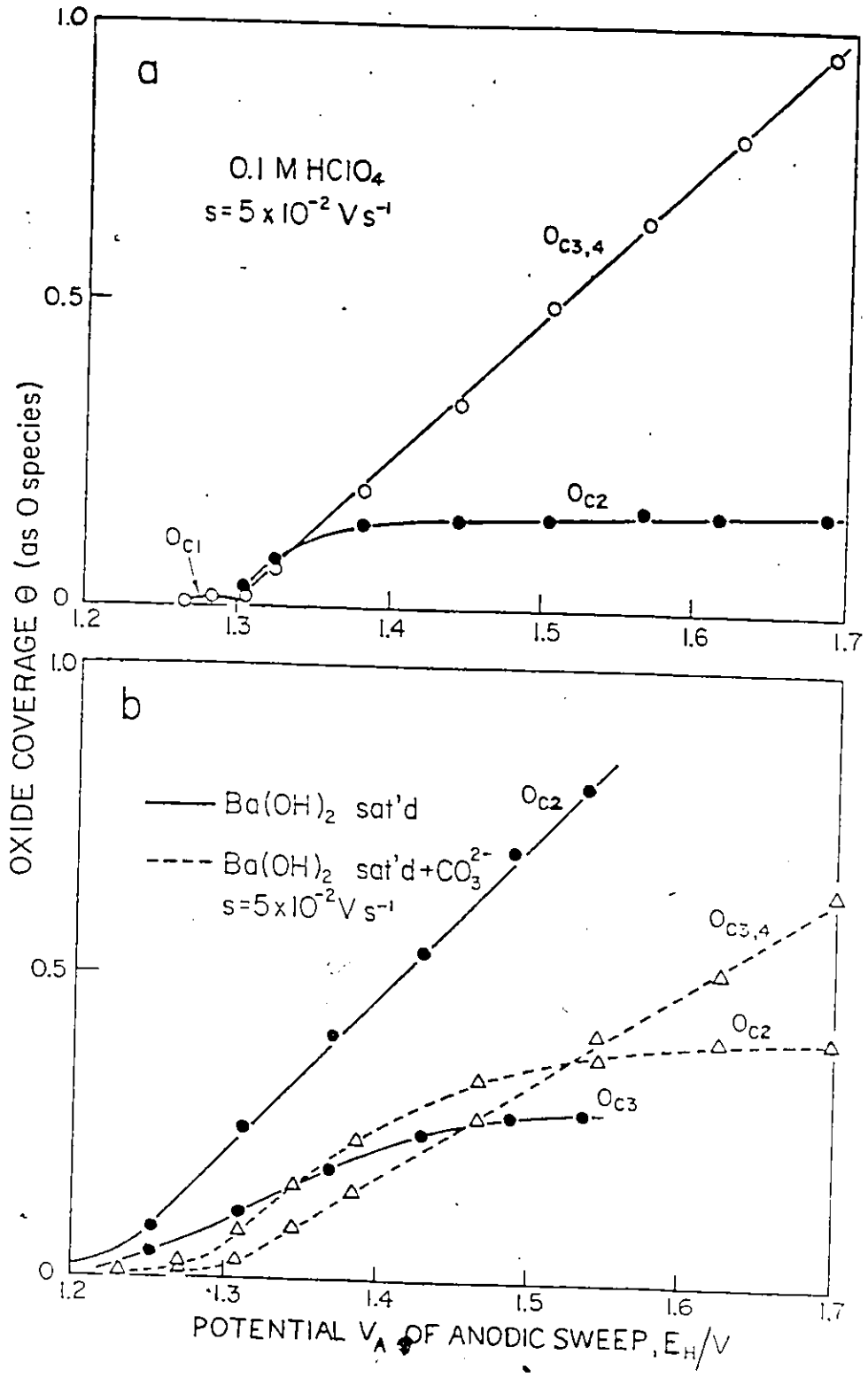

Figure 3-9 Oxide coverages, calculated as O species (2e/Au atom), for the distinguishable stages in cathodic reduction i vs V profiles at Au. Sweep rate = 0.050 V s^{-1} (a) 0.1 M $HClO_4$; (b) $Ba(OH)_2$, (——) saturated, (-----) saturated + CO_3^{2-}

can accept a more or less constant co-occupancy of anions and other O species but the relative amounts of these can depend on the type of ion adsorbed and its concentration.

In the case of Au in $Ba(OH)_2$ solutions, the development of comparable quantities of species reduced in the O_{C2} and O_{C3} regions is to be noted: In the purest aq. $Ba(OH)_2$ (Fig. 3-8a), the O_{C2} peak is predominant while in the CO_3^{-2} containing solution (Fig. 3-8b), the O_{C3} component becomes eventually predominant. This behavior is strikingly different from that in $HClO_4$ or H_2SO_4 solution but is more similar to that in Na_2CO_3 (Fig. 3-4b). In the presence of traces of CO_3^{-2}, the system behaves like that for acid or Na_2CO_3 solutions, with O_{C2} attaining a limited coverage of ca 0.40. Values of the limiting coverages attained by the O_{C2} state in various solutions are shown in Table 3-1. The value of the limiting coverage for O_{C2} is higher for less strongly adsorbed anions and is lower for more strongly adsorbed anions (e.g. SO_4^{-2}). An important feature of the anodic oxidation behavior of Au in $Ba(OH)_2$ is that, in CO_3^{-2}-free solution, the critical state of the film required (cf refs. 189, 198) for onset of O_2 evolution is attained some 150 - 200 mV lower than in the CO_3^{-2} containing solution. This state of the film corresponds to a degree of oxidation of at least one O on each Au atom. This explains an important point in electrocatalysis for oxygen evolution - the state of the oxide surface as determined by anion adsorption can be a major factor in anode performance.

TABLE 3-1

SOLUTION	LIMITING COVERAGE (as O species) FOR O_{C2} STATE
0.5 M H_2SO_4	0.11
0.1 M $HClO_4$	0.16
0.1 M Na_2CO_3	0.35
0.2 M $Ba(OH)_2$ & CO_3^{-2}	0.40
0.2 M $Ba(OH)_2$	> 0.4

iii) Reversible Stage(s) in Oxide Formation at Au in Alkaline Solution

A striking feature of the behavior of Au in alkaline solution is the appearance, over a broad potential range (0.5 - 1.2 V), of a reversible i vs V profile (Figure 3-8a) up to the potential (ca 1.2 V) at which the main surface oxidation commences. The broad region passes currents much larger than those normally required for double-layer charging (as seen below 0.2 V in Figure 3-8a). Thus the total charge associated with this region (between 0.5 and 1.2 V) after a normal double-layer charge has been allowed for, is ca 35% of that associated with formation of an OH monolayer.

This result can be interpreted either as due to formation of 35% of a normal OH monolayer or formation of a full monolayer of "OH" with an electrosorption valency γ of 0.35, i.e., with OH species as $OH^{(1-0.35)-}$. The latter seems probable and would be consistent with the strong adsorption of OH^- deduced by Bodé et al[191] and for the unusually wide range of potentials over which the supposed OH layer is adsorbed, associated with repulsion effects

In carbonate solution, a somewhat similar situation is observed (Figure 3-4b), especially with currents being observed in the usual double-layer charging region of the i vs V profiles that are larger than those attributable to double-layer charging.

Some insight into the nature of these currents may be gained from Figure 3-10 which shows three i vs V profiles for a full monolayer of oxide taken in 0.1 M Na_2CO_3 at 297 K at a sweep rate of 0.050 V s^{-1}. The first sweep, taken from 0.34 V

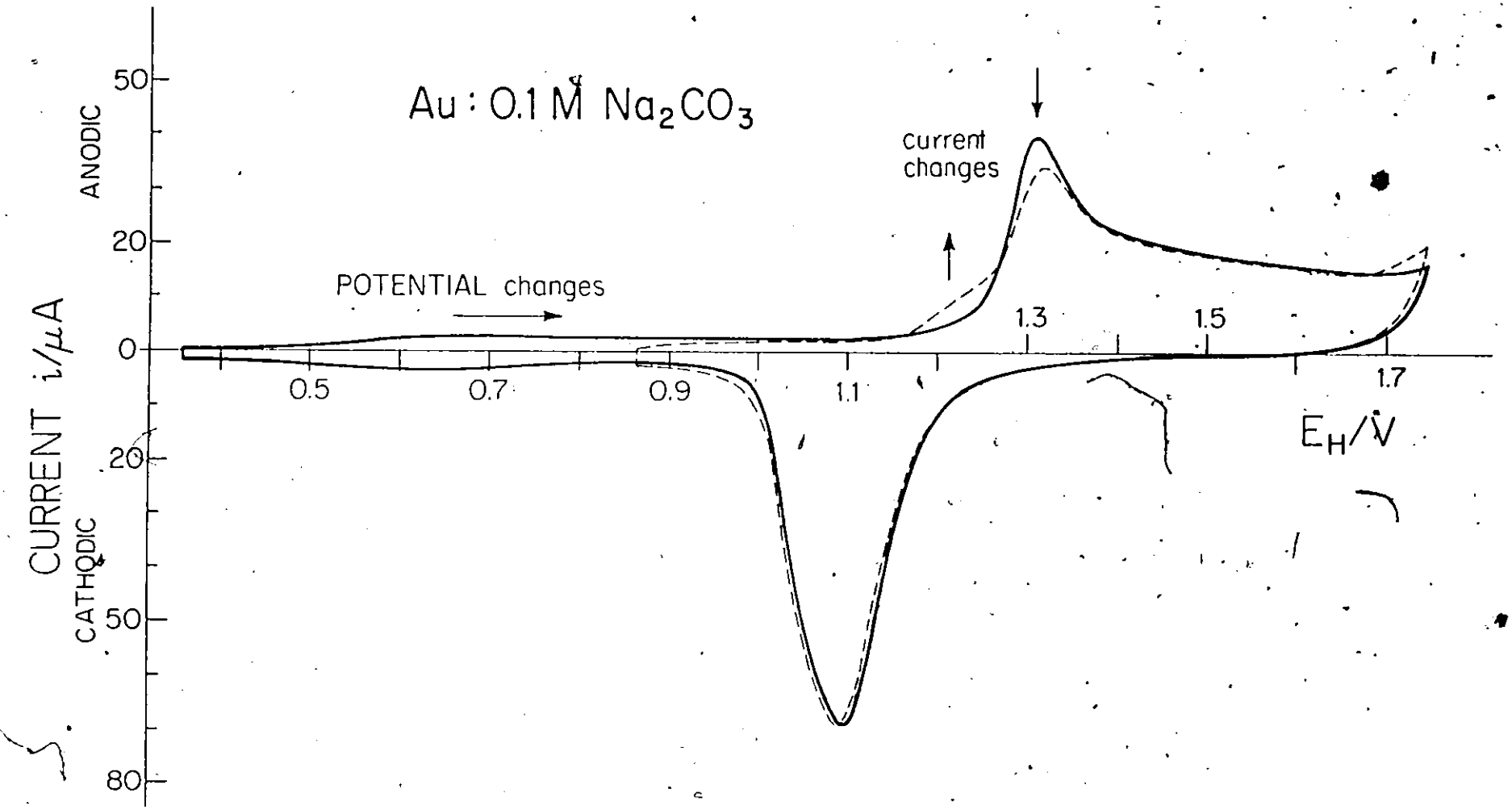

Figure 3-10 Potentiodynamic current-potential profiles for Au in 0.1 M Na_2CO_3 at 0.050 V s^{-1} 297 K, for a series of increasing cathodic end potentials.

to 1.74 V, is similar to that shown earlier in Figure 3-4b for 0.1M Na_2CO_3. The former profile records the negligible effect (in comparison with that for 3-4b) of holding the end potential of the cathodic sweep at 0.34 V for 10 seconds.

When the end potential increased to 0.87 V, some dramatic effects are observed. The onset of oxidation begins at 1.17 V with the appearance of a fairly broad peak up to ca 1.27 V. The profiles then coincide briefly, but then the usual O_{A2} peak is diminished by roughly an equivalent amount of charge as that which has flowed in the new peak at lower anodic potential. The profiles then coincide until O_2 evolution commences at 1.70 V. The apparent transference of a certain quantity of oxide formation charge from one state to another has been accomplished in much the same manner as in the results or effects of SO_4^{-2} adsorption (Fig. 3-2) for sulfate ion blockage of state O_{A2} in $HClO_4$ solution. It appears to be a direct transfer from one state to another and is not associated with a progressive or blocking phenomenon.

There is little or no change in the i vs V profile observed when the new potential limit of the cathodic sweep (0.87 V) is maintained for 10 seconds. The effects observed are therefore due to the change of end potential, and are not related to time effects at these potentials.

It is tempting to try to interpret the changes in oxidation peaks in terms of ion effects, and it will be useful to consider the consequences of such an interpretation. If the p.z.c. has been crossed in both these sweeps, little difference should result

in the i vs V profiles. If, on the other hand, the p.z.c. has not been crossed in the sweep taken to 0.87 V but has been in the earlier sweep to 0.34 V, then it would be expected that anion adsorption could be significant in the former case and diminished in the latter, blocking the onset of surface oxidation in the former case. This is certainly not consistent with the observed behavior. The p.z.c. is likely to lie in a potential region somewhere within the potential range above which the onset of surface oxidation has commenced.

These results lead to the important conclusion that the relatively high currents observed over the potential region 0.34 V to 0.87 V must be attributed to formation of some sort of reversibly deposited and reduced oxide. Thus, in the alkaline solution, when the potential limit of the cathodic sweep is 0.87 V, a quantity of surface oxide would still be residing on the surface in an unreduced state.

A type of aging of this oxide evidently occurs, so that once a potential of 1.17 V has been attained in a subsequent anodic sweep, the residual oxide allows the onset of the main surface oxidation process to commence via a different pathway than for the situation where reduction of the oxide has been completed before the next oxidation sweep is applied. The important feature, however, is that the relatively high currents observed in alkaline solutions over what is normally regarded as a "double-layer charging" region are, in fact, attributable to the presence of a reversibly depositable and reducible surface oxide.

5. Variation of Oxide Coverage Associated With Ion Effects

The effects of adsorption of individual anions (e.g. ClO_4^-) can be demonstrated by observing the onset of surface oxidation up to 1.32 V (in $HClO_4$) in cathodic sweeps that have been taken to various potentials nearer to or further from the p.z.c.

i) Effect of End Potential of the Cathodic Sweep

Figure 3-11 illustrates the situation in 1 M $HClO_4$ at a fast sweep rate of 200 V s^{-1} for extents of oxide formation less than 5% of a monolayer. Perchlorate anions desorbed in the cathodic sweep at potentials negative to or near to the p.z.c. have no time to become readsorbed if the following sweep is sufficiently fast (5×10^{-3} s per volt). Consequently, oxidation can commence at lower potentials so that more surface oxide can be formed at 1.32 V. However, if the sweep is taken only over a shorter potential range (1.32 - 0.95 V), the anions are not desorbed in the cathodic-going sweep. Consequently, hardly any oxide can then be formed, and is thus not observed (Fig. 3-11) on reduction.

Figure 3-12 illustrates the same effect in 0.5 M H_2SO_4 solution, where onset of oxidation is delayed by the more strongly adsorbed HSO_4^- ions to approximately 1.40 V. The behavior for a series of diminishing end potentials of the cathodic sweep is shown in Figure 3-12 and it is evident and noteworthy that there is a narrow potential range in which the effect of cathodic end potential is most dramatic. The quantity of oxide deposited (and reduced) is essentially unchanged as V_c is increased from -0.016 V up to 0.998 V but then, over a relatively small potential range (Fig. 3-12b)

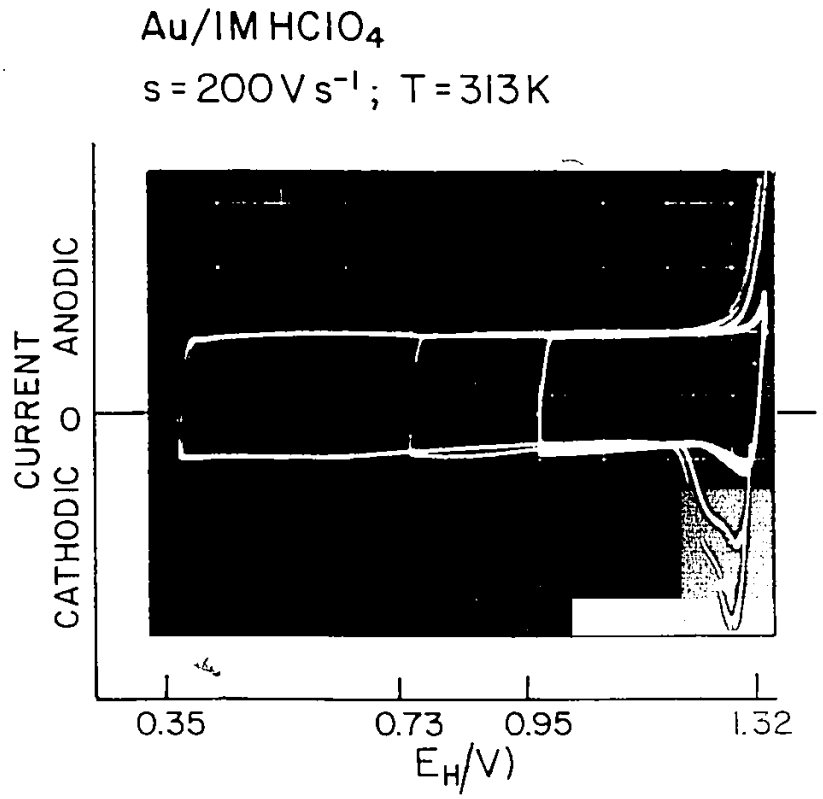

Figure 3-11 Varying extent of reducible surface oxide at Au formed at 1.32 V (E_H), dependent on potential limit of previous cathodic sweep in fast sweep experiments in 1.0 M $HClO_4$ s = 200 V s^{-1}, 313 K

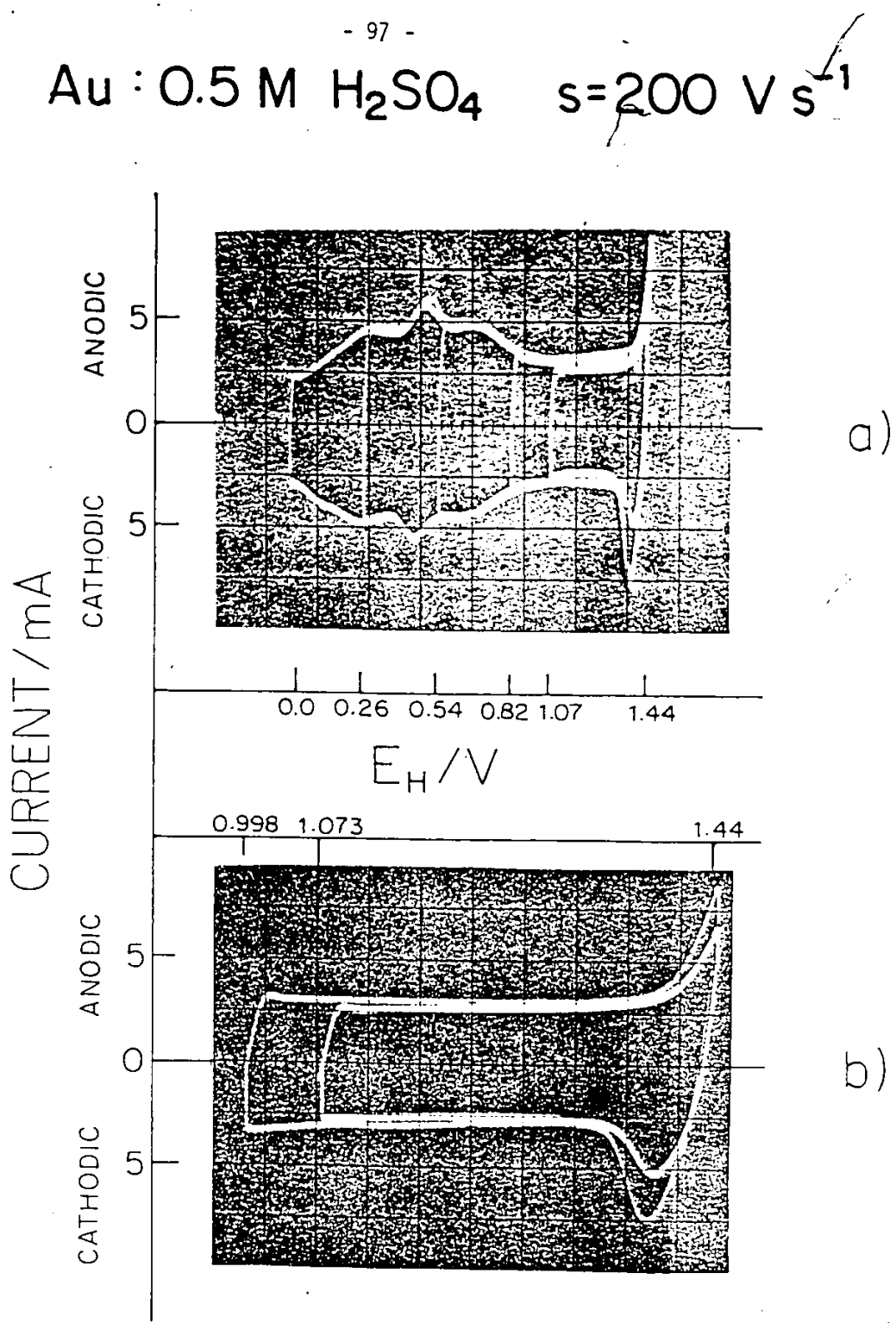

Figure 3-12 Varying extent of reducible surface oxide on Au formed at 1.44 V (E_H), dependent on potential limit of previous cathodic sweep in fast sweep experiments in 0.5 M H_2SO_4. s = 200 V s^{-1}, 293 K. (a) for a series of cathodic end potentials; (b) expanded scale showing principal effect

(0.998 V - 1.073 V), a quite dramatic reduction in oxide coverage is effected. This result is undoubtedly related to the effects of crossing, and then (over some critical potential range) of not crossing the p.z.c. in the cathodic sweep after oxide reduction.

When a somewhat larger quantity of oxide has been deposited, a similar effect is still observed. Figure 3-13 shows how the overall quantity of oxide deposited in several different states is diminished as the end limit of potential in the cathodic sweep is taken to more and more positive values in successive sweeps. When the oxide charge associated with a given cathodic end potential is plotted as a function of that end potential (for a constant anodic sweep end potential), it is quite apparent (Fig. 3-14) that this effect is most dramatic over a fairly narrow range of potential (~ 0.45 V).

Such results must be interpreted in terms of ion adsorption/desorption in relation to the potential of zero charge at Au in each of these media, and whether or not this point is passed in a given sweep. It would appear, then, that ion desorption must play an important, if not major, role in the early stages of anodic oxidation. Thus anion adsorption is a critical factor in the stability of metal surfaces to the onset of oxidation.

Figure 3-15 in 1 M $HClO_4$ solution illustrates the effect of varying the end potential of the cathodic sweep for a somewhat larger quantity of deposited oxide. When the cathodic end potential is increased from -0.186 V to +0.736 V, a substantial decrease in oxide deposited (and reduced) up to the potential of 1.421 V is observed. This is attributed to the increased steady-

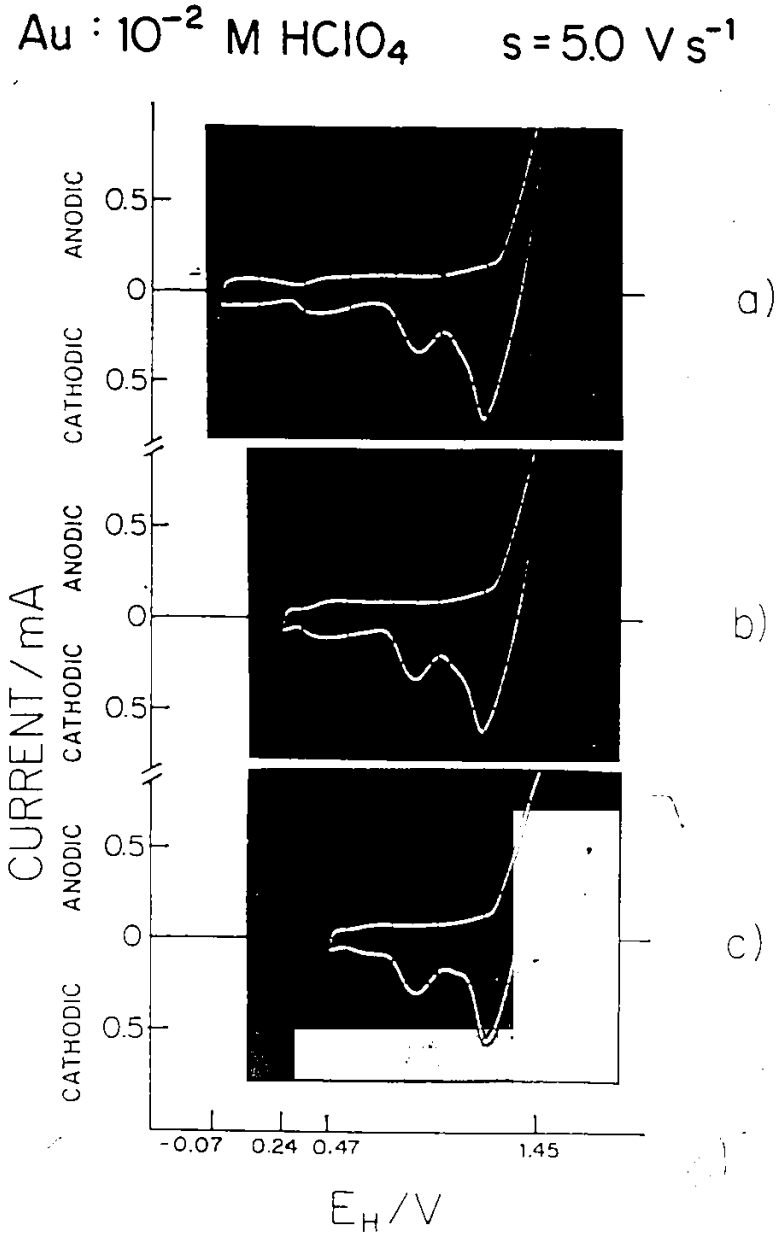

Figure 3-13 Varying coverage of surface oxide on Au formed at 1.45 V (E_H), dependent on potential limit of previous cathodic sweep in fast sweep experiments in 0.01 M $HClO_4$. s = 5.0 V s^{-1}, 298 K. (a) - (d) involving a series of cathodic end potentials;

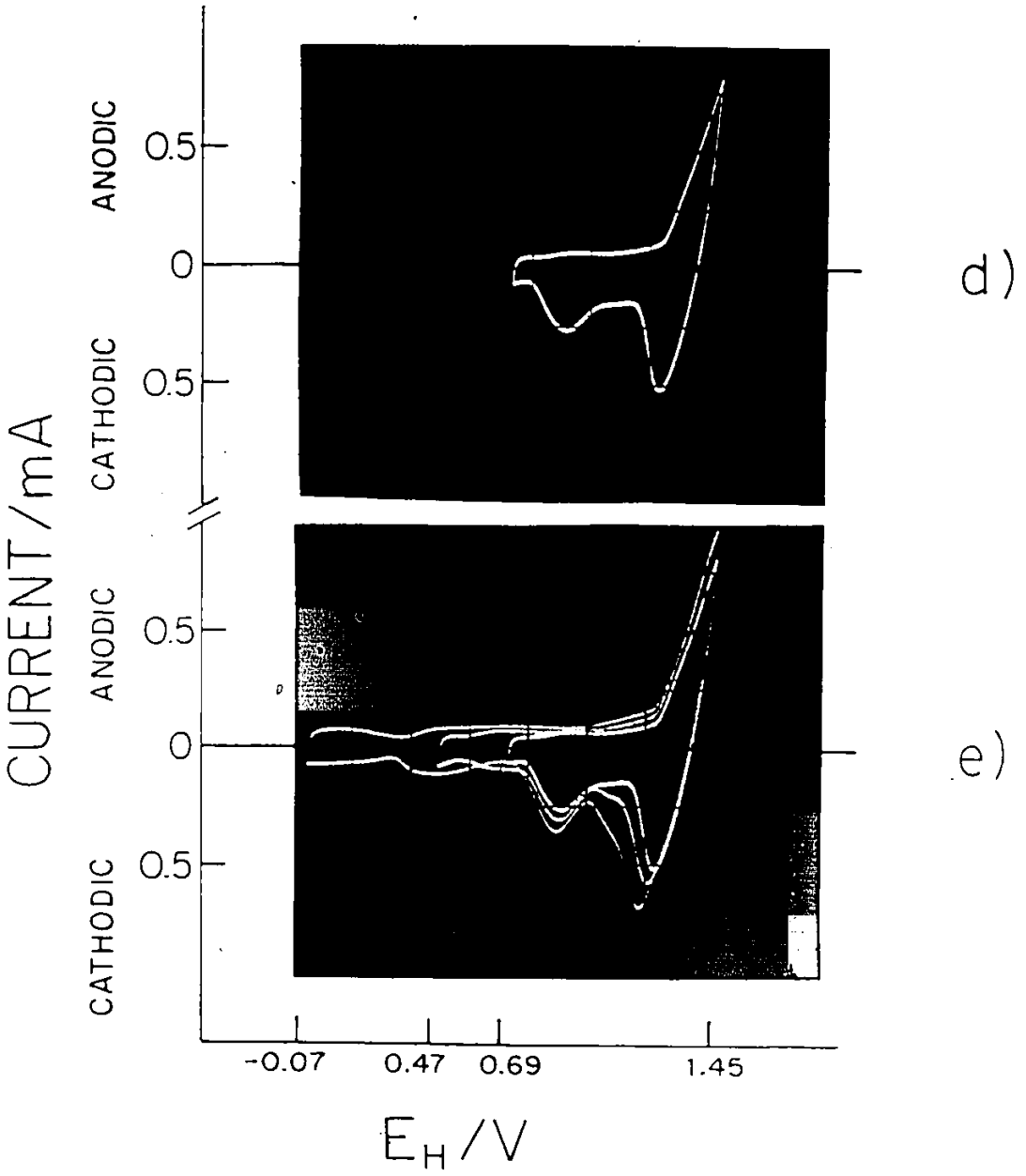

Figure 3-13 Varying coverage of surface oxide on Au formed at 1.45 V (E_H), dependent on potential limit of previous cathodic sweep in fast sweep experiments in 0.01 M $HClO_4$. s = 5.0 V s^{-1}, 298 K. (a) - (d) involving a series of cathodic end potentials; (e), (a), (c) and (d) superimposed

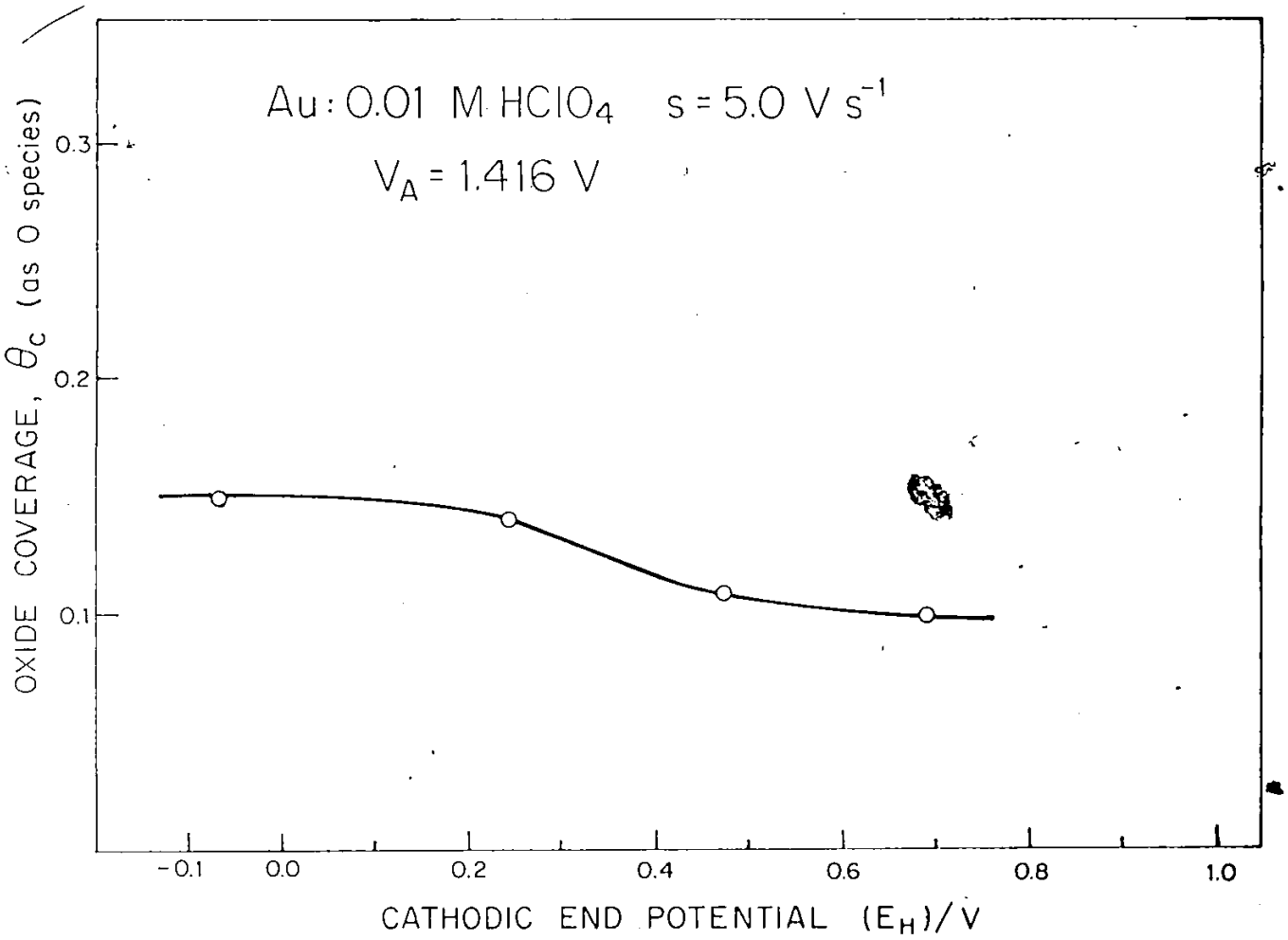

Figure 3-14 Variation of oxide coverage (as O species) formed on Au at 1.42 V (E_H) in 0.01 M $HClO_4$ for a series of end potentials of the previous cathodic sweep. s = 5.0 V s^{-1} 298 K

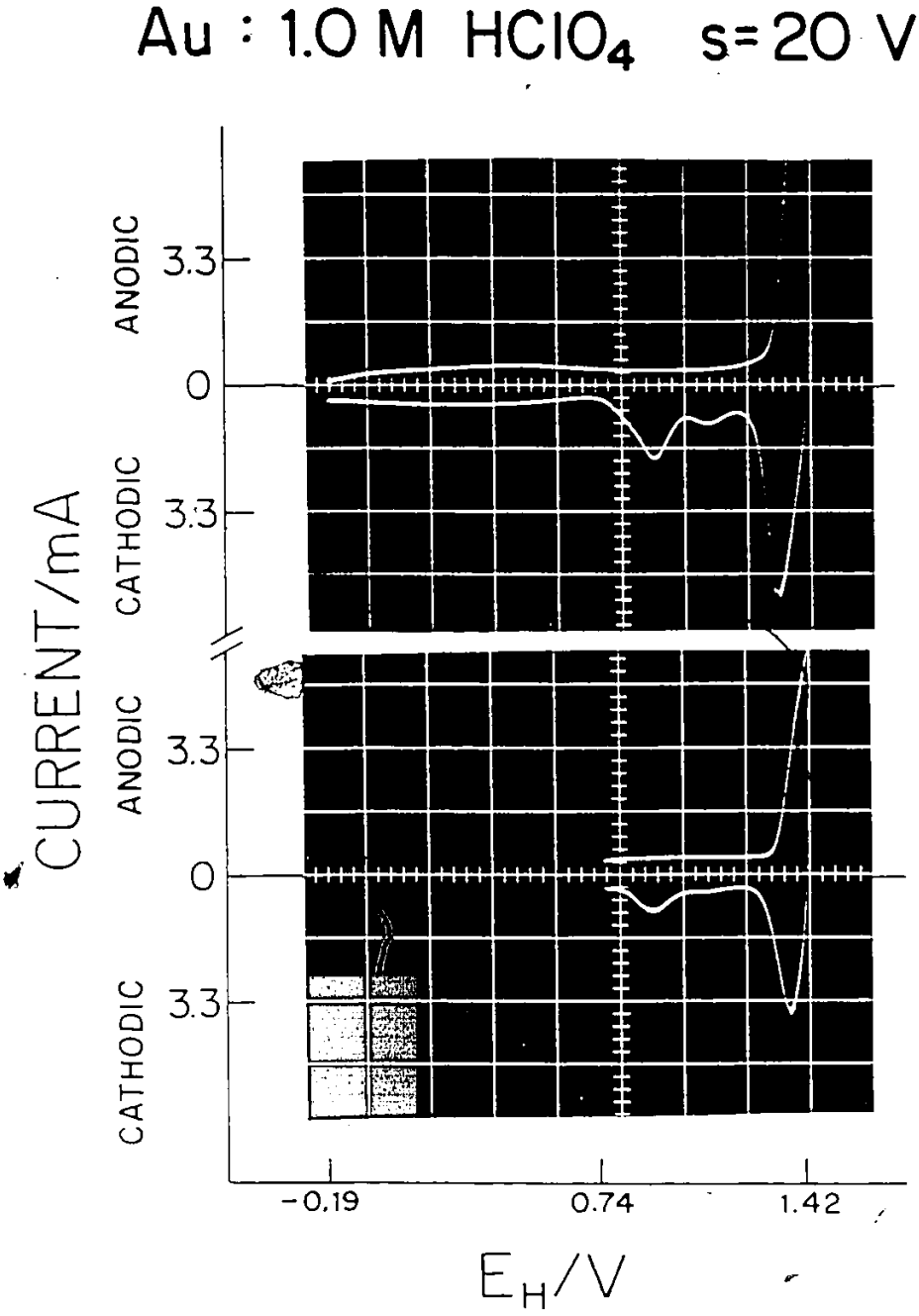

Figure 3-15 Varying extent of reducible surface oxide on Au formed at 1.42 V (E_H), dependent on potential limit of previous cathodic sweep in fast sweep experiments in 1.0 M $HClO_4$. s = 20 V s^{-1}, 297 K

state concentration of anions in the double-layer which exerts a blocking action on the discharge of water to form oxide. This higher surface concentration of anions is a result of the p.z.c. not having been crossed in the cathodic sweep and hence of anions not having been significantly desorbed in that sweep.

The higher surface concentration of anions remaining adsorbed may exert a blocking action in physical (geometric) terms and/or may exert such an effect indirectly by electrostatically lowering the potential drop across the inner-layer. This potential drop is the driving force for discharge from water or of OH^- ions to form oxide. The lowering of this potential cannot be too great, however, since approximately the same distribution of oxide reduction peaks is observed, rather than a situation where the states O_{C2} and O_{C3} have been eliminated, with peak O_{C1} being hardly reduced (in charge) at all. This latter situation is what is seen in studies where the end potential of the anodic sweep is varied.

ii) Time Spent on the Positive Side of the P.Z.C.

Additionally, it was found that time spent on the positive side of the p.z.c. has important effects. These were investigated using the more complicated potential-time program shown in Figure 2-5c, page 49. This program enables the potential of the electrode to be held first for various periods of time on the positive side of the p.z.c. and then scanned to some limit on the anodic sweep, then back to a new limit past the p.z.c. on the cathodic side, and finally back to the anodic limit and then back to the holding potential (Figure 2-5c, page 49). This affords the opportunity of observing

in a rapid "back-to-back" fashion the effects of traversing the potential of zero charge.

The effects appear to be cumulative, as Figure 3-16 illustrates for 1 M $HClO_4$ solution at 200 V s^{-1}. Thus Figure 3-16a is essentially a repetitive sweep profile; holding times of at least 10^{-1} s at V_2 must be employed before any effect is observed (Fig. 3-16b). As holding time is increased, successively larger effects are observed as charge in O_{Cl} becomes smaller. It should be noted that a cathodic sweep taken to low potentials (-0.29 V) is not sufficient to return the charge in O_{Cl} to the value attained in a regular repetitive sweep. This is especially apparent in Figure 3-16d, where τ_h = 10 s and in Figure 3-16e, where the multi-sweep profile is shown superimposed. Thus, in the repetitive sweep profile, larger currents are passed than those generated in the program where the p.z.c. has been crossed once after some period of holding.

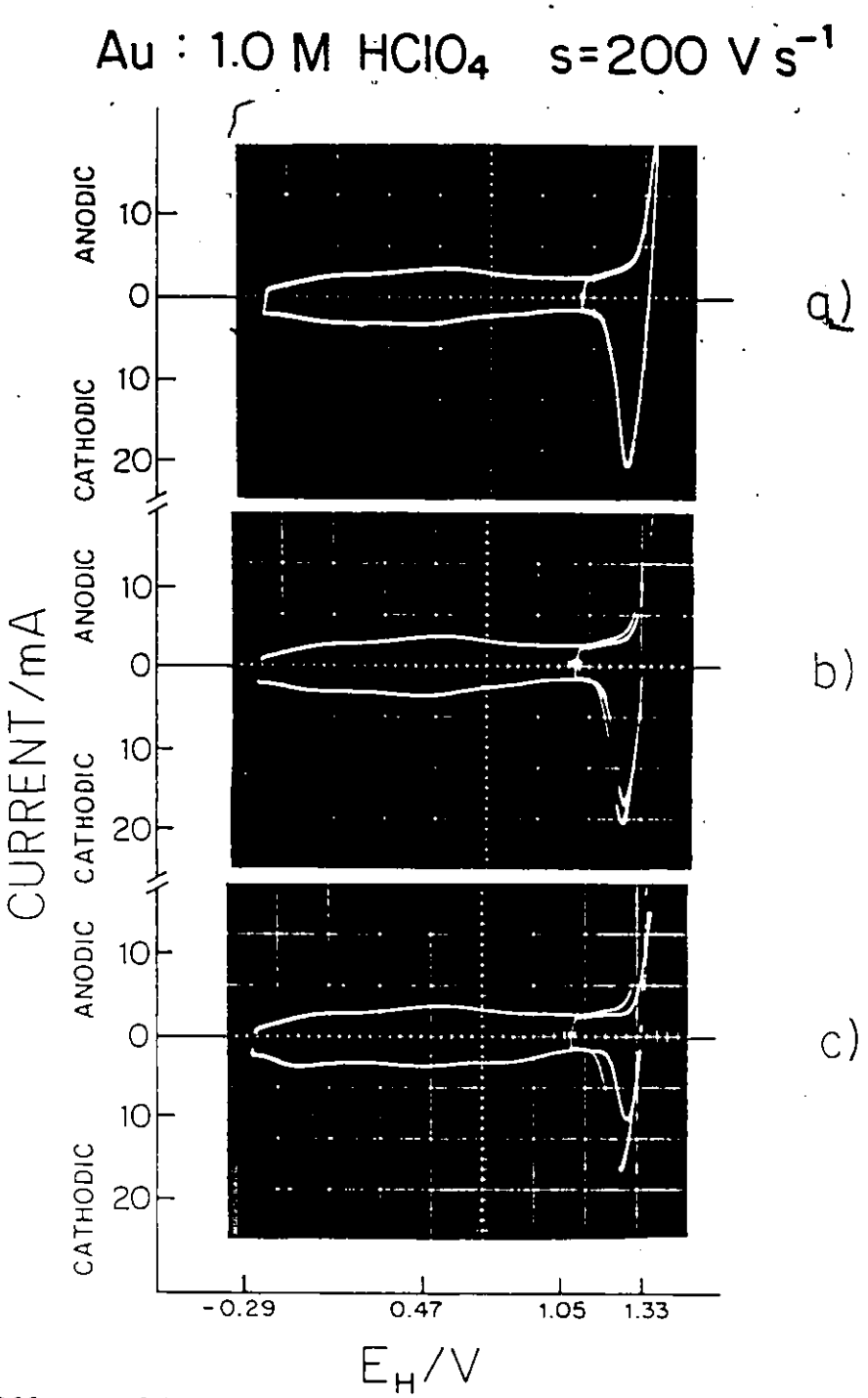

Figure 3-16 Effects of halting a cathodic potentiodynamic sweep at 1.05 V for various periods of time (τ_h) after completion of reduction of oxide previously formed at 1.33 V. The effects observed are in the subsequent re-oxidation to 1.33 V and subsequent reduction to -0.29 V; in 1.0 M $HClO_4$ s = 200 V s^{-1}, 293 K (a) $\tau_h = 10^{-4}$ to 10^{-2} s, no effect observed (b) $\tau_h = 0.1$ s (c) $\tau_h = 1$ s

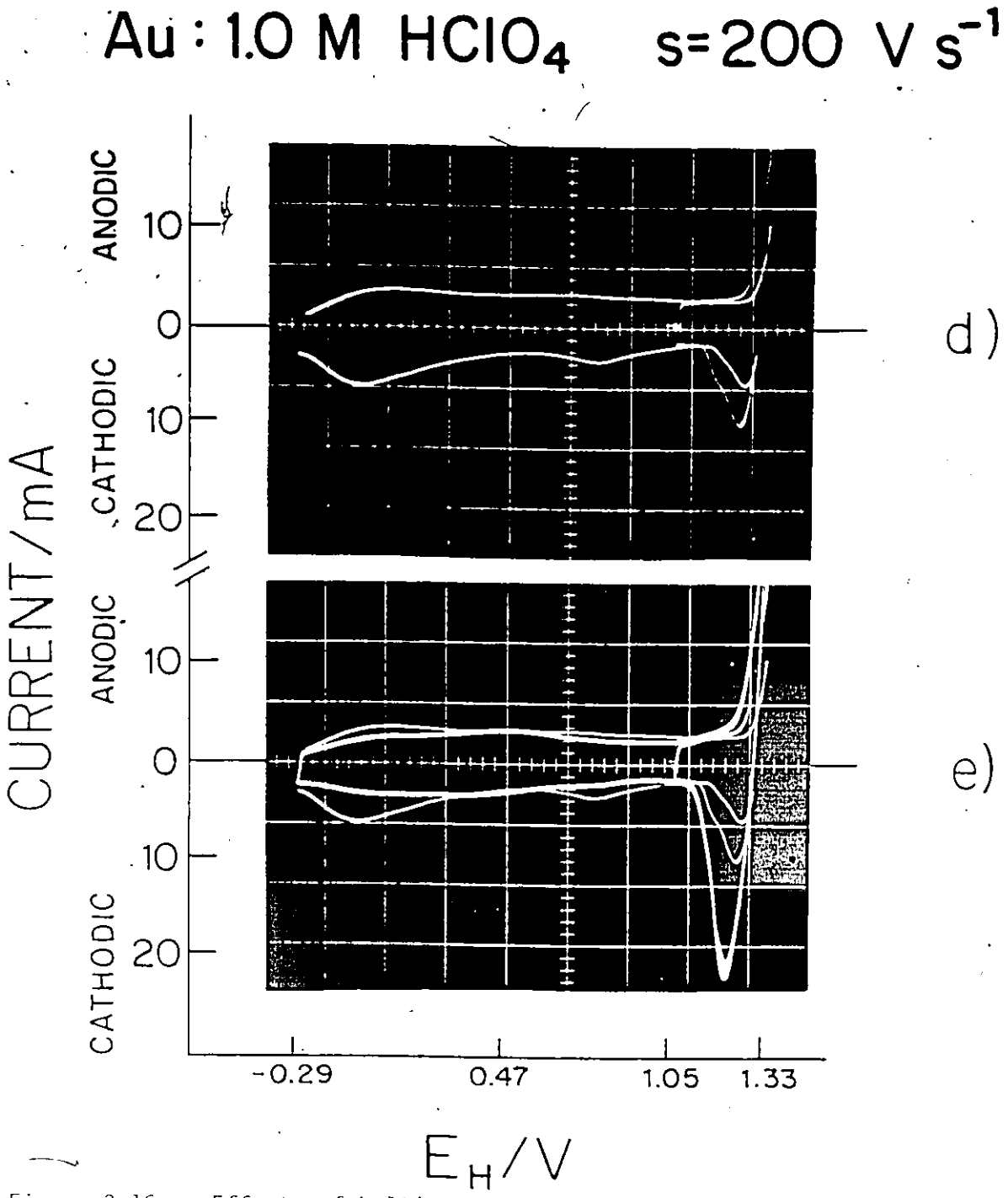

Figure 3-16 Effects of halting a cathodic potentiodynamic sweep at 1.05 V for various periods of time (τ_h) after completion of reduction of oxide previously formed at 1.33 V. The effects observed are in the subsequent re-oxidation to 1.33 V and subsequent reduction to -0.29 V; in 1.0 M $HClO_4$ s = 200 V s^{-1}, 293 K (d) τ_h = 10 s (e) τ_h = 0, 10 s superimposed.

CHAPTER 4

KINETICS OF OXIDE MONOLAYER FORMATION

The investigation of the kinetics of the formation and subsequent reduction of a monolayer of oxide on Au was carried out using three types of experiment which will be described in the next three chapters. Each study provides (a) different types of information concerning the overall process and/or the individual peaks observed in i vs V profiles and (b) allows direct evaluation of the potential dependence of the rate constant to be made at various stages of formation or reduction of the oxide film.

The anodic growth of the oxide formed on Au (described in this chapter) was studied as a function of time (t) and potential (V). Oxide was grown at various constant potentials and the extent of its formation was measured in terms of the charge passed in a subsequent cathodic i vs V profile.

A number of experimental V vs t programs were used before a satisfactory program yielding unambiguous results was established. However, all types of experiments yielded significant i vs V profiles which served (a) to illustrate further the role of ions in the growth mechanism; (b) to enable various distinguishable stages of growth of oxide to be followed at a given potential and (c) to provide valuable kinetic and diagnostic information concerning the stages of oxide growth corresponding to peaks observed in cathodic i vs V profiles.

1) Oxide Growth i vs V Profiles

It will be desirable to illustrate some of the i vs V profiles associated with V vs t programs used in early experiments as well as those associated with the kinetic data presented later in this

chapter.

The first studies of the oxide growth on Au as a function time and potential consisted of experiments in which the potential limit of an anodic sweep taken at moderate and high sweep-rates, was maintained for programmable, controlled periods of time. The first program used is shown in Figure 2-5b, p. 49.

In a typical series of experiments, the potential limit of the anodic sweep was varied over the entire potential range for monolayer oxide formation, with appropriate increments (30 ∿ 50 mV) in potential being selected usually on the basis of the i vs V profiles which resulted.

A given potential limit in an anodic sweep was maintained for controlled periods of time, ranging from 10^{-4} s to 1000 s (taking 3 data points in each decade of time, e.g. 1s, 2s, 5s, 10s).

The analysis of results of these experiments involved an initial inspection of the observed i vs V profiles to establish the relative sequences in which cathodic current peaks grow and their interrelationships. This provided an important supplementary basis for evaluation of the general features, and stages of oxide growth and reduction, discussed in Chapter 3.

Thus Figures 4-1 and 4-2 show the growth of oxide, in terms of the i vs V reduction profiles observed for 1.0 M $HClO_4$ at a sweep rate of 2.0 V s^{-1} when the end potential (1.403 V) of the anodic sweep was maintained for 10^{-4} and 10^{-3} s (giving identical profiles in Figure 4-1, for 10^{-2}, 10^{-1} and 1 s (in Fig. 4-1), for 10 s (in Fig. 4-2) and for 100 s (Fig 4-2). At the shortest holding times,

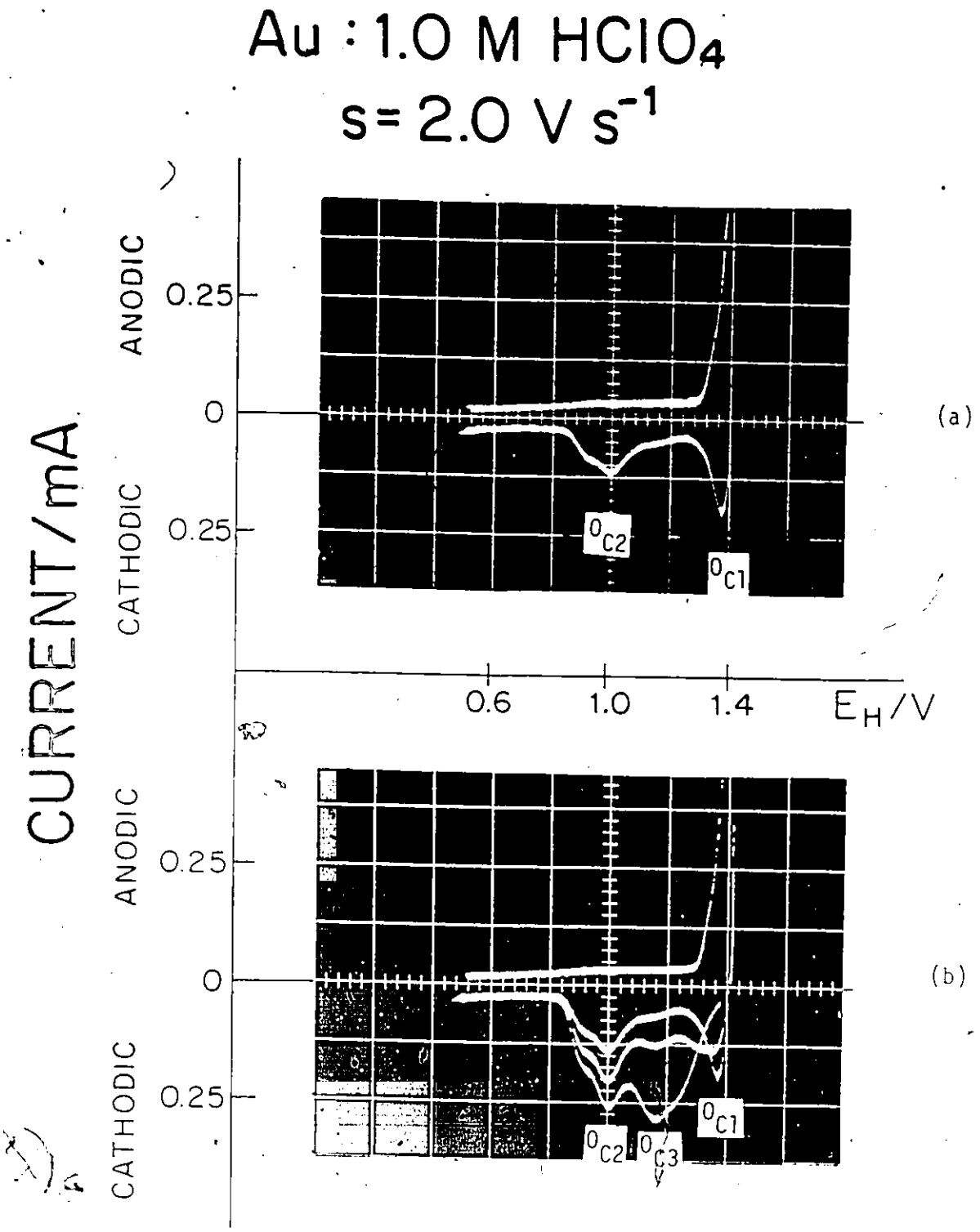

Figure 4-1 Potentiodynamic current-potential profiles for Au in 1.0 M $HClO_4$ at 2.0 V s^{-1} for oxide growth at constant potential of 1.40 V for varying growth times, τ_h, showing development of current peaks for reduction of submonolayer coverages of oxide, 293 K; (a) τ_h = 10^{-4}, 10^{-3} s; (b) τ_h = 0.01, 0.1, 1.0 s.

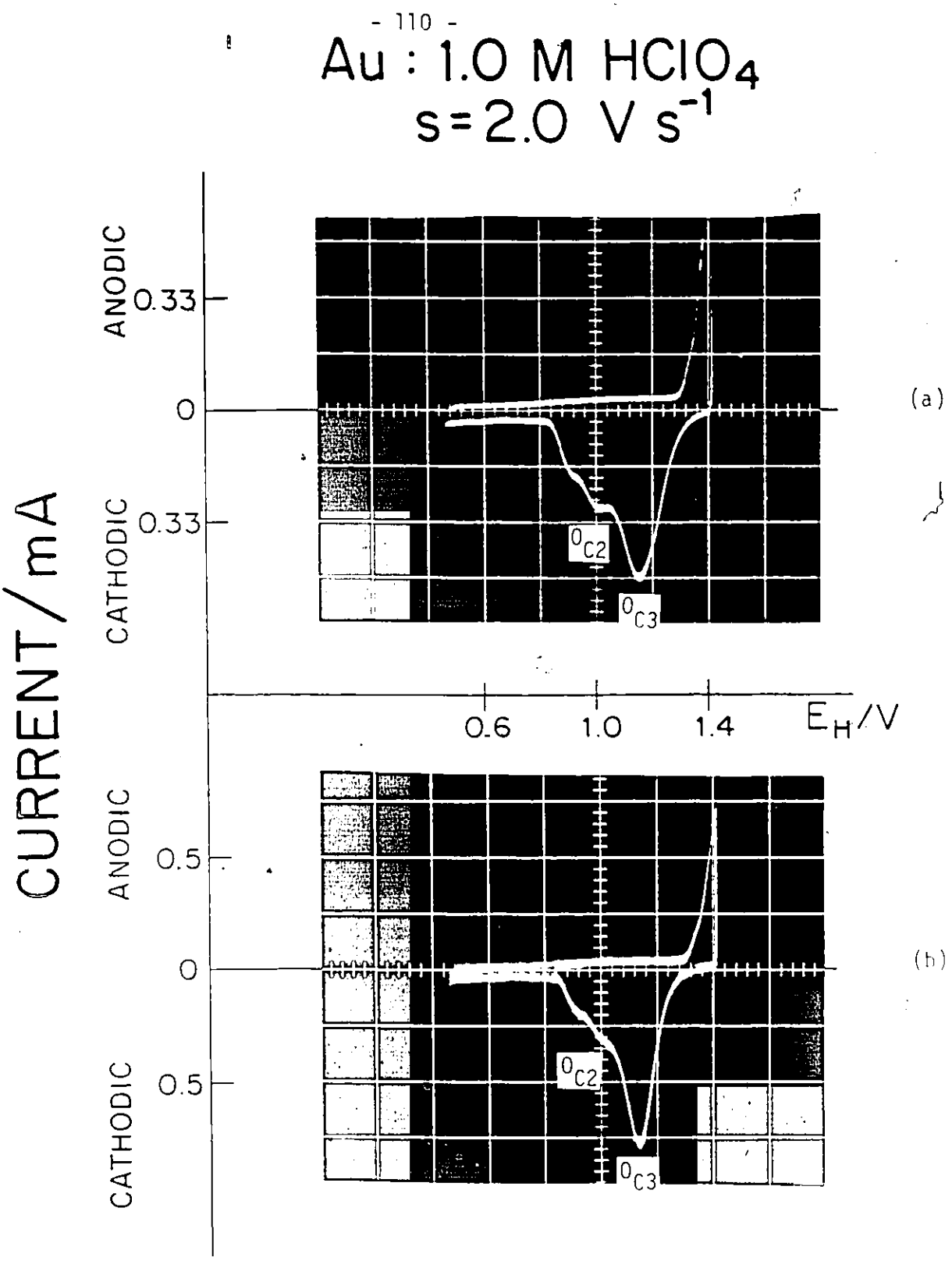

Figure 4-2 Potentiodynamic current-potential profiles for Au in 1.0 M $HClO_4$ at 2.0 V s^{-1} for oxide growth at constant potential of 1.40 V for varying growth times, τ_h, showing development of current peaks for reduction of submonolayer coverages of oxide, 293 K; (a) τ_h = 10 s; (b) τ_h = 100 s.

O_{C1} is the predominant oxide reduction peak with significant oxide coverage being associated also with O_{C2} (and its satellite $O_{C2'}$). A small peak, O_{C3} is barely observable. Longer holding times (Fig. 4-1) lead to an increase in the O_{C2} and ultimately in the O_{C3} states coupled with a continuing decrease in O_{C1}, so that at 1 s holding time, virtually no O_{C1} state is detected and the O_{C3} peak (and $O_{C3'}$) has become the principal state (hereafter referred to as the principal growth peak) in which the main growing state of the film is reduced. The i vs V profiles at τ_h = 10 s and τ_h = 100 s show the continuing growth of peak O_{C3} and saturation of state O_{C2} as observed initially in the general i vs V profiles shown in Chapter 3.

At a sweep rate of 200 V s^{-1} in the same solution and for "holding" at essentially the same anodic end potential, the i vs V profiles of Figure 4-3 are obtained. Increase in τ_h from 10^{-4} s to 10^{-3} s results in a small increase in the O_{C1} state, but also shows some growth in the O_{C2} and O_{C3} states; no peaks of this type are seen at $\tau_h = 10^{-4}$ s. With increasing τ_h state O_{C1} stays essentially the same but substantial increases of coverage in O_{C2} and O_{C3} states arise. Then at $\tau_h = 10^{-1}$ s state O_{C1} starts to decrease dramatically and its peak potential shifts to more cathodic values. The O_{C3} peak becomes the principal growth peak (Fig. 4-3b) with τ_h is a little > 1 s but, simultaneously, state O_{C1} disappears.

In 0.5 M aq. H_2SO_4 for s = 2.0 V s^{-1} and a similar (1.425 V) end potential of the anodic sweep, an analogous trend is observed in the growth and transition of the various peaks associated with the reduction of oxide. Figure 4-4a shows that oxide coverage, in terms of the states of reduction of that oxide, is evenly divided between

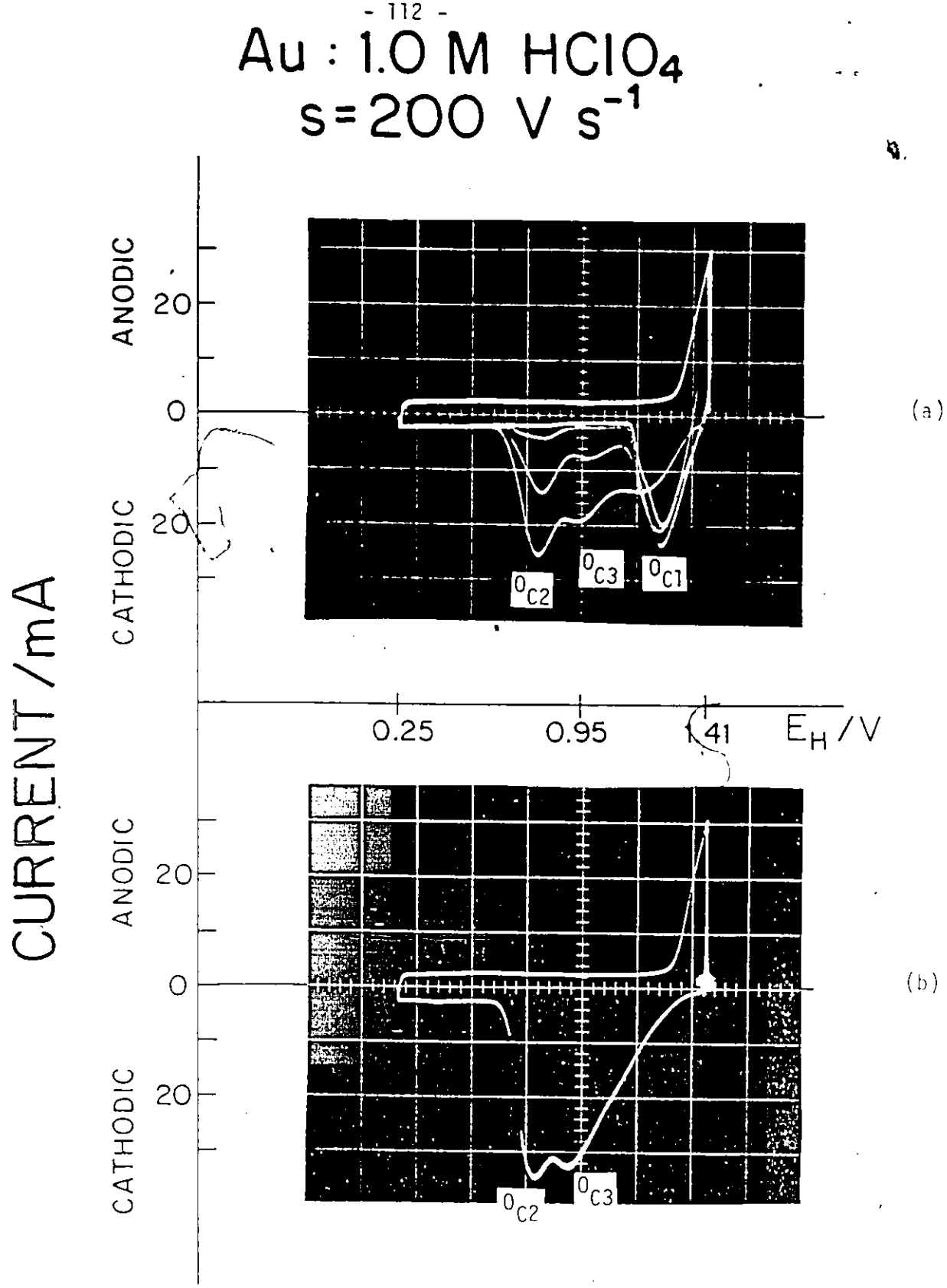

Figure 4-3 Potentiodynamic current-potential profiles for Au in 1.0 M $HClO_4$ at 200 V s^{-1} for oxide growth at constant potential of 1.41 V for varying growth times, t_h, showing development of current peaks for reduction of submonolayer coverages of oxide, 293 K; (a) $t_h = 10^{-4}$, 10^{-3}, 0.01 and 0.1 s; (b) t_h = 1.0 s.

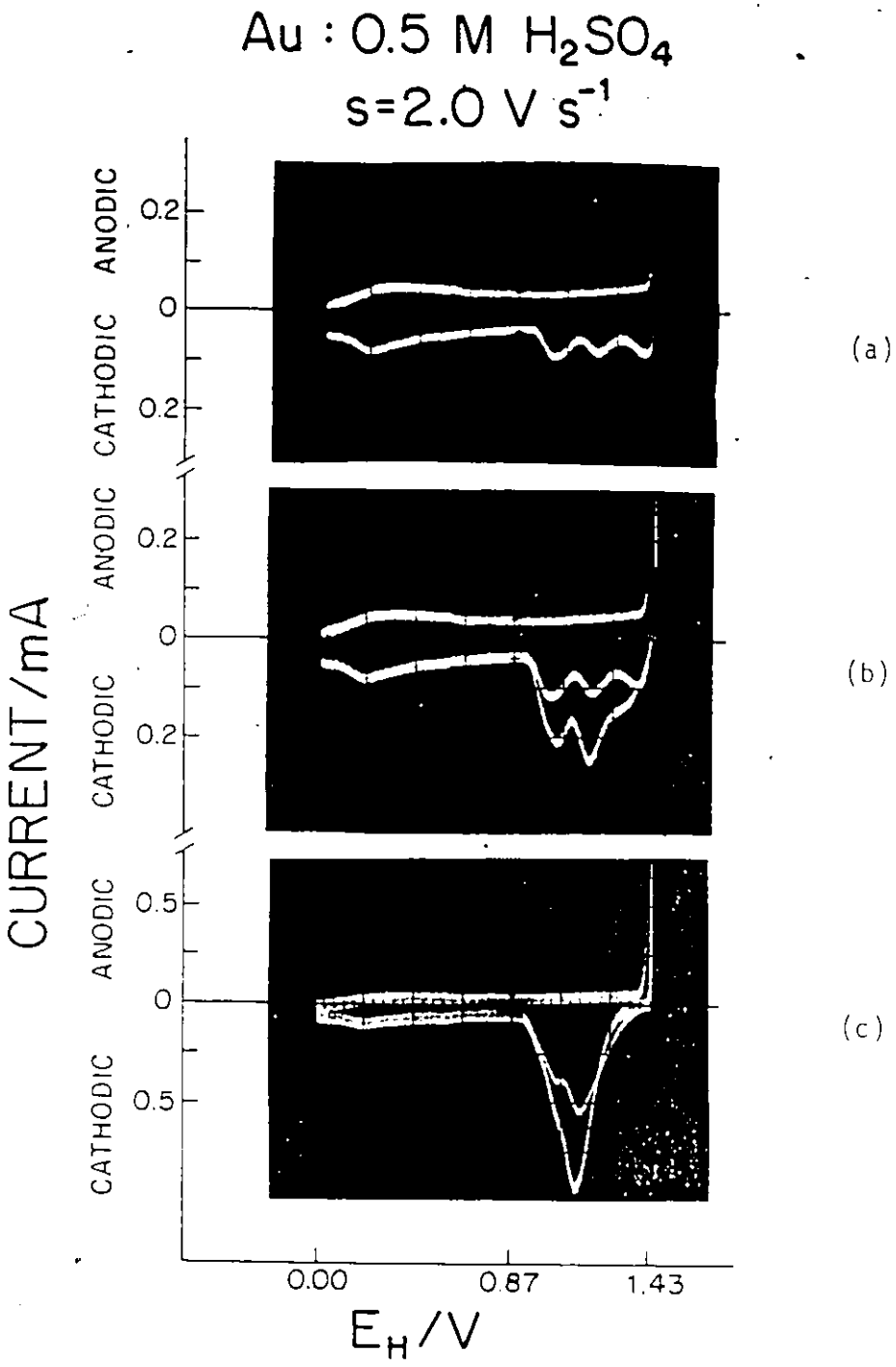

Figure 4-4 Potentiodynamic current-potential profiles for Au in 0.5 M H_2SO_4 at 200 V s^{-1} for oxide growth at constant potential of 1.43 V for varying growth times, τ_h, showing development of current peaks for reduction of submonolayer coverages of oxide, 293 K; (a) τ_h = 10^{-4}, 10^{-3} s; (b) τ_h = 0.01, 0.1 s; (c) τ_h = 1.0, 10 s.

the O_{C1}, O_{C2} and O_{C3} states for $\tau_h = 10^{-4}$ s (and 10^{-3} s). At longer τ_h, (e.g. 10^{-1} s in Fig. 4-4b) the O_{C3} peak has become dominant, the O_{C2} peak has increased somewhat, and the O_{C1} peak has become a shoulder on the anodic side of the O_{C3} peak. When oxide is grown for longer times, (1 and 10 s as shown in Fig. 4-4c), O_{C3} dominates the reduction profile after the O_{C2} state has reached its saturation value. Continuing growth of oxide occurs with reduction through the O_{C3} state and eventually, as a higher extent of oxidation is reached (that is Θ is > 1.0 under these conditions), through a state labelled O_{C4} which has its peak in the same potential region as that associated with the O_{C3} state and is detected by more subtle shifts in peak potential to be discussed later in Chapter 5.

Useful information regarding the variation of oxide coverage as a function of potential can be obtained using data from the integration of charge associated with these i vs V profiles. Thus, it is possible to compare data showing oxide coverage as a function of potential measured after periods of 1.0 second anodic holding (or any other appropriate time) at that potential. Figure 4-5 shows the oxide coverages developed after 1 s of oxide growth in 1 M $HClO_4$ and 0.5 M H_2SO_4 at s = 2.0 V s^{-1} and 200 V s^{-1} as a function of potential (with 1 s holding, or growth of oxide, at each potential).

A number of features of the results shown in this diagram are important. Firstly, after the 1.0 s holding, it appears that the oxide growth pattern becomes independent of sweep rate in both the above electrolytes. However, some of the important differences noted earlier between the results for the two media are not diminished by the holding procedure. Oxide growth is delayed considerably in H_2SO_4

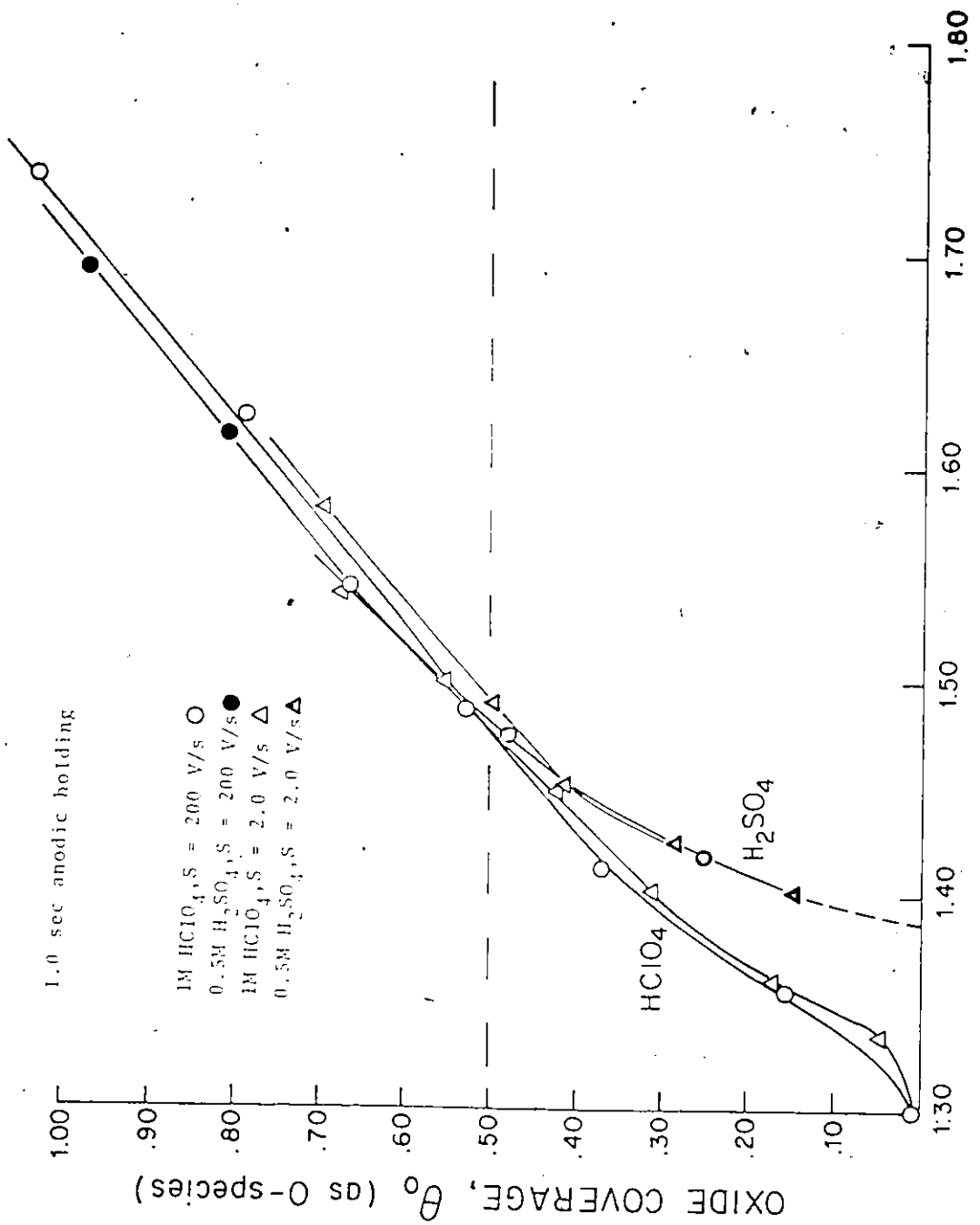

Figure 4-5 Variation of oxide coverage (as O-species) formed on Au in 1.0 M $HClO_4$ and 0.5 M H_2SO_4 for oxide growth for 1.0 s at various growth potentials. Comparison of results for s = 200 V s^{-1} and s = 2.0 V s^{-1}, 293 K.

(due to the anion blocking effect) and the curve for this solution does not "catch up" to the curve for growth in $HClO_4$ for some time. The fact that it should catch up at all, and that at oxide coverage of approximately 0.4 and greater it appears to follow the same oxide growth curve as that for $HClO_4$, is of interest. The growth curves all seem to merge when oxide coverages of 0.4 - 0.5 monolayer are attained and, thereafter, oxide growth is approximately independent of the type of electrolyte. In these two media, then, the influence of individual anions is differentiated dramatically below 0.40 in coverage counted as O species (or almost a full monolayer if O is counted as exclusively due to OH species on the electrode) following which, the effect of the anions present is essentially the same. The ion blocking effect is thus predominant in the initial stages of oxide deposition and growth. In addition, when coverage is considered as being due to O species (and support for this conclusion will be given in what follows), the effect (Fig. 4-5) is strong support for a type of random deposition since ions should be removed from the surface under these conditions already at ca 1/3 monolayer coverage, taking account of their size requirements in adsorption.

2. Oxide Growth V vs t Programs

Important characteristics of the experimental procedure forced the implementation of more complex V vs t programs in order to obtain uncompromised results, i.e., results not made ambiguous solely because of the V vs t program used. The problem is as follows: the deposition of oxide species commences as soon as the potential in an

anodic sweep is raised above a certain critical value (e.g., ca 1.30 V in $HClO_4$ solutions). Then, dependent on the anion of the electrolyte, in measuring oxide growth at, for example, 1.50 V, 200 mV of potential must be traversed over which oxide can already begin to grow before the potential selected as the end potential of the anodic sweep at which the oxide growth kinetics are to be studied, is attained. Thus, it is evident that the sweep time associated with traversing potentials over which some oxidation can occur before the "holding" potential is reached can be quite significant in comparison with the "holding times" when the latter are small. For example, for a sweep rate of 2.0 V s^{-1}, the time to raise the potential by 200 mV in the sweep is already 10^{-1} second. Furthermore, this time cannot be added directly to the time spent at the end potential of the anodic sweep since the sweep time covers a range of varying potentials. For a sweep rate of s and a range ΔV, of V to be traversed, the time involved is $\Delta t = \Delta V/s$.

Moreover, an additional error in growth time and conditions can arise from the reduction sweep, where, because of irreversibility in the process, continuing oxide growth can occur during the early part of the cathodic sweep, before reduction sets in at lower potentials where the current crosses the zero current line.

A special V vs t program was therefore designed (Fig. 2-5d, page 49) in order to minimize the time spent at oxidizing potentials in both the positive-going sweep before the constant potential at which oxide is grown is reached, and in the subsequent cathodic sweep before the potential at which reduction commences is reached. Using this program, experiments were performed in the following solutions:
a) 1.0 M $HClO_4$; b) 0.1 M $HClO_4$; c) 10^{-3} M $HClO_4$; d) 1.0 N H_2SO_4;

e) 0.1 N H_2SO_4; and f) 0.2 M $Ba(OH)_2$.

Approximately 10 - 12 different "holding potentials" were selected within the monolayer oxide coverage region for each solution.

A number of interesting features of the results of this aspect of the work must be considered, and their discussion falls into two categories:

a) the time dependence of oxide growth (θ vs log τ_h)

and b) the i vs V profiles for subsequent reduction of oxide.

3. Charge Data From Oxide Growth

In each solution, the charge or coverage of oxide associated with growth at 10 - 12 constant potentials is measured in the subsequent cathodic sweep at a series of τ_h from 10^{-4} s to 20 s (3 data points per decade of time). These charges, converted to θ_o values, are plotted for each solution as a series of curves of θ vs log τ_h (Figures 4-6 to 4-11).

Typical results are illustrated in Figure 4-12, which shows three distinguishable oxide growth regions which are designated as Stages I, II, and III.

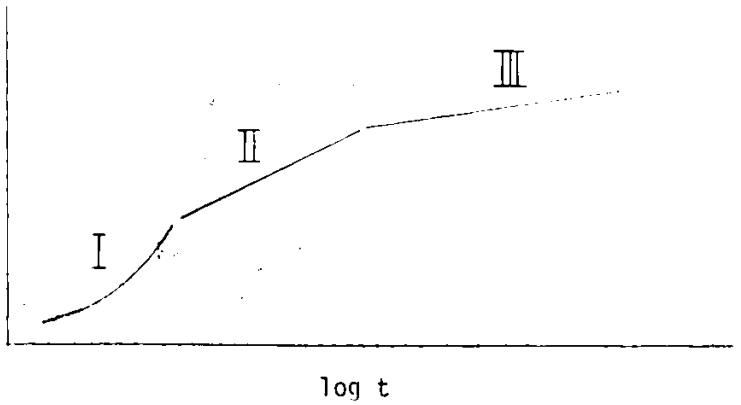

Figure 4-12 General form of data for coverages of grown oxide film vs log τ_h showing three distinguishable stages of oxide growth at constant potential.

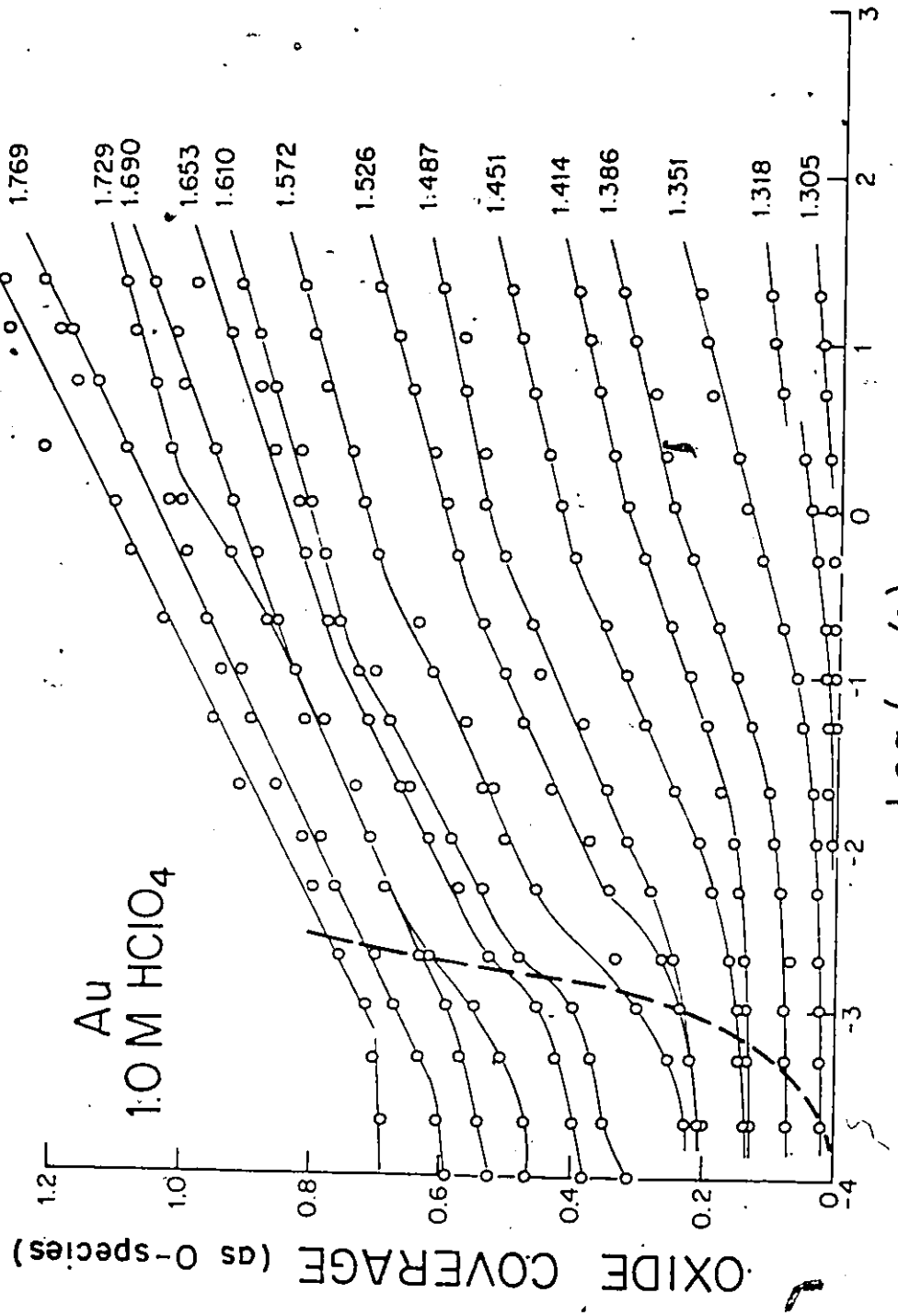

Figure 4-6 Variation of oxide coverage (as O-species) formed on Au in 1.0 M $HClO_4$ at various oxide growth potentials for grwoth periods of 10^{-4} s up to 20 s, 298 K, plotted as θ vs log τ_h.

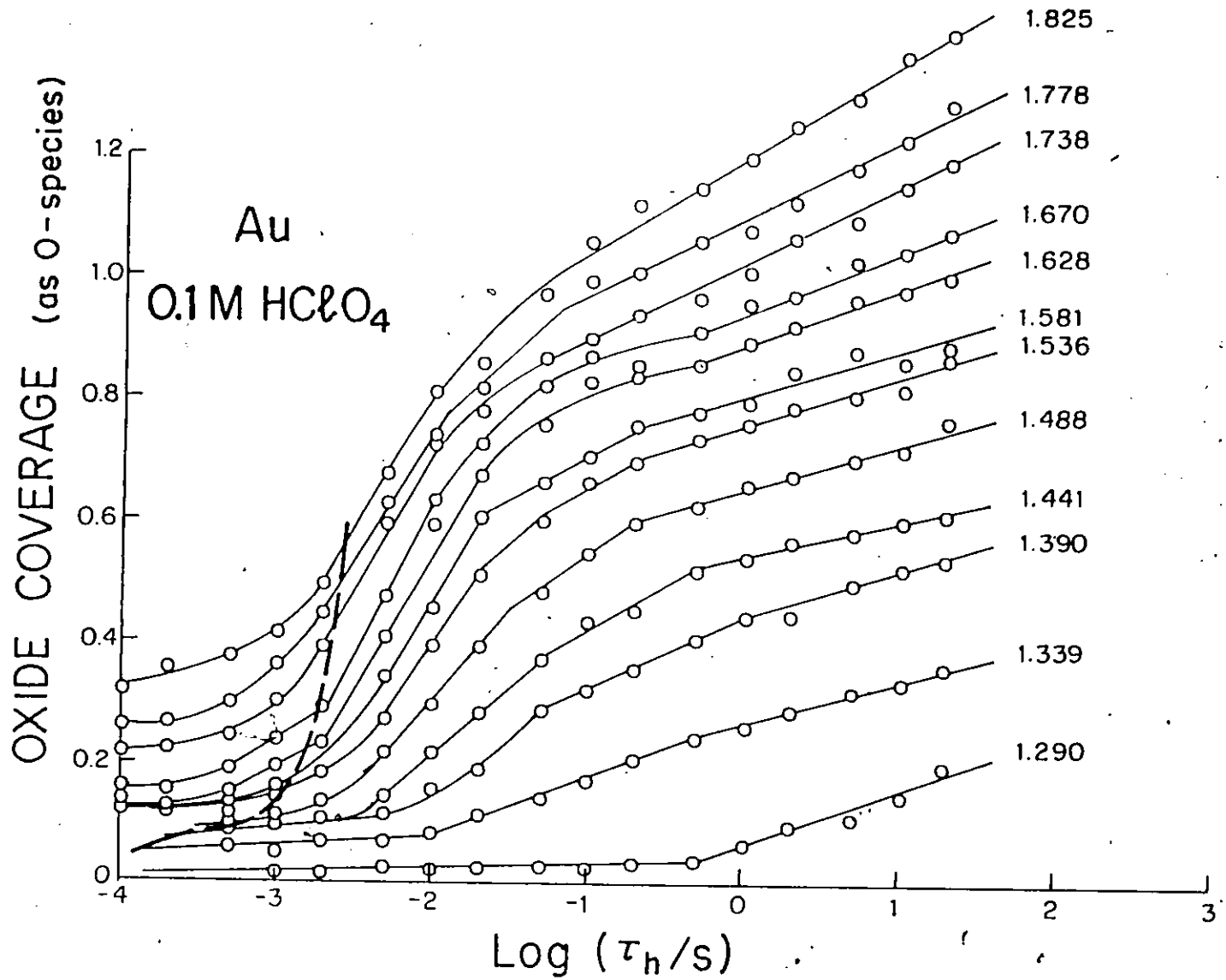

Figure 4-7 Variation of oxide coverage (as O species) formed on Au in 0.1 M $HClO_4$ at various oxide growth potentials for growth periods of 10^{-4} s up to 20 s, 298 K; plotted as θ *vs* log τ_h.

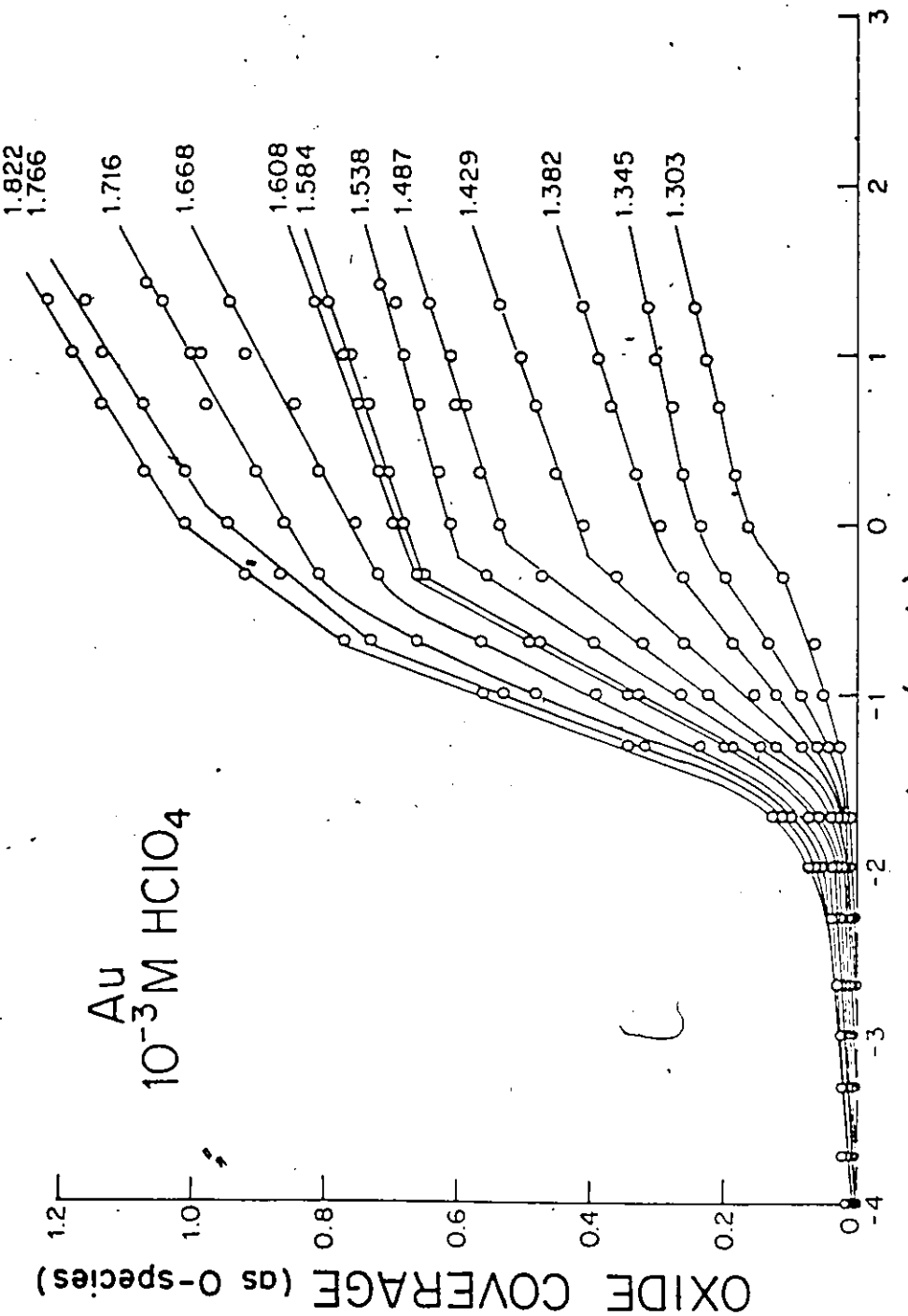

Figure 4-8 Variation of oxide coverage (as O species) formed on Au in 10^{-3} M $HClO_4$ at various oxide growth potentials for growth periods of 10^{-4} s up to 20 s, 298 K; plotted as Θ vs log τ_h.

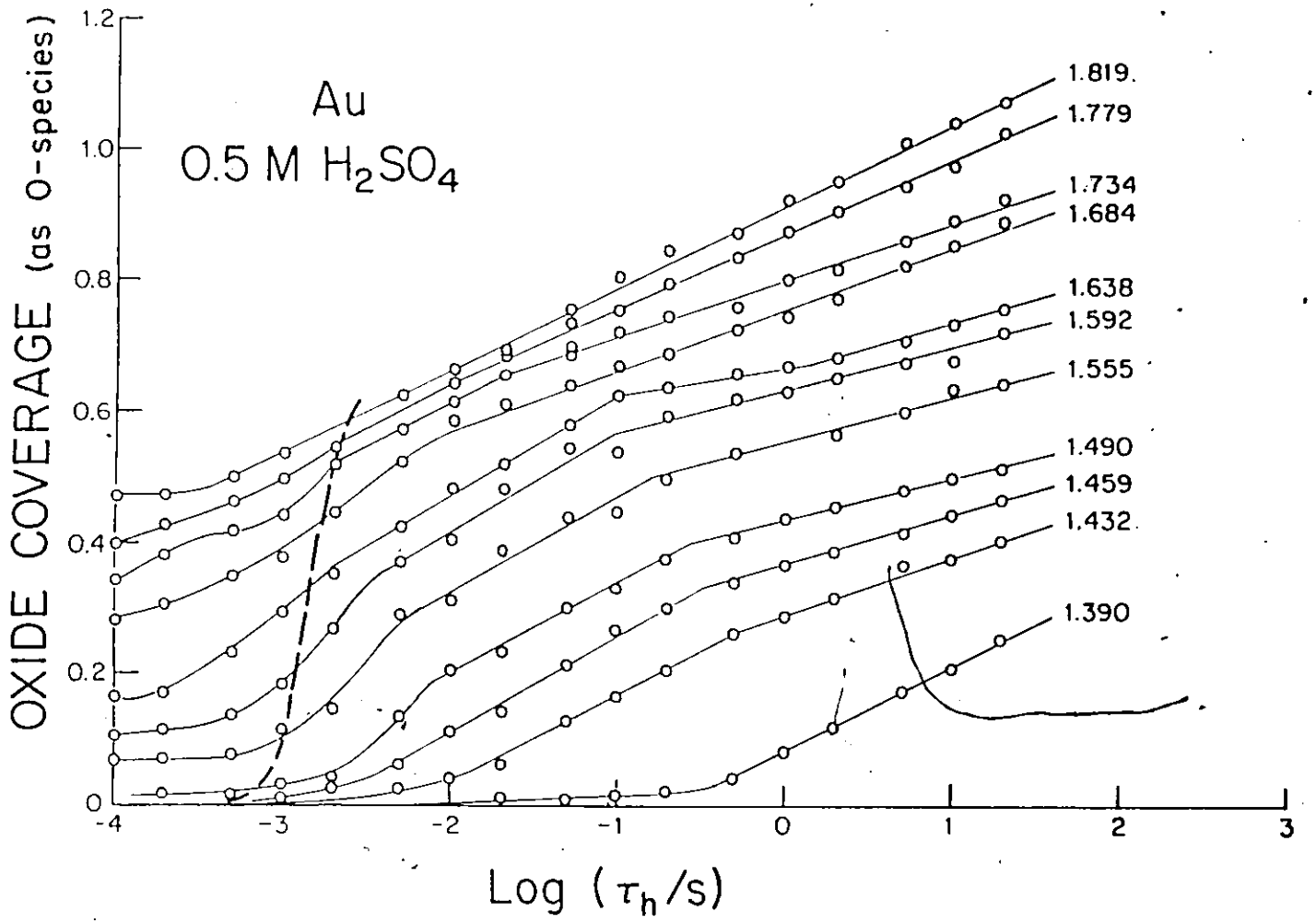

Figure 4-9 Variation of oxide coverage (as O species) formed on Au in 0.5 M H_2SO_4 at various oxide growth potentials for growth periods of 10^{-4} s up to 20 s, 298 K; plotted as θ vs log τ_h.

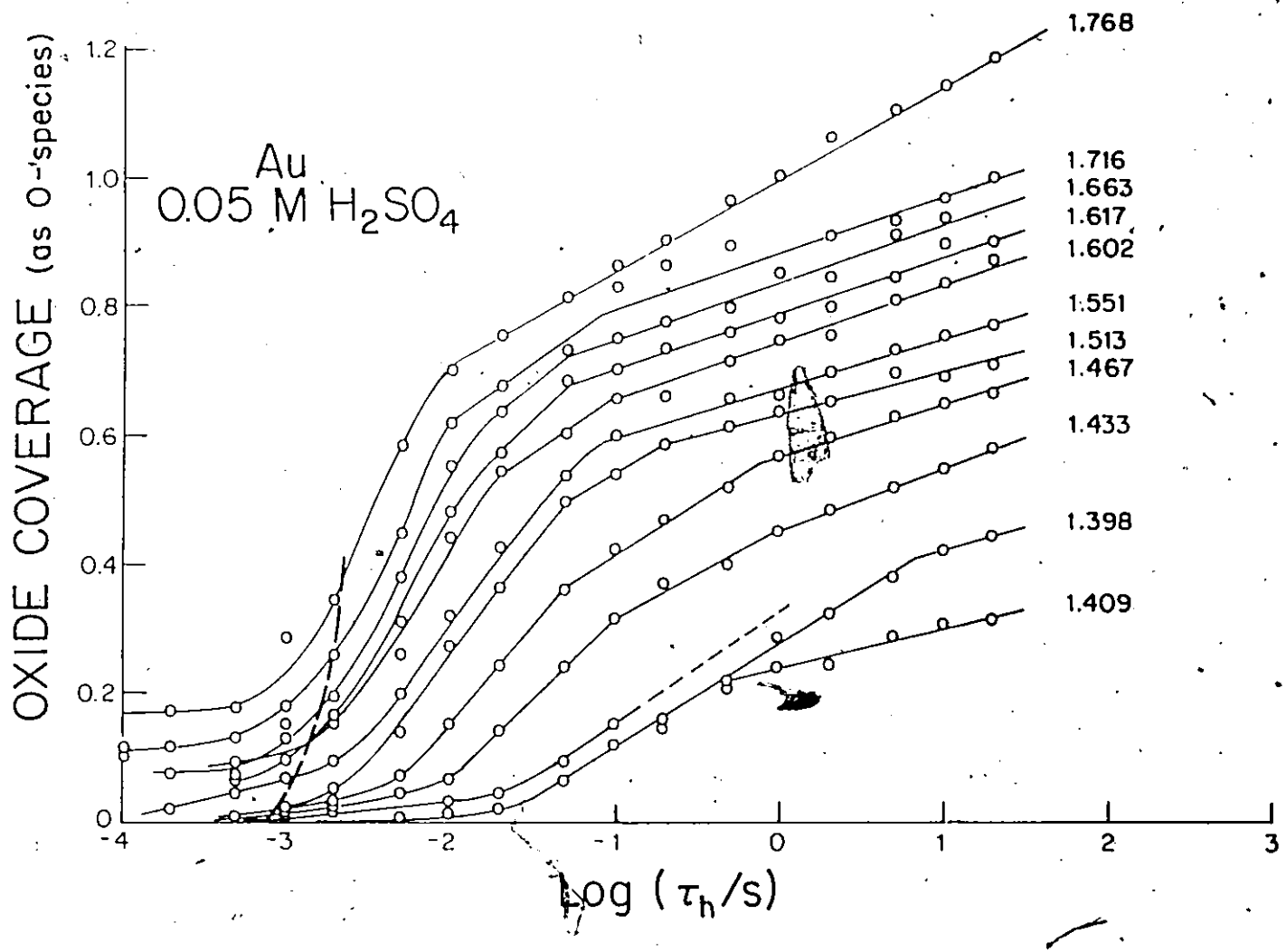

Figure 4-10 Variation of oxide coverage (as O species) formed on Au in 0.05 M H_2SO_4 at various oxide growth potentials for growth periods of 10^{-4} s up to 20 s, 298 K; plotted as Θ vs log τ_h.

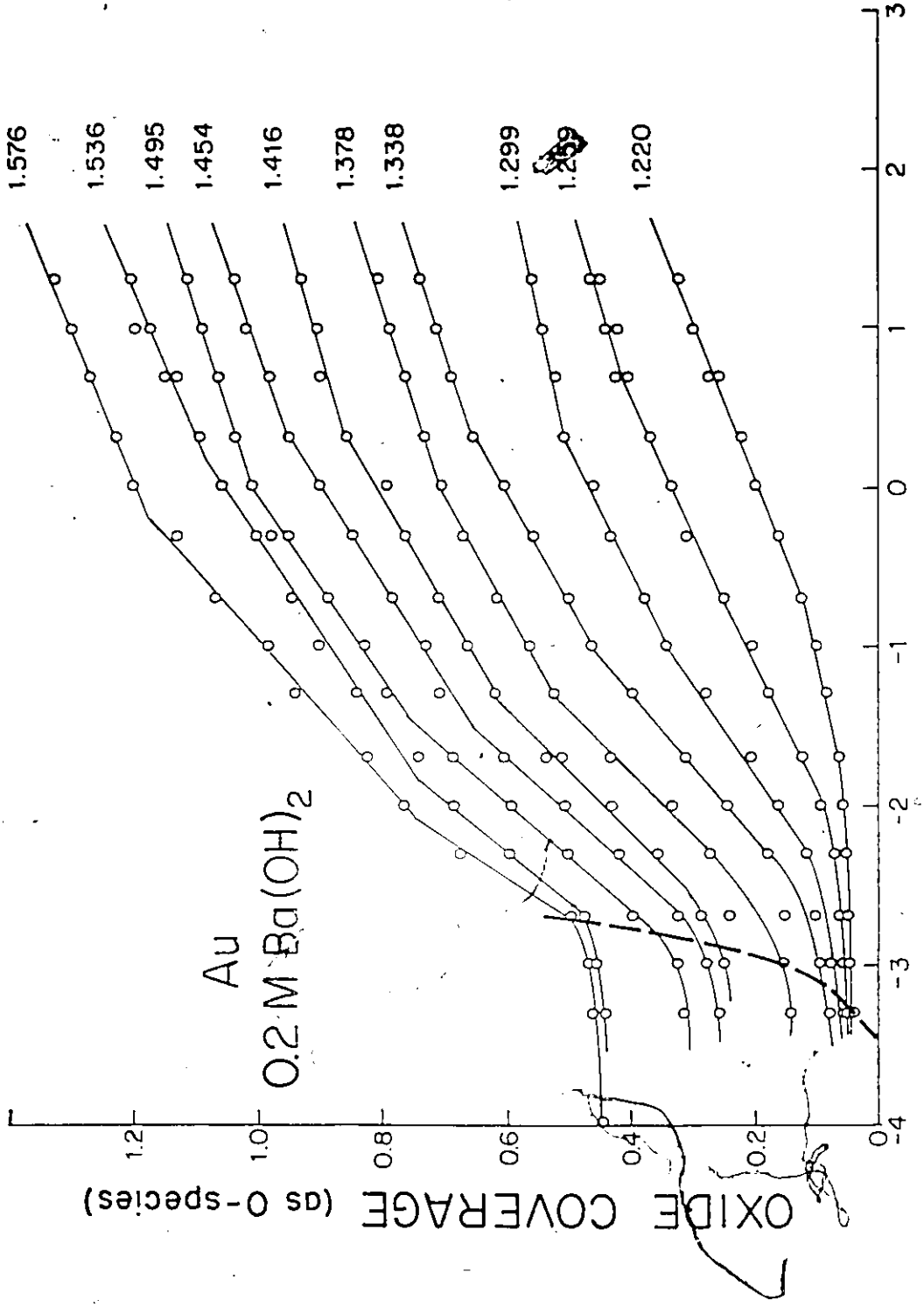

Figure 4-11 Variation of oxide coverage (O species) formed on Au in 0.2 M $Ba(OH)_2$ at various oxide growth potentials for growth periods of 10^{-4} s up to 20 s, 298 K; plotted as θ vs log τ_h.

Close examination of the features of the Θ vs log τ_h curves of Figures 4-6 to 4-11, especially in comparison with Figure 4-12, shows that the type of relations in Figure 4-12 is not found at all the holding potentials in any solution. Stage I behavior is found only at the lowest holding potentials for several reasons:

i) a significant sweep time, τ_s, even at 200 V s^{-1}, can complicate the growth time at the higher end potentials of the anodic sweep (e.g. traversing 200 mV at 200 V s^{-1} takes 10^{-3} s), as explained above;

ii) arguments and calculations about to be presented show that the potentials involved in stage I deposition of oxygen species are well displaced from the reversible condition and therefore lead to deposition of coverages of oxide exceeding those associated with Stage I behavior in immeasurably short times, e.g. 10^{-5} s or less; and

iii) at higher anodic end potentials, it becomes likely that more than one derivative peak (each with significant current in an appropriate deconvolution), is now contributing to oxide growth so that a single growth process is no longer measured over a large enough range of oxide growth potentials to permit the kinetic analysis, described below to be made for a single peak in the profile. Adequate corrections for the sweep time effect have, however, been made in Figures 4-6 to 4-11. The dashed line represents the sweep time, τ_s, associated with time spent at oxidizing potentials in the anodic sweep before the end potential at which growth is measured is attained. Data points to the left of this line involve the sweep time effect and are, therefore, not used in subsequent calculations.

Sections II and III of Figure 4-12 (and in Figs. 4-6 to 4-11) are direct logarithmic relations with a clear discontinuous transition between the two sections, and are observed for all solutions and for all but the highest and lowest "holding" potentials.

Several details of the Θ vs log τ_h plots give insight into the mechanism of oxide growth and, in conjunction with the corresponding i vs V profiles, subsequent reduction of the oxide species involved. The following observations refer to Figures 4-6 to 4-11 and the three stages of oxide growth observed therein.

i) The charge integration reveals that the rate of oxide growth decreases with time throughout the periods of growth, τ_h. A clear break is observed between the two seemingly linear sections of the Θ vs log τ_h plots at higher τ_h (i.e. sections II and III in Fig. 4-12).

ii) The effect of potential on each of the sections II and III is just to raise the curve in Θ for each successive potential. Thus, when slopes $\left(\frac{d\Theta}{d \log t}\right)_V$ are measured for each section and at each potential it can seem that the value of these slopes is essentially constant for each section for the majority of anodic end potentials studied. Figure 4-13 illustrates this constancy for 1.0 M $HClO_4$ and 0.5 M H_2SO_4. As described in the discussion of kinetics which follows, this effect of potential can be employed to calculate an apparent Tafel parameter for Stage II.

4. Kinetics of the Section I (Fig. 4-12) Process

Section I data of Figures 4-6 to 4-11 are represented by a linear log $(1-\Theta)$ vs t relation. It is found that the first stage (I) can be adequately represented by a kinetic equation based on electrochemical control as a rate-determining step. Thus, a linear log $(1-\Theta)$ vs t

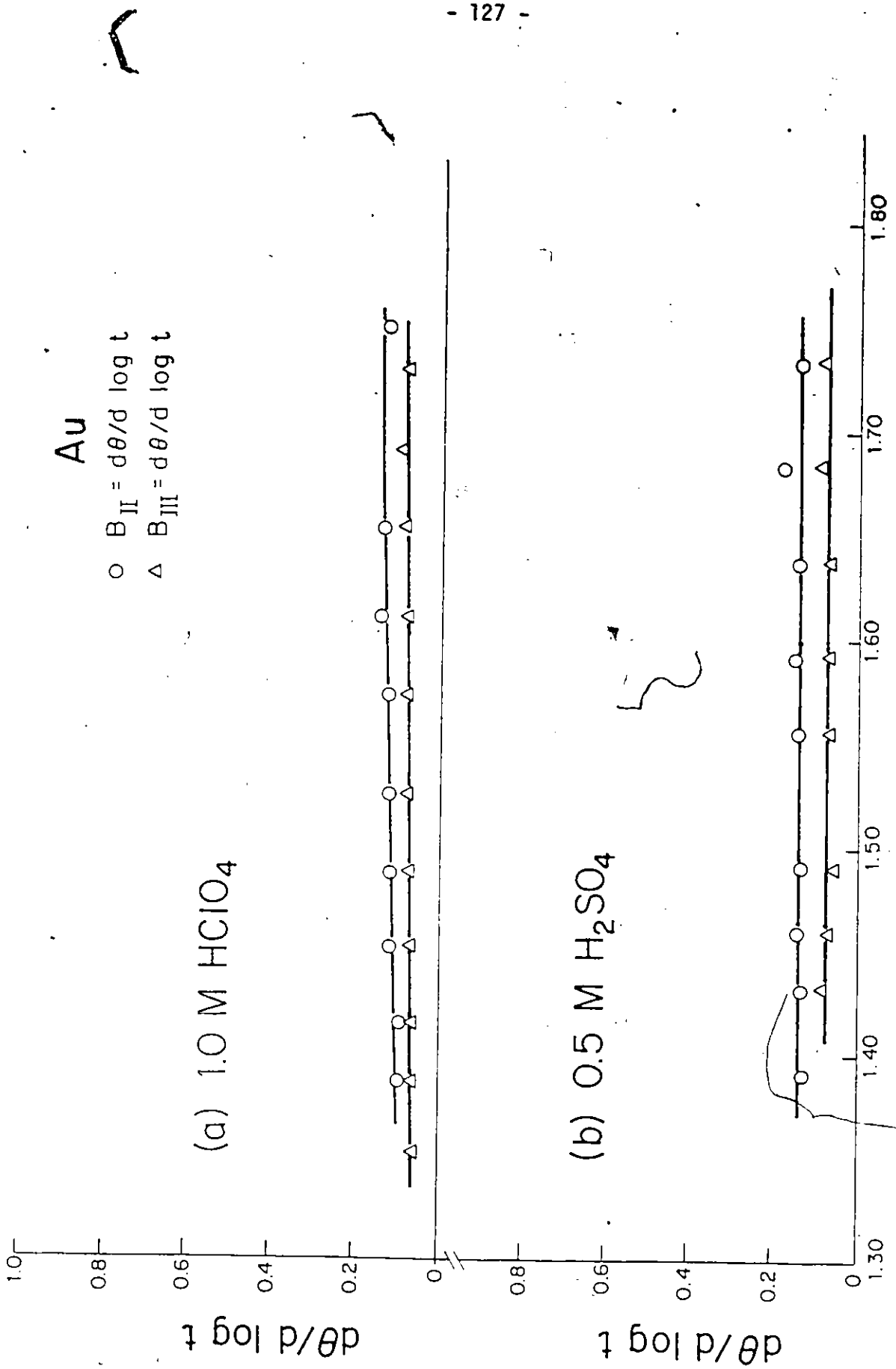

Figure 4-13 Variation of slopes ($d\theta/d \log \tau_h$) observed in stages II and III of oxide growth at constant potential (from Figs. 4-6 and 4-9) as a function of oxide growth potential.

relation develops from a general representation of the rate for the early stages of oxidation for a reaction of the type

$$Au + H_2O = AuO + 2H^+ + 2e \qquad I$$

where $$\text{Rate} = \frac{d\Theta}{dt} = kc_{H_2O}\,(1-\Theta)\,\exp[\alpha 2VF/RF]\,\exp(-g\Theta) \qquad (4\text{-}1)$$

and Θ_T is the coverage due to all deposited species.

It will become apparent that the following derivation is not altered by the actual choice of a reaction for I.

In the early stages of oxide deposition (low Θ), the interaction term in $g\Theta$ may be neglected, giving:

$$\text{Rate} = \frac{d\Theta}{dt} = kc_{H_2O}\,(1-\Theta)\,\exp[\alpha 2VF/RT] \qquad (4\text{-}2)$$

It is not clear whether this assumption is valid because the operative g-value is zero (e.g. for random, early deposition) or because the coverages investigated are quite small (so that $e^{-g\Theta} \rightarrow 1$).

Eqn. (2) may be integrated to give

$$-\ln(1-\Theta) + \ln(1-\Theta_o) = A\,t \qquad (4\text{-}3)$$

where $$A = kc_{H_2O}\exp[\alpha 2VF/RT] \qquad (4\text{-}4)$$

and, for a series of potentials,

$$dV/d\ln A = RT/\alpha F \qquad (4\text{-}5)$$

which gives the Tafel slope, b.

The experimental data obey these equations for a range of potentials in each solution and samples of these plots are shown in Figure 4-14 for 0.05 M H_2SO_4 and for 0.2 M $Ba(OH)_2$. Equation (4-3) fails to represent the data in these figures with the characteristic that a <u>much</u> longer t_h is required to obtain the $(1-\Theta)$ value needed for the straight line relation (e.g. Figure 4-14b for 0.2M $Ba(OH)_2$) to be

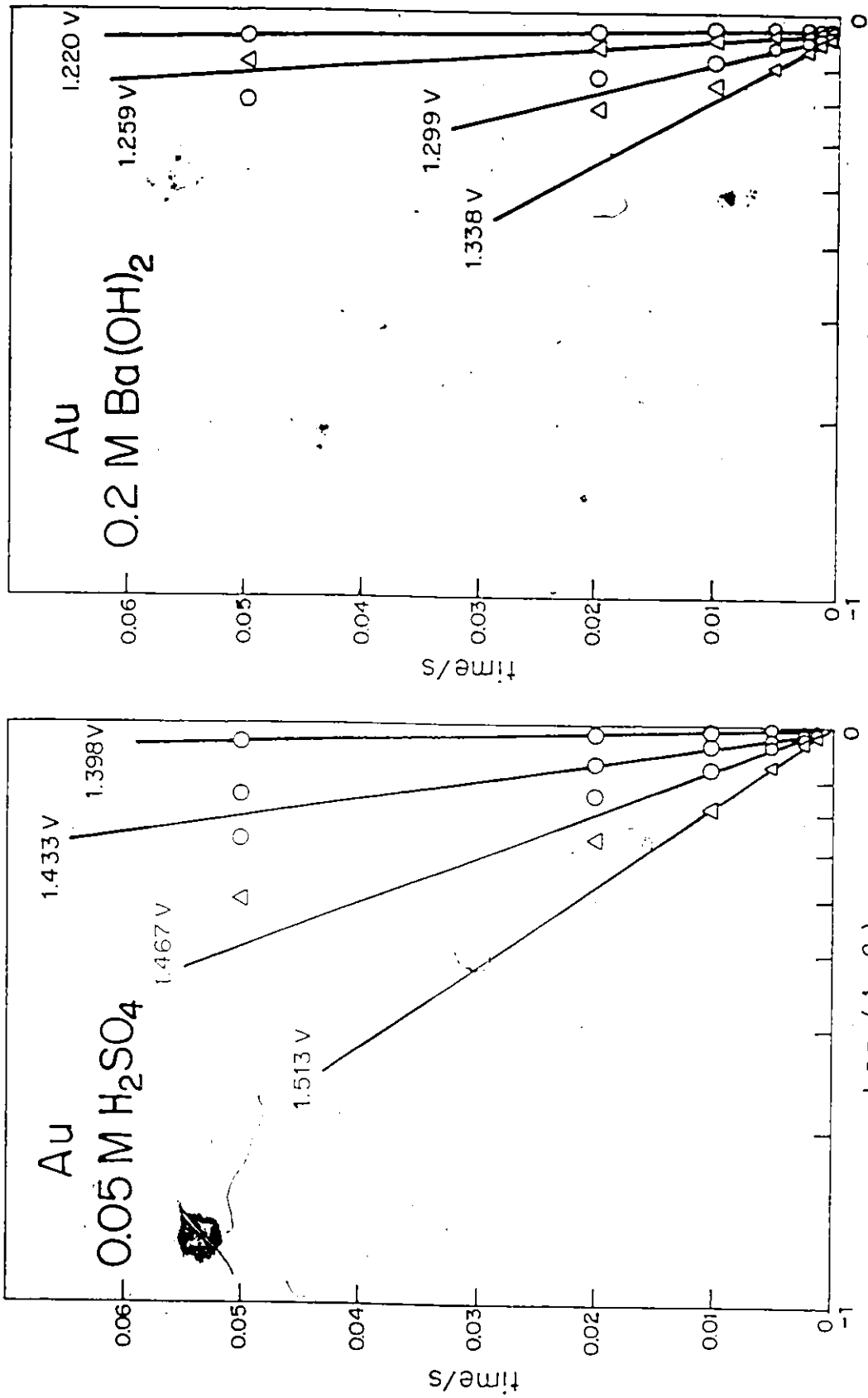

Figure 4-14 Plots of (1 - θ) vs t testing the applicability of eqn. (4-3) for electrochemically controlled oxide deposition at constant potential at Au.

extended. The linear log relation (eqn. 3) is obeyed when sweep-time effects (p.125) do not vitiate the holding time experiments. These figures have been constructed for each solution and have been used to determine A values (eqn. 4-3) for oxide growth rate at each growth potential. These A values are then plotted vs their corresponding potentials for each of the solutions (Fig. 4-15). The gradient of these V vs ln A plots (Fig. 4-15) gives the Tafel slope associated with section I of the Θ vs log τ_h plots as expected from eqn. 4-5. Table 4-1 summarizes those values for several solutions.

TABLE 4-1

SOLUTION	$\frac{dV}{d \log A} = 2.3\ b$
1.0 M $HClO_4$	0.057
0.1 M $HClO_4$	~ 0.060
0.5 M H_2SO_4	~ 0.060
0.05 M H_2SO_4	0.057
0.2 M $Ba(OH)_2$	0.062

The straight line behavior predicted for log A vs V is observed for the range of potentials represented in Figure 4-15 and, for the most part, a Tafel slope of RT/F is observed. There are several possible mechanistic interpretations of such a value for the Tafel slope and they will be discussed subsequently in Chapter 8 after additional kinetic information has been presented. However, one possible hypothesis is that a $2e^-$ charge-transfer step is involved in the rate-controlling step in the initial stages of oxide deposition. However, there are two data points evident in Figure 4-15, for 0.1 M $HClO_4$ and 0.05 M H_2SO_4, where oxide

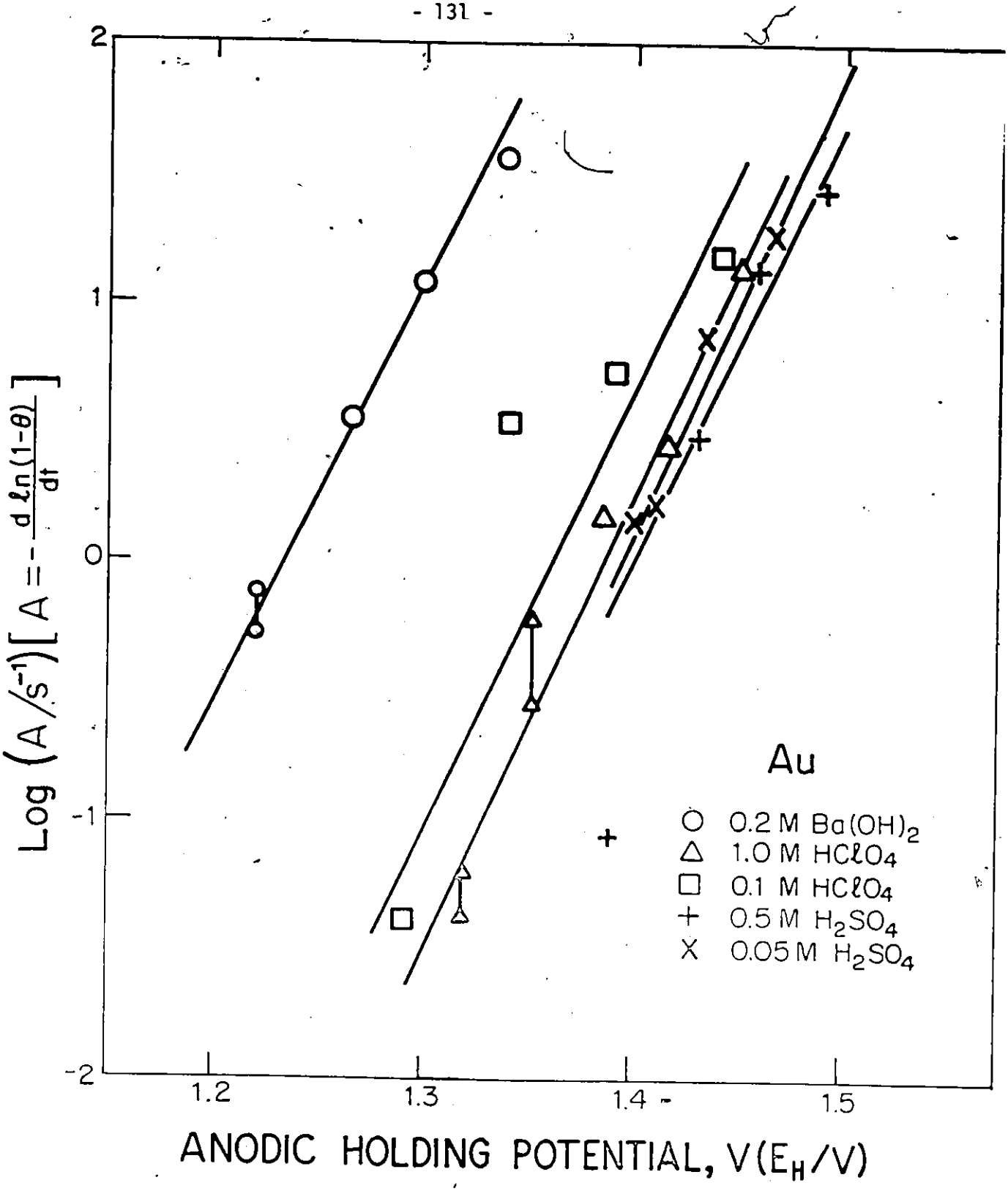

Figure 4-15 Plots of Log A vs oxide growth potentials using eqns. (4-3) and (4-5) to determine Tafel slopes for irreversible, electrochemically controlled oxide deposition in Stage I of oxide growth at constant potential at Au.

growth is measured at a potential very near that at which oxide deposition is first observed in an i vs V profile in the same solution, and for which the value A (from the slope of a plot of -ln (1-θ) vs t) is anomalously low in Figure 4-15 (log A vs V). Similarly, the Tafel slopes evaluated from the variation of peak potential vs log s in sweep rate studies for the initial O_{A2} oxidation peak are very low; they vary somewhat from solution to solution but have values of the order of 20 - 30 mV (see Chapter 6).

The explanation for both these results lies in the effects of ions on the earliest stages of oxide deposition, and the complex interrelationship between ion desorption and concomitant oxidation of the Au surface. Thus, as potential is increased in an anodic sweep, anions are held more strongly to the electrode. These ions must be removed, however, to permit oxidation of the underlying metal.

As it is seen from Figure 4-15, substantial differences in A-values for a given potential are observed for the different solutions and reflect specific ion adsorption effects in relation to electrode potential.

As the potential at which oxide is grown is increased positively, it appears that oxide growth can occur in more than one surface state as indicated by distinguishable peaks in the i vs V profiles. Thus, only that oxide growth which occurs at the lower potentials would have unequivocal value in determining the Tafel parameters for section I (Fig. 4-6 to 4-12).

5. "Direct" Logarithmic Oxide Growth

The second and third stages of oxide growth shown in Figure 4-12, where linear relations between θ and log t are demonstrated, represent

a mechanism for continuation of oxide growth in which physical, i.e. non-electrochemical, steps are apparently rate-controlling. This conclusion is reached because the effect of potential on each of the sections II and III for several different solutions is seen to be simply to raise the respective curves in Θ for each successive potential without changing the slopes of the Θ vs log t relations, as may be seen in Figure 4-13. This also means that the actual rate of reaction at given $t = \tau_h$ is constant, independent of potential. Surprisingly, they are also independent of coverage Θ. These two properties of the behavior seem to indicate firstly that a non-electrochemical reaction is rate-controlling and, more importantly, that rates of oxide growth in these stages are not determined by how much oxide (Θ) has been deposited previously.

A better understanding of the significance of effects of potential in relation to oxide growth can be gained by considering the origin of the direct logarithmic growth laws, as follows.

A direct logarithmic law can easily be derived on the assumption that the rate constant, k, which may or may not be a function of potential V for the deposition/growth process is exponentially dependent on coverage or that the corresponding activation energy increases linearly with coverage. If k is a function of potential [$k = k(V)$], $k(V)$ will probably have the exponential form $e^{-\alpha VF/RT}$ where α is a transfer coefficient. Thus a reaction rate expression

$$\left(\frac{d\Theta}{dt}\right)_V = k(V) \exp(-g\Theta) \qquad (4\text{-}6)$$

would result which can be integrated at constant V, giving

$$\frac{1}{g} \exp[g\Theta] = k(V)\, t + c \text{ where c is an integration constant.}$$

Then $g\Theta = \ln g + \ln k(V) + \ln (t + \frac{c}{k}(V))$

i.e. $\Theta = \frac{1}{g} \ln g + \frac{1}{g} \ln k(V) + \frac{1}{g} \ln (t + \frac{c}{k}(V))$ (4-7)

which is a direct logarithmic law in t when $t >> c/k(V)$, i.e.

$$\frac{d\Theta}{d \ln t} = \frac{1}{g} \quad (4\text{-}8)$$

This equation shows that the slope of the linear sections of the Θ vs log t plots of experimental data would be interpreted in terms of the interaction parameter, g. An alternative significance for the exp $(-g\Theta)$ term is that it arises really from a change of the effective potential difference across the interface due to progressive change of the surface dipole p.d., χ_Θ, proportional to Θ. Thus $V_t = V_o - \chi_\Theta$ could be written for the effective potential V_t operating across the interface during growth at time t. χ_Θ will be approximately proportional to Θ and since k(V) is an exp f(V), the form of eqn. (4-6) would arise from a build up of the surface dipolar layer of O species on the Au surface. A similar effect could arise from changes of anion adsorption.

Equation (4-7) indicates that the progressive increases in Θ observed at a given t for a series of oxide growth potentials may be attributed to the increase of the potential-dependent rate constant k(V) in the term $\frac{1}{g} \ln k(V)$ or to an equivalent increase in the initial oxide coverage at various potentials before the growth in ln t has significantly taken place.

The integrated result, eqn. (4-7) shows that Θ as f(ln t) depends only on 1/g except that the level of Θ values depends on $(1/g) \ln k(V)$ and thus on potential for the case $k = k(V)$. Experimentally, the slopes of given sections of the Θ vs ln t relations are the same at various Θ values, i.e. the rates expressed at $d\Theta/d \ln t$ are independent of Θ. However, this seems inconsistent with the form of eqn. (4-6) but is a result of the

integration operation.

Although direct growth laws in ln t have been used previously (see p. 9 and 10), and were based intuitively on either an exponential term in Θ or in oxide film thickness, δ, the main problem physically with the rate equation (4-6) required to give the ln t relation after integration has not, apparently, been recognized; it is that it contains no term in the fractional free area of the electrode surface $1 - \Theta_T$ (where $\Theta_T = \Theta_O + \Theta$ anions) which would be expected to be required in a rate equation of the type of (4-6) representing, supposedly, continuing deposition or growth of O species.

If such a term is included, then the resulting rate equation, viz. $(d\Theta/dt)_V = k(V)\ (1-\Theta_T)\ \exp\ (-g\Theta)$ cannot be integrated to a direct growth law in ln t. In fact, no other equation, except the obvious one $d\Theta = k(V)\ dt/t$, which has no clear physical significance here, will integrate to a simple relation in ln t. Further, it is not that $1-\Theta_T$ can approach 1, i.e. $\Theta_T \to 0$ as a special case, since the same direct ln t law is found in the present work and in a variety of other studies on very thin oxide film growth where Θ_O or Θ_T is by no mean negligible.

The required rate equation such as (4-6) must therefore be zero order in $1-\Theta_T$ or else there must be a cancellation of Θ terms implicit in $g(\Theta)$ or $k(V)$ with $1-\Theta_T$. How this could arise is physically difficult to visualize.

The required zero order in free area $(1-\Theta_T)$ of the electrode for eqn. (4-6) might arise if the rate-determining process in growth were not the actual deposition reaction itself, e.g. it could be the act of place-exchange of already electrodeposited "AuO" species in small oxide clusters or desorption of an anion, A^-, at a potential growth center (see p. 257).

In the latter case, however, it would be expected that a term in Θ_A would be significant in the rate equation (4-6). At the present time no proper solution to this dilemma can be proposed nor has it been offered in previous literature.

If it is considered that eqn. (4-6) is of the form where k = k(V), then the logarithmic growth lines of Figures 4-6 to 4-11 can be treated according to eqn. (4-7) to obtain the implicit potential-dependence of the growth process, represented by this k(V). Consideration of two conditions provides the required result: (a) when the relation between Θ and time is linear simply in ln t, c/k(V) = 0; then the growth lines can be extrapolated to Θ = 0 giving corresponding times t_o, viz. from eqn. (4-7)

$$0 = \frac{1}{g} \ln g + \frac{1}{g} \ln k(V) + \frac{1}{g} \ln t_o \qquad (4\text{-}9)$$

(b) when t = 1, for various potentials V

$$\Theta_V = \frac{1}{g} \ln g + \frac{1}{g} \ln k(V) \qquad (4\text{-}10)$$

where Θ_V is valuated from the log growth lines.

These relations and the slopes (1/g) of the Θ vs ln t lines enable -ln t_o to be plotted vs V e.g. as shown in Figure 4-16 for Stage II in 0.1 M $HClO_4$. This plot gives a Tafel type relation with a slope, b, of 0.062 V. Similar slopes written as 2.3 b, obtained for other solutions, are listed in Table 4-2.

TABLE 4-2

Solution	2.3b (II)/V
1.0 M $HClO_4$	0.059
0.1 M $HClO_4$	0.062
0.5 M H_2SO_4	0.054
0.05 M H_2SO_4	0.034 (0.101)
0.2 M $Ba(OH)_2$	0.059

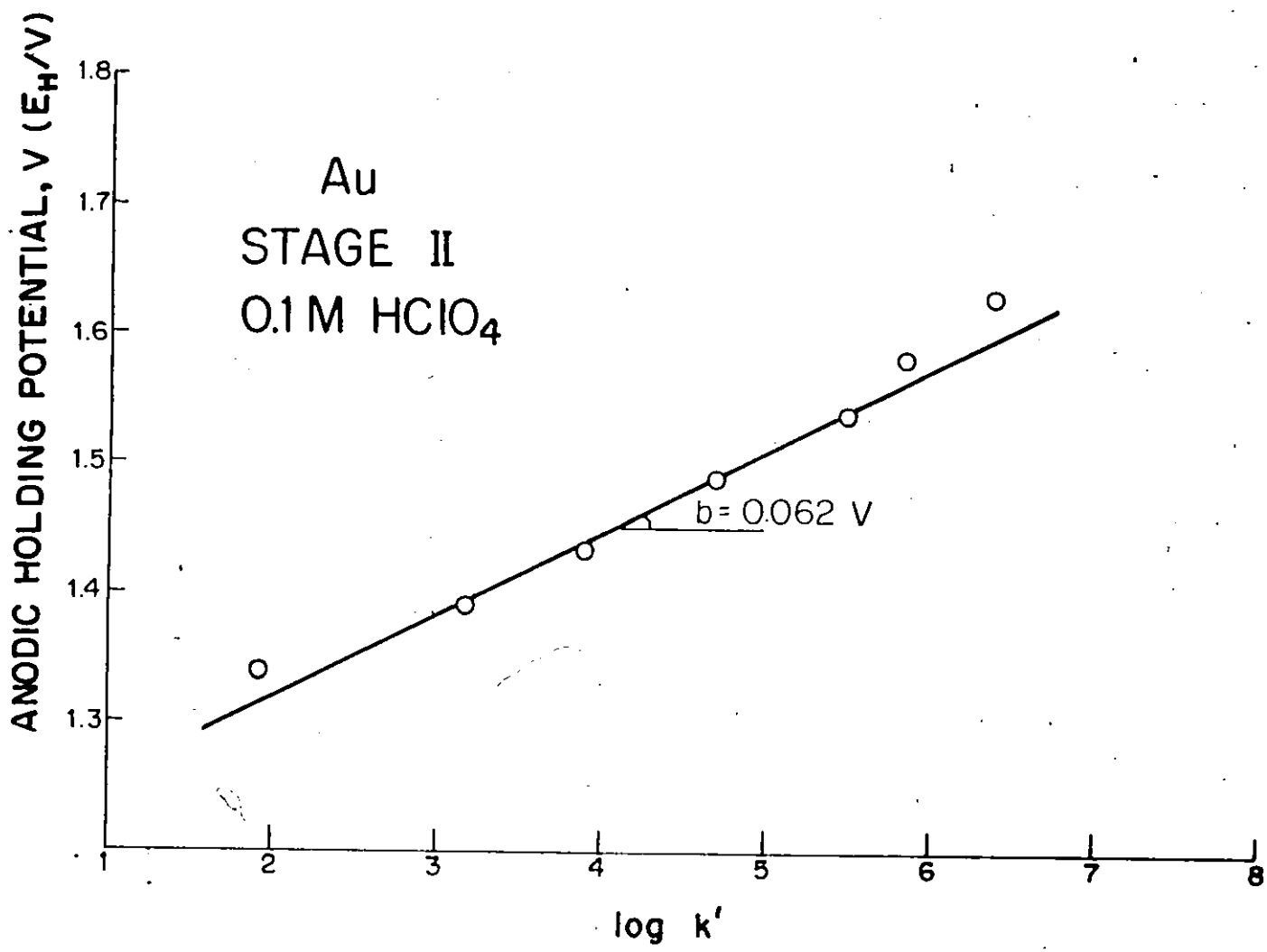

Figure 4-16 Evaluation of Tafel slope using time intercept values (to $\theta = 0$) for Stage II of oxide growth at constant potential at Au at several potentials, 0.1 M $HClO_4$.

It is of interest that most of these slopes correspond to a 2-electron transfer as also deduced from the kinetics of stage I where electrochemical control applies [see section 4 in this chapter].

6. Phenomenology of Oxide Development: The Growth Curves

In general, quite apart from any equations derived above and the question of whether or not straight-line plots of the data are obtained, it is apparent from the θ vs log τ_h curves that, with time, at any given constant potential, oxide growth becomes more and more difficult; thus, the rate of growth of oxide is always decreasing with time (cf. eqn. 4-6) under these conditions. This constitutes strong evidence against the operation of a mechanism of nucleation and growth in the development of the oxide with time at constant potential where a transient in time of the form  rather than  is usually observed.

The charge data indicate that it is possible to observe the second and third stages of oxide growth occurring through exactly the same oxide coverage range, a surprising result. Thus, at different constant potentials, oxide growth is proceeding through the II and III stage mechanisms, corresponding to the θ vs log τ_h plots, over the same coverage range (θ_1 to θ_2), though for different growth times. Thus, for example, Figure 4-9 shows θ vs log τ_h data for 0.5 M H_2SO_4 in which stage III growth is observed at 1.490 V between θ = 0.4 - 0.55 while, at 1.555 V, stage II growth of oxide is seen between θ = 0.3 - 0.56.

At low potentials, it appears that stage III behavior does not take place when the potential is applied up to even 20 s growth time (Figures 4-7, 4-9 and 4-11). It appears, then, that some minimum potential or minimum oxide coverage is required before oxide growth via stage III is observed. Comparison of the θ vs log τ_h data, e.g. for 0.5 M H_2SO_4,

indicates that at a constant growth potential of 1.390 V the break in the Θ vs log τ_h curve (indicating a transition from stage II to stage III conditions) and stage III behavior is not observed even up to τ_h = 20 s and with Θ = 0.25. However, at 1.432 V in 0.5 M H_2SO_4, the transition from II to III is apparent at Θ = 0.26 and τ_h = 0.5 s.

Similarly, it appears that some minimum value of Θ must be attained before stage II behavior is observed.

Since the growth of oxide by stage II or III processes can evidently occur over the same Θ range but at different potentials; it would appear that when some minimum potential or minimum oxide coverage is attained in the oxidation, the transition from stage II to stage III oxide growth is dependent only on time or on some other process dependent on time. This is an interesting and unexpected result.

Comparison of the Θ vs log τ_h figures with the cathodic i vs V oxide reduction profiles used (by integration) to construct them, reveals the important information that, in all solutions, stage II oxide growth is accompanied by an increase in oxide in states which are reduced in the O_{C2} and O_{C3} peaks of the cathodic i vs V sweep profile. However, stage III oxide growth apparently occurs after saturation of the O_{C2} state and proceeds with an increase in only the O_{C3} state (illustrated below Fig. 4-17 to 4-19) in the cathodic sweep profile.

Work on oxide growth on Au published in the literature has usually presented quite different results and conclusions than in this study for several reasons, including the following:

i) Θ values (measured only as $\mu C\ cm^{-2}$) have generally exceeded 1.0 (as O species) in previous work (e.g. Vetter and Schultze on Pt[65] and extended in ref. 59 to Au; also the work of Brummer[54] and Makrides[85]).

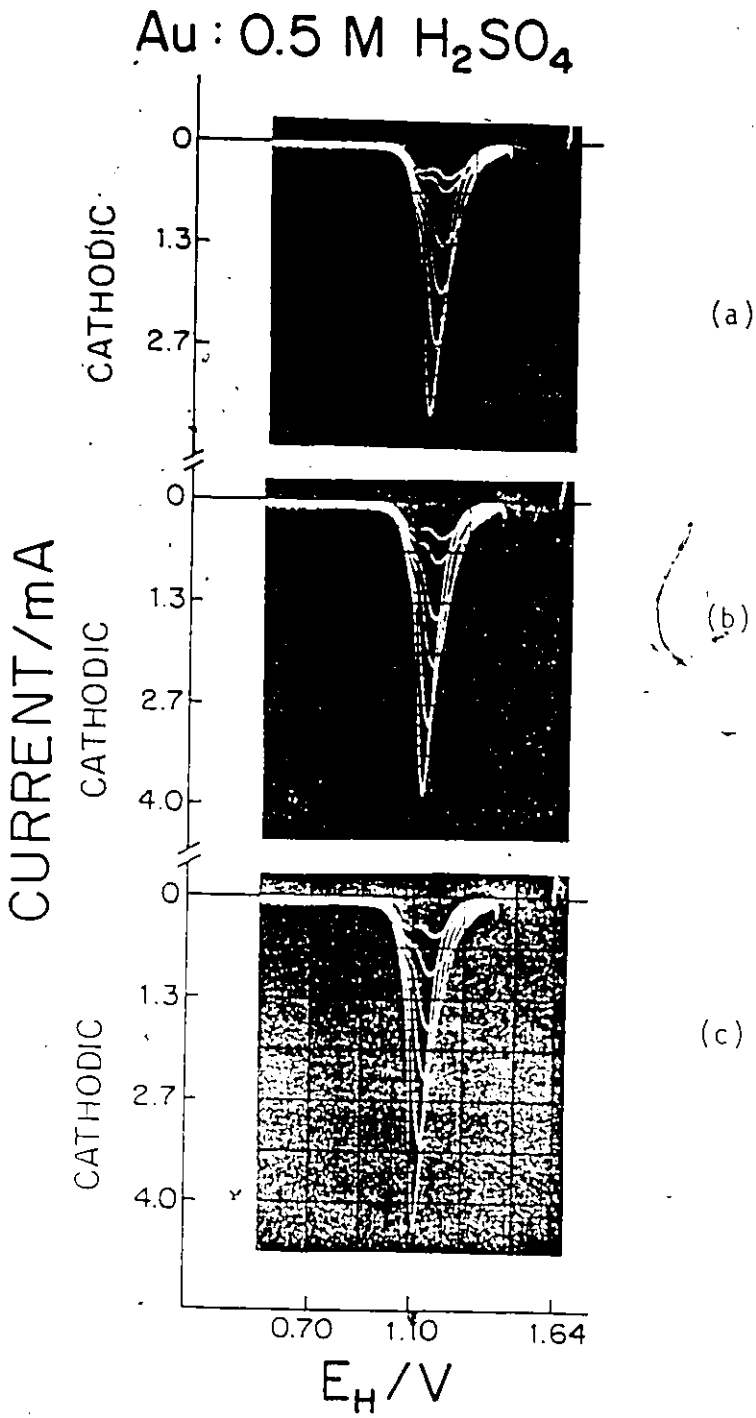

Figure 4-17 Potentiodynamic current-potential profiles for oxide growth at constant potential of 1.64 V at Au in 0.5 M H_2SO_4 for various growth times, τ_h. (a) τ_h = 10^{-4}, 10^{-3}, 10^{-2}, 0.1, 1.0 and 10 s; (b) τ_h = 5.0×10^{-5}, 5.0×10^{-4}, 5.0×10^{-3}, 0.05, 0.5 and 5s; (c) τ_h = 2.0×10^{-4}, 2.0×10^{-3}, 2.0×10^{-2}, 0.2, 2.0 and 20 s.

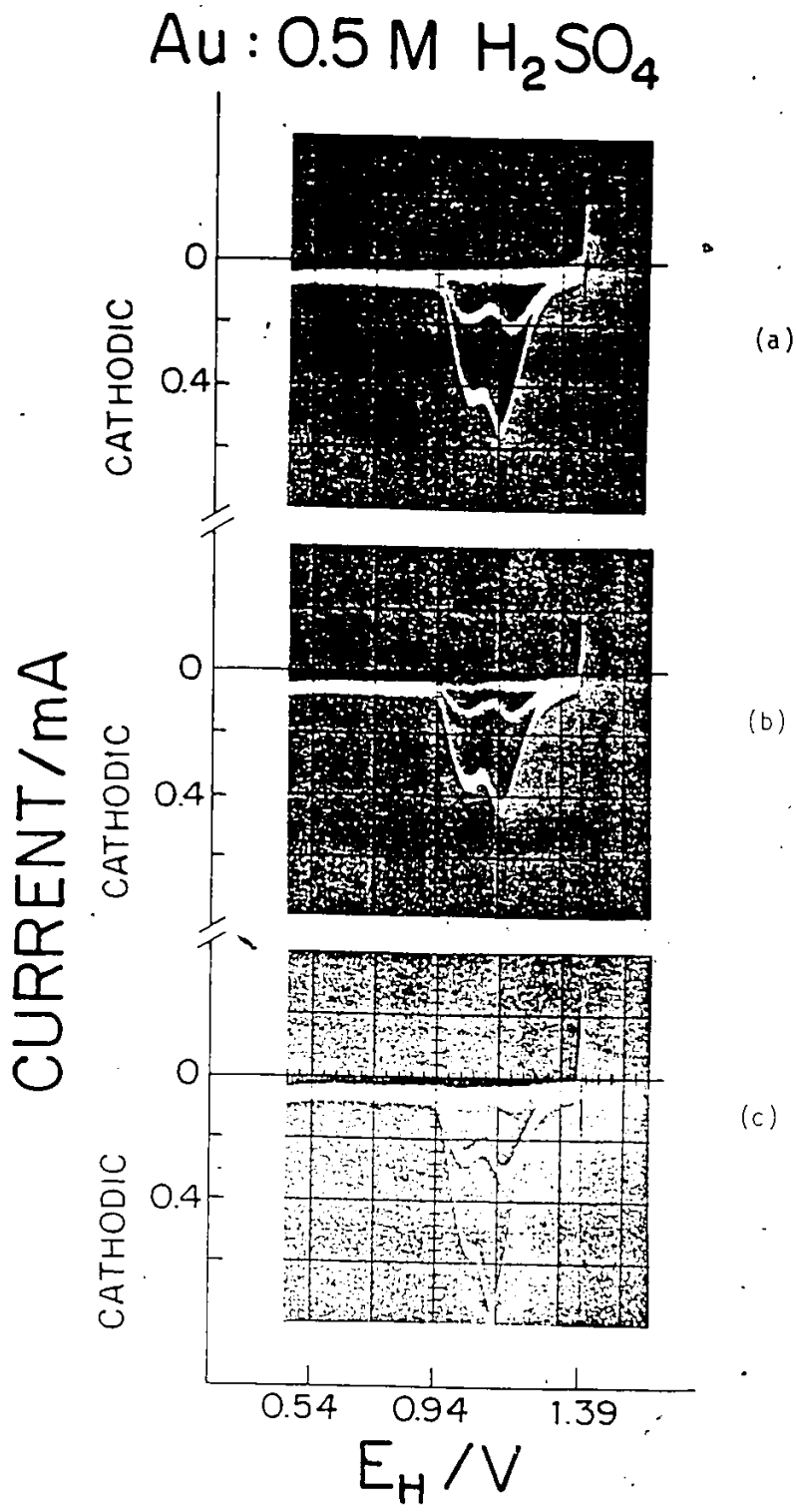

Figure 4-18 Potentiodynamic current-potential profiles for oxide growth at constant potential of 1.39 V at Au in 0.5 M H_2SO_4 for various growth times, τ_h; (a) τ_h = 0.1, 1.0 and 10 s; (b) τ_h = 0.05, 0.5 and 5 s; (c) τ_h = 0.2, 2.0 and 20 s.

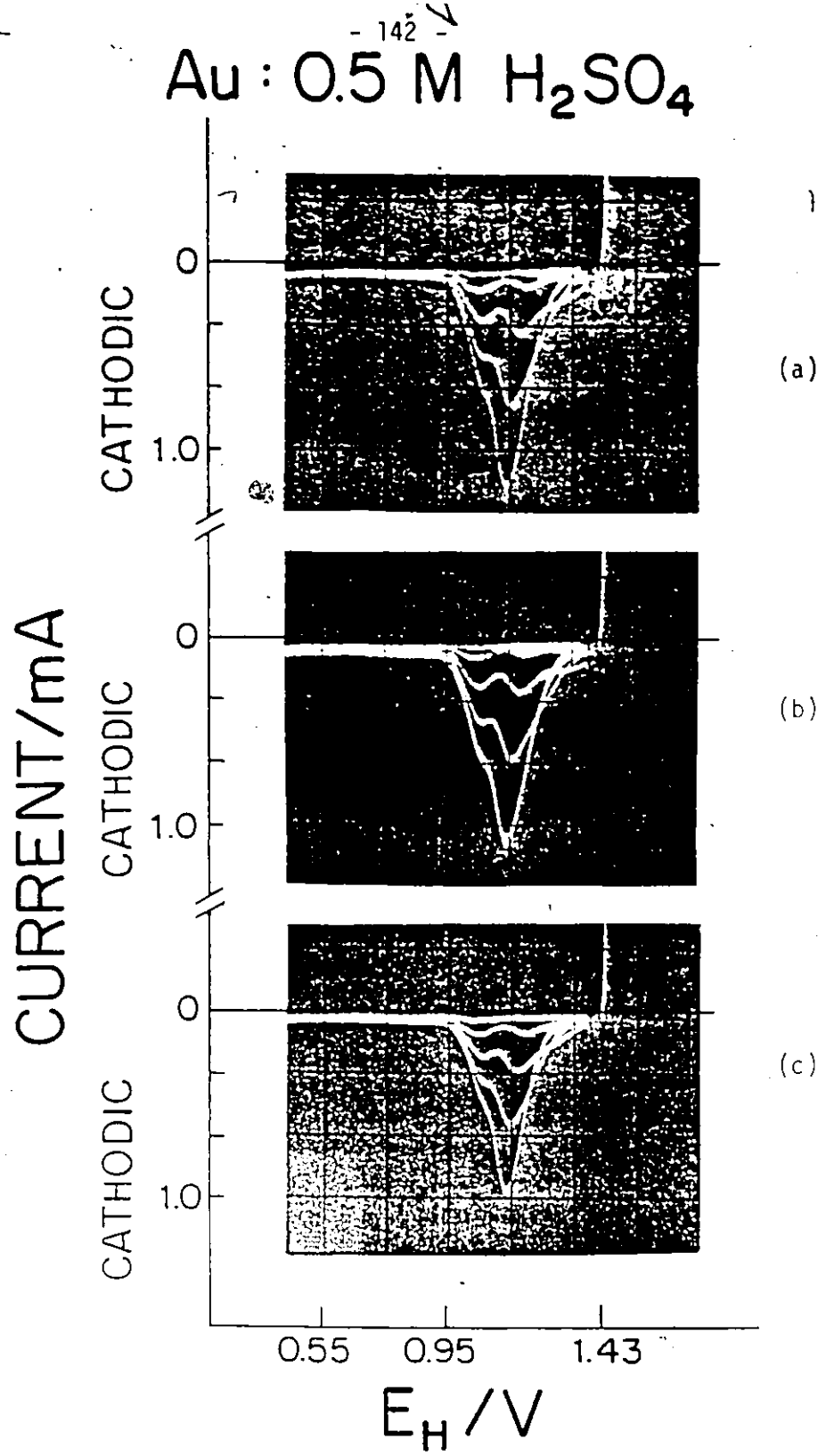

Figure 4-19 Potentiodynamic current-potential profiles for oxide growth at constant potential of 1.43 V at Au in 0.5 M H_2SO_4 for various growth times, τ_h; (a) τ_h = 0.01, 0.1, 1.0 and 10 s; (b) $\tau_h = 5.0 \times 10^{-3}$ 0.05, 0.5 and 5 s; (c) τ_h = 0.02, 0.2 and 20 s.

Thus the investigations did not apply extensively to growth in the submonolayer region investigated in the present work.

ii) Constant potentials used to grow oxide were generally around 1.8 V and higher at Au. This not only guarantees that oxide coverages greater than one monolayer will arise, but also introduces the probability of interfering reactions (e.g. O_2 evolution)[54,65,85].

iii) Time values investigated in some studies (during which simple dependence of Θ on log τ_h is said to occur) are 10^2 s or greater, much longer than the growth times investigated in the present study.

The submonolayer stages of oxide growth observed in the present work could not be detected at growth times of this relatively large order of magnitude. Such studies may actually indicate that stage III oxide growth involves a continuing, longer-term oxidation mechanism by which thicker oxides are formed on Au.

iv) Growth potentials were studied at intervals too great to detect the subtleties of submonolayer oxide growth (e.g. in the work of Gilroy on Pt[83]).

7. Reduction in Cathodic i vs V Profiles after Oxide Growth

Some further aspects of the stages of growth behavior of oxide films on Au are clarified by examination of the i vs V profiles for reduction of oxide films previously grown under controlled conditions. Other details on reduction are given in Chapter 5.

For each experiment in which oxide was grown at some constant potential for controlled periods of time, the subsequent i vs V reduction profiles provide information concerning the reduction of oxide species formed under the given conditions of growth potential and time. In particular, the quantitative evaluation of several diagnostic parameters (described on pages 55 to 59) clarifies several aspects of the oxide growth

curves (Figs. 4-6 to 4-11), especially for the direct logarithmic sections.

The development of the individual current peaks for reduction of oxide as growth time at constant potential or as growth potential is increased has been described earlier in this chapter (p. 111).

For very short times of growth, oxide grows with an increase in both the O_{C3} and O_{C2} peaks. It is evident (Fig. 4-17) that O_{C3} becomes the principal state through which the growth oxide film is reduced (i.e. the main "growth-peak") and the O_{C2} state becomes saturated. Thereafter O_{C2} is seen simply as a shoulder on the cathodic side of the main peak for the reduction of the growing oxide.

The peak potential of the O_{C3} reduction process moves to less positive values as higher extents of oxidation are attained. Simultaneously the peak itself becomes narrower as larger extents of oxide are reduced through state O_{C3}.

At fairly low oxide growth potentials, such as 1.390 V (Fig. 4-18) and 1.432 V (Fig. 4-19), it is evident (a) that oxide developed in the early stages of growth is reduced through the O_{C3} and O_{C2} states; (b) that the O_{C2} state becomes saturated at some value specific for the solution and (c) that subsequent oxide reduction occurs mainly through the O_{C3} state.

Several of these points may be quantified by evaluation of appropriate diagnostic parameters (see Chapter 3, p. 56). Figure 4-20 illustrates data from Figure 4-18 for growth associated with the O_{C2} peak showing that, while i/s increases with growth time, the peak potential, V_p, is virtually unchanged. At higher potentials and oxide-coverages, it appears also that i/s for O_{C2} reaches some constant saturation level, and that V_p for O_{C2} continues to remain constant. Exact measurement of these parameters is difficult at higher coverages due to the influence of the much

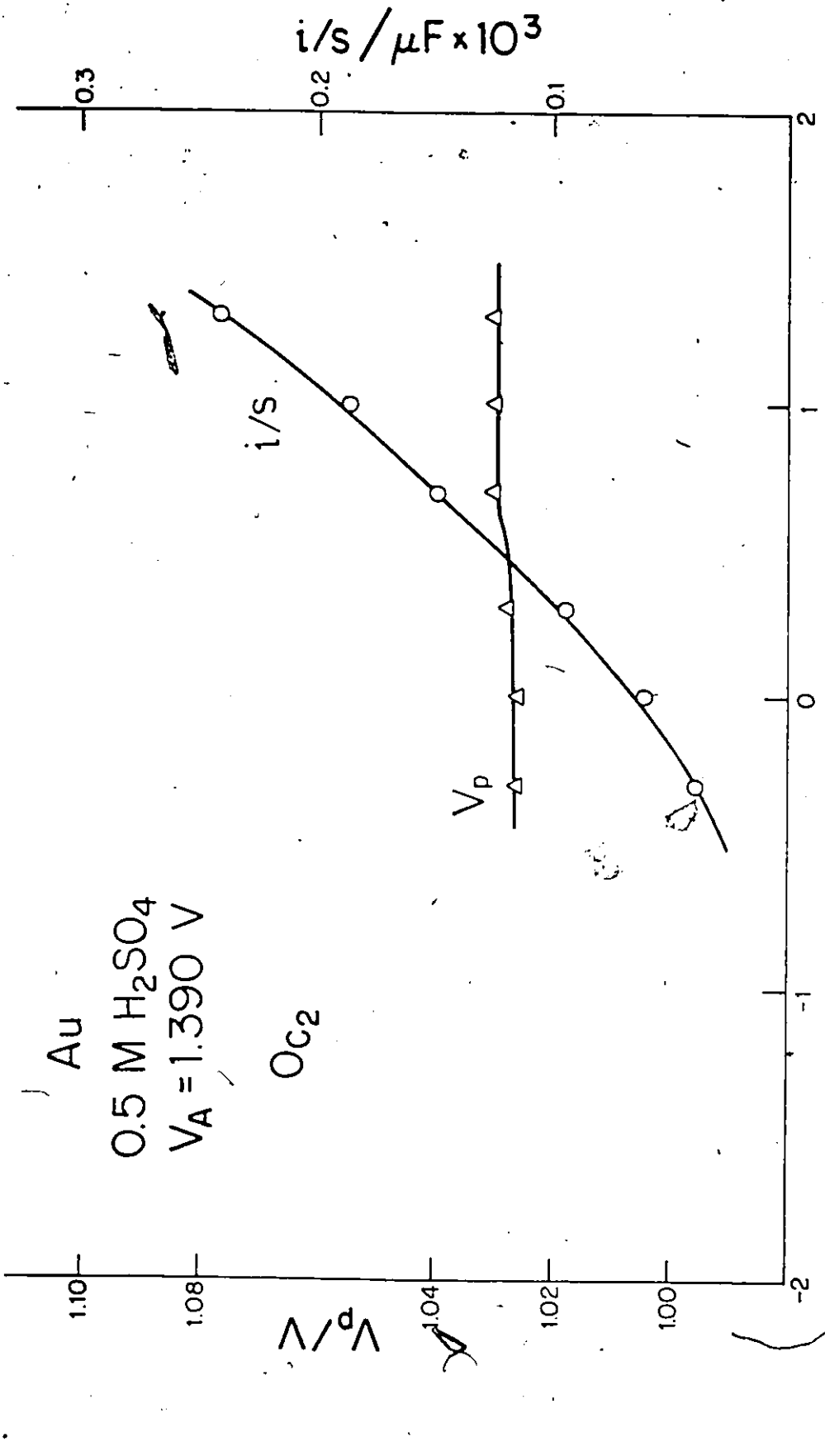

Figure 4-20 Variation of diagnostic parameters V_p and i/s for current peak O_{C2} in reduction i vs V profiles for oxide grown at constant potential of 1.39 V at Au in 0.5 M H_2SO_4 for various periods of time.

larger peak, O_{C3} (Fig. 4-19). For the latter peak, Figure 4-21 shows that i/s continues to increase with increasing time and V_p (O_{C3}) shows no sign of being constant but becomes more and more cathodic (i.e. the oxide species becomes harder to reduce) at longer growth times.

Additional data for higher coverages can be more revealing. Figure 4-22 shows the variation of i/s vs log τ_h for the O_{C3} peak for oxide grown at 1.638 V; the corresponding i vs V profiles are shown in Figure 4-17. The value for i/s increases smoothly with log τ_h from 10^{-3} s to 10 s. There is a slight break in i/s vs log τ_h at 0.2 ~ 0.5 s which coincides with the change of oxide growth kinetics from stage II to stage III. In addition, Figure 4-23 illustrates the concomitant shift in peak potential for O_{C3} over the same range of growth times and also shows the variation of peak half width parameter, $\Delta V_{1/2}$, as a function of time of oxide growth. It appears that V_p (O_{C3}) is constant at low growth times but begins to decrease smoothly with increasing growth time beyond ca 10^{-2} s. Comparison with the original Θ vs log τ_h data (Fig. 4-9) shows that 10^{-2} s, at this growth potential, is approximately the time at which oxide growth through stage II begins, although it may be complicated by the sweep time τ_s. The decrease of $\Delta V_{1/2}$ (O_{C3}) with log τ_h, also represented in Figure 4-23, shows that at higher levels of oxide coverage, a g-factor associated with the O_{C3} state must become progressively smaller. This is apparent from visual inspection of the i vs V profiles but is in direct contrast with the results obtained from one interpretation of the plots of Θ vs log τ_h, that is that g-values apparently increase at higher levels of oxidation. This apparent contradiction will be examined in subsequent chapters, but it indicates that the processes involved in oxide deposition and reduction are fundamentally different.

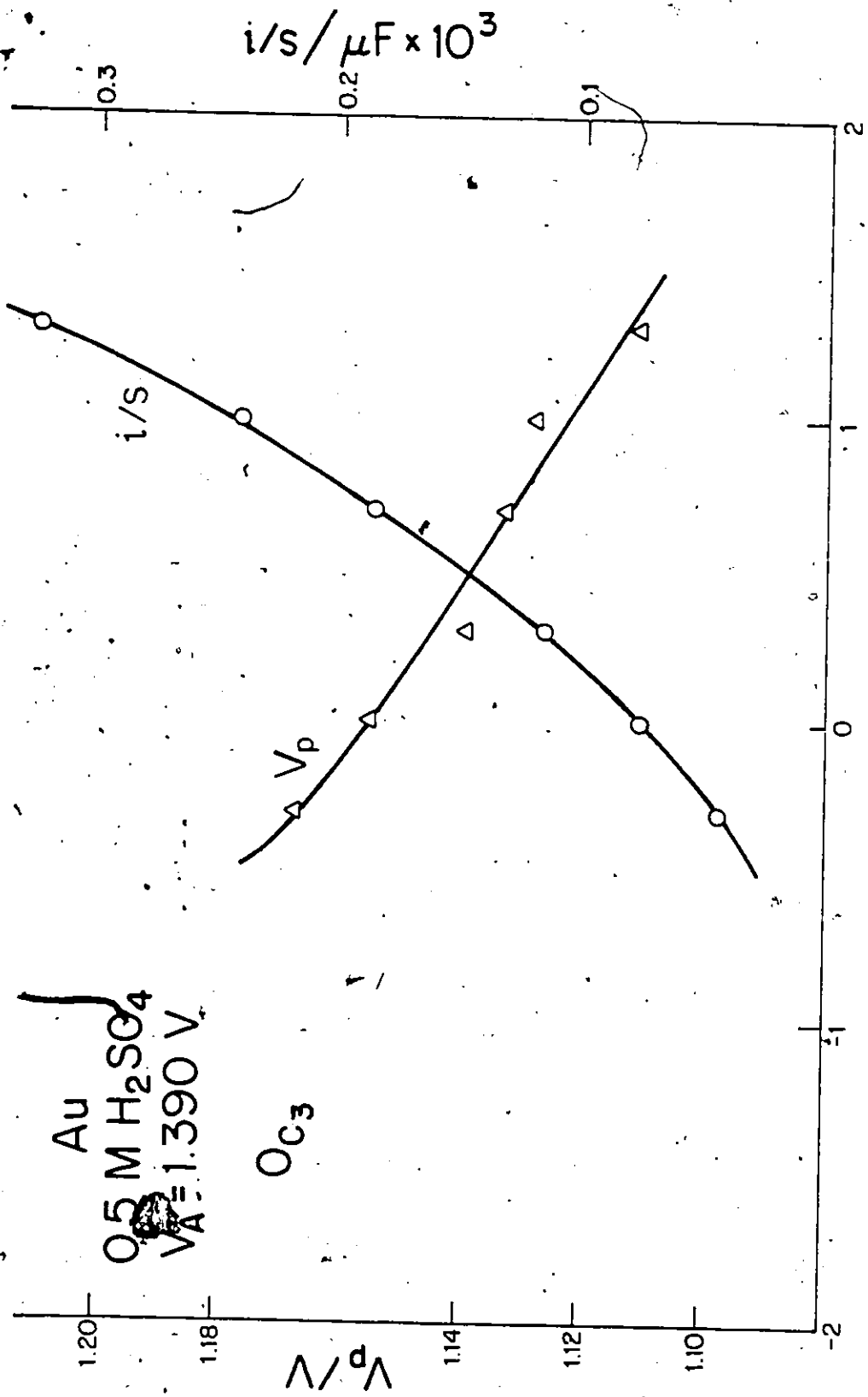

Figure 4-21. Variation of diagnostic parameters V_p and i/s for current peak O_{C3} in reduction i vs V profiles for oxide grown at constant potential of 1.39 V at Au in 0.5 M H_2SO_4 for various periods of time.

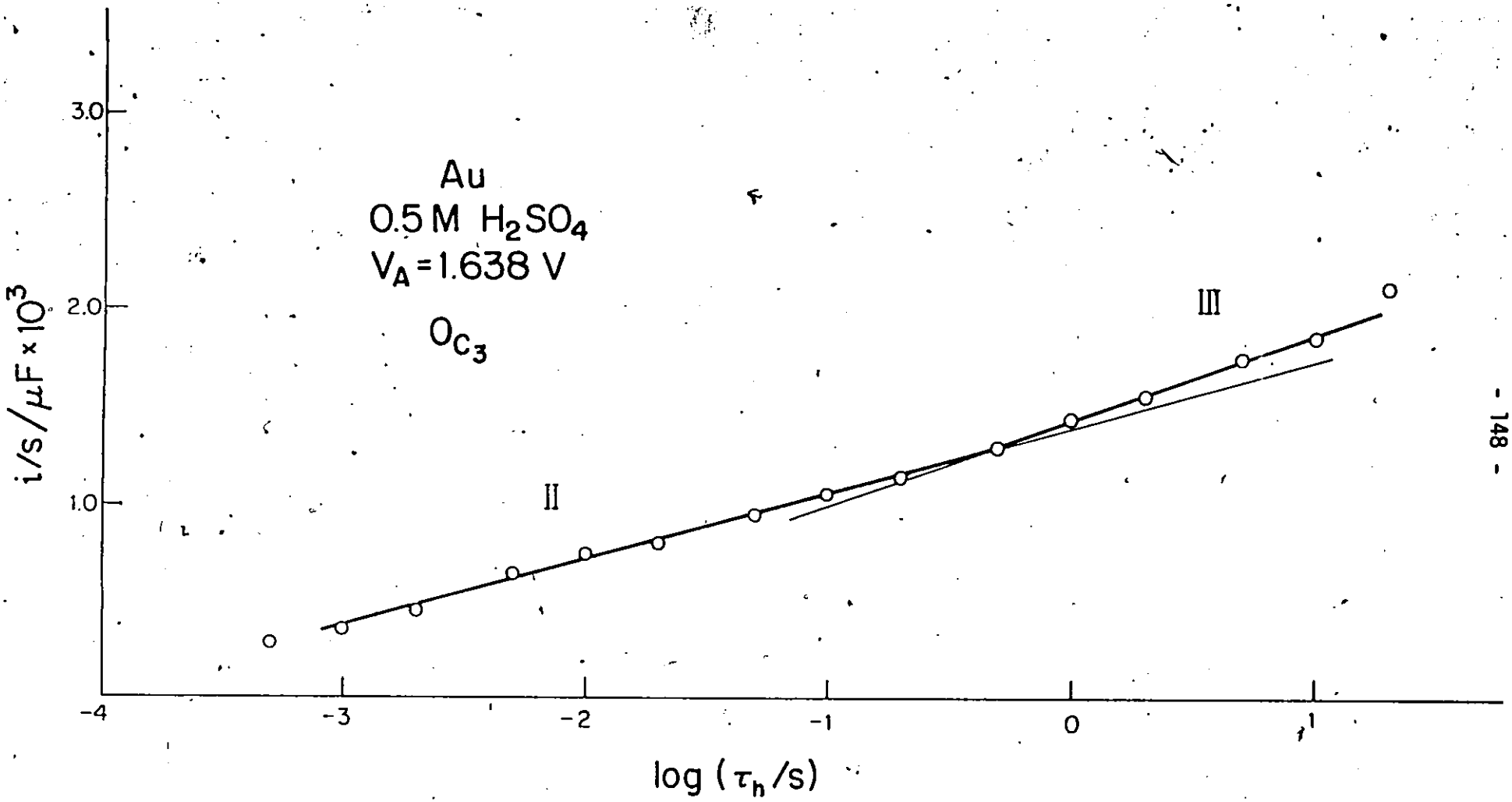

Figure 4-22 Variation of i/s for current peak O_{C3} in reduction i vs V profiles for oxide grown at constant potential of 1.64 V at Au in 0.5 M H_2SO_4 for various periods of time.

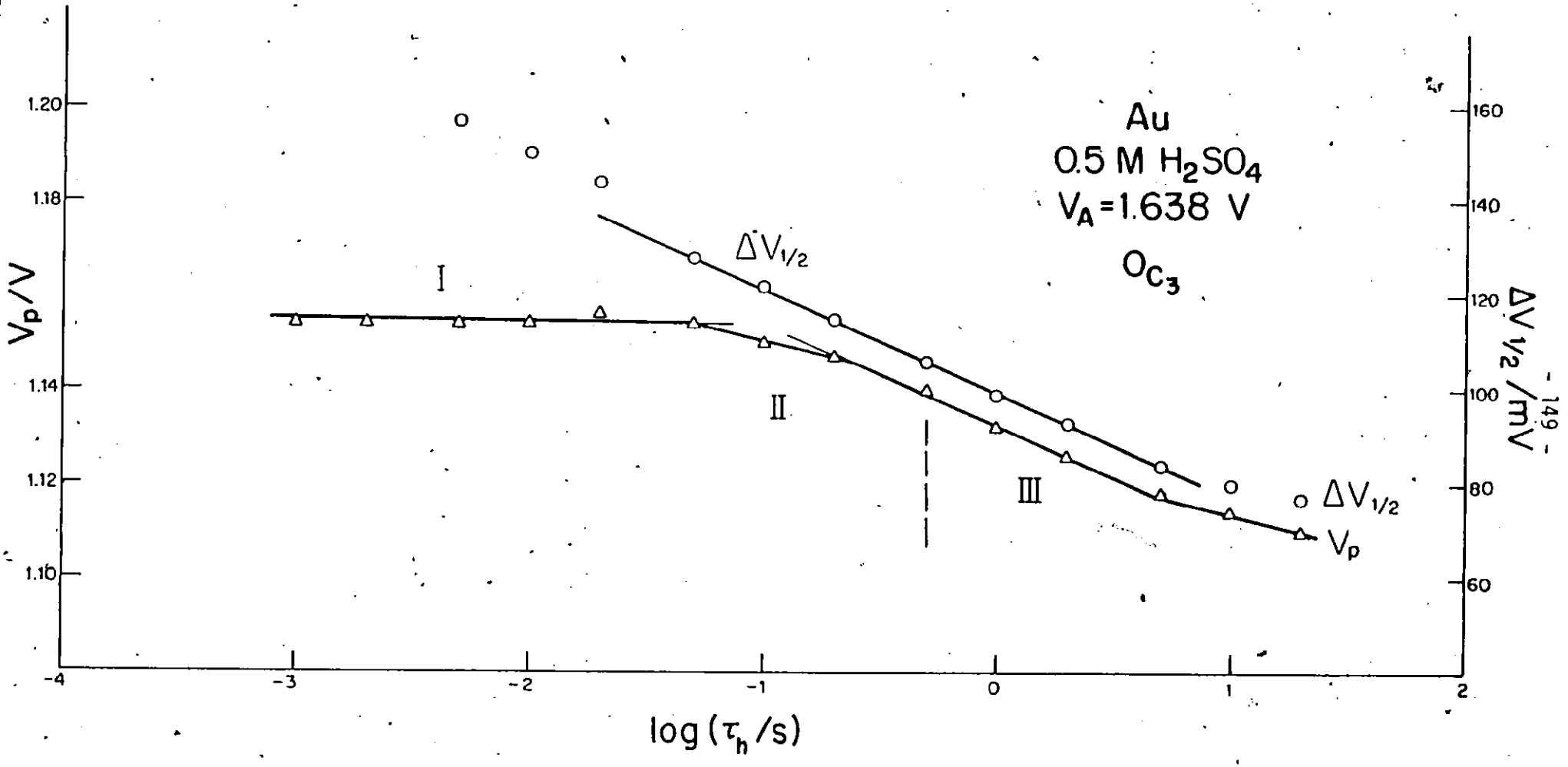

Figure 4-23 Variation of diagnostic parameters of V_P and $\Delta V_{1/2}$ for current peak O_{C3} in reduction i vs V profiles for oxide grown at constant potential of 1.64 V at Au in 0.5 M H_2SO_4 for various periods of time.

It should be noted that while the interaction parameter indicates formation of a more stable species at higher oxide coverages (Fig. 4-23), the peak potential (V_p) also shows that, at higher coverages, the oxide formed is more and more stable (i.e. more negative potentials must be applied in a potential sweep before it can be reduced).

Also, the experimental quantity i/s plotted in Figure 4-22 as f(log τ_h and the quantities V_p and $\Delta V_{1/2}$ shown in Figure 4-23 clearly support the observation of two stages of direct logarithmic growth at constant potential.

8. Discussion of Overall Features of the Processes

The growth of oxide through the O_{C2} state is distinctly different from oxide growth with reduction through the O_{C3} state. As the O_{C2} state saturates, both its V_p and the i/s remain approximately constant except at low coverages. Even then, when i/s is increasing, V_p (O_{C2}) remains constant (Fig. 4-20).

Growth of oxide, as indicated by its reduction through the O_{C3} state, appears to be the main process.

Unlike the O_{C2} state, O_{C3} does not saturate; it is the main peak for reduction of previously grown oxide. The V_p (O_{C3}) decreases with growth time, τ_h, and, coupled with the known aging effect [21], would seem to indicate that some reorganization of the oxide is occurring as oxide coverage increases. This reorganization involves the formation of an organized, more stable oxide (having lower V_p and small $\Delta V_{1/2}$ in reduction), usually considered as a two-dimensional network phase, the reduction of which is effected with a lower value of the interaction parameter, g. Since one interpretation of the 2-stage Θ vs log τ_h behavior is that oxide growth occurs with an increase of the g value, it is apparent then that there

must be fundamental differences between the mechanism of formation of oxide in the growth process and the mechanism of subsequent reduction of that oxide. Thus, reduction cannot be the same, in reverse, as the process of oxidation.

CHAPTER 5

KINETICS OF REDUCTION OF SURFACE OXIDE AT Au

The potential vs time program described in Figure 2-5e, page 49 was used as part of a systematic attempt to evaluate the kinetics of reduction of the various states of surface oxide that are developed in the course of monolayer oxide formation at Au. In these experiments, oxide species were deposited in a potentiodynamic sweep at moderate rates (typically 0.050 V s^{-1}) up to appropriate end potential limits (V_1) in the anodic sweep, thereby varying the oxide coverage. The oxide thus formed is partially reduced to varying extents in a subsequent cathodic sweep down to some systematically variable potential (V_2) at which the reduction of oxide has become observable. Maintenance of such potentials (V_2) for controlled periods of time, τ_h, (typically 0.1 s up to 200 s) permits evaluation of the kinetics of reduction of the oxide from known initial coverage at constant potential as a function of that potential, V_2. Under optimal conditions, the kinetics of changes of individual states of the oxide film, corresponding to resolved peaks in the i vs V profile for the reduction of the film, can be separately evaluated.

Experiments of this type were performed in the following solutions and conditions:

a) 1.0 M $HClO_4$; V_A = 1.623 V, 1.512 V;

b) 1.0 M $HClO_4$ with SO_4^{-2} contamination;

c) 0.05M H_2SO_4, T = 298 K; and

d) 0.05M H_2SO_4, T = 273 K.

The general form of a succession of cathodic i vs V profiles obtained in these measurements is illustrated in Figures 5-1 and 5-2 for solutions 0.05M in H_2SO_4 and 1.0M in $HClO_4$ respectively. A striking feature of these i vs V profiles, especially in comparison with the behavior observed when the growth of oxide is followed in time (Chapter 4), is the relatively long times required to reduce the oxide and to follow its reduction stages. Thus, in oxide growth, the process must be followed on an oscilloscope because holding for times τ_h produces substantial effects already at 10^{-4}, 10^{-3} and 10^{-2} s. In cathodic reduction kinetics on the other hand, virtually no effects are observable until τ_h becomes of the order of 0.1 s and longer. In addition, the process(es) of reduction appear to take place via the O_{C3} state before any reduction of oxide occurs through the O_{C2} state. Thus, in Figure 5-1, a comparison of the profiles in the family generated after initial, partial reduction of oxide in the cathodic sweep down to 1.191 V shows that the major component of the oxide remaining at this point of the sweep is reduced quite quickly through the O_{C3} peak. After a potential of 1.191 V has been maintained for 5 s, the only oxide species remaining on the surface are reduced through the O_{C2} state (cf. especially for the time range τ_h = 1.5 s to 5 s, during which the O_{C3} state is the only one through which reduction is apparent at 1.191 V). Figure 5-2 for reduction at 1.205 V of oxide formed in 1 M $HClO_4$ in an anodic sweep up to 1.638 V shows similar behavior. After oxide reduction for 3 s at 1.205 V, there is apparently no oxide remaining

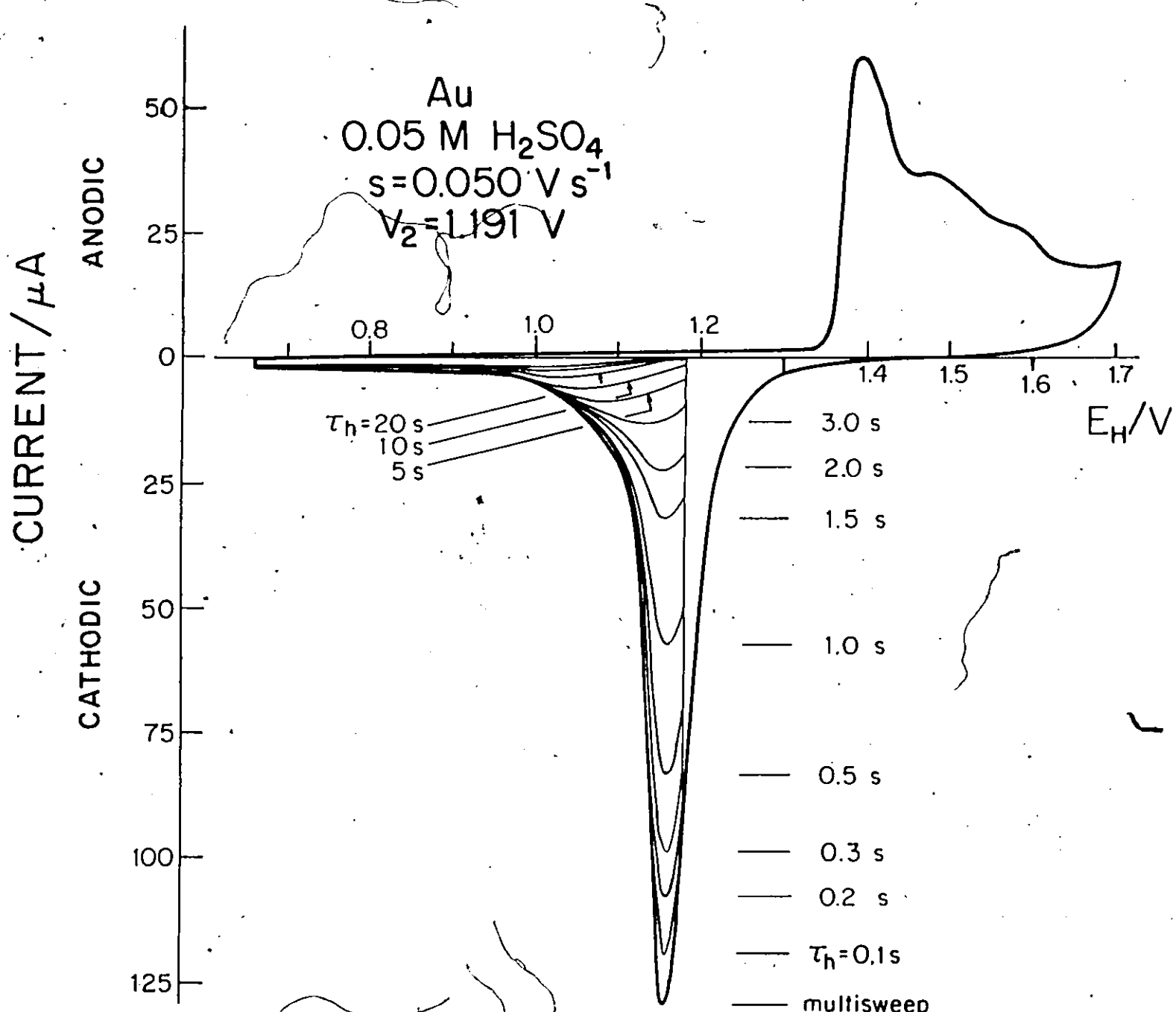

Figure 5-1 Cyclic-voltammetry i vs V profiles for Au in 0.05 M H_2SO_4 showing the partial reduction of oxide to 1.19 V, and continued reduction after maintaining this potential for periods of time τ_h = 0.1 s to 20 s. s=0.050 V s^{-1}, 298 K.

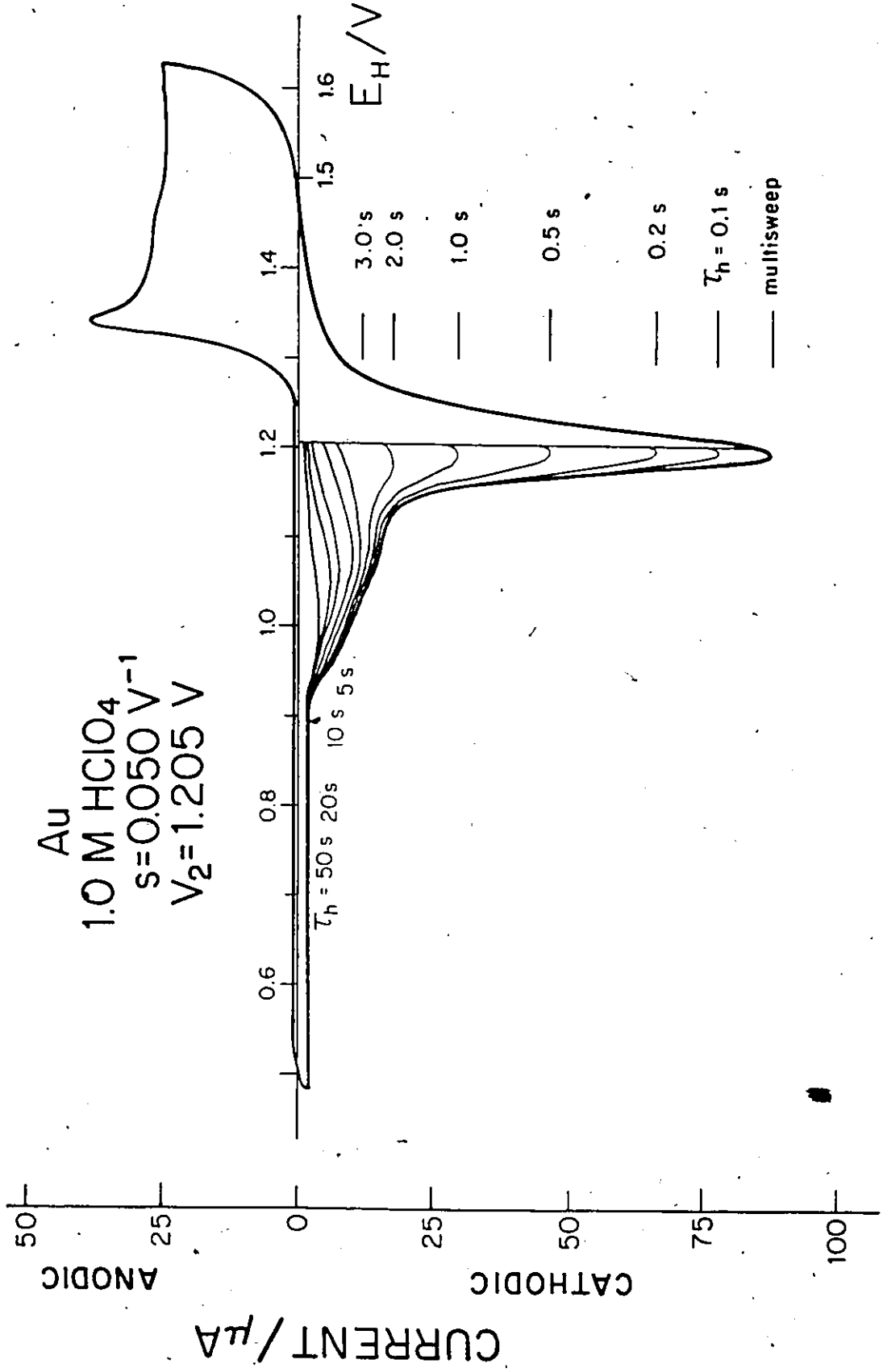

Figure 5-2 Cyclic-voltammetry i vs V profiles for Au in 1.0 M $HClO_4$ showing the partial reduction of oxide to 1.205 V, and the effects of reduction at constant potential (1.205 V) for periods of time τ_h = 0.1 s to 50 s as shown in continuation of the reduction potential sweep. s = 0.050 V s^{-1}, 298 K.

available for reduction in the O_{C3} state. However, the O_{C2} state has not diminished in coverage (charge) at all. A further contrasting feature, then, is that, of the amount of oxide remaining on the surface when the reduction potential of 1.205 V is reached in the cathodic sweep, that portion which is normally reduced via the O_{C3} state is removed completely in 3 s. An additional 47 s is required before almost complete reduction of the remaining oxide is accomplished with consumption of the species corresponding to the O_{C2} peak.

The current-time relations obtained at various potentials in these experiments were integrated and Figures 5-3 and 5-4 illustrate the resulting charges plotted as coverage Θ (calculated as O-species, 400 $\mu C\ cm^{-2}$ for the monolayer) as a function of log time (τ_h) for 1.0 M $HClO_4$ and 0.05 M H_2SO_4 solutions (T = 273K), respectively.

Both these figures show that while a relatively large quantity of charge can be passed initially in a short time, there is a levelling off of the reduction rates at longer τ_h. As the measured values of oxide charge become comparable with the saturation coverage level for the O_{C2} states at long τ_h, an almost logarithmic relation is observed between Θ and τ_h. The question arises: must oxide reduction through the O_{C3} state be completed before reduction through the O_{C2} state can begin, or is reduction through the O_{C2} state simply characterized by a rate constant orders of magnitude smaller than that for oxide reduction through the O_{C3} state? Attempts to answer various aspects of this question will be made in the material which follows in the subsequent chapters.

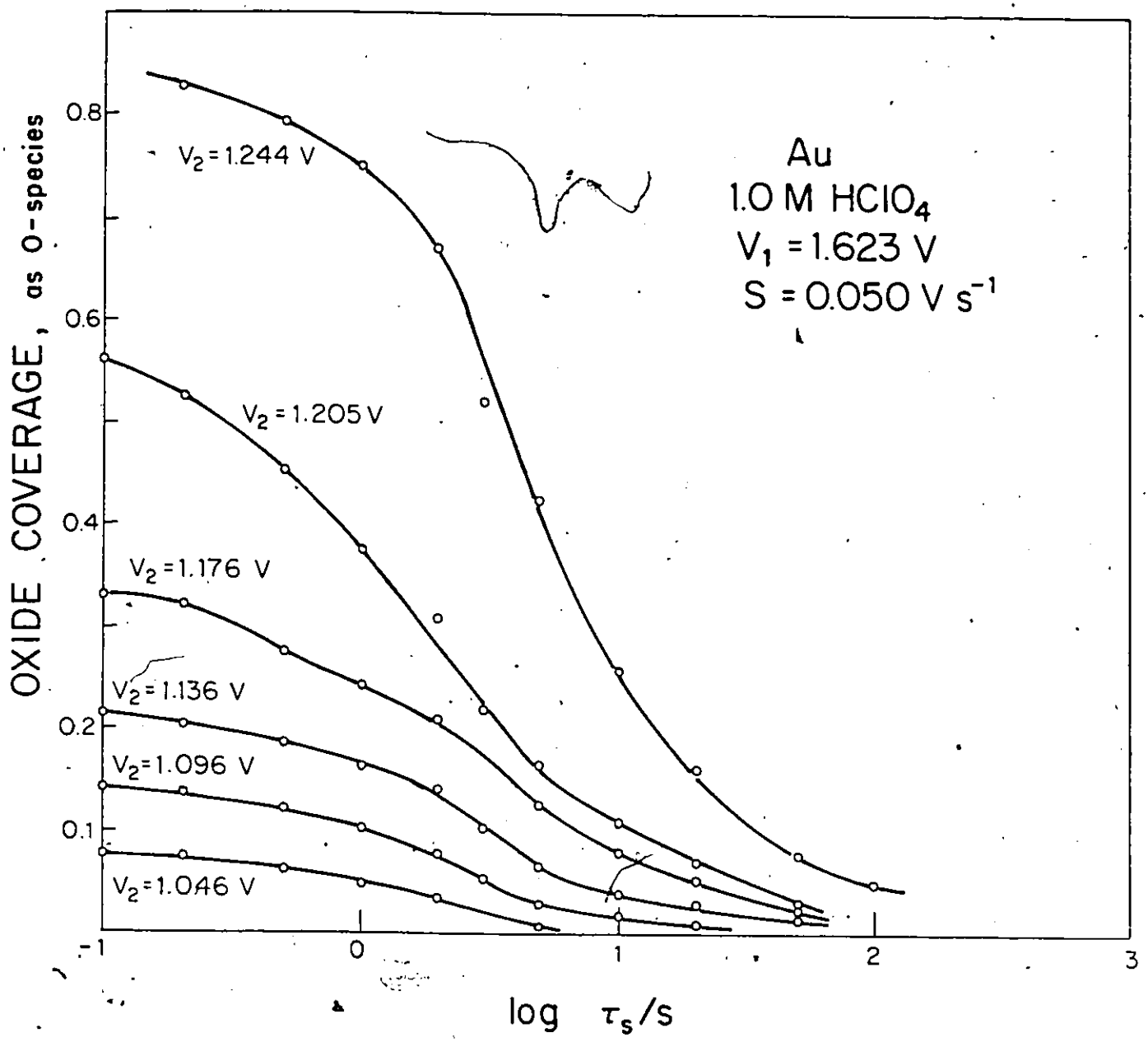

Figure 5-3 Variation of oxide coverage (O species) remaining on Au electrode in 1.0 M $HClO_4$ after oxide reduction at various constant potentials from 1.244 V to 1.046 V for various periods of time τ_h = 0.1 s to 100 s. s = 0.050 V s^{-1}, V_1 = 1.623 V, 298 K.

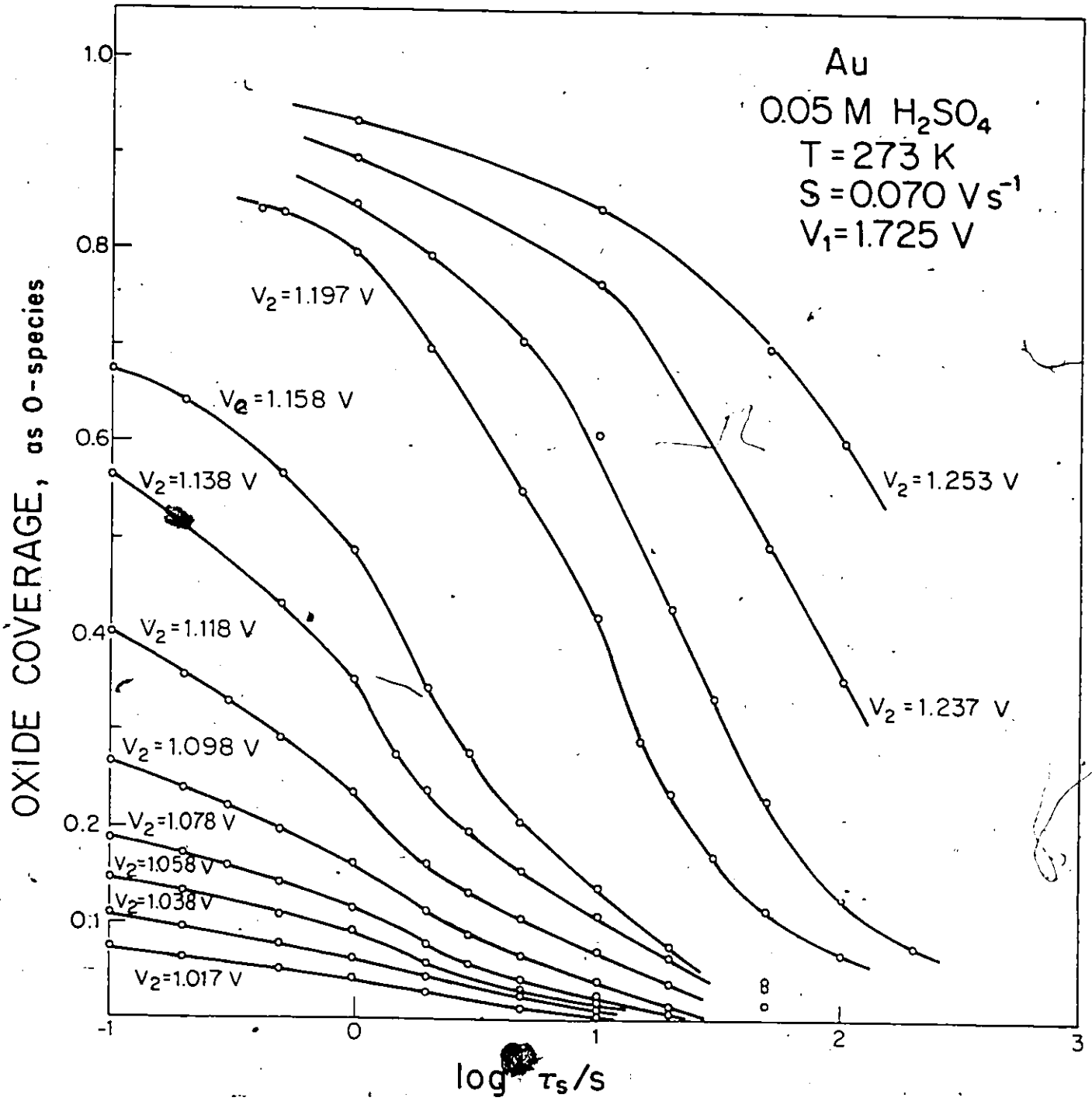

Figure 5-4 Variation of oxide coverage (O species) remaining on Au electrode in 0.05 M H_2SO_4 after oxide reduction at various constant potentials from 1.253 V to 1.017 V for various periods of time τ_h = 0.1 s to 200 s. .s = 0.050 V s^{-1}, V_1 = 1.725 V, 298 K.

Attempts were made to evaluate the applicability of any one of several common, and other less common rate-law expressions (e.g. $\theta^{1/2}$ vs t, $\theta^{3/2}$ vs t and some others) to the integrated charge vs time data of Figures 5-3 and 5-4, and to similar data for other solutions investigated.

Only one relation could be found which was suitable (in fact, the fit was excellent, see Figure 5-6) and that was the relation which can be derived for a simple irreversible electrochemical reduction process in which ln θ is linear in time τ_h.

This relation evolves from consideration of the reduction of oxide as being represented very generally by the equation

$$AuO + 2H^+ + 2e \rightleftharpoons Au + H_2O \qquad (5\text{-}1)$$

assuming "O" species are the principal chemisorbed entities. The actual choice of reduction reaction does not interfere with the following derivation. The assumption will be justified in detail in the final chapter, but a 1-electron oxidation or reduction is not indicated either through appearance of a current peak due to such a process or through the observation of appropriate Tafel slopes for a 1-electron process. Thus, experimentally, there is no evidence for the existence of OH species on Au (e.g. see Chapter 4 for Oxide Growth) and supporting evidence would be easily found if a 1-electron reaction took place.

A general expression for the rate of reduction according to eqn. (5-1) follows as:

$$\text{Rate} = \frac{d}{dt}(1 - \theta_T) = k(c_{H^+})^2 \theta_o \exp[-2(1-\beta)VF/RT] \qquad (5\text{-}2)$$

and for $\theta_T \approx \theta_o$

$$\frac{d}{dt}(1-\theta_T) = \frac{d}{dt}(1-\theta_o) = -\frac{d\theta_o}{dt} \qquad (5\text{-}3)$$

Then

$$-\frac{d\theta_o}{\theta_o} = k(c_H{}^+)^2 \exp[-2(1-\beta)VF/RT]dt \qquad (5\text{-}4)$$

which gives on integration

$$-\ln \theta_o + \ln \theta_o \text{ (init.)} = A(V).t \qquad (5\text{-}5)$$

where

$$A = k(c_H{}^+)^2 \exp[-2(1-\beta)VF/RT] \qquad (5\text{-}6)$$

For a given solution, a series of potentials is studied so that:

$$\ln A = \ln k + 2 \ln c_H{}^+ - 2(1-\beta)\frac{VF}{RT} \qquad (5\text{-}7)$$

which allows a direct evaluation of $dV/d \ln A$ to be made which is seen to be the Tafel parameter

$$\frac{dV}{d \ln A} = \frac{-RT}{2(1-\beta)F} \qquad (5\text{-}8)$$

for the surface process involved

Consideration of a q-factor

The rate equations derived above have not included the influence of the so-called interaction "g" parameter. Inclusion of such a factor requires the rate expression to be written as:

$$\text{Rate} = -\frac{d\theta_o}{dt} = k\,\theta_o \exp(g\theta_o)(c_H{}^+)^2 \exp[-2(1-\beta)VF/RT] \qquad (5\text{-}9)$$

Rearranging gives

$$-\frac{\exp(-g\theta_o)}{\theta_o} d\theta_o = k(c_H{}^+)^2 \exp[-2(1-\beta)VF/RT]dt \qquad (5\text{-}10)$$

which integrates to give a series solution

$$A\,t = \ln \frac{\Theta_{in}}{\Theta} + g\,(\Theta-\Theta_{in}) + \frac{g^2}{4}\,(\Theta_{in}^2-\Theta^2) + g^3\,(\Theta^3-\Theta_{in}^3) + \ldots\ldots$$

$$= -\ln\Theta + g\Theta - \frac{g^2\Theta^2}{4} + \frac{g^3\Theta^3}{16} \ldots\ldots\ldots + \text{const.} \qquad (5\text{-}11)$$

where the constant is

$$\ln \Theta_{in} - g\Theta_{in} + \frac{g^2}{4}\,\Theta_{in}^2 - \frac{g^3}{16}\,\Theta_{in}^3 + \ldots\ldots \qquad (5\text{-}12)$$

and Θ_{in} is the initial coverage at $\tau_h = 0$.

A useful first approximation, which takes interaction effects into account, is given as

$$A\,t = -\ln\Theta + \ln\Theta_{in} + g\Theta - g\Theta_{in} \qquad (5\text{-}13)$$

It should be possible to obtain a best fit value for the g-factor for a set of experimental data through computer optimized selection of g values.

However, the results referred to above are found to be fitted by a g-factor close enough to zero that the interaction effect may be neglected; then equation (5-5) may be used, i.e. linear plots of $\log\Theta$ vs τ_h should be obtained over a wide range of time and reduction potentials, as is found from the experimental data (Figures 5-5 and 5-6).

The aim of the experimental study undertaken was to analyze the kinetics of reduction through states O_{C3} and O_{C2}. The equations derived above have a validity at any given potential, but the investigation of a series of reduction potentials so that the Tafel parameter (eqn. 5-8) can be evaluated, is valid only when one reaction (with one E°) is predominant throughout the potential range involved. If two reactions

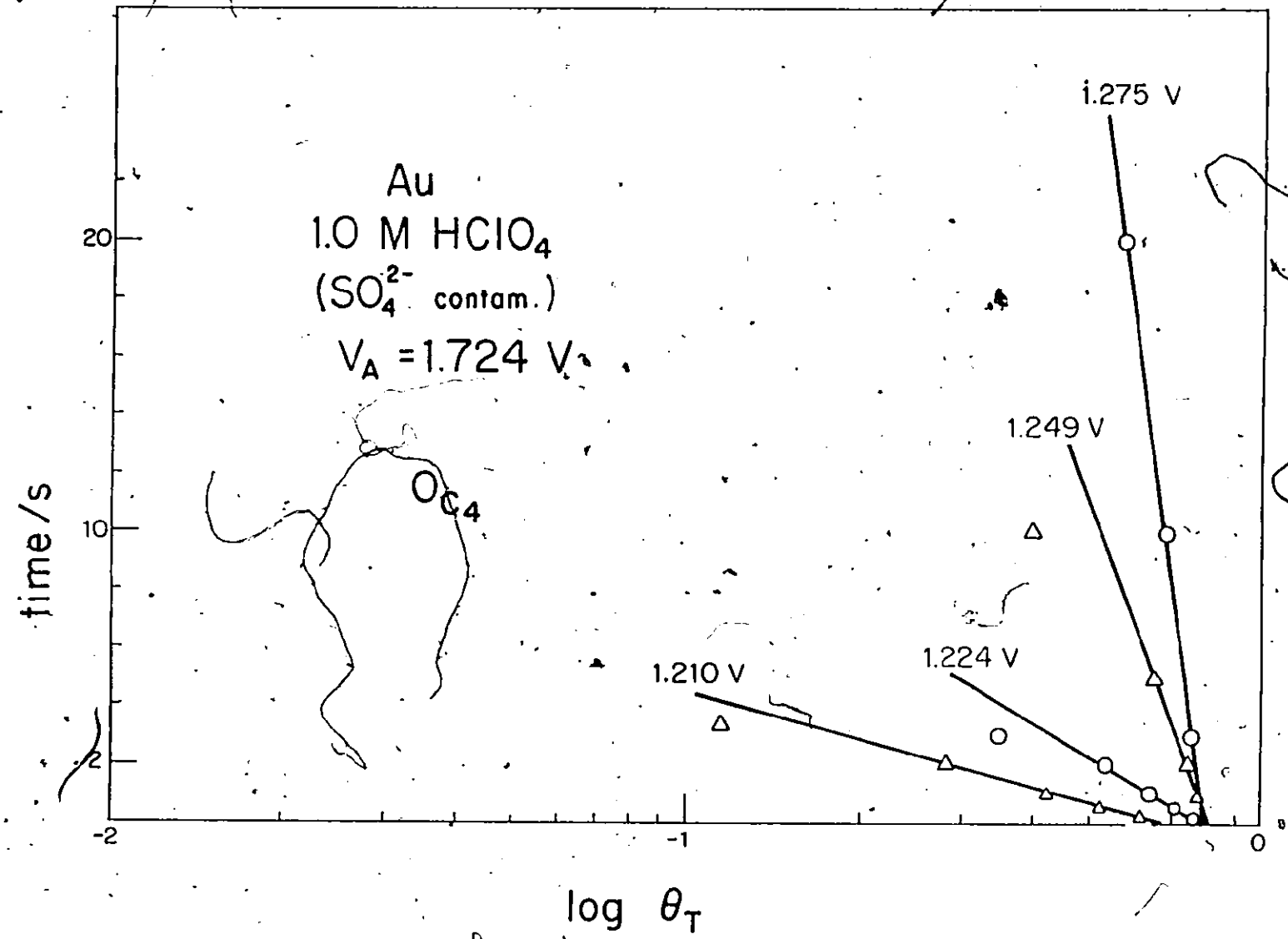

Figure 5-5 Plots of log θ_T vs t testing the applicability of eqn. (5-5) for electrochemically controlled reduction of oxide at constant-potential for O_{C4} current peak in SO_4^{2-} contaminated 1.0 M $HClO_4$.

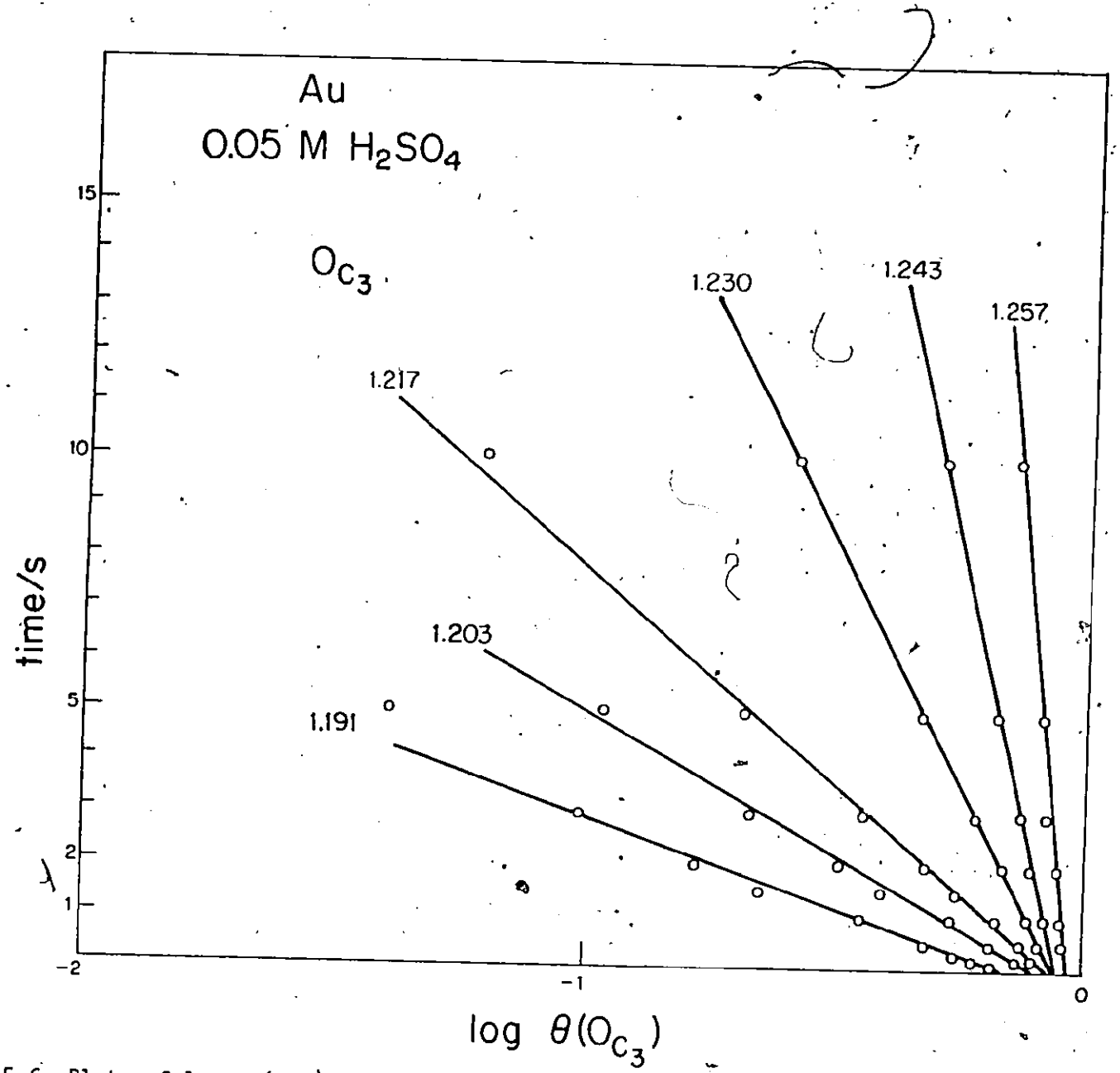

Figure 5-6 Plots of log Θ (O_{C3}) vs t testing the applicability of eqn. (5-5) for electrochemically controlled reduction of oxide at constant potential for O_{C3} current peak in 0.05 M H_2SO_4.

(assumed independent) are occurring simultaneously at a given potential, the total rate is of course, the sum of the individual rates. However, in a study conducted over a range of potentials, the relative contributions of the reactions involving the two stages O_{C2} and O_{C3} to the net rate observed at each potential is changing (assuming different E°'s and / or Tafel slopes) so that the potential dependence cannot be evaluated. It is for this reason that the studies described in this chapter were not extended to include alkaline solutions (especially 0.2M $Ba(OH)_2$) where the peaks observed in oxide reduction are so close together, on the potential scale, that the component processes O_{C3} and O_{C2} cannot be studied separately. It is fortuitous, then, that the reduction of oxide in the O_{C3} and then in the O_{C2} state appears to progress sequentially, as noted above (see Fig. 5-1 and 5-2). Reasons for this effect are suggested in Chapter 8.

1. Evaluation of Kinetics of Oxide Reduction

For each solution, it is apparent from inspection of the respective i vs V profiles that there are ranges of reduction potentials and ranges of reduction (or holding) times of the order of a decade or more for which virtually one state only is the significant one through which oxide is reduced. Thus, when V_2 (see program in Fig. 2-5e, p. 49) is held at relatively high values, the measured reduction currents are almost entirely associated with the O_{C3} state; however, at much lower potentials, the O_{C2} peak appears to be the only peak through which the remaining oxide is reduced.

Subsequent data analysis confirms the conclusions based on visual inspection of the i vs V profiles and, at potentials in the mid-range of reduction, especially where deconvolution of the reduction peaks demonstrates overlapping between constituent peaks, a substantial deviation from the expected linear behavior according to eqn.(5-5) is observed in the kinetic relations described above. The analysis also leads to the indication of the role of a reduction process involving a state O_{C4} in which higher oxides (see also Chapter 7) are reduced at potentials similar to those observed for the O_{C3} peak. Some evaluation of the kinetic parameters for reduction in this state has been possible.

Integrated charge vs time data from the experimental i vs V profiles were plotted as log Θ vs time, τ_h. The results obtained indicated adherence to equation 5-5 and are shown in Figure 5-5 for the O_{C4} state in sulfate-contaminated 1.0 M $HClO_4$, and in Figure 5-6 for the O_{C3} state in 0.05 M H_2SO_4. The data for the O_{C4} peak are less extensive due to the small quantities (coverages) of higher oxide associated with this state that are expected to be formed at the anodic end potentials employed. Deviation from a straight line plot arises as the oxide species reduced in state O_{C4}, is exhausted and reduction in the O_{C3} state begins. Thus, for reduction at 1.249 V (Figure 5-5), the oxide coverage Θ at τ_h = 10 s is much lower than would be expected by reduction through state O_{C4} alone; thus, reduction through state O_{C3} has apparently become significant. Data used for evaluation of oxide reduction through the O_{C3} state (e.g. Figure 5-6) have been corrected for the coverage of that quantity of oxide reduced through

state O_{C2}.

Attempts were made to evaluate reduction through the O_{C2} state by a similar procedure, starting at the most cathodic potentials (and long times) where changing coverages could be associated strictly with reduction via the O_{C2} state. Unfortunately, only a few potentials were available for which it could be clearly shown that reduction occurs through the O_{C2} state alone. This problem arises mainly from overlap between the relatively small O_{C2} peak and the "cathodic" tail of the larger O_{C3} peak. In addition, there are inherent difficulties encountered in monitoring the charges (as Θ) of low Θ-level species, and in following changes in Θ with the required accuracy.

The slopes ($d \ln \Theta/dt$) at each reduction potential (Figs. 5-5 and 5-6) and for each solution, give values for the "A" term in eqns. (5-5) and (5-6); these values are recorded in Table 5-1 and illustrate the relative rates of reduction of the oxide which had been previously formed in each solution under conditions where the rates could be evaluated without ambiguity. "A" values for each solution are plotted in Figures 5-7 and 5-8 as a function of reduction potential ($\log A$ vs V_H) and verify the potential-dependence of rate expected from the previously derived equation (eqn. 5-8) in that straight line relations are observed. Figure 5-7 shows the potential-dependence of the rate for oxide reduction through the O_{C4} state and Figure 5-8 the corresponding potential-dependence for reduction through the O_{C3} state. The slopes obtained from these figures as $dV/d \log A$ give the Tafel slopes (eqn. 5-8) for the reaction

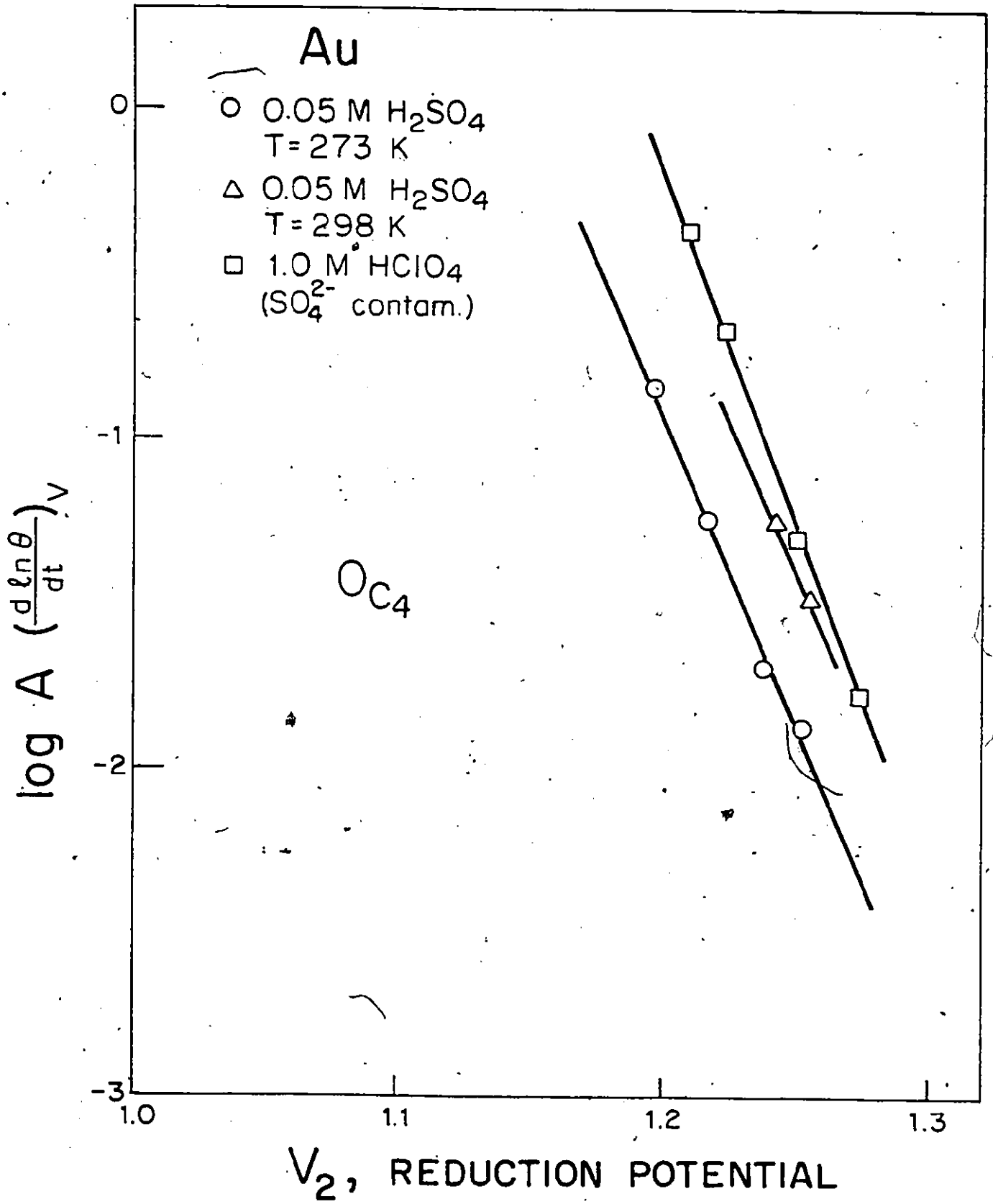

Figure 5-7 Plots of log A vs oxide reduction potentials using eqns. (5-5) and (5-8) to determine Tafel slopes for electrochemically controlled oxide reduction in O_{C4} for various solutions.

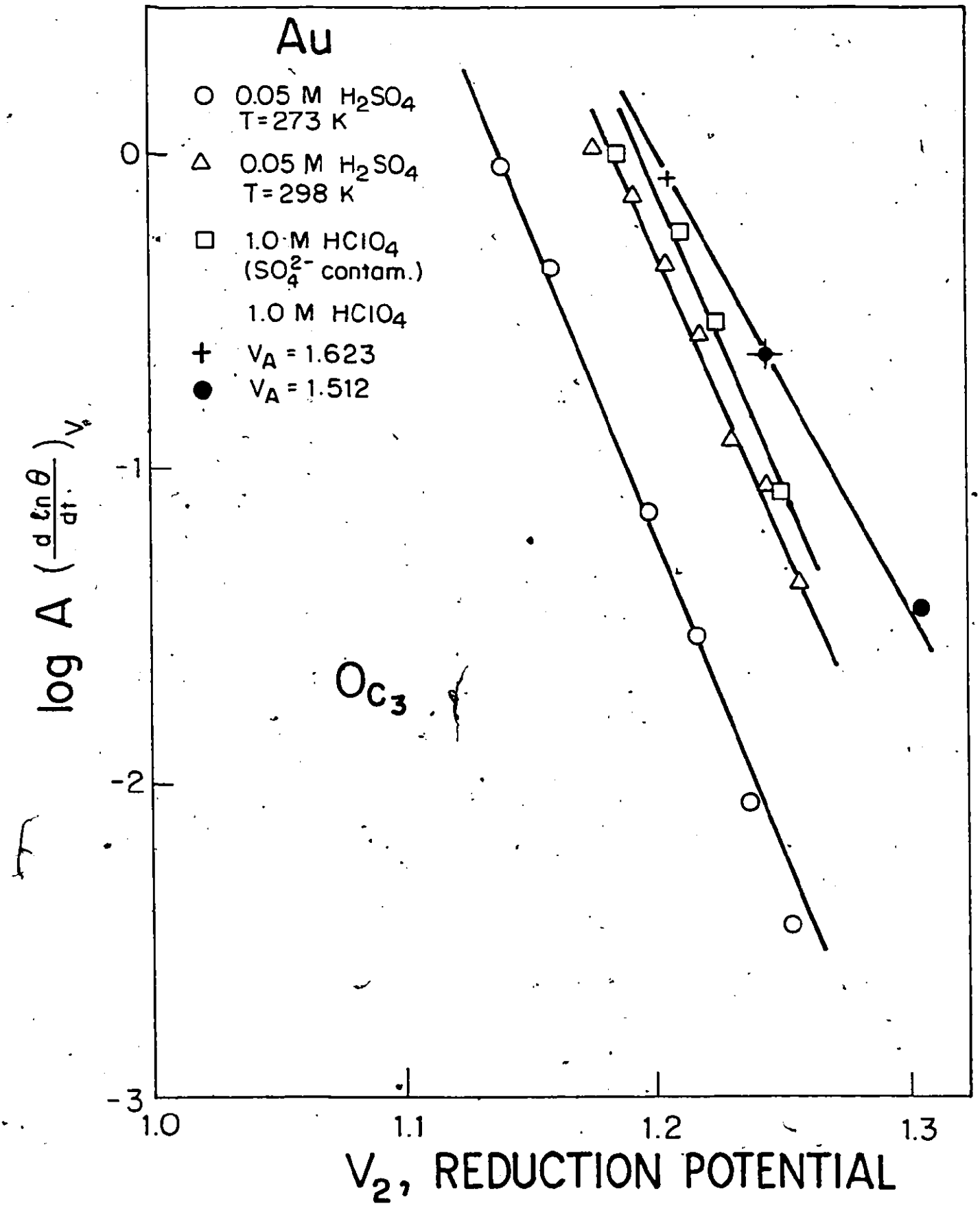

Figure 5-8 Plots of log A vs oxide reduction potentials using eqns. (5-5) and (5-8) to determine Tafel slopes for electrochemically controlled oxide reduction in O_{C3} for various solutions.

TABLE 5-1

Solution	Reduction Potential, V_2	A (O_{C3}) $d\ell n\Theta/dt(s^{-1})$	A (O_{C4}) $d\ell n\Theta/dt(s^{-1})$
1.0M $HClO_4$; SO_4^{-2} contaminated	1.185	1.00	-
	1.210	0.56	0.43
	1.224	0.29	0.21
	1.249	0.082	0.050
	1.275	-	0.017
1.0M $HClO_4$ V_1 = 1.623V	1.176	1.15	-
	1.205	0.85	-
	1.244	0.23	-
1.0M $HClO_4$ V_1 = 1.512V	1.244	0.23	-
	1.306	0.036	-
0.05M H_2SO_4 T = 298 K	1.177	1.05	-
	1.191	0.73	-
	1.203	0.45	-
	1.217	0.27	-
	1.230	0.12	-
	1.243	0.088	0.055
	1.257	0.044	0.033
0.05M H_2SO_4 T = 273 K	1.138	0.91	-
	1.158	0.44	-
	1.197	0.073	0.14
	1.217	0.029	0.055
	1.237	0.0087	0.020
	1.253	0.0035	0.013

associated with each reduction peak (Table 5-2).

The results indicate that a 2-electron transfer is involved as the rate-determining step for the reactions giving rise to both O_{C3} and O_{C4} peaks in all solutions at 298 K (theoretical value for 2e transfer = 0.059V) and at 273 K (theoretical value = 0.054V). Further justification for the conclusion regarding a 2-electron process will be given in Chapter 8.

TABLE 5-2

Solution	(dV/d log A)/V	
	O_{C3}	O_{C4}
0.05M H_2SO_4 T = 273 K	0.051	0.054
0.05M H_2SO_4 T = 298 K	0.055	0.058
1.0M $HClO_4$ SO_4^{-2} contaminated	0.054	0.048
1.0M $HClO_4$ 1.623 V and 1.512V	0.068	-

These results show that it is possible to evaluate the potential-dependence of the appropriate rate constants. Also, since the peaks observed in an i vs V reduction profile are more clearly differentiated than those observed in oxide deposition, it is apparent that the measured rates and Tafel slopes obtained may be more directly ascribed to the kinetic behavior of a particular surface state (i.e. corresponding to a peak in an i vs V profile) than those obtained in the experiments in which oxide growth kinetics were studied (Chapter 4).

i) Significance of the O_{C2} Reduction Peak

It has not proven possible to characterize satisfactorily the kinetics of oxide reduction through the O_{C2} state. Examples of linear dependence of Θ on log t and log Θ on t have both been obtained though, for the most part, data are available over less than two decades of time. In addition, problems in accurately measuring and detecting changes in low levels of oxide coverage ($\Theta \simeq 0.10$ and less) are unavoidable so that kinetic determinations of the type used here may not be able to be carried out reliably for the O_{C2} state.

ii) Effects of Various Anions

The effects that various anions of the supporting electrolyte have on the processes of reduction of oxide are best illustrated by referring to Figures 5-7 and 5-8. In Figure 5-8, for example, the solutions associated with each line in the figure from left to right, are aq. H_2SO_4 at 273 K aq. H_2SO_4 at room temperature, sulfate-

contaminated aq. $HClO_4$ and finally, very pure, 1M aq. $HClO_4$ solution. The same trend is observed as the order of increasing A values at given constant potential (Table 5-1). When the known (Chapter 3) trend of strength of ion adsorption is considered, namely that SO_4^{-2} or HSO_4^- ions are adsorbed much more strongly than ClO_4^- ions, it becomes apparent that strongly adsorbed ions inhibit reduction to some extent, although the mechanism of that reduction (i.e. in terms the slope of the d log A/dV lines) is not affected significantly. Again, the state of the metal-oxide appears to be the primary determinant of the mechanism of reduction of that oxide.

iii) Nucleation & Growth

The i vs V profiles obtained in the reduction experiments provide extensive information on oxide reduction as a function of time and reduction potential, V_H, during cathodic sweeps.

The important question arises whether the reduction processes occur through a mechanism of nucleation of holes in the oxide film or by random removal of oxygen species in the monolayer. A distinction between these two types of mechanism can be made by conducting a potential sweep experiment in which the sweep is taken rapidly to some intermediate potential in the i vs V reduction profile and then held constant. If a nucleation process were involved in reduction, the current would tend first to increase and then decrease during this holding time. In all reductions and at many potentials investigated in the range over which reduction is observed, no behavior of this kind was ever observed.

Similarly, if a potential sweep is taken to some intermediate potential in the anodic i vs V profile, and then held constant, only continuously decreasing anodic currents are always observed - never an increase followed by a decrease as would be expected were a nucleation and growth process involved. Similar effects observed in the study of oxide growth will be discussed in Chapter 7, but the behavior observed constitutes strong evidence that a mechanism of hole nucleation and hole expansion is not operative in the reduction of the oxide monolayer on Au so that some other process of reduction is involved, as will be discussed in Chapter 8.

CHAPTER 6

SWEEP RATE DEPENDENCE OF OXIDE FORMATION AND REDUCTION BEHAVIOR

1. Purpose of Investigations at Various Sweep Rates

The potentiodynamic method used in the present work is essentially a modulation technique in which electrical perturbations can be addressed to an electrode interface over various time scales determined by the potential sweep rate, dV/dt. Accordingly, this method is very convenient for following the kinetic response of surface processes to various rates of modulation. In particular, it is useful for following a) the transition from kinetic reversibility to irreversibility in a surface process and b) the kinetic coupling between two-stage surface processes at electrodes. Diagnostic criteria of peak shapes enable various conditions or mechanisms to be distinguished.

2. Distinguishable States of Electrodeposited Oxygen Species at Au Electrodes

The current-potential profiles at polycrystalline Au shown earlier, e.g. in Figures 3-5 and 4-1 to 4-4, demonstrated that several distinct and reproducible states of submonolayer quantities of oxide on Au can be resolved in the oxidation and reduction i vs V profiles before monolayer oxidation is completed. These states are functions of the solution composition and the end potential of the anodic sweep, and are intrinsic features of the oxide growth behavior on Au; arguably[129], they are common to the initial stages of oxide growth processes on all noble metals.

An essential procedure for investigation of the kinetics of these submonolayer processes is the measurement of the sweep rate dependence of the peak potentials of the states resolved in the formation and reduction of the oxide species on Au and the evolution of the shapes of the peaks themselves (see Chapter 3, p. 56).

Such investigations are complementary to those described in the previous two chapters in which the processes of oxide formation and

reduction, studied as a function of potential, were described. Although important quantitative relations were found in the experimental data for, e.g., oxide growth as a function of time, usually several processes in the potential ranges involved, make significant contributions to the experimental quantities being measured.

The methods to be described here permit individual resolved processes in the surface oxidation to be studied, and give quantitative information on the kinetics of the individual processes and their respective reversibilities.

Use of diagnostic parameters of i vs V profiles for surface reactions, described earlier in Chapter 3, p. 56, provides important bases for interpretations of the results to be described in the material which follows.

In the experiments described below, the variation of peak potentials, V_p, for the various current peaks observed in the anodic and cathodic sections of the i vs V profiles was studied as a function of sweep rate, s, and (for reduction) of oxide coverage generated in the previous anodic sweep under various conditions.

In the reduction studies, each set of experiments was performed at constant oxide coverage. This condition, which is required on account of the complicating effects which arise from the variation of V_p with coverage, was accomplished by depositing oxide at a fixed, "slow" sweep rate which was smaller than the sweep rates to be employed subsequently in the cathodic direction. A range of submonolayer oxide coverages on Au was studied by means of measurements of this type, with s between 0.05 V s^{-1} and 200 V s^{-1}, in the following solutions: (a) 1.0 M $HClO_4$; (b) 0.1 m $HClO_4$; (c) 10^{-3} M $HClO_4$; (d) 0.5 m H_2SO_4; (e) 0.05 M H_2SO_4; (f) 5×10^{-4} M H_2SO_4; (g) 0.2 M $Ba(OH)_2$; and (h) 0.1 M Na_2CO_3.

3. General Features

Typical effects of variation of s on the i vs V profiles are illustrated, for fairly low s values, in Figure 6-1 for monolayer oxide formation and reduction in 10^{-3} M $HClO_4$. The profiles shown here are recorded on a constant i/s setting of instrument sensitivities, so that a capacitance scale results (i = Cs).

The following general features are to be noted:

i) In oxidation profile, the capacitance for the initial, reversible deposition of oxide (state O_{A1}*, $\theta < 0.1$) is constant and independent of s, indicating that the peak is for a reversible process. Deviations begin to occur only at potentials approaching the O_{A2} peak, where current contributions from the latter process begin to be significant.

ii) With increasing s, the deposition of oxide, observed in the current peak O_{A2}*, occurs with a broadening of the peak and a shift of V_P to more positive values.

iii) Peak O_{A3} cannot be well resolved under these conditions.

iv) V_P, for the broad peak O_{A4}, and the current minimum, Q_B (cf Burshtein[183]), shifts to more positive values with increasing s without much change of capacitance, indicating that the process is irreversible over the range of s employed.

v) The overall shapes of the anodic i vs V profiles do not depend very much on s.

However, the cathodic reduction profiles are much more dependent on s, even in the ranges s = 0.01 to 0.10 V s^{-1}. The major peak, O_{C3}, through which oxide is reduced, becomes much broader with increasing s

---

* Definitions of these and other states are given on p.70 with respect to Figure 3-5.

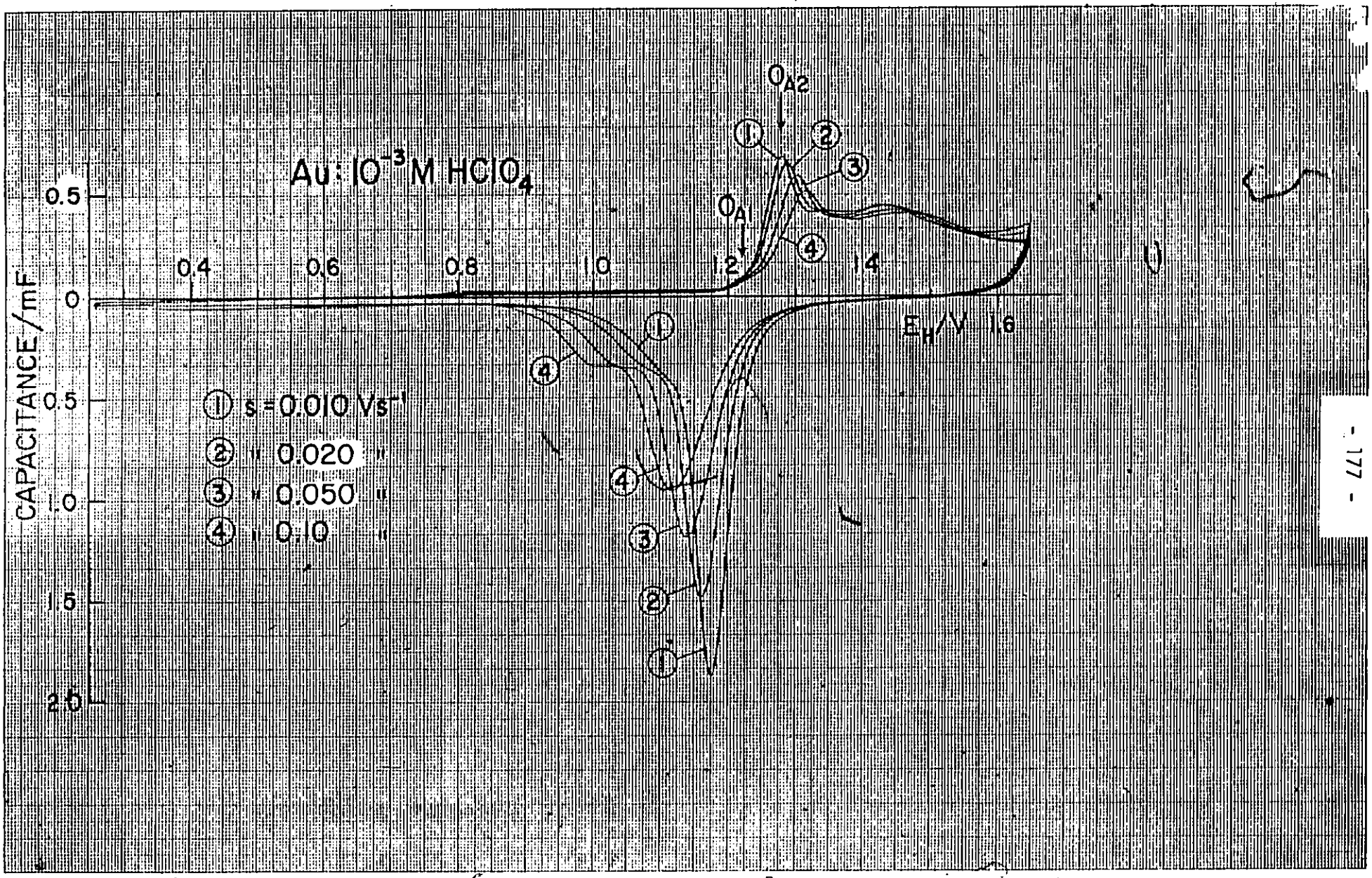

Figure 6-1 Potentiodynamic current-potential profiles for Au in 10^{-3} M $HClO_4$ for monolayer oxide formation and reduction at various sweep rates of 0.010 V s^{-1} to 0.10 V s^{-1}, 298 K.

and its V_p becomes less positive in the usual way[132] due to kinetic effects.

Theoretically[132], a broadening of a peak (for a 1 electron process) from a half width of 0.093 to 0.126 V and the drop of the associated capacitance to 73% of its reversible value is expected to occur as the surface process is driven from reversible ($s < s_o$) to irreversible ($s > s_o$) behavior. The observed changes in the O_{C3} peak ($\Delta V_{1/2}$: 0.059 to 0.110 V and C from 1.85 to 0.9 mF) are, however, larger than this and must therefore reflect a complex surface reaction probably with a pre-electrochemical step which supplies the electrochemically active species. At higher s, this time-dependent step effectively spreads out the availability of this electroactive material for reaction over a wider potential range as the sweep progresses, giving a broadening of the peak (cf Fig. L2, p. 59). A quite different behavior is observed for state O_{C2}, although the $V_{1/2}$ values for this peak are not easily measured due to some overlap with the much larger O_{C3} peak. The most striking feature of the O_{C2} peak is the independence of its i/s on s. The constancy of i/s and the shift of V_p with s indicate that a simple irreversible surface reaction is involved.

Quantitative treatment and further discussion of these effects follows, but the trends discussed above must be kept in mind.

4. Sweep Rate Dependence of Anodic Peaks

Although several anodic i/s peaks can be distinguished in the surface oxidation of Au, their overlap (cf Fig. 6-1) prevents quantitative analysis of their form, e.g. through $\Delta V_{1/2}$ evaluation.

Figure 6-2 illustrates the variation of V_p with log s for two states (O_{A2} and O_{A4}) of surface oxide formation on Au in 1.0 M $HClO_4$, and is representative of the dependence of V_p on log s for all the solutions studied. The variation of the potential of the "Burshtein minimum" (V_B) with sweep rate is also shown. The dependence of V_p on log s for the other

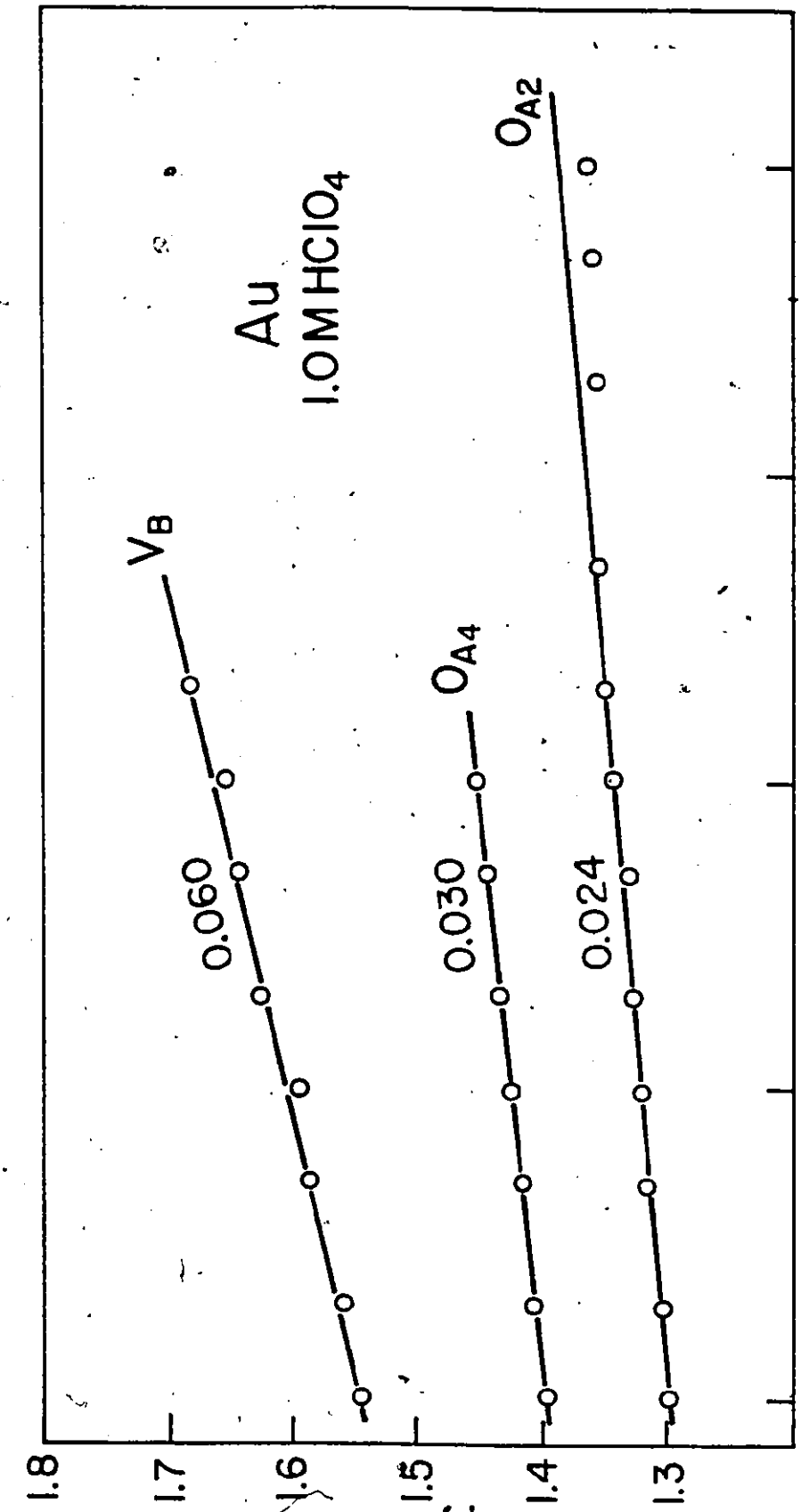

- Figure 6-2 Variation of V_p with log s for two states of surface oxide formation (O_{A2} and O_{A4}) and the "Burshtein minimum" on Au in 1.0 M $HClO_4$.

identifiable peaks cannot be followed for more than a decade of s due to peak overlap problems.

The variation of V_p with log s for peak O_{A2} is linear over more than four decades of s (Fig. 6-2), with a slope of 24 mV. The O_{A4} state behaves similarly (over 2 decades), giving a slope of 30 mV. Figure 6-3 shows corresponding behavior for alkaline [0.2 M $Ba(OH)_2$] solutions at 298 K. Linear V_p *vs* log s relations are also observed, again with low slopes.

The results for various solutions are summarized in Table 6-1. Some data for resolvable peaks, other than those referred to in Table 6-1, can also be obtained but only over a small range of s before overlap effects eliminate resolution. In clean 0.5 M H_2SO_4, for example, five current peaks (excluding the initial O_{A1}) can be identified and followed as a function of sweep rate over a limited range of s values (*ca* 0.001 to *ca* 0.1 V s^{-1}) with a $dV_p/d \log s$ of 0.023, 0.035, 0.018, 0.020 and 0.030 V/decade s.

From these results, it is evident that the peaks observed for oxide deposition are not highly sensitive to sweep rate, in contrast to the results (below) for the cathodic current peaks observed in reduction of that same oxide.

These slopes are surprisingly low for a surface process and would conventionally indicate that a multi-step mechanism is involved, which is actually hardly possible here. This important result will be examined in more detail in Chapter 8.

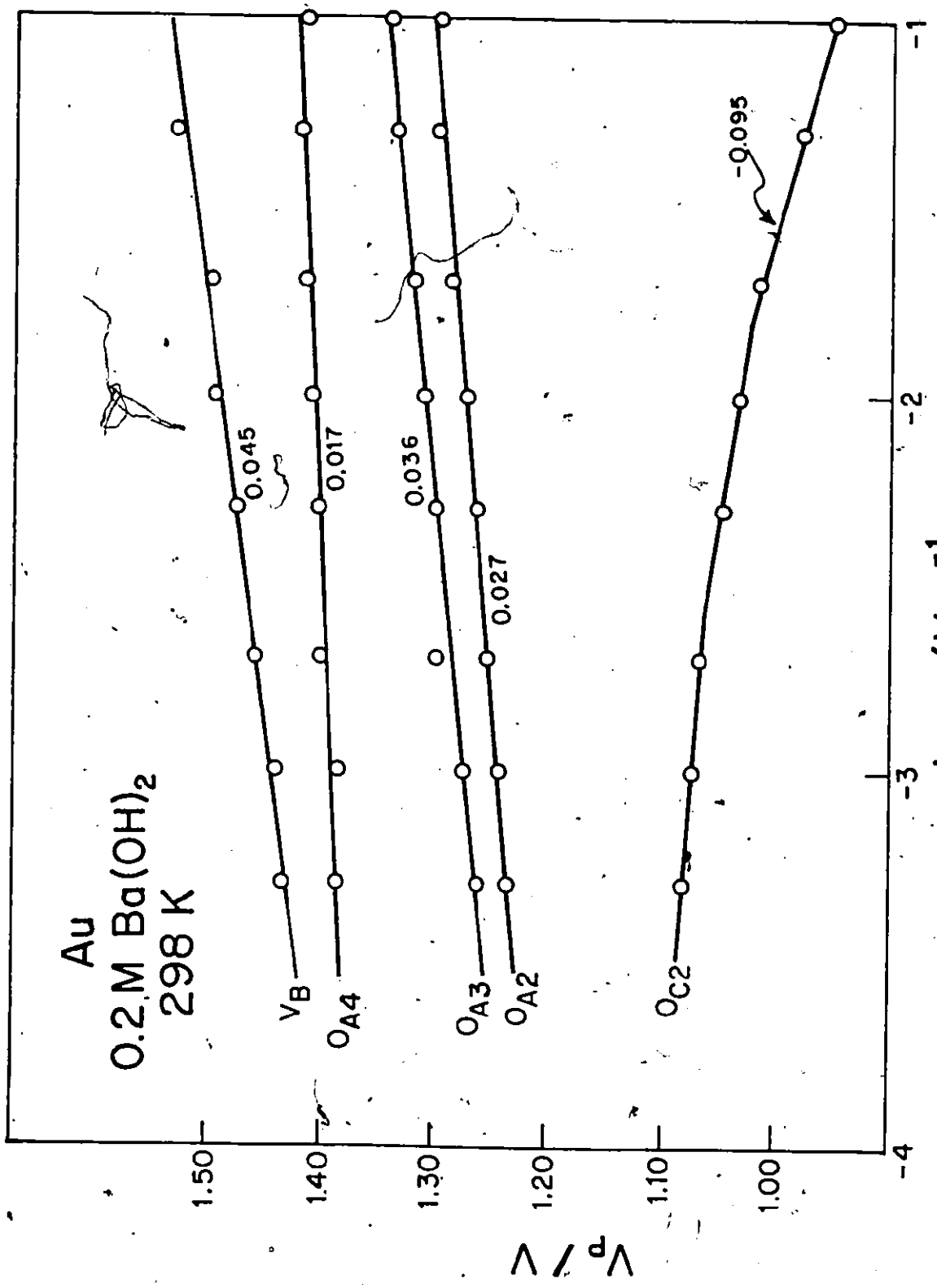

Figure 6-3 Variation of V_p with log s for several states of surface oxide formation on Au in 0.2 M $Ba(OH)_2$.

TABLE 6-1

$dV_p/d \log s$ for Oxide Deposition Processes at Au

Solution	O_{A2} (onset peak)	O_{A3}	O_{A4}	V_B
1.0 M $HClO_4$	0.024	-	0.030	0.060
0.1 M $HClO_4$	0.020	0.045	0.025	0.090
10^{-3} M $HClO_4$	0.038	-	0.040	0.085
0.5 M H_2SO_4	0.023	0.035	0.030	0.040
0.5 M H_2SO_4(273 K)	0.028-0.038	-	-	0.055
0.05 M H_2SO_4(293 K)	0.030-0.038	-	-	0.062
0.1 M Na_2CO_3	0.045	-	-	-
0.2 M $Ba(OH)_2$(273 K)	0.042	-	-	-
0.2 M $Ba(OH)_2$(298 K)	0.027	0.036	0.017	0.045

5. Sweep Rate Dependence of Cathodic Peaks

Cathodic sweep experiments reveal more details of the behavior states of surface oxide at Au than are obtainable in anodic sweep, because the additional effects of (a) the end potential, V_A, in the previous potential sweep and (b) the time of holding at V_A can be independently varied, as well as the sweep rate itself in the cathodic transient. Better evaluation of the diagnostic parameters can then be made.

When low coverages of oxide species are studied ($\theta_o < 0.1$), it is possible to determine the influence of sweep rate on the current peak for reduction of oxide in state O_{C1} (Fig. 6-4 for 0.1 M $HClO_4$). The results show that this species behaves kinetically in a very reversible way. Thus, V_p is essentially independent of s until $s > 10$ V s^{-1}.

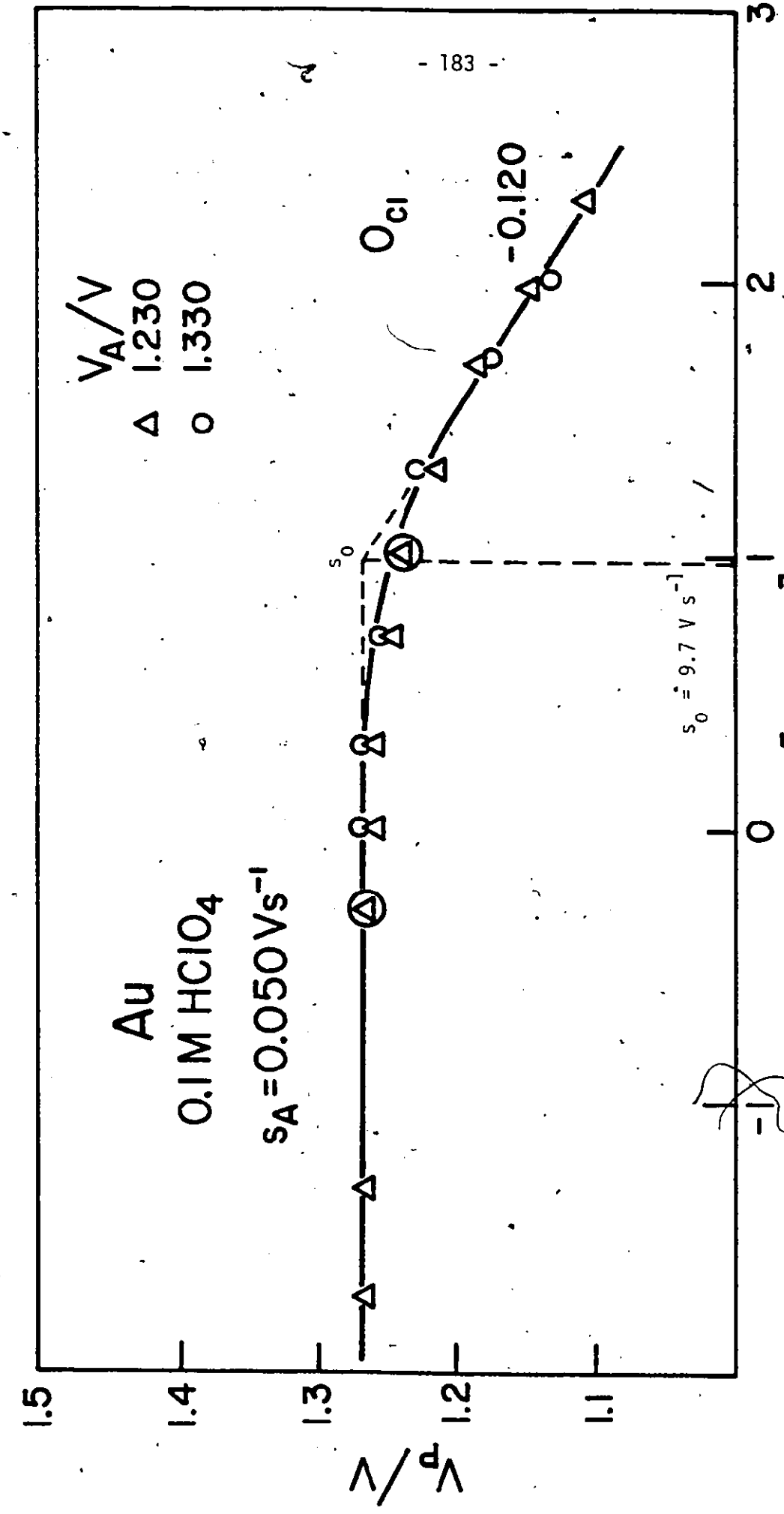

Figure 6-4 Variation of V_p with log s for reduction of oxide in state O_{Cl} on Au in 0.1 M $HClO_4$, 298 K.
$s_o = 9.7\ V\ s^{-1}$.

Thereafter $dV_p/d \log s \simeq 0.12$ V, i.e. 2RT/F. The corresponding s_o[185] value is 9.7 V s^{-1}. While results of this nature were obtained in several solutions, V_p for O_{C1} cannot be accurately followed if $s > 200$ V s^{-1} due to uncompensatable "iR drop" effects. This limits, practically, the range of s for which linear variation of V_p with log s can be observed for peak O_{C1} to a single decade of sweep rate or less.

As was also shown in Figure 6-1 (and earlier in Fig. 3-1) the other major peaks for reduction of oxide do not show reversible behavior, even at the lowest sweep rates employed. In 1.0 M $HClO_4$ at 298 K (Fig 6-5), V_p for O_{C3} is linear in log s with $dV_p/\log s \simeq 0.070 \sim 0.080$ V for several oxide coverages. Similarly, the behavior of O_{C2} gives $dV_p/d \log s \simeq 0.060 - 0.075$ V (decade s)$^{-1}$. In 0.5 M aq. H_2SO_4 (298 K), for a series of oxide coverages, $dV_p/d \log s \simeq 0.055 - 0.070$ and $0.052 - 0.060$ V (decade s)$^{-1}$ for states O_{C3} and O_{C2}, respectively (Fig. 6-6).

In alkaline solution, namely carbonate-free 0.2 M $Ba(OH)_2$, a different result is obtained. As discussed in Chapter 3, oxide species deposited in this medium are not reduced in the O_{C3} state in sufficient quantity to allow accurate quantitative measurements, although a small "O_{C3}" state can be seen to be present. The peak potential for the principal peak through which reduction of oxide species occurs, now O_{C2}, does exhibit the usual log relation between s and V_p (Fig. 6-7) over several decades of s. $dV_p/d \log s$ varies from $0.092 - 0.107$ V (decade s)$^{-1}$. The additional log region for V_p below $s = 0.10$ V s^{-1} (Fig. 6-7) cannot be well characterized; there is no sharp transition to reversible behavior.

The variations of the diagnostic parameters $\Delta V_{1/2}$ and i/s with log s (Chapter 3, p. 56) are shown in Figure 6-8. One group of the original i/s vs V profiles from which these data were obtained is shown

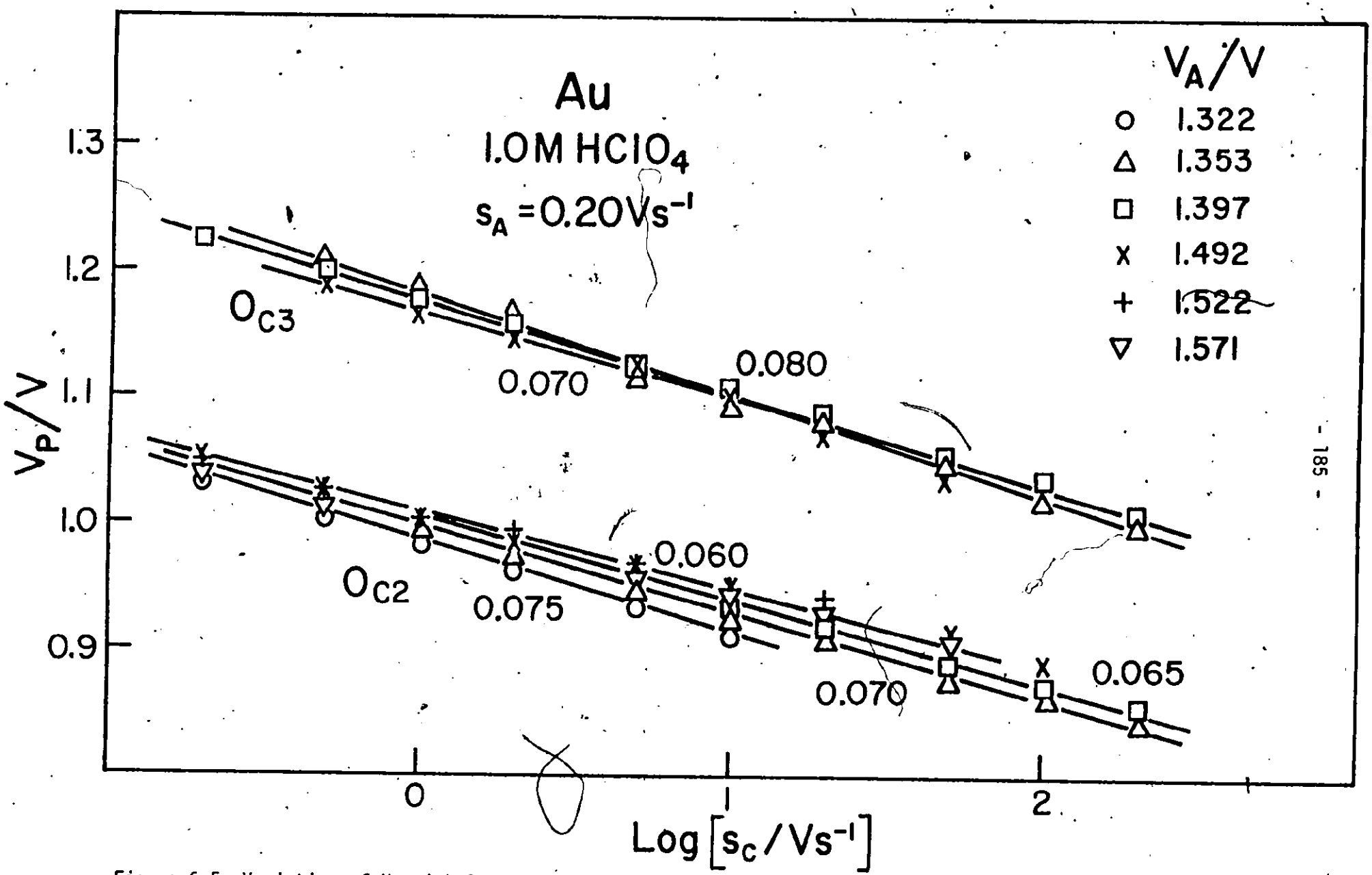

Figure 6-5 Variation of V_p with log s for reduction of varying amounts of oxide (previously deposited at 0.2 V s^{-1}) in states O_{C3} and O_{C2} on Au in 1.0 M $HClO_4$, 298 K.

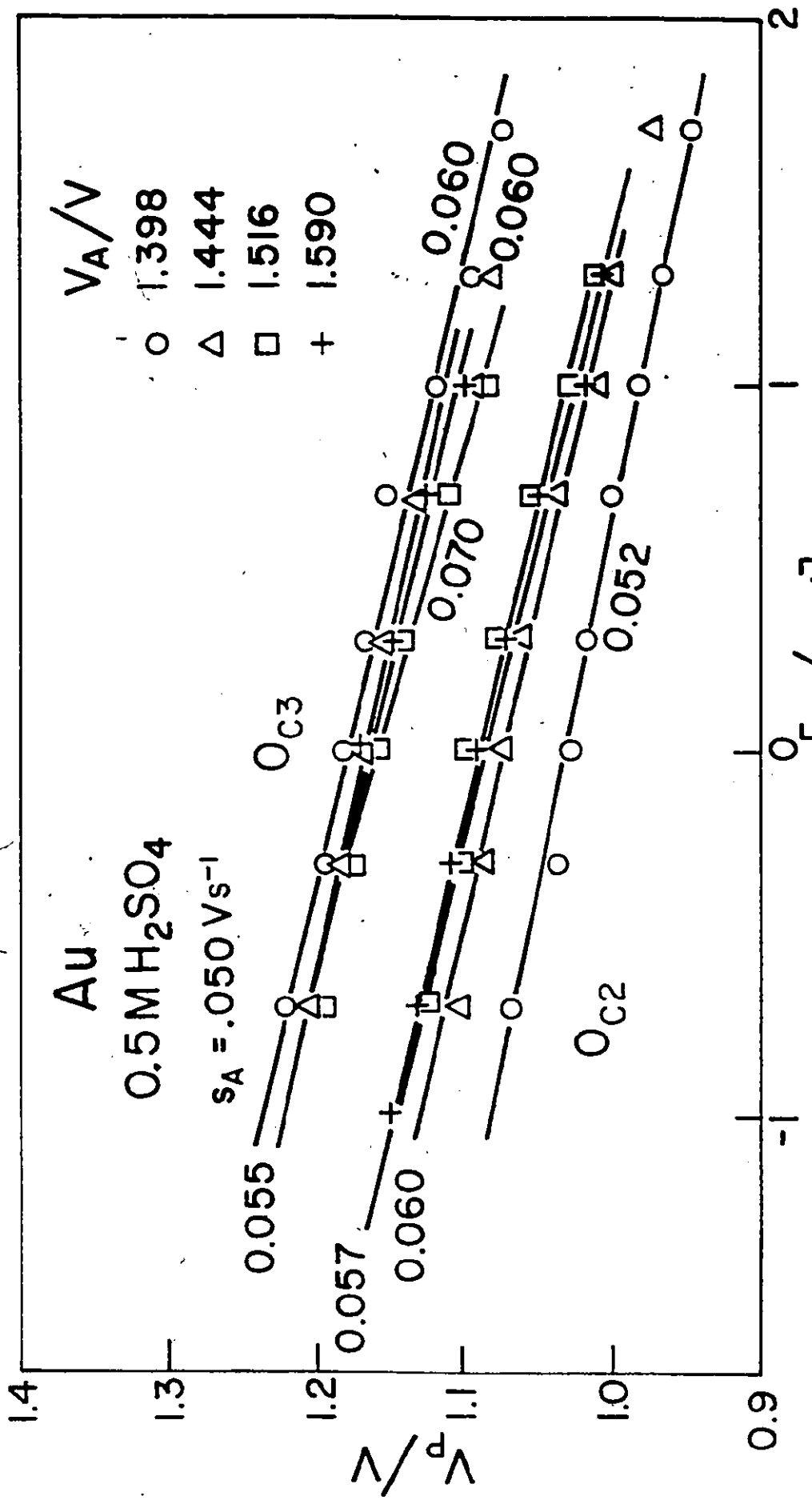

Figure 6-6 Variation of V_p with log s for reduction in states O_{C3} and O_{C2} of varying amounts of oxide previously deposited at 0.05 V s^{-1} on Au in 0.5 M H_2SO_4, 298 K.

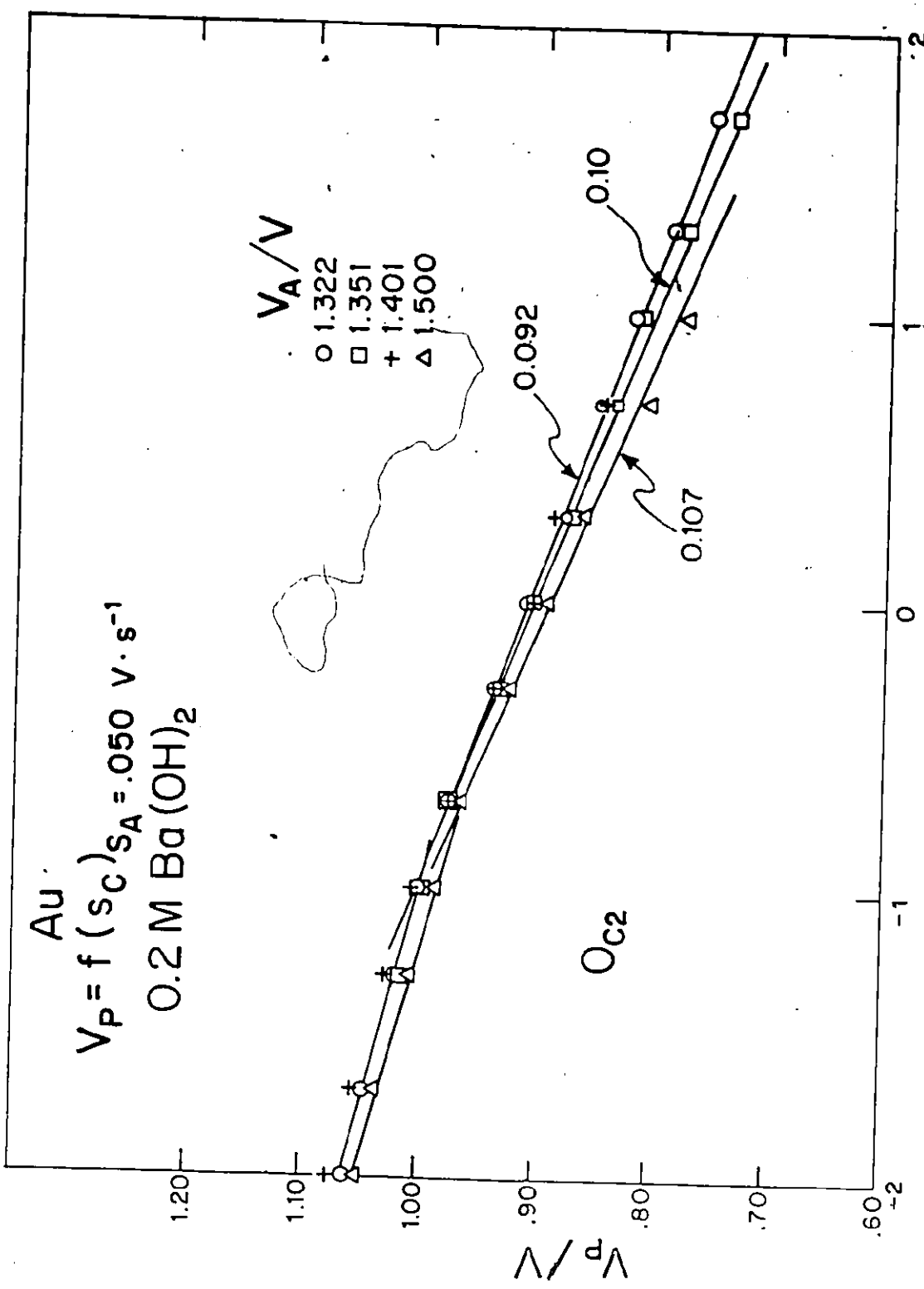

Figure 6-7 Variation of V_p with log s for reduction in state O_{C2} of varying amounts of oxide previously deposited at 0.050 V s^{-1} on Au in 0.2 M $Ba(OH)_2$, 298 K.

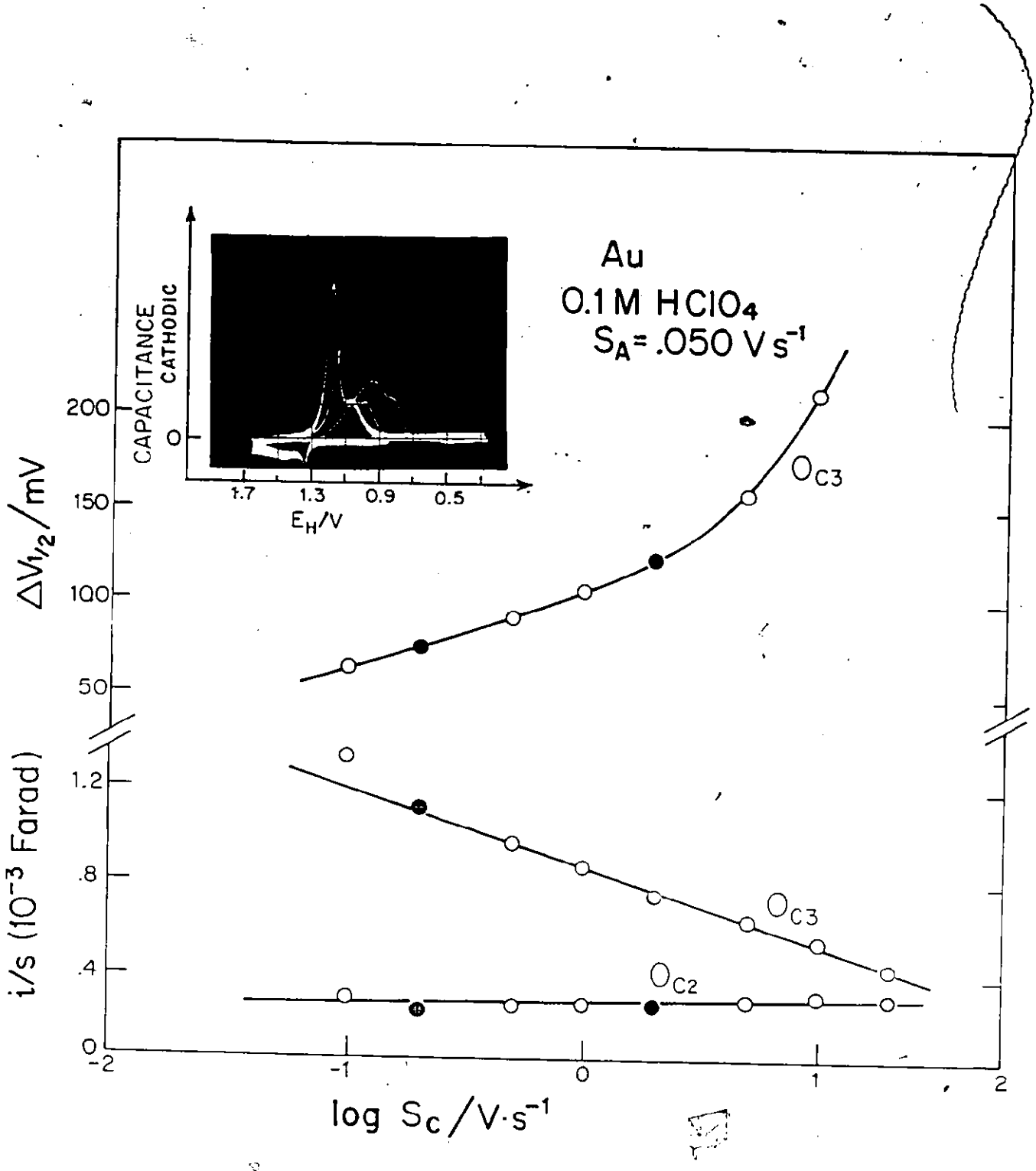

Figure 6-8 Variation of diagnostic parameters $\Delta V_{1/2}$ and i/s with log s for reduction in states O_{C3} and O_{C2} of oxide previously formed at 0.050 V s^{-1} on Au in 0.1 M $HClO_4$, 298 K.

in the upper part of the figure. Figure 6-8 shows quantitatively what was described earlier in section 3), i.e. the continuing decrease of capacitance, C, for state O_{C3} as s is increased, in quite striking contrast with the essentially constant C values for oxide reduction through state O_{C2}. Similar results are found for reduction of oxide states in all the acid solutions studied.

$\Delta V_{1/2}$ values for the O_{C3} peak increase in roughly logarithmic fashion with s (Fig. 6-8), and then, as s > 1.0 V s^{-1}, an even larger increase is observed. As discussed in section 1), such an increase in $\Delta V_{1/2}$ is larger than can be due to a simple surface reaction, and indicates that a 2-step reaction could be involved with a pre-electrochemical step.

Similar results for $\Delta V_{1/2}$ are shown in Figure 6-9 for 10^{-3} $HClO_4$, where it is seen that $\Delta V_{1/2}$ increases very rapidly from 60 up to > 160 mV as s is increased from 0.010 to 0.50 V s^{-1}. As was discussed in Chapter 1, several authors have argued that the reduction of oxide monolayers occurs through a mechanism of nucleation and growth (or nucleation of holes when referring to oxide reduction). However, theoretical evidence (discussed in Chapter 3, p. 56) now indicates that the highest value for $\Delta V_{1/2}$ which can be observed when a mechanism of nucleation and growth ("n + g" in Fig. 6-9) is operative (nucleation of holes when referring to oxide reduction) is 63 mV[132] and this value is exceeded in the present experiments for all but the very lowest sweep rates at which oxide reduction has been studied (Fig. 6-9). Thus, a mechanism of nucleation of holes for oxide reduction is not supported by these results, nor by some other experimental behavior to be discussed on p. 259.

Theoretically[132], $\Delta V_{1/2}$ values are much larger than for nucleation and growth if the mechanism involves simply irreversible random

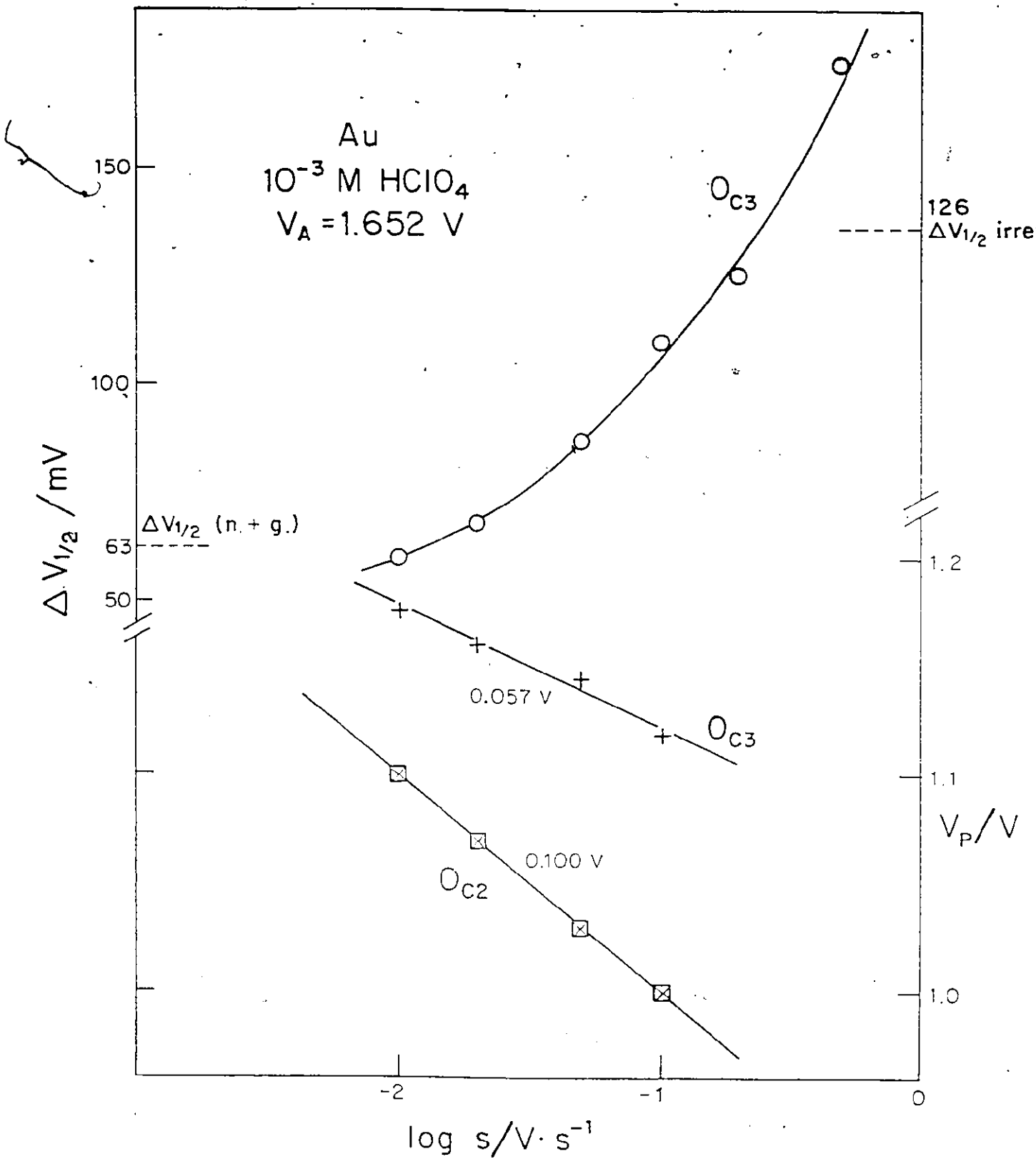

Figure 6-9 Variation of diagnostic parameters V_P and $\Delta V_{1/2}$ with log s for reduction in states O_{C3} and O_{C2} of oxide previously formed to V_A = 1.652 V at Au in 10^{-3} M $HClO_4$, 298 K.

deposition. Thus, under the latter conditons, $\Delta V_{1/2}$ should be 126 mV[132] if the interaction effects are negligible (g = 0). Experimentally, this value is exceeded for oxide reduction at only the highest sweep rate employed (Fig. 6-9). The values obtained for $\Delta V_{1/2}$ (O_{C3}) are consistent theoretically with an irreversible random process occurring under conditions where weakly attractive interactions (g small and negative) operate between the oxide species.

It is important to emphasize, however, that these increases in $\Delta V_{1/2}$ with increasing sweep rate are larger than those predicted theoretically[132] for the effect of sweep rate on a simple (1-electron) electrochemical process in transition from reversible to irreversible behavior. Thus, if a physical or chemical step in the mechanism of reduction of oxide is coupled with the electron transfer step, it introduces a kinetic time effect in a linear sweep experiment, manifested by peak broadening. Such an effect is strongly indicated by the experimental results. The existence of such a step, which must be relatively slow compared with the electrochemical step(s), accounts for the reduction of an increasing quantity of oxide in the O_{C3} state at lower sweep rates when additional time is available for the time-dependent (chemical) process to take place during the sweep. There is considerable support for this interpretation of the present results, based on computer simulation of the kinetic behavior of surface reactions[131] referred to in Chapter 3, p. 59. This behavior will be examined in more detail in Chapter 8.

Figure 6-9 shows the variation of V_p (O_{C3}) and V_p (O_{C2}) with log s. For the data of this figure, however, the sweep rates employed for oxide formation and reduction were identical, so that oxide coverages are somewhat higher for oxide deposited at the lower, than at

the higher, sweep rates. Since V_p for the larger peak O_{C3} is displaced to more cathodic potentials at higher coverages, this results in the slope $dV_p/d \log s$ for the smaller O_{C2} state somewhat higher than should otherwise be expected.

In alkaline solution [carbonate-free $Ba(OH)_2$], the peak i/s value for the "main growth peak", O_{C2}, shows the same decrease in value with increasing s as is observed for the O_{C3} peak in acid solution (Fig. 6-8). It is, however, not possible to measure accurately the various quantities associated with the O_{C3} current peak in this medium. $\Delta V_{1/2}$ values for O_{C2} follow the same trend, and with similar values, as already described for O_{C3} in acid solutions (Figs. 6-8 and 6-9).

The dependence of V_p on log s, for various ranges of s and oxide coverages, is summarized in Table 6-2 for results obtained in the seven electrolyte solutions used.

TABLE 6-2

$dV_p/d \log s$ For Oxide Reduction Processes At Au, in V (Decade s)$^{-1}$

Solution	O_{C1}	O_{C3}	O_{C2}
1.0 M $HClO_4$	-	0.070-0.080	0.060-0.075
0.1 M $HClO_4$	0.120	0.060-0.068	0.075-0.085
10^{-3} M $HClO_4$	0.110	0.060	0.100
0.5 M H_2SO_4	-	0.050-0.070	0.052-0.060
0.05 M H_2SO_4	-	0.060-0.070	0.070
0.1 M Na_2CO_3	0.070	0.055-0.060	0.085-0.110
0.2 M $Ba(OH)_2$	0.080-0.095	0.040-0.060	0.090-0.107

The ranges of values shown for O_{C3} and O_{C2} in acid solutions are

derived from the results of many measurements at varying oxide coverages. The other data are less extensive.

It appears that an average, or typical value of $dV_p/d \log s$ for O_{C1} would be ca 0.12 V (decade s)$^{-1}$, for O_{C3}, it would be ca 0.060 V (decade s)$^{-1}$ and for O_{C2} ca 0.060 V (decade s)$^{-1}$ or more. It may be misleading, however, to round off these values for the sweep rate dependence of V_p to values of theoretical significance, e.g. 0.060 V, viz. 2.3 RT/F as we have done here. The i vs V profiles (e.g. Fig. 6-1) show that the slope for O_{C2} is significantly higher than that for O_{C3}, so that peak O_{C2} appears to "move out" from under O_{C3} as s is increased. Hence, the values for $dV_p/d \log s$ for these two peaks cannot be equal.

Additionally, only 2 or 3 points are available for evaluation of the effect of sweep rate on V_p for O_{C1} due to the high s_o for this peak. At such high sweep rates, uncompensatable "iR drop" effects vitiate the accurate evaluation of $dV_p/d \log s$.

It is to be noted that the $dV_p/d \log s$ values for the peaks resolved in cathodic sweeps (Table 6-2) do not correspond in any simple way with any of the values (Table 6-1) for oxidation peaks observed in anodic sweeps. The latter values are usually lower, in fact surprisingly low, for a surface process. They would conventionally indicate that a multi-step mechanism is involved. These differences are due in part to kinetic effects associated with slow anion adsorption/desorption processes which are connected with the kinetics of the oxide formation or reduction processes themselves, as will be discussed in Chapter 8.

6. Summary

The following general points are to be noted:

a) The slopes of the anodic i/s vs V profiles are similar, in a general way, for the various solutions (p. 69) investigated, including alkali [$Ba(OH)_2$] (apart from the unusual behavior in the so-called double-layer region [Fig. 3-8]).

b) The onset of surface oxidation and the overlap of peaks O_{A1}, O_{A2} etc. depends on the anion of the electrolyte, because of ion adsorption effects (Fig. 3-2).

c) The i/s values for the various anodic peaks are comparable, that for O_{A2} being the largest.

d) Although the $\Delta V_{1/2}$ value for the first main peak in surface oxidation of Au is ca 70 mV, the remainder of the anodic oxidation i vs V profile requires a "g" factor value of ca 12 to account for its spread as is also found for the oxide film at Pt beyond the monolayer OH stage.

e) Broadening of an i vs V profile with increasing s can also arise when a chemical step is kinetically coupled with an electrochemical one. Then peak broadening ($\Delta V_{1/2}$ unusually large) can arise with increasing sweep rate, even when $q = 0$. Cases like this can arise in the present work.

f) Apart from the small quantity of oxide deposited and reduced reversibly in the O_{A1}/O_{C1} region, reversible behavior for which $dV_p/d \log s = 0$ is not observed even at the lowest sweep rates. This must be attributed, we believe, to time-dependent, non-electrochemical steps in oxide growth and reduction, as well as to slow anion adsorption/desorption processes.

g) Diagnostic parameters (e.g. $\Delta V_{1/2}$ for O_{C3}) indicate that oxide reduction is not a simple surface reaction, but rather a 2-step process with a pre-electrochemical step. Also, a mechanism of "nucleation and growth" (or nucleation of holes in reduction) is not supported.

Interpretations of these important results, and the nature of the time-dependent non-electrochemical processes, will be suggested in more detail in Chapter 8.

CHAPTER 7

HIGHER EXTENTS OF OXIDATION AND THE EFFECTS OF AGING OF THE OXIDE

In preceding chapters, detailed information was given on the kinetics of oxide growth and reduction, especially with regard to the influence that variables such as potential and type of electrolyte have on the constituent processes. However, it is desirable to learn more about the interrelationships between the various states which give rise to the current peaks in the i vs V profiles.

While some experimental observations on this question were already discussed in Chapter 3, important additional information is provided from studies of "aging" of the oxide film.

Recent work in the literature shows that oxide films in the monolayer range on Pt[20,128] and on Au[118] undergo some aging processes. In particular, the kinetics of electrochemical reduction processes are sensitive to aging of the oxide, as revealed for Pt by Conway et al[20,21] in acid aqueous systems and by Arvia[192,193] in molten salt systems. More recently, Arvia[118,119,128] has extended his investigations to include what he has termed "dynamic aging" of oxide monolayers at Pt[119,128] and Au[118,119] electrodes in aqueous acid solutions. Arvia, who observed the type of aging described below, has also indicated[12] that both anodic and cathodic potentiodynamic i vs V profiles depend strongly (e.g. the peak potentials, V_p) on both the rate of potential sweep and the end potential reached in the anodic sweep, and that these effects, he supposed, are related to aging of the oxide. Such a conclusion, is clearly not supported experimentally for anodic sweeps (Chapters 3 and 6), and is justified only under circumstances in which, and to

the extent that, the strong dependence of various current peak parameters on sweep rate referred to is greater than that normally associated with sweep rate effects for kinetically irreversible current peaks Effects of this nature have been found for oxide monolayer reduction at Au and were described in the previous chapter.

Aging effects are manifested as shifts of potentials of reduction current peaks to less positive values under circumstances where conditions have been chosen so that total oxide coverage remains constant, i.e. no net electrochemical formation or reduction occurs in the aging period. Results of this kind have been verified in the present work and a more comprehensive investigation of aging effects has been made.

The special V vs t program used to evaluate the aging effects was shown in Figure 2-5f (p.49). After formation of an oxide film under the required conditions, partial reduction of that film is allowed to occur in the subsequent cathodic sweep.

Following this procedure, two types of subsequent potential change are addressed to the electrode:

(i) After the partial reduction, the oxide film is re-formed up to the same positive end potential as in the previous sweep.

(ii) After the first formation of the oxide film, partial reduction and re-formation of the film, as in (i), is conducted but in a repetitive manner, often at elevated sweep rates. Finally a reduction curve is taken and compared with that in a single anodic/cathodic sweep.

Briefly, the results of procedures (i) and (ii) are as

follows: (i) after this procedure, the i vs V profile for the next anodic sweep is very different from that for a complete sweep on a previously unoxidized surface; (ii) after this procedure, for a controlled period of aging, the final complete reduction profile is very different from that observed in a normal cyclic sweep over the full potential range. The aging effect depends appreciably on the potential limit (V_2 in Fig 2-5f, p. 49) in the particular reduction sweep i.e. on how much coverage of oxide remains after the partial reduction.

Experiments of these kinds enable growth of oxide, from a pre-existing partially complete oxide film, to be studied; this incomplete film is different from that which would exist on the surface at the same potential had it been grown directly from an initially bare surface.

Thus, appropriate choice of the potential limit for partial reduction can selectively eliminate all or part of the oxide reduced in a given state (e.g. O_{C3}). In this way, the effect of commencing redeposition and growth of an oxide film without the oxide species corresponding to e.g. the O_{C3} reduction peak can be followed, i.e. on a surface with only oxide in the O_{C2} state present. Also, multiple cycling (e.g. for 20 minutes at sweep rates > 2 V s^{-1}) enables quite small changes in the states of the oxide film to be selectively distinguished as the aging process continues.

Before proceeding further with this discussion, it is necessary to describe briefly the behavior of "higher" extents of surface oxidation that are developed in the course of the aging treatment. We shall not discuss these effects further because they correspond to oxide deposition above the monolayer level.

1. Extents of Oxidation Greater than a Monolayer

Extents of oxidation greater than a monolayer can be achieved at Au, as at Pt, and refer to species deposited beyond the nominal monolayer limit of $\Theta_O = 1$ (oxide counted as O species). Such oxide species develop on Au under strong anodic polarization or when the oxide film is aged in a cycling regime over a restricted (oxidizing) potential range. In either case, the oxide film thickens with the appearance of new characteristic current peaks observed in the cathodic i vs V profile, with less positive peak potentials.

The development of higher coverages in oxides deposited from 0.05 M H_2SO_4 at 273 K is indicated in the family of i vs V profiles shown in Figure 7-1, recorded for a series of successively increasing end potentials in the anodic sweep. Profile #1 shows oxide formation up to ca 1.0 monolayer (as O species). The reduction of this oxide occurs predominantly through the O_{C3} state, although some reduction through O_{C2} is evident.

The continuous shift of potential (V_p) for this reduction peak to less positive values as the degree of oxidation of the electrode is increased in successive sweeps indicates that the oxide formed is more and more stable with respect to reduction. That is, more cathodic potentials must be applied in order to reduce the oxide. This implies that a more stabilized oxide phase is produced under these conditions, presumably because the application of higher potentials and an increasing amount of time spent at these oxidizing potentials has enabled a more complete re-organization and stabilization of polar oxide species in the growing oxide to be attained. This behavior is evidently coupled with the trend to multilayer oxide formation as $Q > 400\ \mu C\ cm^{-2}$.

As the quantity of oxide deposited becomes increased in

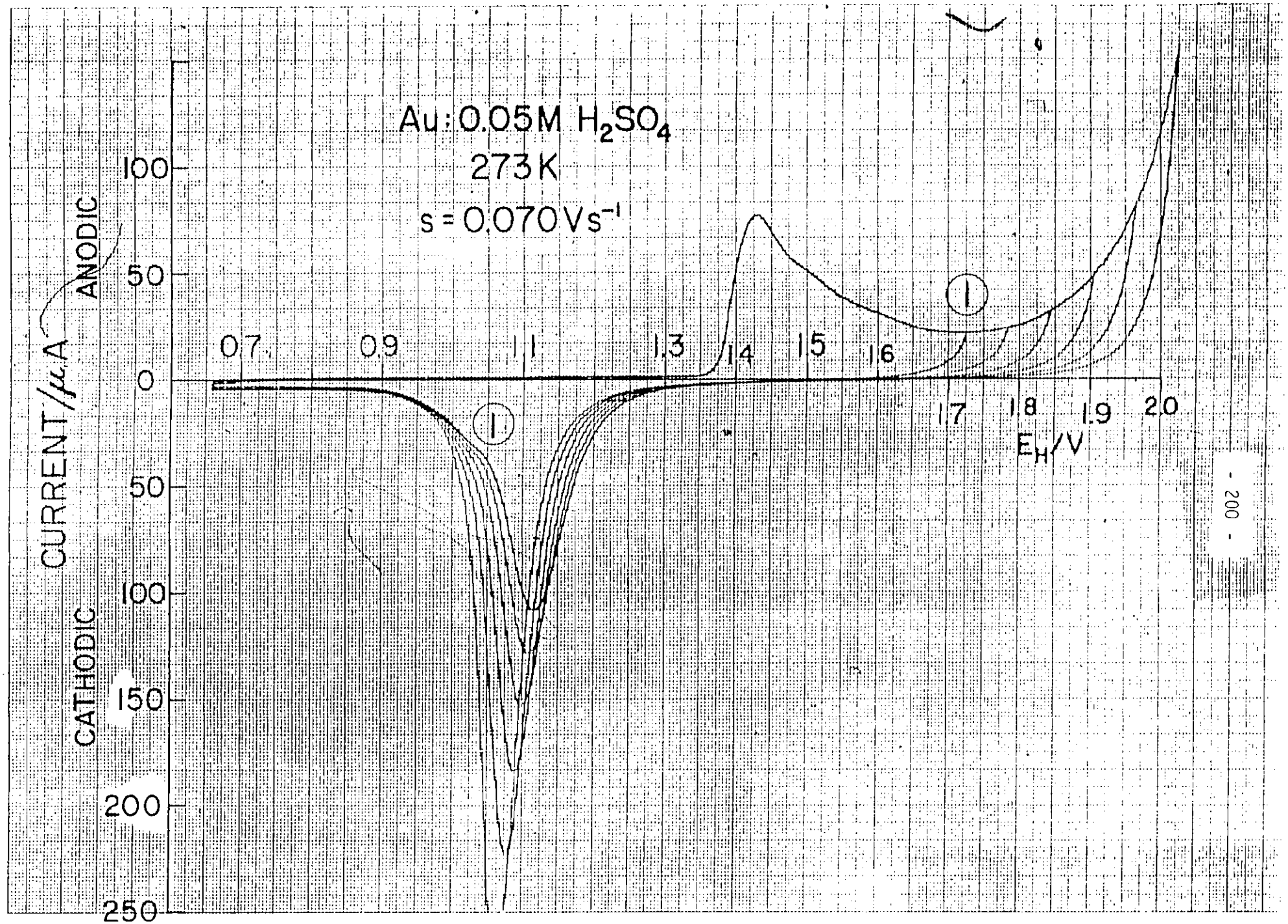

Figure 7-1 Potentiodynamic current-potential profiles for Au at 0.070 V s^{-1}, 273 K, taken to a series of anodic end potentials in 0.05 M H_2SO_4, illustrating extents of surface oxidation beyond one monolayer (as O species).

successive sweeps taken to progressively higher potentials, the oxide reduction behavior changes.

The current peak, O_{C2}, apparently at saturation coverage, ceases to be observable when reduction proceeds from higher coverages. Even before the highest level (θ_o = ca 2 monolayers of O) of oxide deposition observed in Figure 7-1 is attained, reduction appears to occur in a single current peak. It is believed that this corresponds to reduction of an oxide film greater than a monolayer in average thickness, as opposed to reduction of submonolayer quantities of oxide for which multiple cathodic peaks are observed as in Figure 3-5 and 4-1 to 4-4.

When the oxide film is formed in 0.2 M $Ba(OH)_2$ at s = 2.0 V s^{-1}, similar behavior is observed. In Figure 7-2a a series of i vs V profiles are recorded for oxidation at a series of higher potentials in successive 100 mV increments up to 1.90 V.

In reduction of oxide deposited in the anodic sweep taken to 1.90 V, a new current peak (besides the dominant O_{C2}) emerges at potentials ca 100 mV more positive than O_{C2}, as well as substantial reduction currents at potentials just negative to O_{C2}. (Note, it is the O_{C2} rather than the O_{C3} peak in $Ba(OH)_2$ which is associated with reduction of the main anodically grow species.

The effects of aging of oxide formed in aq. $Ba(OH)_2$ under these conditions are seen in Figure 7-2b, where a series of reduction profiles recorded after a series of aging re-oxidation cycles between 1.10 and 1.80 V are shown. The effect of the longest aging time (2.5 minutes) on the i vs V profile is seen in Figure 7-2c, superimposed on the normal multi-sweep profile for potential taken to +1.80 V, E_H. The relative extent of oxidation of the Au surface with the aged oxide is ca 2 expressed as "θ_o".

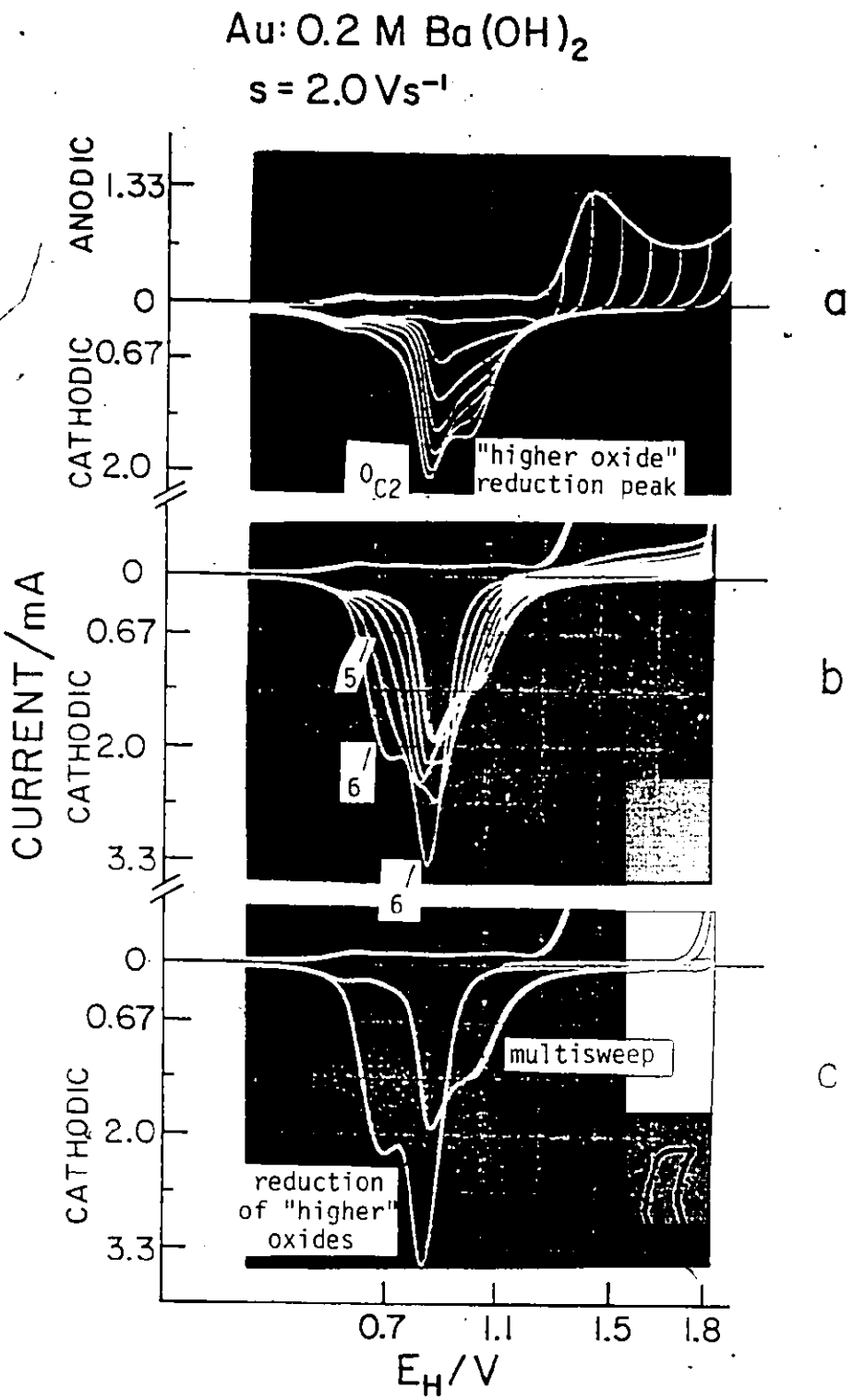

Figure 7-2 Potentiodynamic current-potential profiles for Au at 2.0 V s^{-1}, 298 K in 0.2 M $Ba(OH)_2$ for (a) a series of anodic end potentials; (b) development of higher extents of surface oxidation through dynamic aging of oxide and (c) comparison of monolayer oxide reduction profile with highest coverage profile of (b)

The emergence of a peak in the profiles of Figure 7-2a which may be attributed to reduction of a more extensively formed ($\Theta_o > 1$) oxide film, is seen also in the profiles of Figure 7-2b. However, as the currents in the emerging peak become larger, the peak potential shifts to less positive values and this peak eventually becomes the main one observed for oxide reduction as in Figure 7-2c. The O_{C2} state has become saturated at ca its value in Figure 7-2a. In addition, the increasing currents observed on the cathodic side of the O_{C2} peak in Figure 7-2a have now become so appreciable that a new major current peak evidently develops, as seen in curves 5 and 6.

The results indicate that some additional states of the oxide film can be distinguished beyond those attributable to monolayer processes and before "bulk" ($\Theta_o \pm$ ca 3) oxide deposition becomes established. These peaks are associated with reduction of the more extensively oxidized ($\Theta_o > 1$) surface. Note that when a true "bulk" species is formed its reduction will occur at a constant potential, apart from kinetic and iR effects. The progressively narrowing peaks as "Θ_o" increases beyond 1 indicates a gradual approach to "bulk" behavior in this respect.

2. Aging of the Oxide

The use of aging V vs t programs to study oxide growth has the advantage that oxide growth processes are altered in a sensitive way depending on the aging history and the potential limits of the aging cycles. Multiple cycling during aging can effectively enhance, or "develop", quite small effects otherwise not detectable.

Figures 7-3 to 7-6 show the effects of varying the reversal potential, V_2, in the program of Figure 2-5f, p.49 for oxide formation and reduction in 0.05 M H_2SO_4 in a sweep up to 1.47 V. The profiles of Figure 7-3 are obtained after aging for 1 minute in cycles at 1.0 V s^{-1}

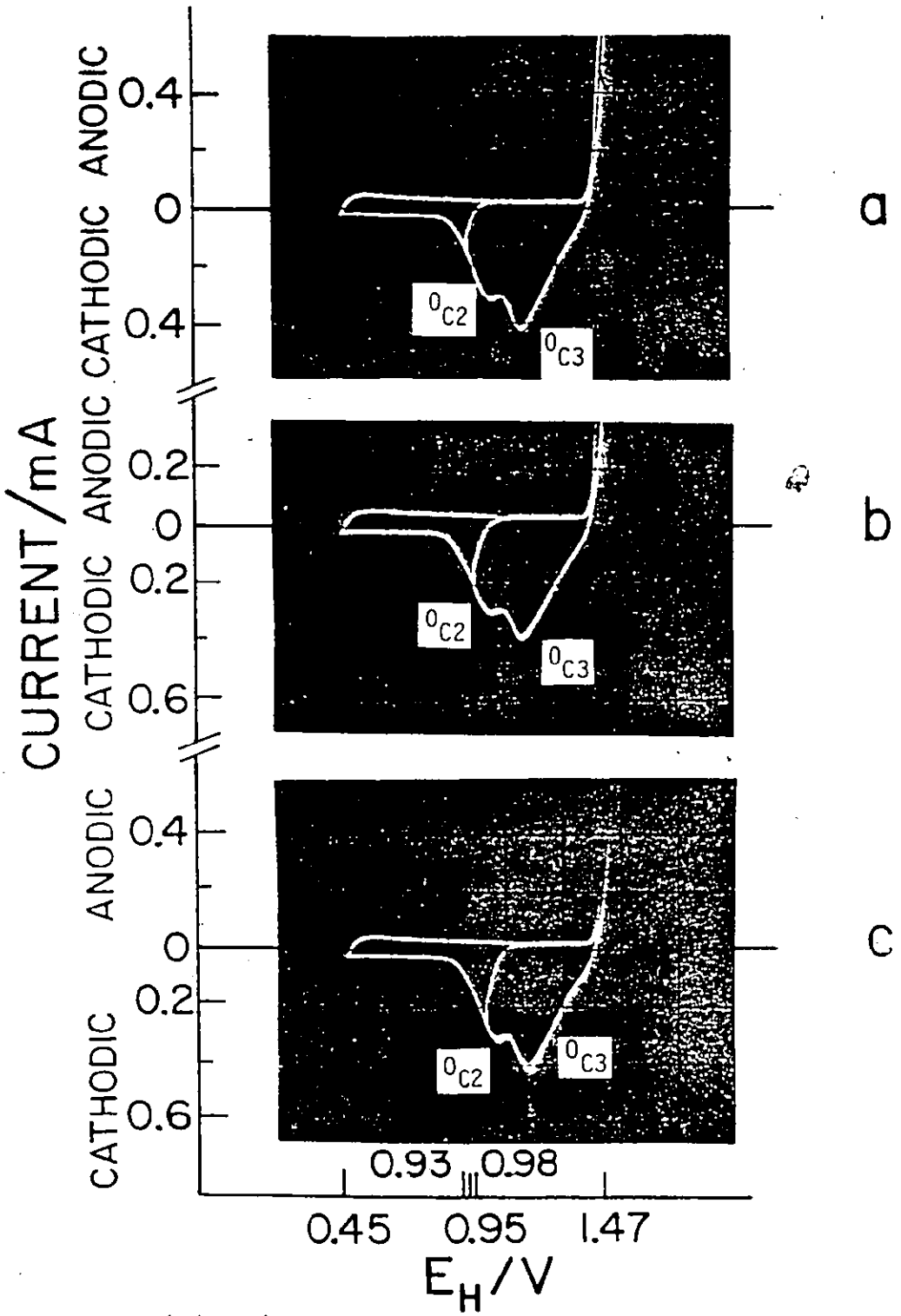

Figure 7-3 Potentiodynamic current-potential profiles for Au at 1.0 V s^{-1}, 298 K in 0.05 M H_2SO_4 for reversal of the cathodic potential sweep at various potentials, V_2, and "dynamic aging" of the oxide to 1.47 V for 1 minute using program f, Figure 2-5, p. 49: (a) V_2 = 0.93 V; (b) V_2 = 0.95 V and (c) V_2 = 0.98 V

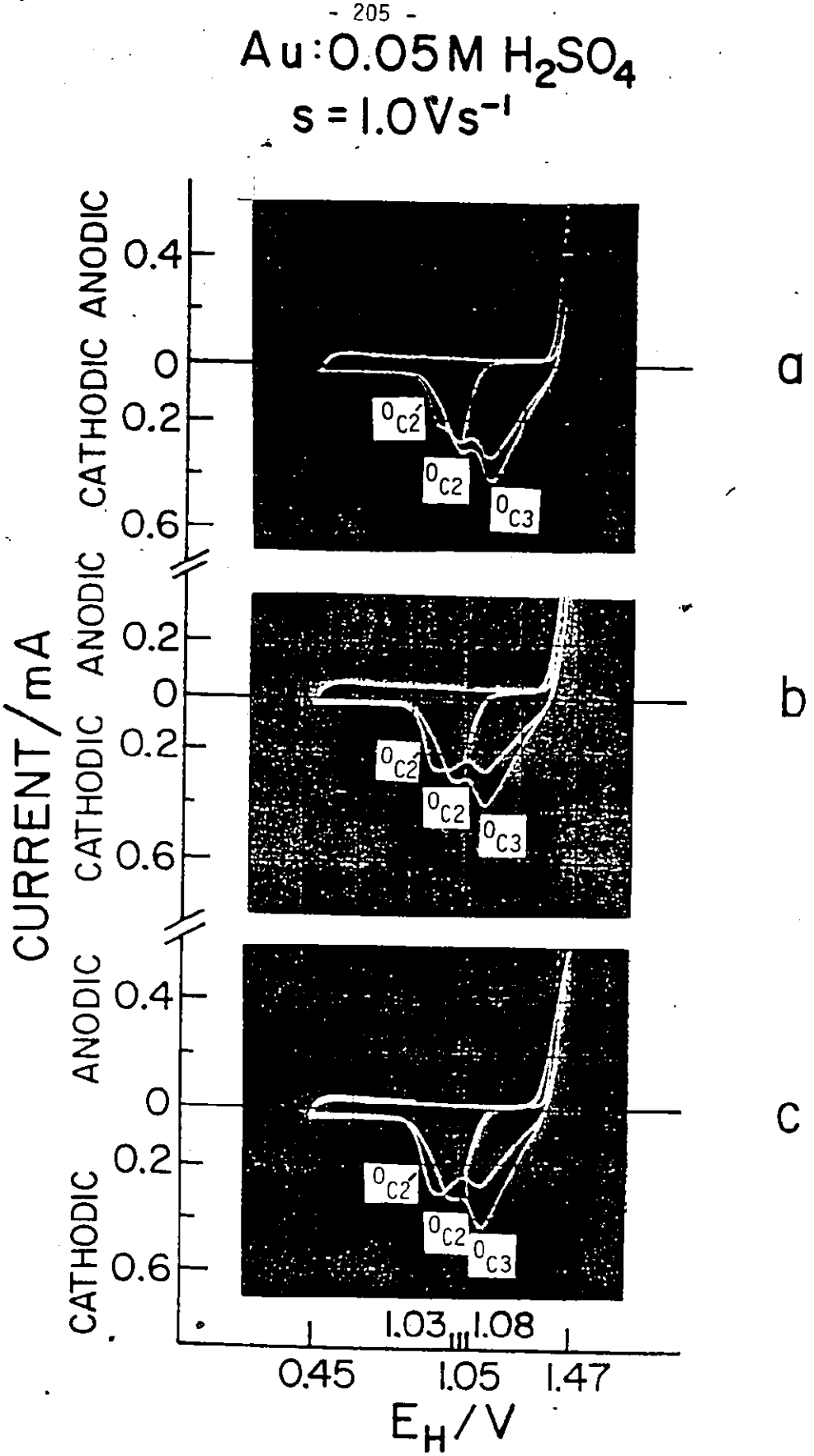

Figure 7-4 Potentiodynamic current-potential profiles for Au at 1.0 V s^{-1}, 298 K in 0.05 M H_2SO_4 for reversal of the cathodic potential sweep at various potentials, V_2, and "dynamic aging" of the oxide to 1.4- V for 1 minute using program f, Figure 2-5, p. 49: (A) V_2 = 1.03 V; (b) V_2 = 1.05 V and (c) V_2 = 1.08 V

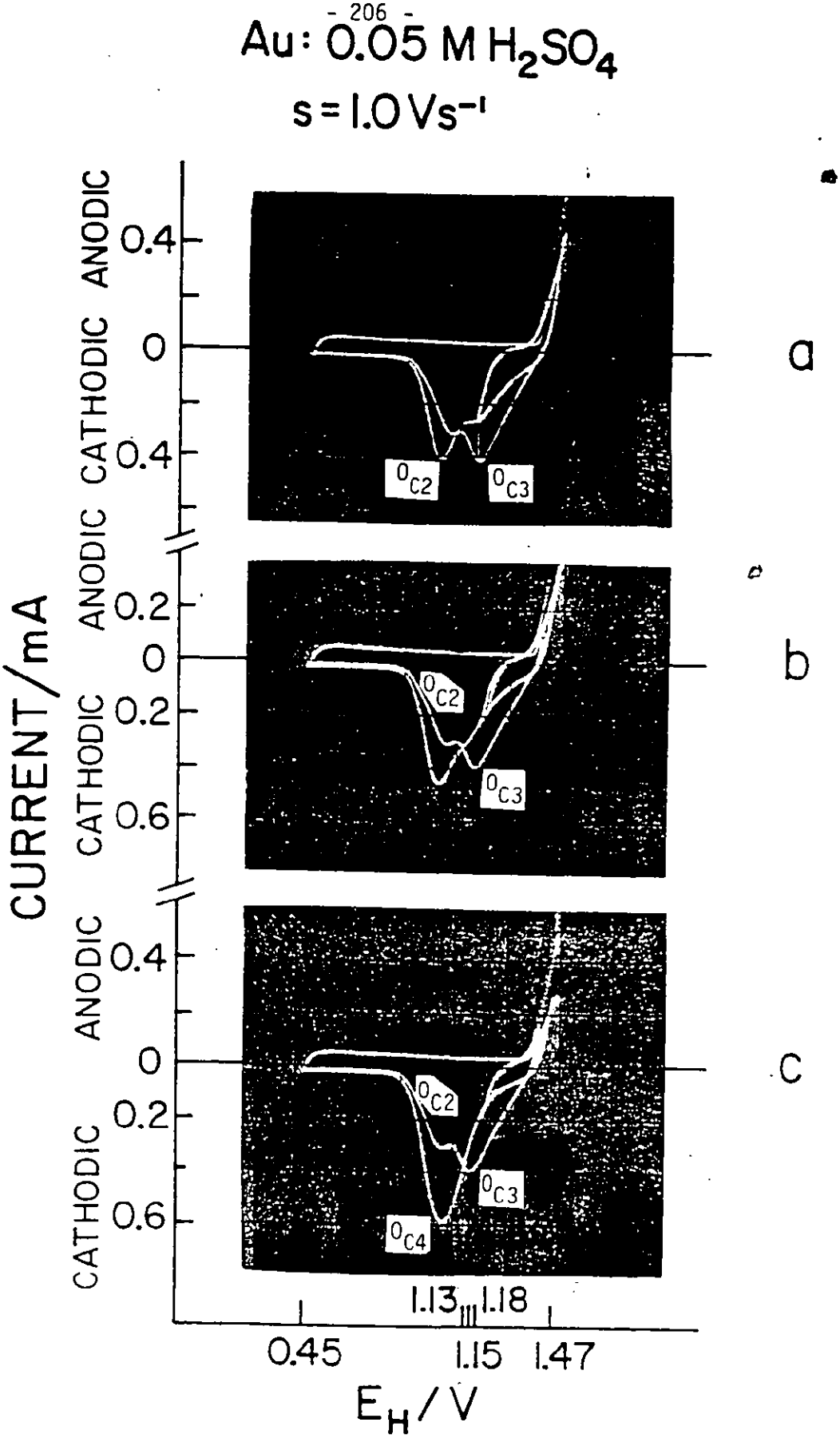

Figure 7-5 Potentiodynamic current-potential profiles for Au at 1.0 V s^{-1}, 298 K in 0.05 M H_2SO_4 for reversal of the cathodic potential sweep at various potentials, V_2, and "dynamic aging" of the oxide to 1.47 V for 1 minute using program f, Figure 2-5, p. 49: (a) V_2 = 1.13 V; (b) V_2 = 1.15 V and (c) V_2 = 1.18 V

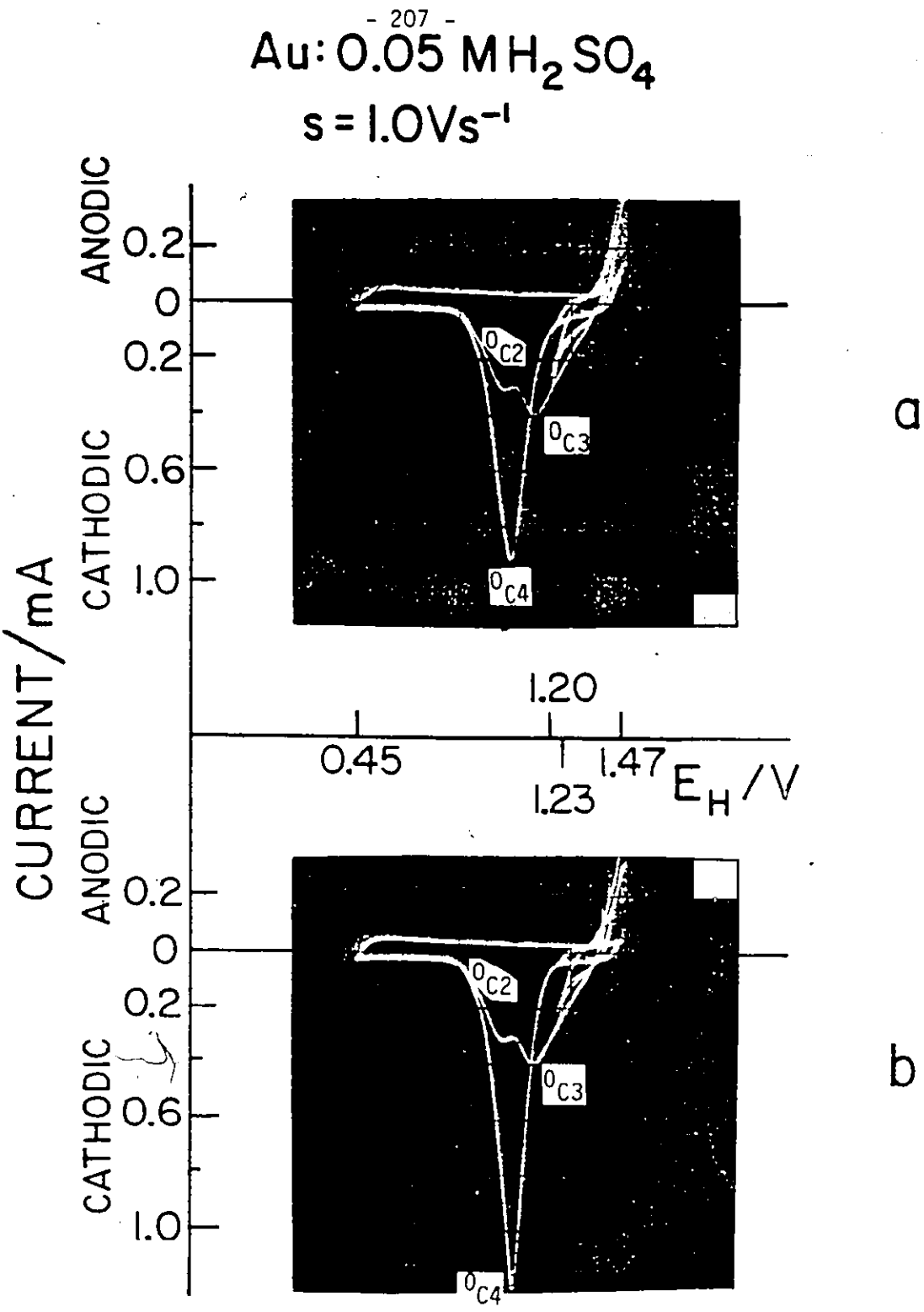

Figure 7-6 Potentiodynamic current-potential profiles for Au at 1.0 V s^{-1}, 298 K in 0.05 M H_2SO_4 for reversal of the cathodic potential sweep at various potentials, V_2, 1 minute using program f, Figure 2-5, 0. 49: (a) V_2 = 1.20 V; (b) V_2 = 1.23 V

between 1.47 V and the selected value of V_2, and show that no effect of aging is seen in the reduction current profiles until the reversal potential has been increased to 0.98 V (Fig. 7-3c); the lowest value of V_2 for which an effect can be observed. The lack of any aging effect under these conditions must be attributed (at $V_2 < 0.98$ V) to the complete reduction of the oxide (after sweep reversal) before oxidation currents re-commence in the anodic sweep, even when the cathodic limit of "partial" reduction is 0.98 V. The currents observed after sweep reversal are still cathodic for close to 100 mV along the reverse (anodic) sweep (Fig. 7-3c), i.e., until the potential has been raised to ca 1.1 V. Apparently a bare metal surface has been restored at this potential in the profile, following the reversal of sweep in the anodic direction. The behavior here (Fig. 7-3c) is typical of slowness in the reduction process as was indicated by the holding experiments described in Chapter 4.

The i vs V profiles in Figure 7-4 show the first effects of aging as V_2 is increased to 1.03, 1.05 and 1.08 V, respectively. Under these conditions, aging of the oxide results in a slight reduction of the overall quantity of oxide on the electrode surface, as measured in the final reduction of the aged oxide. In addition, the distribution of reducible oxide species shifts with increasing V_2 so that smaller quantities of O_{C3} charge, and larger quantities of O_{C2} (and especially O_{C2}') charge can be detected. These conditions of repetitive cycling apparently allow the oxide species reduced in peak O_{C2} to accumulate at the expense of those giving rise to O_{C3}. Since the aging program is expected to produce an ionic environment at the electrode interface in which the average, or steady-state concentration of anions is diminished as compared to multisweep conditions as V_2 increases, a

tentative explanation for these results may center on the influence of anions on the reduction of the oxide species, as will be discussed further in Chapter 8.

Alternatively, the formation of oxide species reduced through O_{C2} may be blocked by anions, so that a surface environment, from which these anions have been largely eliminated, may permit the accumulation of these species beyond previous limits or saturation levels (Chapter 3).

It must be borne in mind, however, that for $V_2 > 0.98$ V oxide is not completely removed from the electrode before subsequent oxidation (after sweep reversal) commences at potentials > 1.4 V. This remaining oxide may serve as a base for the next cycle of oxide growth and partial reduction but, because of the manner in which O_{C2} charge accumulates, it appears that oxide is deposited on the remaining bare metal surface with the same distribution between reduction states as would normally be expected. Thus, O_{C2} is accumulated in successive cycles necessarily at the expense of O_{C3}. This is of fundamental importance; it implies that the states O_{C2} and O_{C3} are <u>not fixed stoichiometrically</u> either as well defined different chemical species or as the same species but deposited on different crystal planes of a polycrystalline surface.

As V_2 is increased further, the same trend continues, with increasing reduction of oxide being observed in the O_{C2} state in the final reduction profile (Fig. 7-5). When V_2 is sufficiently high, a critical aging condition is apparently established for which the total measured oxide species on the electrode increases during the aging (Fig. 7-5c for $V_2 = 1.18$ V).

A further increase in V_2 (Fig. 7-6) results ultimately in

reduction of the oxide film in a single large peak, whose V_p increases to slightly more positive potentials as oxide coverage increases (cf Figs. 7-6a and 7-6b). This behavior is contrary to that observed in the usual aging effect and, in conjunction with the increase in the overall oxide coverage which is observed when V_2 exceeds a critical value (cf Fig. 7-5b and c and Fig. 7-6a and b), must be attributed to the reduction of oxide at $\theta_o > 1$. Thus the shift in V_p to more positive values arises on account of superposition of significant currents for reduction of more extensively formed oxide films.

Similar behavior is observed in an experiment on the aging of an oxide at a low coverage ($\theta_o \simeq 0.2$) in 0.05 M H_2SO_4 solution: the initial oxide formation and the eventual oxide reduction are carried out with $s = 0.10\ V\ s^{-1}$ but the aging is conducted at $s = 10\ V\ s^{-1}$.

For these conditions, aging still continues after 90 minutes (Fig. 7-7) of cycling, although most of the effect is completed after just one minute. The trend described above, in which a progressive increase in oxide species reduced in the O_{C2} state occurs during aging, apparently at the expense of oxide species reduced via O_{C3}, is evident in these profiles. Figure 7-7 also shows the final anodic oxidation sweep in the aging process before final reduction of the aged oxide is recorded. The oxide deposition profiles obtained in this way indicate that, as aging processes continue, smaller currents are observed in subsequent anodic oxidation regions of the aging sweeps. This indicates that the build-up of oxide species eventually reduced as O_{C2}, and the increasing quantity of such species not reduced in the cathodic sweep down to V_2, apparently has a blocking effect on further surface oxidation. This

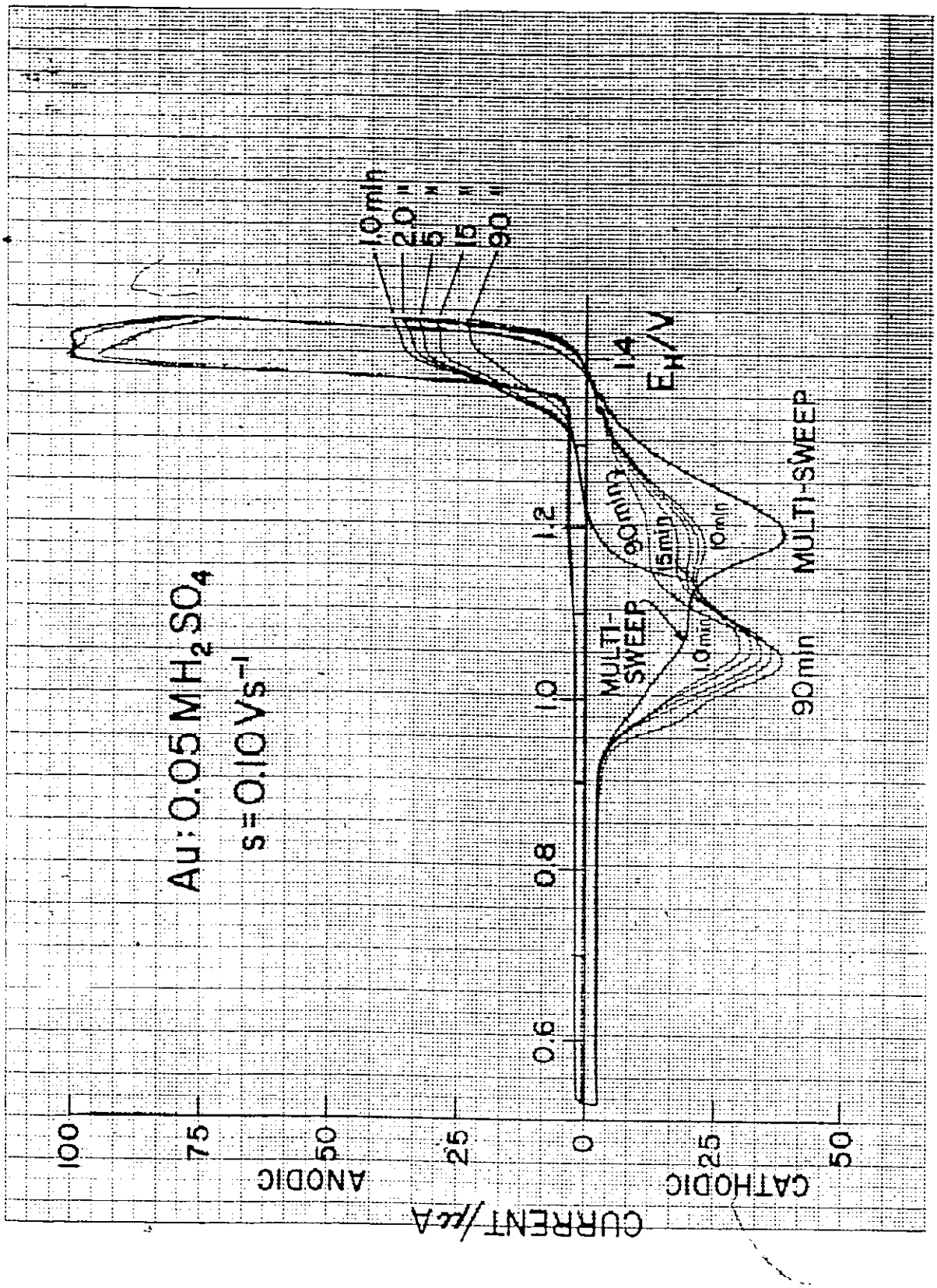

Figure 7-7 Potentiodynamic current-potential profiles for Au at 0.10 V s^{-1}, 298 K in 0.05 M H_2SO_4 for reversal of the cathodic potential sweep at V_2 = 1.14 V and "dynamic aging" of the oxide at 10 V s^{-1} to 1.45 V for various periods of time using program f, Figure 2-5, p. 49

indicates strongly that the species first formed in oxidation are the last to be reduced in the cathodic sweep. That this aging effect occurs even at low coverages of oxide ($\theta_o \approx 0.2$) is rather surprising and is an important clue towards understanding the processes giving rise to these peaks. In addition, a saturation coverage level is usually associated with oxide reduction via O_{C2} in H_2SO_4 solutions.

It is clear that the aging process allows about twice the level of oxide species associated with the O_{C2} state to be formed on the electrode than was earlier (Chapter 3) associated with supposed saturation of that state observed (Figs. 3-3, 4-4 and 4-19) in H_2SO_4 solution. A detailed explanation of these and related effects will be given in the following chapter, correlating the results described in earlier chapters.

In a similar experiment, ca 0.9 monolayer of oxide formed in the same solution was aged (though with V_2 = 1.12 V compared with 1.14 V above) for up to 10 hours, again with aging performed in a cycling regime at s = 10 V s^{-1} (Fig. 7-8).

A very dramatic increase in coverage of species reduced as O_{C2} is observed in the final reduction of oxide after aging, again at the expense of species giving rise to the reduction current peak O_{C3}. Also, the currents measured in the oxide deposition profile significantly decrease, especially in the early stages of oxidation. This illustrates again the relationship of first formed oxide species to those reduced last in a cathodic sweep.

Similar effects are observed for aging of oxide films in $HClO_4$ solution.

Studies on aging in 1.0 M $HClO_4$ do illustrate some differences in aging behavior (Fig. 7-9): when V_2 is increased up to 1.25 V,

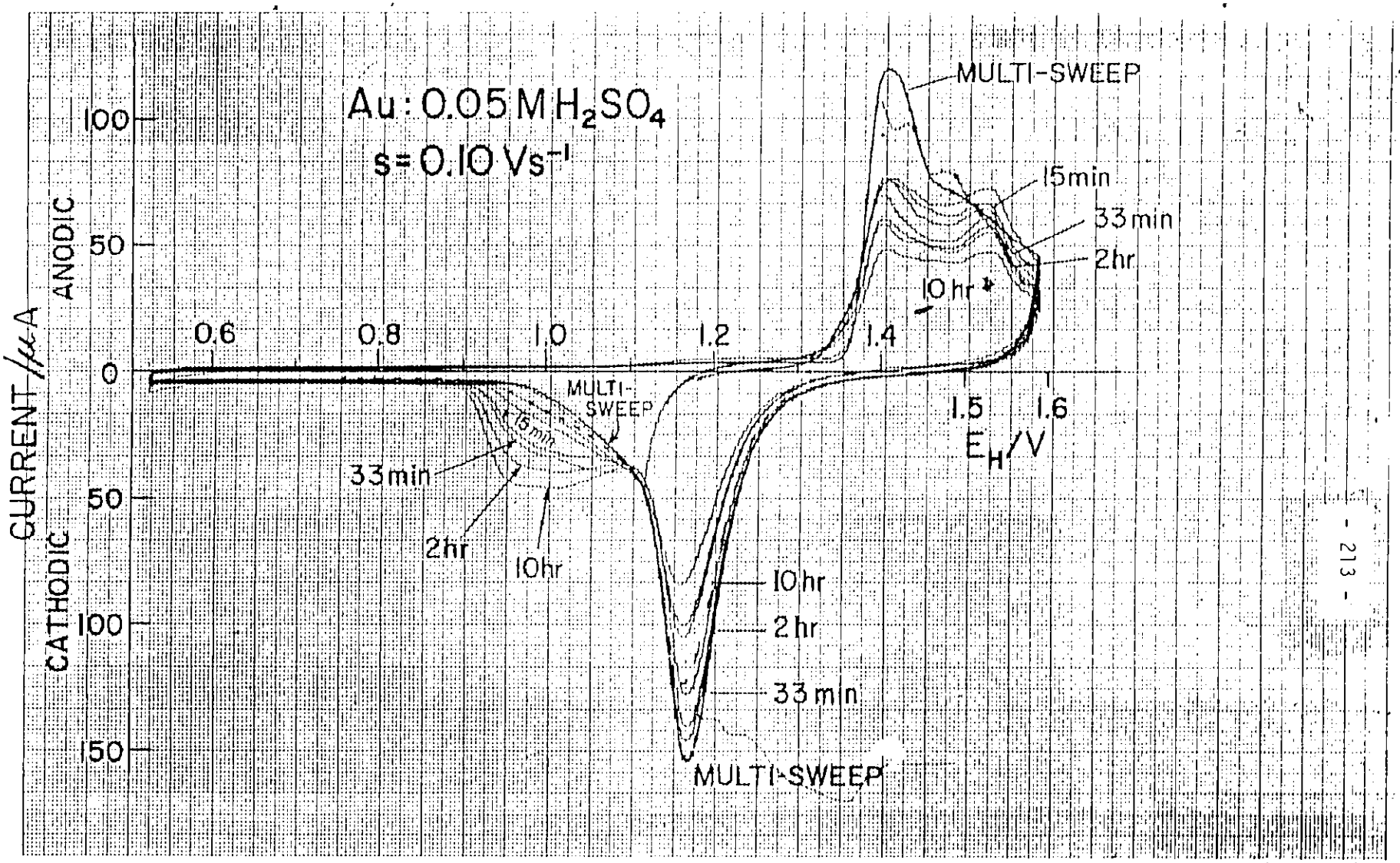

Figure 7-8 Potentiodynamic current-potential profiles for Au at 0.10 V s^{-1}, 298 K in 0.05 M H_2SO_4 for reversal of cathodic potential sweep at V_2 = 1.12 V and "dynamic aging" of the oxide at 10 V s^{-1} to 1.59 V for various periods of time using program f, Fig. 2-5, p. 49.

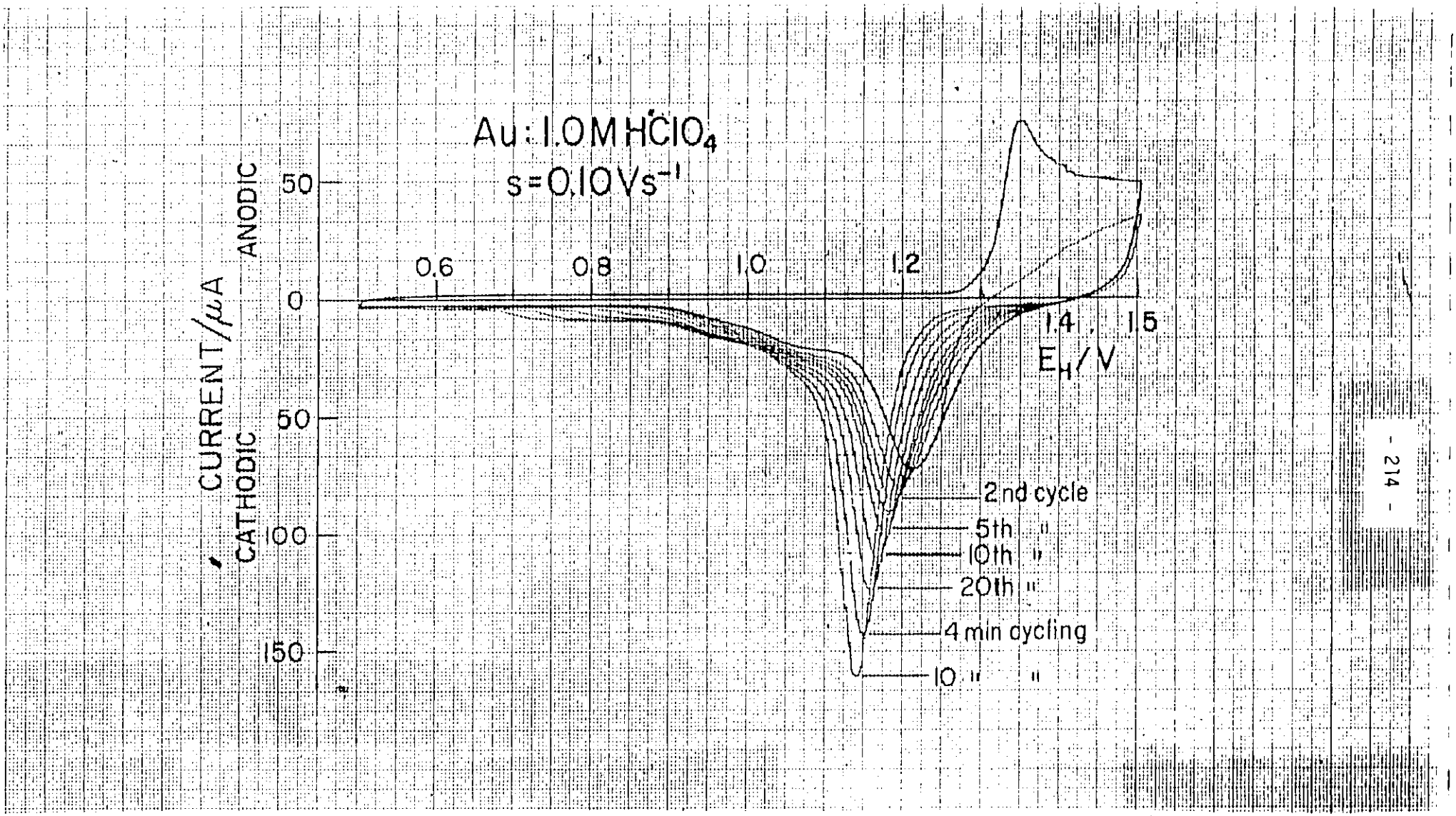

Figure 7-9 Potentiodynamic current-potential profiles for Au at 0.1 V s^{-1}, 298 K in 1.0 M $HClO_4$ for reversal of the cathodic potential sweep at V_2 = 1.25 V and "dynamic aging" of the oxide at 10 V s^{-1} to 1.50 V for various periods of time using program f, Fig. 2-5, p. 49.

the principal result of aging is an increase in currents for state O_{C3} with a continuous shift of V_p (O_{C3}) to lower potentials for longer aging times and increasing coverages. However, the quantity of charge associated with oxide reduction in the O_{C2} state is apparently unchanged by the aging process. Thus, potential cycling between 1.25 V and 1.50 V "ages" the oxide with an overall growth and thickening of the oxide film (growth not necessarily occurring in the same fashion as oxide growth at constant potential) producing some higher oxide species. This behavior is in contrast to that observed in aging procedures employing lower V_2 values for which some transformation of oxide species occurs so that more oxide is reduced in state O_{C2} at the expense of that in O_{C3}.

An interesting feature of the reduction of more extensively formed oxides produced after longer aging times is that a constant-current tail is observed in the cathodic sweep at potentials negative to the O_{C3} peak, e.g. as in Figure 7-9, and becomes longer as the extent of surface oxidation increases. This behavior, similar to that found in oxidation of metal films on Au when alloying occurs, is presumably due to slow emergence of sorbed O species by diffusion from within the metal. However, simulation studies[132] provide an alternate explanation for this affect in terms of sequential chemical-electrochemical reaction kinetics as shown in Figure L-2, p. 59 and discussed further in the next chapter.

Importantly, currents of this type are not observed in the first multi-sweep profile after the aging experiment, thus indicating that the O sorption has been effected by the aging process and is associated with the formation of the film with $\theta_O > 1$ by that process.

The same behavior is seen in Figure 7-10. In this experiment, the potential limit of each anodic sweep is set at 1.604 V, permitting

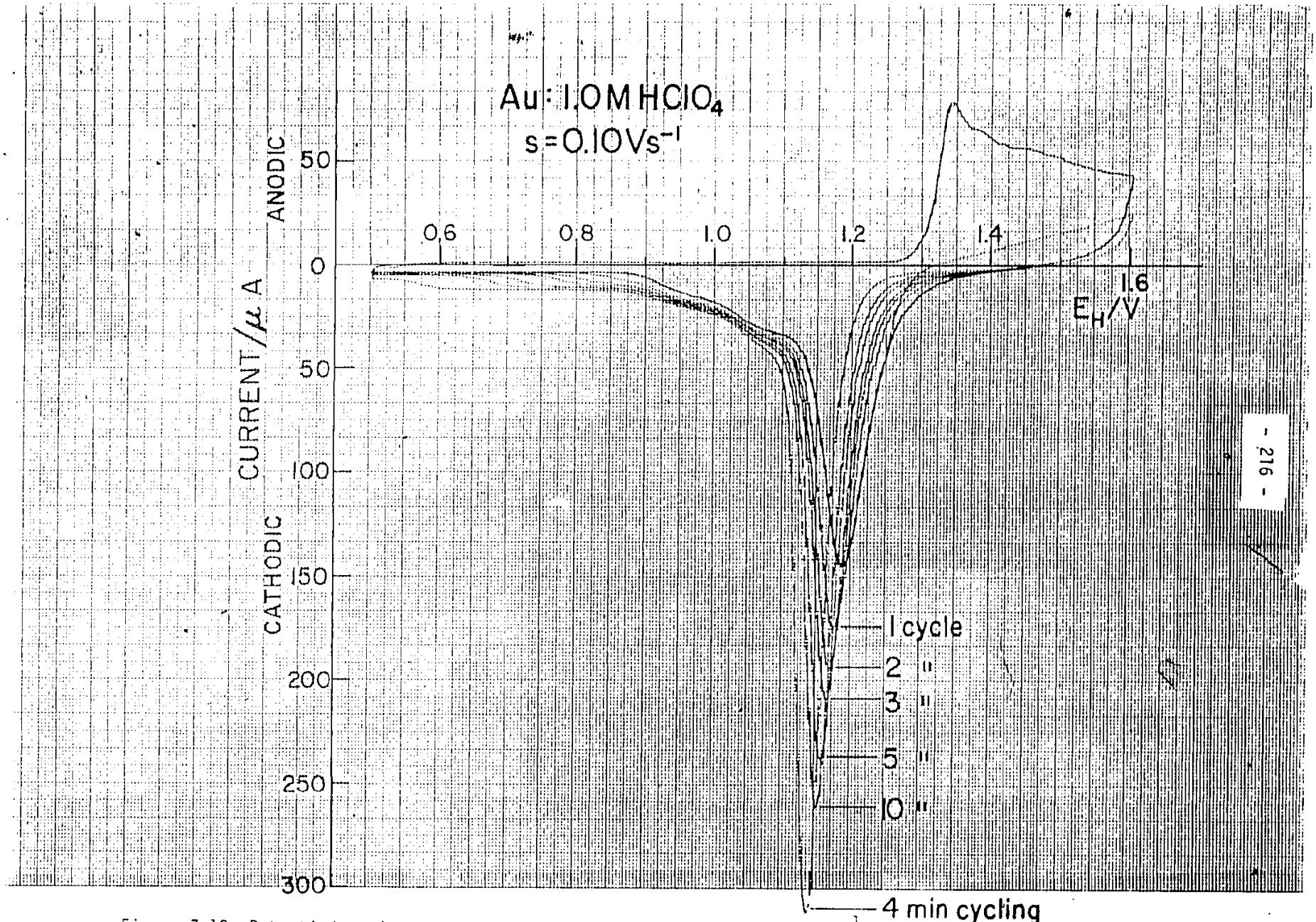

Figure 7-10 Potentiodynamic current-potential profiles for Au at 0.1 V s^{-1}, 298 K in 1.0 M $HClO_4$ for reversal of the cathodic potential sweep at V_2 = 1.26 V and "dynamic aging" of the oxide at 10 V s^{-1} to 1.60 V for various periods of time using program f, Fig. 2-5, p. 49.

a higher initial degree of surface oxidation to be attained. The constant current tail in these experiments is extended for each successively higher degree of surface oxidation reached.

Summary

The aging experiments have permitted study of the growth and thickening of oxide films for relatively positive potentials, V_2, of partial reduction. Under these conditions, correspondingly larger residual quantities of oxide are available as a base for further growth when further deposition of oxide begins in a following anodic sweep.

The aging of submonolayer quantities of oxide, especially with appropriate choice of V_2, shows the interchange of oxide from species reduced as O_{C3} to those reduced as O_{C2} during aging.

The appearance of an apparently diffusion-controlled limiting current tail in oxide reduction profiles (expecially of higher oxides), perhaps due to slow emergence of sorbed O species from within the metal electrode, has important implications for the mechanism of oxide film growth beyond a monolayer of O species. However, another explanation for this behavior exists.

The aging effects observed in this study indicate the important role of non-electrochemical, time-dependent steps in the overall process of stabilization of an oxide film.

The nature of these effects will be discussed further in the next chapter.

CHAPTER 8

Mechanisms of Formation and Reduction of Oxide Monolayers and Submonolayers on Gold Electrodes

The experimental results for oxide formation and reduction which have been presented in the preceding chapters will be examined in relation to the following three questions:

1) What is the significance of the various distinguishable current peaks for deposition and reduction of monolayer quantities of oxide observed in i vs V profiles?

2) What mechanism can be invoked to explain the charge-time data for oxide growth and reduction? That is, what mechanisms can result in kinetics linear in $\ell n\ \theta$ vs t (p.126) and in θ vs log t, independent of V, (p.132)?

3) What are the mechanisms operative in oxide deposition and reduction?

1. Recapitulation of Critical Experimental Results

Several results from the study of oxide growth and reduction at constant potential must be correlated with results from sweep rate studies in order to understand the overall processes. It must be mentioned that the potential-step method by which oxide is grown in the growth kinetics measurements described in Chapter 4 can be expected to produce kinetic results inherently different from those obtained by the linear potential-sweep method.

The important facts can be summarized as follows:

i) In deposition and reduction of oxide monolayers on Au, multiple states of adsorption of OH or O species below monolayer coverage are resolved in the i vs V profiles. As is well known, the i vs V

profiles for surface oxide formation and reduction are very different, indicating hysteresis in these processes. Oxide deposition takes place initially in a potential sweep in the O_{A1} state, which is reversibly reduced (Fig. 3-5a). Three or four current peaks may usually be observed, before oxide coverages of ca 0.25 are attained. Continued deposition occurs over a broad range of potentials, without further current peaks being easily distinguishable before monolayer (0) coverages are attained. While little quantitative information can be deduced concerning the current peaks for oxide deposition, due to the overlap of component peaks, there are several important features of the current peaks observed during reduction of oxide over the potential range of a cathodic sweep. Firstly (Fig. 3-5a), low quantities of oxide ($\theta < 0.1$) may be reversibly reduced under appropriate conditions in a reduction peak O_{C1}, which apparently saturates at coverages (as O species) of ca 0.1 monolayer. Of the several peaks observed in the cathodic sweep for acid solutions, the potential for O_{C2} is the least positive. The coverage associated with it saturates at ca 0.1 monolayer and its peak potential is independent of coverage. The exact level of saturation and the exact potential are a function of solution composition (Figs. 3-3, 3-4, 3-8 and Table 3-1). The main current peak for reduction of oxide, O_{C3}, is observed at intermediate potentials (Figs. 3-3 to 3-5).

ii) The early stages of oxide deposition are extraordinarily sensitive to the type and concentration of ions of the electrolyte, even at very high dilutions. In oxide growth at constant potential, such effects, however, are no longer distinguishable from electrolyte to electrolyte when oxide coverages of ca 0.25 and greater have been

attained (Figs. 4-5 to 4-11).

iii) The growth of oxide at constant potential as a function of time (Figs. 4-6 to 4-12) proceeds in three distinguishable stages:

a) An initial stage of electrochemically controlled growth, for which linear log θ vs t relations are observed, giving Tafel slopes of the order of 60 mV (decade)$^{-1}$, independent of the type of solution.

b) Two stages of physically controlled growth, for which linear θ vs log t relations are observed. The observed constancy of the slopes $[d\theta/d(\log t)]_V$ for each of these two stages of oxide growth is independent of the nature of the solution in which the oxidation is carried out. This independence of solution composition is a strong indication of the importance of metal/oxide interface properties in the rate-controlling process in the oxide growth mechanism. Also, the observation that oxide may apparently grow through the same coverage range by different mechanisms (at different potentials) provides important information for evaluation of suggested reaction mechanisms.

4) The reduction of oxide at constant potential through stage O_{C3} takes place with an electrochemical process as the rate-controlling step, for which a linear log θ vs t relation is observed. The Tafel parameter, 2.3 b, associated with this reaction is reproducibly ca 60 mV (decade)$^{-1}$. While nucleation and growth is usually indicated as a likely mechanism of such experimental behavior, information from several types of experiments show that a mechanism of nucleation and growth of oxide or nucleation of holes in reduction is not operative (pages 172 and 189).

5) The sweep rate dependence of anodic V_p values for several

distinguishable peaks gives low slopes, $dV_p/d \log s$, in the range ca 20-30 mV. The cathodic current peaks are more strongly sweep rate dependent, with $dV_p(O_{C3})/d \log s \simeq 60$ mV and a corresponding value for O_{C2} of at least 60 mV or more.

In addition, several diagnostic parameters provide important insight into the processes giving rise to these current peaks; in particular, i/s for O_{C3} decreases continuously as log s increases while i/s for O_{C2} is constant over a wide range of s. Also, $\Delta V_{1/2}$ for O_{C3} increases continuously with increasing log s, indicating that the electrochemical reduction process manifested in peak O_{C3} is coupled with a time-dependent physical or chemical process, whereas the O_{C2} process corresponds to a simple surface reaction.

6) The effects of aging of the oxide film under various conditions indicates the importance of a physical or chemical process in the overall stabilization of the film. Under certain conditions, the oxide can be aged in such a way that growth of oxide, subsequently reduced in peak O_{C2}, may be increased apparently at the expense of oxide ordinarily reduced in peak O_{C3} (see Figs. 7-7 and 7-8).

These main experimental conclusions are important in providing an insight into the overall mechanism of monolayer oxide deposition and reduction at Au.

2. Chemical Species Formed as Oxide

As we have seen in Chapter 4, p.130), the earliest stages of growth of oxide at constant potential are apparently governed by an electrochemical rate-controlling step. The interpretation of the electrochemical b parameters obtained from plots of log A ($A = \frac{d \ln(1-\theta)}{dt}$

vs potential, Figure 4-15, must be based on examination of an overall mechanism of oxide growth. We shall attempt first to establish the nature of the chemical species formed in oxide deposition and reduction before the overall mechanisms of these reactions are treated.

i) Role of Ion Coverage Terms in Rate Equation Expressions

It is difficult to find a way of properly expressing a term in the surface concentration of ions, Θ_{A^-}, which could be used as a stoichiometric measure of their important effects in an overall rate equation for the formation of surface oxide. The following considerations are, however, helpful:

1) At potentials just below the onset of oxide deposition where $\Theta_o = 0$, Θ_{A^-} is probably near to unity, taking account of anion size and hydration. However, it is physically possible to adsorb more ions onto the electrode surface. This was demonstrated by the experiments in which the end potential of a cathodic sweep is increased to values beyond the point of zero charge (Figs. 3-11 to 3-15). In results of experiments not shown, the deposition of very low coverages of oxide may be completely blocked by appropriate increases of the cathodic end potential. While the "physical" or geometrical fractional coverage, Θ, of the ions themselves is considerably less than unity, the blocking action of these ions indicates that the electrostatic range of influence of these ions corresponds to "total" coverage of the electrode (Fig. 3-2). Thus at all ion coverages:

2) Θ_{A^-} is not stoichiometric in its effect, that is, the effective Θ_{A^-} is not a strict measure of the number of ions present per cm^2 on the electrode surface, but is rather a measure of their electro-

static effect - i.e. their co-circle of influence is much larger than their cross-sectional area.

3) There probably exists a complex function by which θ_A- changes as the other surface concentrations, and the potential, increase in a potential-sweep experiment. Each surface species, e.g. MOH or MO, would be expected to exhibit a different interaction with the adsorbed ions present at the surface. Thus, there are several unknowns in the overall relation between θ_A- and potential, and other θ quantities.

We may therefore consider that the mechanisms below will generate the same types of rate equations, regardless of whether or not ions are represented, through their coverages, in separate terms in these expressions. When adsorbed ions are present, their effect is more usefully expressed in terms of a change of the reversible potential E^r for a given stage of O deposition and/or the q-factor (see p. 56) for the given reaction.

ii) Mechanisms and Equations for Oxide Monolayer Deposition

First it is necessary to develop the argument and present the evidence that the principal species directly deposited in the oxide monolayer are O rather than OH, as this determines how coverage measurements are related to evaluation of charge passed as a function of potential and how the current peaks observed in the i vs V profiles are to be interpretted. Also, since most of the results to be considered refer to monolayer or submonolayer quantities of O ($Q < 400\ \mu C\ cm^{-2}$), we shall not be concerned with stoichiometric bulk-type species such as "AuO", "AuOOH" or "Au_2O_3" such as have been considered in earlier work (e.g. refs. 14-16,110,111) where more extensive oxidation of Au surfaces was

involved.

If lateral interaction effects between species in an electrodeposited monolayer are significant, they must usually be introduced into the rate equation for the electrodeposition process through the usual exp [± gΘ] terms. However, the gΘ terms do not enter into the determination of limiting values of the Tafel slope[130].

We consider first the reaction sequence where O species on Au, represented by "AuO", are formed from initially electrodeposited OH species on Au, represented by "AuOH"; these species are not, of course, stoichiometric compounds AuOH or AuO. Thus,

1)	$Au + H_2O \longrightarrow AuOH + H^+ + e^-$	Discharge
	$1-\theta_T \quad C_{H_2O} \qquad \theta_{OH} \qquad C_{H^+}$	
2)	$AuOH \longrightarrow AuO + H^+ + e^-$	Oxidation of chemisorbed species
	$\theta_{OH} \qquad \theta_O \qquad C_{H^+}$	
3)	$AuO \longrightarrow OAu$	Reconstruction of monolayer oxide film
	$\theta_O \qquad \theta_{OAu}$	

where θ_T is total surface coverage by all adsorbed species, θ_{OH} and θ_O are coverages due to OH and O species, respectively, and θ_{OAu} is coverage of place-exchanged oxide. Rate constants for the three steps are k_1, k_2, and k_3 for the forward direction of the reactions.

When step 1) is the rate-controlling step, the reaction current density is given by

$$i = 2Fk_1C_{H_2O}\,(1-\theta_T)\,\exp\,[\beta VF/RT] \qquad (8\text{-}1)$$

If it can be assumed that θ_T is very small in the earliest stages of oxide deposition, i.e. when $1-\theta_T \simeq 1$, then

$$i = 2Fk_1 C_{H_2O} \exp [\beta VF/RT] \qquad (8\text{-}2)$$

and, with $\beta = 0.5$* at 298 K

$$\frac{dV}{d \log i} = 0.12 \text{ V/decade } i \qquad (8\text{-}3)$$

Tafel slopes having this value are not observed experimentally (e.g. Fig. 4-15 and Table 4-1).

When step 2) is rate-controlling, step 1) may be assumed in quasi-equilibrium, which allows the introduction of an expression for Θ_{OH} as f (potential). Assuming the Langmuir isotherm applies, i.e. interaction effects are neglected, the reaction current density is

$$i = 2Fk_2K_1(1-\Theta_T)[C_{H_2O}/C_{H^+}] \exp [(1 + \beta)VF/RT] \qquad (8\text{-}4)$$

When it is assumed that $\Theta_T \approx 0$, eqn. (8-4) gives, for $\beta = 0.5$ at 298 K:

$$\frac{dV}{d \log i} = 0.040 \text{ V/decade } i \qquad (8\text{-}5)$$

This value for the Tafel slope is also not observed experimentally.

For another simplifying situation, when Θ_T is essentially only Θ_{OH}, and Θ_{OH} is close to unity and constant while Θ_O is assumed to be quite small, the current density is given by

$$i = 2Fk_2 \exp [\beta VF/RT] \qquad (8\text{-}6)$$

$$\frac{dV}{d \log i} = 0.12 \text{ V/decade } i \qquad (8\text{-}7)$$

This situation only arises when OH species cover virtually the entire surface before O species are formed, a sequence of events

---

* This is usually taken to be true for virtually all charge-transfer reactions and is based on Brønsted's principle applied to effects of changes of electrode potential on electrochemical free energy of activation.

and a resulting Tafel slope which is also not supported by the experimental results.

When more than one surface species is present on the electrode in significant quantities at the same time, it is not possible to make simplifying assumptions to establish Tafel slopes for realistic limiting cases since the term $(1-\Theta_T)$ contains more than one unknown (i.e. Θ_{OH}, Θ_O, Θ_{OAu}).

When step 3) is rate-controlling, the preceding steps may be treated as being in quasi-equilibrium, as before, and the value of Θ_O may be found from the isotherm. Assuming Langmuir conditons, the expression for Θ_O is

$$\Theta_O = K_1 K_2 (1-\Theta_T)[C_{H_2O}/C_{H^+}{}^2] \exp [2VF/RT] \qquad (8\text{-}8)$$

and the corresponding reaction current density is

$$i = 2Fk_3\Theta_O \qquad (8\text{-}9)$$

A number of limiting cases then follow as:

i) when Θ_T is low, i.e. Θ_{OH}, Θ_O and Θ_{OAu} are $\ll 1$

$$i = 2Fk_3K_1K_2[C_{H_2O}/C_{H^+}{}^2] \exp [2VF/RT] \qquad (8\text{-}10)$$

so that $$\frac{dV}{d \log i} = 0.030 \text{ V/decade} \qquad (8\text{-}11)$$

Although Tafel slopes of ca 30 mV are seen for the s-dependence of V_P for Θ_{A2}, it is difficult to imagine place-exchange (step 3) control at such low coverages.

ii) for low Θ_{OH} with high Θ_O, i.e. where $\Theta \longrightarrow 1$,

$$i = 2Fk_3 \text{ or } 2Fk_3 (1-\Theta_{OAu}) \qquad (8\text{-}12)$$

which is potential independent. This relation for i is not observed.

iii) the experimentally observed Tafel slope of 60 mV is obtained however if conditions of low Θ_O but with high Θ_{OH} are assumed, i.e. when $\Theta_{OH} \longrightarrow 1$ and is constant so that

$$i = 2Fk_3[K_2/C_{H^+}] \exp [VF/RT] \qquad (8\text{-}13)$$

then $$\frac{dV}{d \log i} = 0.060 \text{ V/decade} \qquad (8\text{-}14)$$

This agrees with the experimentally determined Tafel slope of 60 mV, but the initial assumption of $\Theta_{OH} \longrightarrow 1$ is hardly justifiable, e.g. at low degrees of oxidation of the surface of Au. Also, a peak for OH monolayer formation is not resolved.

If oxidation of the species AuOH to AuO (reaction equations 1 and 2) were rate-controlling, it should be possible to distinguish a separate current peak corresponding to the prior (fast) reaction 1):

$$Au + H_2O \overset{fast}{\dashrightarrow} AuOH + H^+ + e^-$$

at a sufficiently high sweep rate. A wide range of sweep rates was used (0.0005 V s^{-1} - 1000 V s^{-1}) but such a current peak (or a sweep rate dependent separation of the component peaks in the oxide deposition i vs V profile) was never observed. The same argument would hold for any second step of a sequence being the r.d.s., e.g. reaction 5) in the following 2-step sequence 4), 5):

4) $Au + H_2O \longrightarrow AuO + 2H^+ + 2e^-$

5) $AuO + H_2O \longrightarrow AuOOH + H^+ + e^-$

Thus it would be expected that a distinct current peak would be observed for reaction 4) at very high sweep rates; this is not observed.

It is concluded that the O_{A1} process is not associated with step 1) producing OH species on Au. If such a process were rate-controlling,

a Tafel slope of 0.12 V/decade would be expected, at least for low θ_T in the early stages of deposition. Instead, the experiments at various sweep rates reveal Tafel slopes (Table 6-1, p. 182) of the order of 20-30 mV only for the earliest stage of oxide deposition. In addition, a Tafel slope of the order of 60 mV was obtained for the oxide growth kinetics reported in Chapter 4.

In summary then, the absence of a resolvable current peak attributable to initial formation of OH species and the failure of the behavior observed at high sweep rates to support the existence of such species, seems to indicate strongly that O rather than OH species are the initially formed entities in surface oxide deposition at Au.

Moreover, the type of analysis just described in sections (i) to (iii) above for the mechanism producing OAu in 3 steps (p.226) has been applied in the present work (see Appendix I) to a large number of mechanisms which produce final states of adsorbed O species represented by AuO, or AuOOH in a variety of rate-controlling steps and sequences of electrochemical and chemical steps. A summary of the results of this analysis for oxide deposition in acid solutions is given in Appendix I. This analysis does not, however, reveal a realistic mechanism for oxide deposition which predicts (even in limiting cases) the 60 mV Tafel slopes observed experimentally, besides the direct formation of an O species on Au.

This interpretation may not exclude the transient formation of AuOH species. However, these species must be converted to AuO species in a fast step 2) reaction, so the overall deposition of O species behaves kinetically as a 2-e process. An analogous case is the observed 2-e

reaction for deposition of zinc on Zn or into Hg. It is to be concluded that there is no experimental evidence supporting OH species in oxide deposition or reduction.

The differences in Tafel slopes for the anodic deposition of O species derived from either sweep rate or slow growth experiments described in Chapters 4, 5 and 6 (viz. oxide growth and sweep rate studies on oxide formation and reduction), are interesting and provide insight not only into the oxide growth processes but also the significance of the experimental techniques themselves. Thus, we have mentioned earlier (p.218) that the method by which oxide is grown in the oxide film growth kinetics measurements of Chapter 4 can be expected to produce results inherently different from those obtained by the potential-sweep method. The growth of oxide in a potential-step type of experiment takes place at constant potential and is measured as a function of time only.

As potential is increased in a sweep, deposition of additional oxide is made possible thermodynamically and kinetically during the sweep in contrast to the situation at constant potential. Thus, during a sweep, there is, of course, an implicit growth time Δt ($=\Delta V/s$) associated with sweeping through a range, ΔV, of oxide deposition potentials at a sweep rate, s, once oxide species commence being deposited.

The potential-step experiments on oxide growth at constant potential (program f on p. 49) are conducted using a sweep rate which is sufficiently high that irreversible charge transfer behavior is encountered so that the oxide growth kinetics measured are necessarily under electrochemical control. The sweep rate studies described in Chapter 6, on the other hand, do not reveal reversible current peaks, except in the earliest stages of deposition (cf. Figures 3-5a and 4-1) in the O_{Al}/O_{Cl}

region but not at low sweep rates. In fact, a dependence of V_p on log s of 20 ~ 30 mV for θ_{A2} is actually observed over several decades of sweep rate; thus, reversible behavior is not encountered even at the lowest sweep rates employed (e.g. 0.0005 V s^{-1} in Figure 3-1). This behavior must be attributed to the strong blocking and interaction effects of anions, especially in the early stages of deposition.

With respect to the reaction mechanism 1), 2), 3), we have next to consider the consequences of step 3) of this sequence being rate-controlling. The appropriate limiting case here is for low θ_T, for which a Tafel slope of 30 mV $(decade)^{-1}$ is predicted [eqn. (8-11)] or for high θ_T, b $\longrightarrow$ 0 for place-exchange control. The experimental results for low θ_T indicate that 2.3 b ≈ 60 mV, so that step 3) cannot be the rate-controlling process under either of the above conditions.

The analyses of the consecutive reaction sequences given above, involving 1-electron transfer steps show that either Tafel slopes equal to the observed value of 60 mV/decade are not predicted or, if they are, the result is based on an unrealistic limiting condition. It therefore appears that initial oxide deposition in the submonolayer is best represented by an effective 2-e discharge of water to form AuO species directly in the reaction

$$4)\quad Au + H_2O \longrightarrow AuO + 2H^+ + e^-$$
$$\qquad 1-\theta_T \quad C_{H_2O} \qquad\quad \theta_O \quad C_{H^+}$$

At low θ_O in this reaction, the current-density is obviously given by

$$i = 2Fk_4 C_{H_2O} \exp[2\beta VF/RT] \qquad (8\text{-}15)$$

which gives the experimentally observed Tafel slope of 0.060 V/decade

taking $\beta = 0.5$ as usual and $T = 298$ K.

3. Place-Exchange Steps Following Reaction 4)

For a full representation of the mechanism of oxide growth and aging effects at Au, it is necessary to reconsider the place-exchange step 3) [p.226, this chapter) viz.

3) $\underset{\Theta_0}{AuO} \longrightarrow \underset{\Theta_{OAu}}{OAu}$

which must follow step 4) in the course of the overall reaction.

If step 3) were rate-controlling, the assumption of quasi-equilibrium in step 4) allows the isotherm

$$\Theta_0 = K_4 (1-\Theta_T)[C_{H_2O}/C_{H^+}{}^2] \exp [2VF/RT] \qquad (8\text{-}16)$$

to be written for coverage by O species. Then, in the usual way, the current density is

$$i = 2Fk_3K_4(1-\Theta_T)[C_{H_2O}/C_{H^+}{}^2] \exp [2VF/RT] \qquad (8\text{-}17)$$

Limiting cases follow then as:

a) $\Theta_0 \longrightarrow 1$

$$i = 2Fk_3 \text{ or } 2Fk_3(1-\Theta_{OAu}) \qquad (8\text{-}18)$$

which gives a potential-independent current

b) If $\Theta_0 \simeq \Theta_T$, we find for low Θ_T

$$i = 2Fk_3K_4[C_{H_2O}/C_{H^+}{}^2] \exp [2VF/RT] \qquad (8\text{-}19)$$

so that $$\frac{dV}{d \log i} = 0.030 \text{ V/decade} \qquad (8\text{-}20)$$

While it was stated that the latter Tafel slope is not observed experimentally in the initial stages of oxidation of Au the range of 2.3 b values predicted under conditions for which the place-exchange step 3)

is rate-controlling is 0 to 30 mV decade^{-1}, corresponding to eqns. (8-18) for high θ_0 or (8-20) for low θ_0, respectively.

It is expected that place-exchange will not predominate as the rate-controlling step in oxide deposition until the later stages of monolayer formation have been reached. Under the latter conditions, when place-exchange is the rate-controlling process, the above equations for this case show that potential would exert a relatively small influence (e.g. 0 ~ 30 mV/decade in the analysis just presented) on the rate of reaction.

4. Mechanisms for Reduction of Oxide

Several mechanisms for oxide reduction were considered in Chapter 5, but the analysis can be shortened considerably if it has been determined that O rather than OH species are produced in the primary oxide deposition step. Evidence for such a step was given in section 2 of this chapter.

Here we shall consider the reduction of AuO species back to "bare" Au metal sites from an initial state constituted of varying quantities of place-exchanged material ("OAu"), depending on the total oxide coverage and other factors such as aging and ambient temperature.

Two points must be stressed in relation to the mechanism of reduction. Firstly, there is experimental evidence supporting the existence of some non-place-exchanged material in oxide monolayers in the demonstrated aging effect in which the peak potential for oxide reduction shifts to less positive values at constant oxide coverage after some period of aging. This effect is interpreted as a continuing place-exchange and ordering of the surface dipole array of O species with time to form a more stable, two-dimensional network of oxide. Moreover, it is reasonable to consider

that non-place-exchanged entities adjacent to an OAu species constitute part of the place-exchanged network, and experience the same stabilization as the actual place-exchanged O species within the network. Thus, a 2-dimensional "block" of oxide, of undetermined size, is incrementally stabilized by each place-exchange event.

Secondly, the work described in Chapter 5 has demonstrated that reduction of oxide occurs under electrochemical control with a measured Tafel slope of 60 mV (decade)$^{-1}$. This conclusion means that the hysteresis or irreversibility observed in an i vs V profile between deposition of oxide and the subsequent reduction of that oxide cannot be attributed to a physical process such as the reverse act of place-exchange. It is simply due to irreversibility of an electrochemical process. Hence, reverse-place exchange, which is expected to occur before reduction of any "turned-over" oxide can take place, must be a relatively fast process. In the present work, this was an unexpected result (cf p.164).

The reduction of oxide in acid solution must therefore involve the reaction

$$AuO + 2H^+ + 2e \longrightarrow Au + H_2O \qquad (8\text{-}21)$$

as a rate-controlling step, so that the current density is given by

$$i = 2Fk\ \theta_O (C_{H^+})^2 \exp\left[-2\beta VF/RT\right] \qquad (8\text{-}22)$$

For large θ_O and for $\beta = 1/2$, this gives for the Tafel slope

$$\frac{dV}{d \log i} = 0.060\ V(\text{decade})^{-1} \qquad (8\text{-}23)$$

In alkaline solution, a similar expression for the potential-dependence of rate is obtained because of the postulated 2-electron

transfer of charge. The actual reaction in that case is, of course,

$$AuO + H_2O + 2e \longrightarrow Au + 2OH^- \qquad (8\text{-}24)$$

5. Origin and Significance of Current Peaks in the i vs V Profiles

The question of which species and reactions can be associated with the various current peaks for oxide deposition and reduction is a central issue in the overall understanding of these processes.

In the course of an anodic sweep, a certain critical potential must be attained before currents for oxide deposition are observed. This potential depends on the type of solution involved and reflects, in particular, the varying strengths of adsorption of anions (competitive adsorption or blocking effect) from the electrolyte.

The first peak observed for oxide deposition and reduction is for the reversible surface reactions, O_{Al}/O_{Cl}. It is seen in different solutions, e.g. $HClO_4$ or H_2SO_4, at quite different potentials, even though the nature of the peak and the reaction processes are apparently the same. Therefore, depending on the anion environment of the electrodeposited species, the potential for the initial surface process, O_{Al}/O_{Cl}, on Au can vary appreciably. These facts strongly suggest that the deposition of the first O species is a random and reversible process but that the presence of co-adsorbed ions modifies the reversible potential for this surface process on account of interaction effects due to these ions. Thus, anions apparently cover the electrode substantially, as indicated by the blocking effect, and the first oxide species are deposited, as O on Au (designated "AuO"), in their midst, probably without requiring ejection of the ions, as illustrated in Figure 8-1a.

The observed reversibility of the initial deposition/reduction

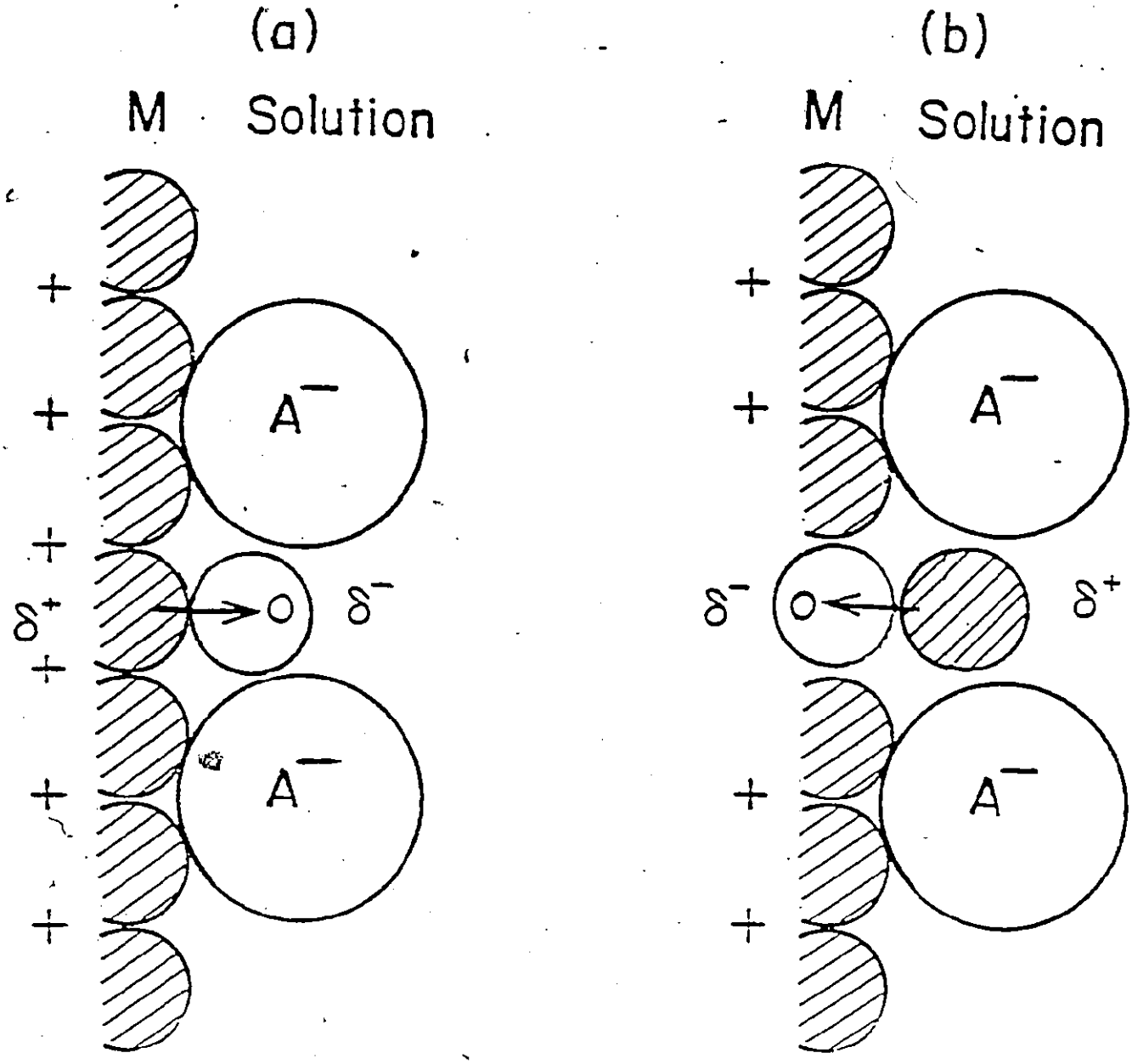

O_{Al} / O_{Cl}

Initially deposited species in presence of anions

O_{C2}

Remaining place-exchanged species after reconstruction and reduction of most of the oxide film

Figure 8-1 Model of anion interaction effects and promotion of place-exchange in initial stages of metal oxidation and final stage of oxide reduction

indicates that the process is a random one on the surface, not involving the slow place-exchange step; also the observed reversible potential, E°, for the reaction must refer to the deposition and reduction of oxide species in the presence of anions on the surface. This E° is thus not the true (unknown) reversible potential for the initial surface process but depends on the anions present. This situation is analogous to the usual effect of ionic strength on the emf of a cell, due to ionic interaction effects. With desorption of ions, the E° will shift to less positive values. A crude representation of the situation is illustrated in Figure 8-1a but the ions shown need not be as close to deposited O species as depicted. This model is strongly supported by the experimental results. The O_{A1}/O_{C1} process loses its reversible character with time due to the place-exchange reaction, and with increasing oxide coverage as more O species become deposited sufficiently "close" to each other, giving rise to lateral interaction effects which will promote place-exchange.

The key to understanding the nature of all the current peaks that are resolved lies in the answer to the following questions: What oxide species

i) occupies ca 0.1 monolayer or less and, in fact, saturates at approximately this value?

ii) must be present initially in a randomly deposited state, i.e. not in agglomerates? And

iii) is surrounded by ions?

An obvious and, it is believed, correct answer to this question is the species corresponding to the O_{C1} state. On reflection, however, it is apparent that the O_{C2} state must also fit this description. Oxide

reduced in this state is the last oxide to remain on the surface in a cathodic sweep and is present in quantities of the order of 0.1 monolayer (e.g. see Fig. 5-1) depending on the electrolyte. As the experimental results indicate (as described especially in Chapters 6 and 7, pages 194 and 212), this species must be randomly distributed over the electrode surface. In addition, it is likely that anions will quickly re-adsorb during oxide film reduction as bare metal sites become generated. If, then, exactly the same description applies to the O_{C1} and O_{C2} states, what can be so different about these species that a further -400 mV or more of potential is required to reduce O_{C2} than O_{C1} species (in 1.0 M $HClO_4$)?

Consideration of Figure 8-1a suggests that only one critical factor could be different, that is that the dipole of "AuO" could be inverted due to a place-exchanged situation (Figure 8-1b) so that an anion-stabilized arrangement of surface dipoles develops as illustrated in Figure 8-1b. There are two additional compelling reasons for this interpretation:

a) An oxide film about to be reduced in a cathodic sweep must present a variety of sites for possible reduction, with varying energies or potentials required to effect reaction. Some O species will be place-exchanged with the oxide end of the "dipole" down (OAu) into the metal. It would be expected that these species are more difficult to reduce. Adjacent to the latter species, an oxide O atom will be projecting out towards the solution and would be expected to be somewhat more available for reduction. However, this species also experiences considerable stabilization as an element of a place-exchanged network. Also present

on the surface, there must be a great number of species not so closely linked with a place-exchanged entity, perhaps only two or three lattice sites away, where the O end of the AuO surface dipole will be projecting towards the solution.

It seems probable that reduction must proceed under electrochemical control initially at sites of this nature, corresponding to peak O_{C3}, and must ultimately progress via "fast" reverse place-exchange in such a manner that the last remaining species on the electrode surface during reduction would be expected to be of the ion-stabilized, place-exchanged type (OAu, abbreviated henceforth as ↓), as represented in Figure 8-1b.

b) The other fundamental consideration involves the earlier experimental evidence (Chapter 3, p.61) which indicates the important role of ions not only in blocking the onset of oxide deposition but in a general way in establishing the energies of the initially formed oxide (up to coverages of 0.3 - 0.4 monolayer). It seems reasonable to assume that ions must have a similar importance as they re-adsorb on the electrode during reduction. This is confirmed by the varying saturation values encountered for state O_{C2} in different electrolytes (see Figs. 3-3 and 3-4, and Table 3-1).

A general representation of the relative potentials for these current peaks and O species is shown below.

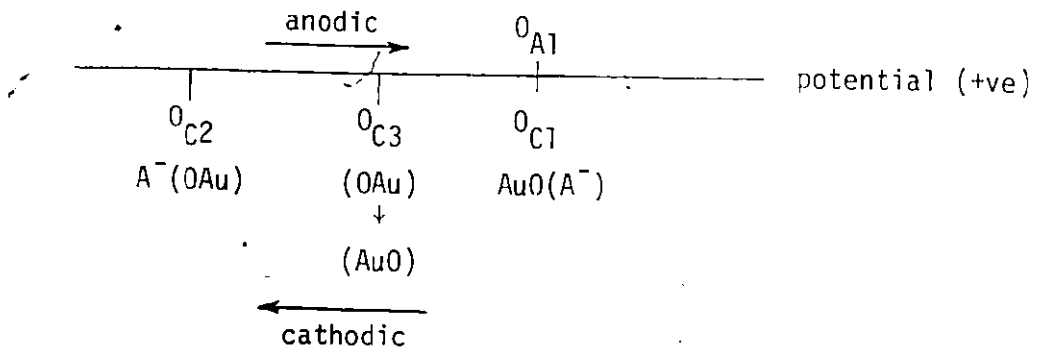

i) Role of a Physical Process in Oxide Reduction

In Chapter 3, the general features of the processes of oxide growth and reduction were described. In particular, the sequences of development of current peaks in i vs V profiles as a function of potential, time and oxide coverage were explored. It was found that, in acid solutions, the first deposited species is O_{A1}, which is reduced as O_{C1}. Subsequent deposition of oxide occurs with the appearance (firstly) of an O_{C2} state in reduction followed shortly by the appearance of O_{C3}. Up to coverages of ca 0.3, after saturation of the O_{C2} state, the profiles reveal that more oxide is actually reduced in the O_{C2} state than in O_{C3} (see Figs. 3-3, 3-4, 3-5, 4-1 and 4-3). The latter state becomes, however, the main peak (state) through which higher coverages of oxide are reduced. In the light of the results mentioned in the previous paragraph and in the previous section, it is now possible to reach a better understanding of the experimental results obtained and the nature of the physical step which must be occurring during reduction. We know already that this step must be relatively fast, as argued in Chapter 5, p. 159.

The ion/oxide-dipole/ion configuration shown in Figure 8-1a is inherently unstable. With time, it would be expected that a more stable configuration would result either from the place-exchange act, producing the stabilized dipole-ion configuration, or from the slow expulsion of ions from sites adjacent to O on an Au site. This latter event is probably related to the displacement of the peak potential, V_p, for O_{C1} to less positive potentials after saturation of that state. The presence of O_{C2} must mean that substantial quantities of place-exchanged material, stabilized by the presence of anions, may be found on the surface, even at low coverages of oxide (< 0.3), and this must be attributed to the ability of anions to promote this place-exchanged state on the grounds of favorable

OAu dipole-ion stabilization. This provides an additional explanation for the loss of reversibility of the O_{A1} process with time or with increasing oxide coverage and, in general, for the dramatic difference between the i vs V profiles for deposition and reduction of larger quantities ($\Theta > 0.2$) of oxide. These profiles are so different because the constituent processes are very different; because of the role of the coupled physical processes of place-exchange, they are not simply the reverse of one another.

O_{C3} represents reduction of oxide from domains of two-dimensional surface lattice in the absence of ions.

Ion assisted place-exchange can occur only in the early stages of oxide deposition on account of the area requirements for adsorption of anions. It is evident from the results described earlier (see Chapter 4, p.114) that, beyond ca 0.3 monolayer, ions play little or no role in the mechanism of oxide growth at constant potential. It appears that up to such a coverage as ca 0.3, deposition of O species takes place either as an essentially random process or in an open regular overlay structure, and co-adsorbed ions may be present up to that limit. Few or no ions can remain on the electrode surface beyond this coverage limit if the O species retain a spaced out overlay or random structure, due to the anions co-area requirement.

It appears that most of the oxide is reduced in just one state, namely O_{C3}. This is evidence (together with the experimental result that reduction takes place under electrochemical control; see Chapter 5, p.159) that the act of reverse place-exchange (reverse of step 3, p.231) is fast with respect to the electrochemical reduction reaction. Moreover, co-operative movements of a series of AuO entities may be possible in

response to reduction of an AuO species within an oxide network (a type of "flip-flop" process which would be represented as ↑↓↑↑ ⟶ ↓↑↓↑ in an element of the oxide lattice). The reason that one predominant peak for reduction of oxide from $\theta > 0.3$ is observed is that the reaction of reverse place-exchange is fast and continues to regenerate AuO with the O ends of the dipoles directed towards the solution (even sections such as ↓↑↓ can become ↑↓↑).

Reduction is observed to occur through essentially one state (O_{C3}) until ions begin to re-adsorb on the electrode. When an ion adsorbs in proximity to a place-exchanged AuO dipole, it essentially freezes that AuO in the place-exchanged state. Its action would thus be to slow down the rate of the reverse place-exchange by several orders of magnitude because of the stability of the adsorbed ion-dipole pair. In addition, it produces a fixed quantity of such pairs, depending on the area requirements of O + adsorbed anion, leading to saturation values of O_{C2} which are anion-dependent, as observed.

It is not clear whether the actual reduction of oxide in peak O_{C3} takes place randomly or whether a type of nucleation of holes is operative. Both mechanisms may be operative. If a random reduction occurs, it would be expected (considering that most anions adsorbed occupy at least three lattice sites) that anions could not-re-adsorb until most of an oxide monolayer had been reduced. In fact, bigger anions would require more space and would result in lower values for the saturation level of O_{C2} since, on the average, more reduction of oxide through O_{C3} would be required before anion re-adsorption could occur. Such a trend in saturation values is supported by the experimental results (e.g. see Figs. 3-3, 3-4) and especially the results for borate solutions (Fig. 3-4c).

Alternatively, if a mechanism of nucleation of holes is considered, it must be envisaged that, after a hole has been created through reduction of one AuO entity, a surrounding ring of oxide would be quickly reduced. However, as soon as the hole created in this manner becomes large enough, (a few O diameters) an anion could quickly adsorb, "freeze" some adjacent place-exchanged material and halt the chain of reduction events. In this way, the nucleation mechanism would not be detectable by the usual experimental criteria discussed earlier (p.189, Chapter 6). However, a saturation value for O_{C2} inversely related to anion size is predicted for this mechanism as well.

There are other determinants of the saturation values for O_{C2} (see Table 3-1, p.90): The rate of ion adsorption must be moderately fast in relation to the rates of the reduction reactions. The rate of anion re-adsorption may differ somewhat for various types of ions. The strength of adsorption to the metal should determine the surface concentration of anions in conjunction with other factors such as the degree of hydration of the ion and the surface dipole moment. The known strength of adsorption of ions (pages 22 and 81) is inversely related to the saturation values for O_{C2} coverages. The energy of stabilization of the oxide surface dipole by the ion should be reflected, it is proposed, by the difference of potential between the O_{C1} and O_{C2} peaks for the various electrolytes.

On the above model, a much higher saturation level for O_{C2} is expected in alkaline than in acid solutions. The ion OH^- is much smaller than the anions available in strong acid solutions and could occupy only one lattice site per ion. It would thus be expected to be able to re-adsorb already at higher remaining coverages of oxide in the reduction

process. Furthermore, the OH^- ion is actually generated in the double-layer as a product of the reduction of oxide in alkaline solutions (eqn. 8-25) and thus does not have to diffuse to the electrode prior to adsorption.

The experimental results are consistent with these proposals: much higher saturation levels for O_{C2} are actually found experimentally for alkaline solutions, thus supporting the nature of this proposed effect.

In 0.2 M $Ba(OH)_2$ solution, two contrasting types of oxide growth were encountered. When carbonate concentration has been depressed to sufficiently low values, a mechanism of oxide growth is observed by which a monolayer of oxide is formed at ca 1.5V and is reduced primarily through what appears to be the O_{C2} state. When traces of carbonate are present, however, a monolayer of oxide is formed at 1.7 V and the familiar pattern of reduction of oxide, primarily through O_{C3}, with saturation of the O_{C2} state, at higher levels is observed. This result is attributed, in part, to the fact that carbonate ion is more strongly adsorbed than hydroxyl ion, and is also a larger ion so that, when carbonate is present even in trace quantities, it is this which determines the mode of growth and reduction.

One interpretation of the increased stability of a monolayer of oxide (as determined by the potential for formation of the monolayer in an anodic potential sweep) formed in the absence of carbonate ion is that OH^- has been able to adsorb on the electrode surface and promote place-exchange up to higher coverages before oxide growth forces the ejection of the ion. This does not adequately explain the high values obtained for O_{C2} coverage (higher than 0.5) and the failure of the state to saturate. It may be that a type of cation-stabilized oxide has been formed under these conditions due to the presence of the high charge-density Ba^{++} ion.

A striking feature of the behavior of Au in alkaline solution in general, and in 0.2 M $Ba(OH)_2$ in particular, is the appearance, over a

broad potential range (0.5 - 1.2V), of a reversible i vs V profile (Figure 3-8) up to the potential ca 1.2V at which the main surface oxidation apparently commences. The total charge associated with this region (between 0.5 and 1.2V) after a normal double-layer charge has been allowed for, is ca 35% of that of an OH monolayer, or 17% of the charge associated with formation of a monolayer of O species. This result may be related to another experimental observation, namely that the charge associated with reversible deposition/reduction of oxide (O_{Al}/O_{Cl}) is much lower in alkaline (especially 0.2 M $Ba(OH)_2$ than in acid solution. In alkaline solution, the OH^- ion would not be expected to block oxide deposition since it is the reactant. However, other anions more strongly adsorbed than OH^- (Fig. 3-8) will always be present in varying quantities sufficient to account for the O_{Al}/O_{Cl} behavior. The lower quantity of O_{Al}/O_{Cl} observed in alkaline solution must reflect the diminished importance of these ions in blocking oxide deposition because of the direct discharge of OH^- ion to form oxide. In addition, the blocking effects of any non-dischargeable anions have been diminished since in alkaline solutions the potential of the p.z.c. is now expected to be in the range of potentials (> 1.2 V) where oxide deposition commences, thus greatly diminishing the concentration of anions in the double-layer. Under these conditions, the deposition of oxygen species may now occur at, and be spread out over, much lower potentials (between 0.5 V and 1.2 V) rather than be blocked by local electrostatic and interaction effects due to other anions until a potential of 1.2 V or higher is attained, as in acid solutions, where the p.z.c. is ca 0.4 - 0.6 V, E_H.

6. Additional Evidence Supporting Ion-Assisted Place-Exchange

i) Sweep Rate Studies

Many experimental results have been introduced into the

preceding discussion in an attempt to propose a consistent overall mechanism of oxide formation and reduction. It will be useful now to examine briefly some additional results presented in the earlier chapters in order to verify and corroborate the interpretations of the experimental behavior which have been suggested in the preceding sections.

An analysis of experimental data obtained for varying sweep rates was presented in Chapter 6 and showed that a physical, though not rate-controlling, step was involved in the reduction of oxide. The decrease in i/s for the O_{C3} peak as the sweep rate in oxide reduction transients was increased, is strikingly evident in Figure 8-2 for 0.1 M $HClO_4$ solution. Simultaneously, the $\Delta V_{1/2}$ for the O_{C3} process increases dramatically and does so beyond the extent attributable[132] to sweep rate (kinetic) effects alone.

The time effect involved here does not increase the charge in O_{C2}; thus, the i/s value for this state is constant over two decades of s as seen in Figure 8-2. This constant value indicates that the coverage in this state is established reproducibly by the sequence of events in reduction of oxide, regardless of the sweep rate employed and of the considerable changes observed in similar current peak parameters for the O_{C3} state in response to changing sweep rate. It would appear that re-adsorption of anions is fast throughout this range of sweep rates, not only relative to the rate of reduction but also to the rate of reverse place-exchange. Under these conditions, no matter how quickly, or slowly, the reduction of oxide is carried out, anions evidently rapidly re-adsorb on the electrode surface adjacent to remaining place-exchanged oxide species and "freeze" those species until they are reduced in the O_{C2} state.

Similarly, the manner in which the O_{C3} peaks spreads out

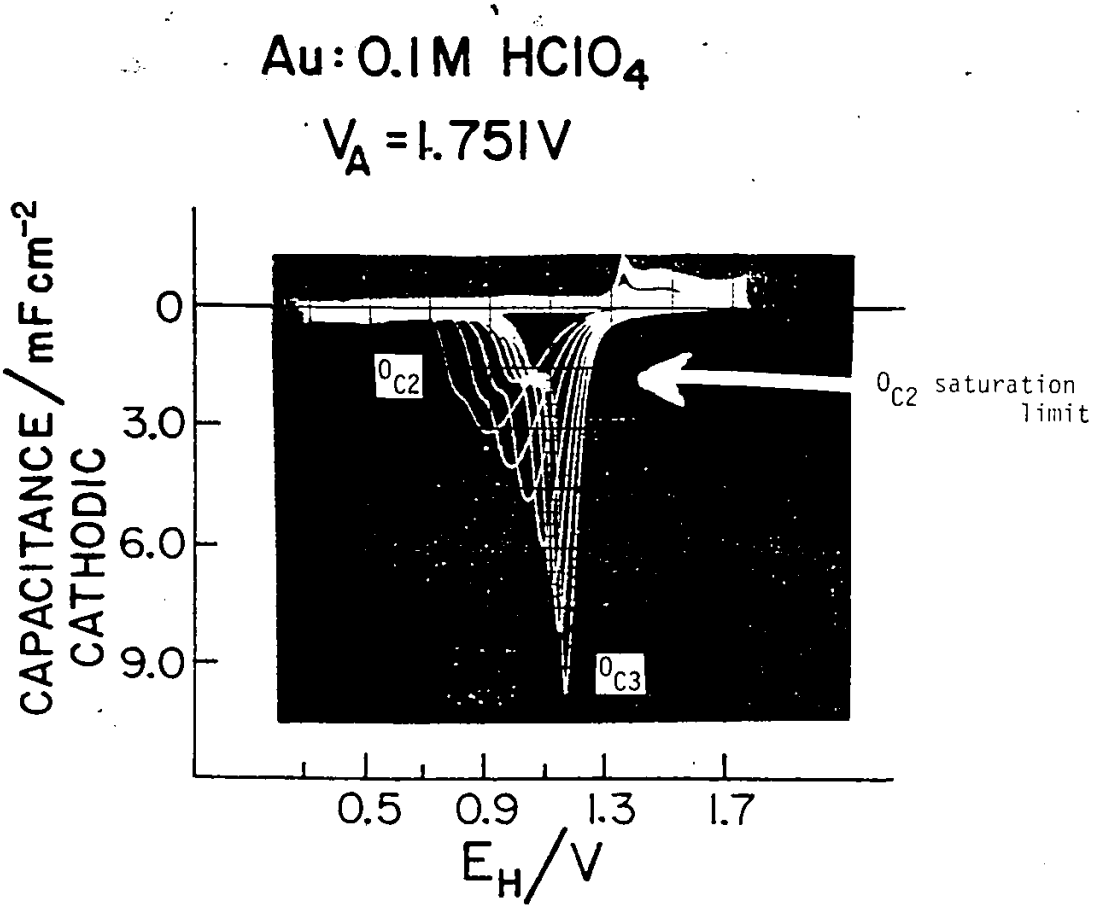

Figure 8-2 Potentiodynamic current-potential profiles for Au for reduction of oxide (formed at 0.050 V s^{-1} to 1.751 V) at sweep rates of 0.20, 0.50, 1.0, 2.0, 5.0, 10 and 20 V s^{-1}

(viz. increases $\Delta V_{1/2}$ with increasing s) over a wider potential range than is due solely to sweep rate (kinetic) effects in the charge transfer step as sweep rate is increased indicates that the rate of reverse place-exchange is exerting considerable influence on the shape of the i vs V profile. At these higher sweep rates, the reduction of an oxide species occurs over a wider potential range than at lower s because the electro-active material is not supplied sufficiently rapidly by the reverse place-exchange step. In the experiment referred to in Figure 8-2, O species were deposited at a constant anodic sweep rate in order to study the effect of sweep rate at constant charge in subsequent cathodic sweeps. An increase in total oxide is still observed at the lower sweep rates but this is attributable to the time spent at oxidizing potentials in the cathodic sweep before reduction of oxide commences.

The potential observed for reduction of oxide as O_{C2} implicitly includes an additional potential which must be applied in order to overcome the extra stability of the ion-dipole pair (see p.237) (i.e. O_{C2} in relation to O_{C1}). In $HClO_4$ solution, this potential is ca 0.40V which, for a two-electron reaction, corresponds to ca 80 kJ mol^{-1}.

ii) Aging Effects

Under appropriate conditions of aging of the oxide, it is possible to increase the quantity of oxide reduced as O_{C2} apparently at the expense of oxide normally reduced as O_{C3}. In these experiments, it was observed that a critical potential existed for partial reduction of oxide before such an effect was observed. This potential must be associated with the state of the oxide at which re-adsorption of ions commences. The latter effect would be expected to aid place-exchange and a re-ordering of oxide (albeit only to a small degree) in the subsequent sweep.

When several sweeps are performed in succession in an aging program (see Fig. 2-5f), the quantity of oxide reduced as O_{C2} becomes significantly increased at the expense of that in the O_{C3} state. When the sweep reversal potential, V_2 (see program f, p. 49), is above this critical value, the aging of the oxide results in net growth of oxide and a consequent increase in charge or coverage of O species.

iii) Temperature Effects

The hypothesis of ion-assisted place-exchange may be tested by performing experiments under conditions, e.g. at elevated temperature, for which the reduction of oxide proceeds to greater extents through O_{C3}, at the expense of O_{C2}. In the extreme, a single state (O_{C3}) for reduction is observed. By performing the oxidation and reduction at elevated temperatures, we are actually able to observe this effect. Thus, in Figure 8-3, for reaction at 365 K, it is seen that the O_{C2} state has essentially disappeared. These results indicate that at higher temperature, the rate of reverse place-exchange has increased relative to that for ion re-adsorption.

Although the reduction of oxide is still not reversible under these conditions, it is apparent that an oxide monolayer can be reduced over a narrow range of potentials, with no evidence of the O_{C2} state towards the end of the monolayer reduction process.

However, a potential sweep taken under exactly the same conditions of temperature, potential and electrolyte but employing a sweep rate 2000 times faster than that which gives the behavior in Figure 8-3, shows that the temperature-generated increase in the rate of reverse place-exchange may be negated by the higher sweep rate (Fig. 8-4). These conditions make it possible for the effect of ions "freezing" the place-exchanged

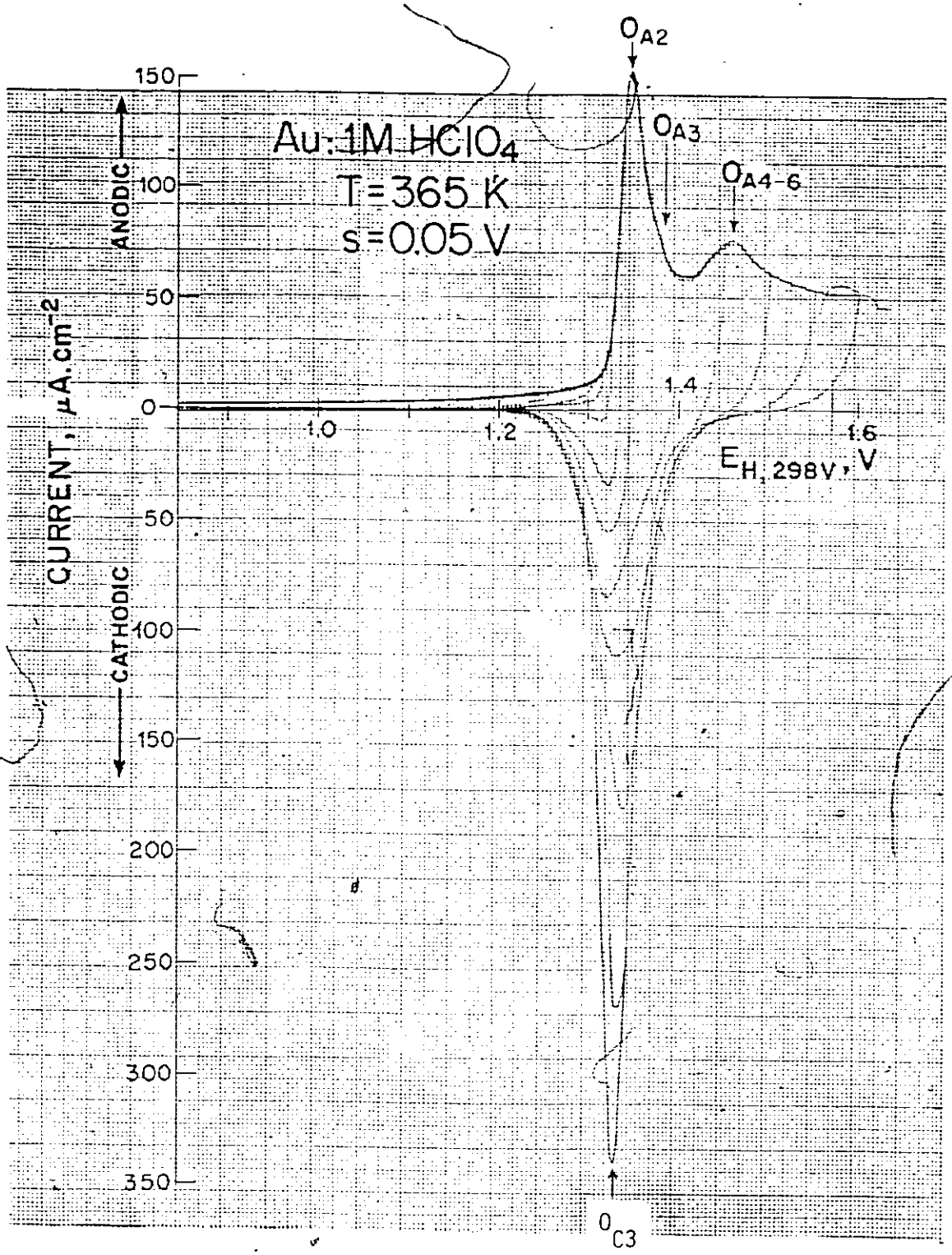

Figure 8-3 Potentiodynamic current-potential profile at Au in 1 M $HClO_4$ at 365 K, s = 0.050 V s^{-1}

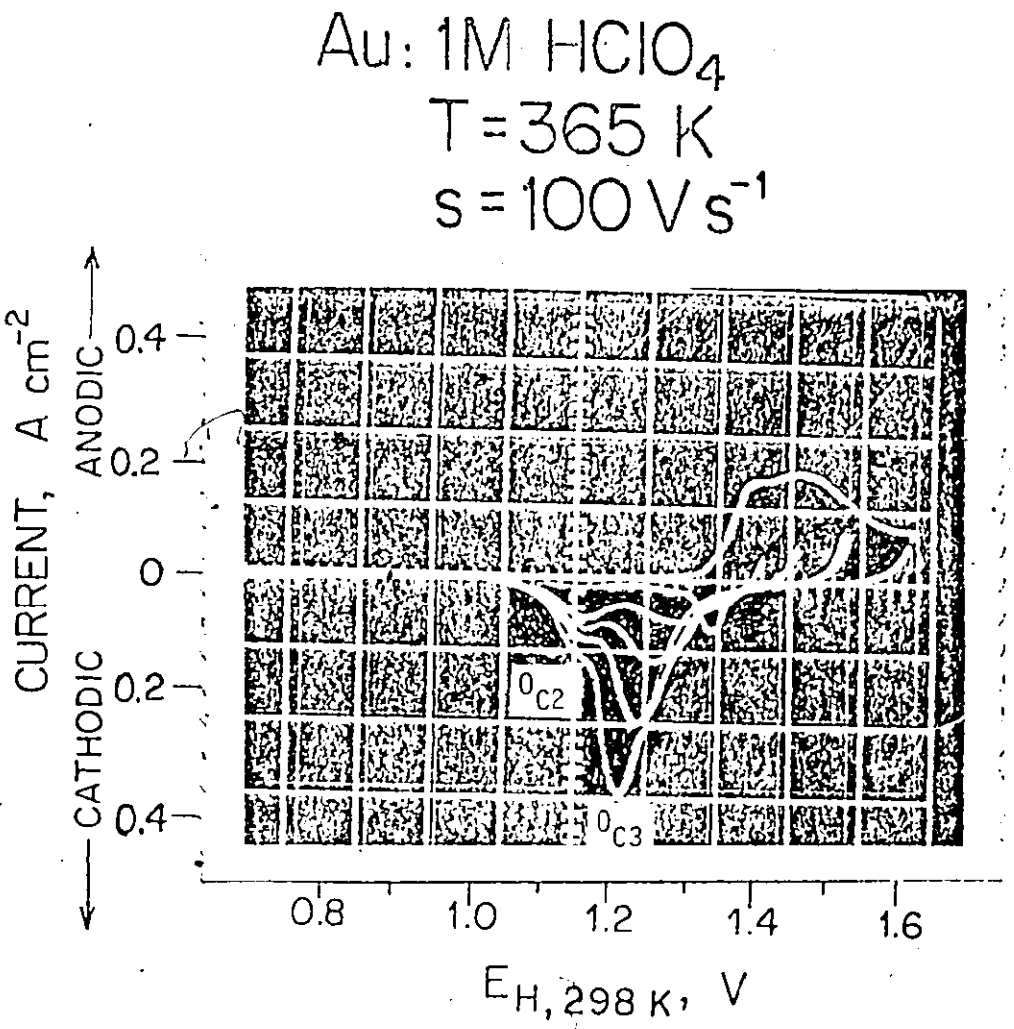

Figure 8-4 Potentiodynamic current-potential profile at Au in 1 M $HClO_4$ at 356 K, s = 100 V s^{-1}

material to be observed; thus, a sizeable coverage of the O_{C2} state is produced, even at the elevated temperature. In other experiments with different electrolytes or at lower sweep rates at 273 K, a substantial increase in the coverage of the O_{C2} state is also observed with respect to that generated in otherwise identical experiments performed at higher temperatures.

iv) Applicability of the Mechanism of Oxide Formation and Reduction to other Noble Metals

In relation to the explanation of oxide reduction in stages O_{C1}, O_{C2} and O_{C3} at Au, it should be mentioned that very similar behavior has recently been found in this laboratory for the case of Pt. An example in which O_{C1}, O_{C2} and O_{C3} components are observed in reduction of an oxide monolayer at Pt is shown in Figure 8-5. Details will be described elsewhere[194]. These results show that the sequence of stages of oxide reduction at Au (see Figs. 3-5 and 4-1) are therefore not peculiar to this metal or to some specific crystal faces of the Au wire samples used in the present work, but rather that the overall effects appear to be general.

Quantitatively, the place-exchange process on Au takes place much more rapidly than at Pt and this is consistent with the lower boiling point (cited earlier) of Au than that of Pt and the lower heat of vaporization of Au (310 kJ mol^{-1}) compared with that for Pt[3] (510 kJ mol^{-1})[67].

7. Mechanisms and Laws for Oxide Growth

It is now finally possible to turn to the overall mechanism of deposition of oxide at Au and suggest some important steps in the process of accumulation of a monolayer of oxide. Here reference will be made to the oxide growth curves (θ vs log τ_h) described in Chapter 4, where it was shown that several distinguishable stages of oxide growth

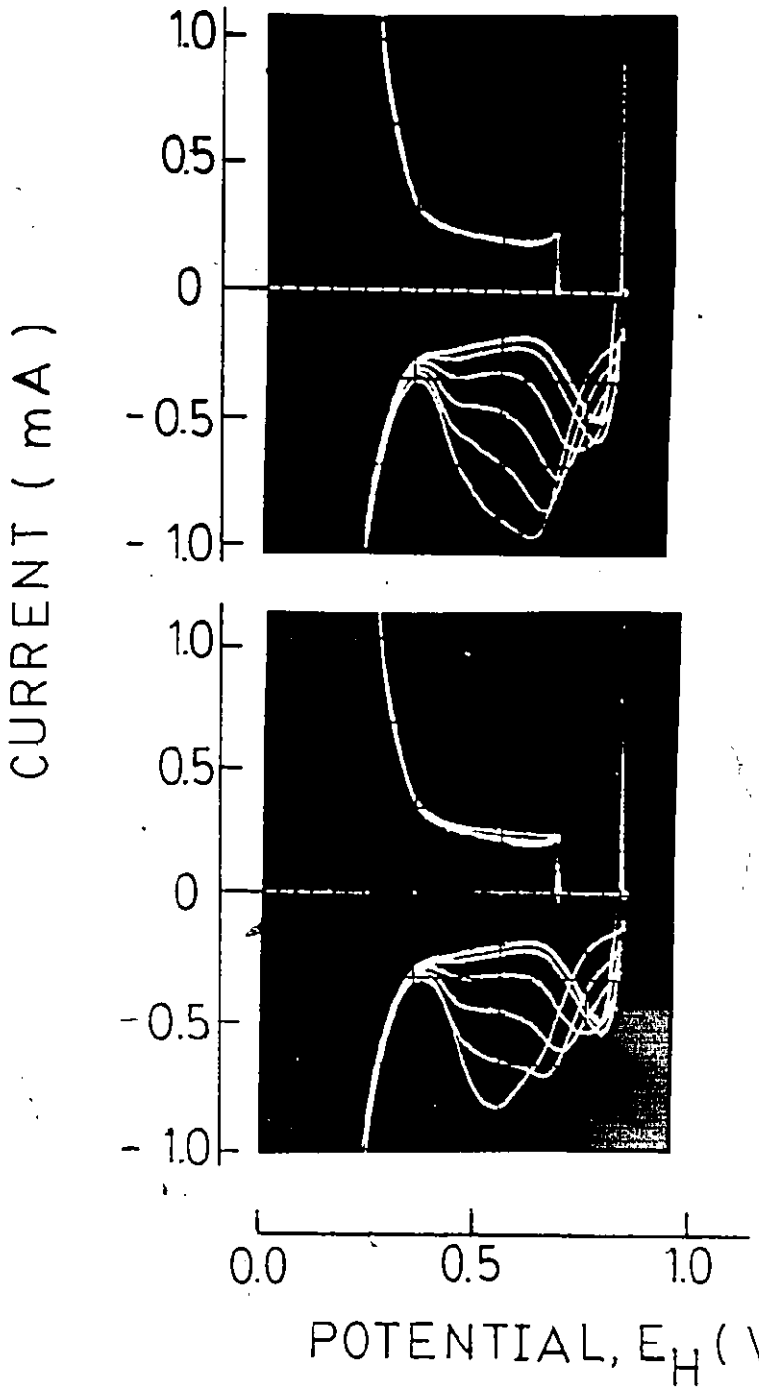

Figure 8-5 Cyclic-voltammetry i vs V profiles for Pt in 0.5 M H_2SO_4 at 298 K for various τ_h = 0, 10^{-3}, 10^{-2}, 10^{-1}, 10^{0}, 10^{1} and 10^{2} s at V_a = 0.9 V E_H; (a) 0.5 M H_2SO_4; (b) 0.5 M H_2SO_4 + 1 x 10^{-6} M KCl.

(I, II and III) are involved (Fig. 4-12).

Of particular interest, first of all, is the observation that Stage III behavior is not seen at any growth potential for coverages $\theta < 0.25$ (Figs. 4-6 to 4-11, Chapter 4). In fact, the oxide growth curves (Figs. 4-6 to 4-11) provide a fairly accurate determination ($\theta = 0.25$) of this "threshold" level of oxide coverage apparently required before Stage III can be observed. For the lowest oxide growth potentials employed, the first stage of oxide growth operates up to quite high τ_h (e.g. to almost 5 s in Figure 4-7 for 0.1 M $HClO_4$). This mean that electrochemical control is maintained until this time, as indicated by the linear log $(1-\theta)$ vs t plots (Fig. 4-14), indicating that random depositon of oxide species can occur, even over this time period. A saturation level of the order of 0.1 monolayer or so is observed for the electrochemically controlled stage of oxide deposition. Growth of oxide at low potentials can continue for long periods of time before Stage II growth takes over as the rate-controlling process. Stage II behavior can continue, however, at higher potentials up to oxide coverages of ca 0.6 or so in acid solutions before Stage III behavior predominates. Nevertheless, Stage III can commence already at coverages as low as $\theta = 0.25$ for relatively low growth potentials.

The key to understanding these results lies in the fact that each ion occupies at least three, and perhaps more, metal atom lattice sites on the exposed electrode surface. It is likely that Stage III represents oxide growth under conditions in which anions are no longer present on the electrode surface or at least not present in significant quantities. Thus, an oxide coverage of ca 0.25, especially when that oxide has a substantial degree of random character, or is a regular overlay structure, may be sufficiently high that no anions can remain on

the electrode surface. As might be expected, the "threshold" level for Stage III in 0.2 M $Ba(OH)_2$ is somewhat higher than that observed in acid solutions: it is ca 0.4. This is consistent with the much smaller size of the OH^- ion that of ClO_4^-, SO_4^{-2} or CO_3^{-2}, as was mentioned in relation to saturation levels for O_{C2} (p.241).

If a saturation value does exist for Stage I, and there is strong indication that one does, then Stage II growth may proceed with a constant number of "growth centers" available for continued deposition and growth of surface oxide. These centers are not nuclei for growth in the sense of mechanisms involving nucleation and growth but originate from some initial extent of deposition of O species in Stage I. They can, however, act as centers directing where continuing growth will tend to occur. Thus, as an ion is desorbed adjacent to oxide species deposited in Stage I, several additional sites for O deposition are immediately made available, i.e. the physical step of ion desorption is rate-controlling for the further growth of the film. The rate of reaction may be dependent, however, on a pre-existing, almost constant coverage by the species previously deposited under electrochemical control or it may depend on the rate at which anions are displaced from the electrode surface, or diffuse on it, making several additional sites available simultaneously for oxide deposition.

In the first case, the dependence of reaction rate on Θ_O would be the same at every potential because the coverage of O species electrochemically deposited in Stage I appears to attain a constant value before some other slower growth process (based on the coverage attained in this stage I) takes place. The available coverage of species deposited as growth centers in Stage I, decreases with continuing oxide deposition in the same manner with time at different potentials, so that no direct Θ-dependence is expected in eqn. (4-6), p. 133.

In the second interpretation, it might be expected that the rate of reaction would be proportional to the surface concentration of ions, a quantity which cannot be accurately determined. Such a concentration would be related to oxide coverage by an expression involving a (1-θ) term. The electrode is best thought of, however, as offering no "free" surface sites in the conventional sense i.e. 1-θ is zero. It is apparent that ions are always held strongly to the electrode in acid solution (except at extreme cathodic potentials) and prevent oxide deposition until an ion desorbs or is ejected from the electrode surface. The free sites thus created tend immediately to be covered with newly deposited oxide, maintaining essentially "complete coverage" of the electrode.

It is important to emphasize that the blocking effects of adsorbed anions can extend beyond their physical size. Desorption of a perchlorate ion, which physically occupies three Au lattice sites, may actually make available, for example, ten Au sites for further oxide deposition, taking into account local interactions, as mentioned earlier.

These considerations suggest that there exists an inherent chemical reason for two stages of oxide growth to develop after Stage I. The deposition of oxide under electrochemical control in Stage I (Fig. 4-12) of oxide growth (or as is resolved in the early stages of a potential sweep) establishes an initial coverage of oxide randomly dispersed amidst, or in an overlay with, anions (O_{Al} process) on the electrode surface. Significant quantities of ion-assisted, place-exchanged oxide should result before ions are displaced from the electrode. A certain amount of O_{Al} species, represented in Figure 8-1a, must be present during oxide deposition. This Au-O dipole will tend to repel adjacent ions, as will additional, potential-dependent deposition of oxide in the immediate neighboring area. As an ion is displaced from the surface, creating free sites for deposition next to existing O species, two distinct states in the oxide monolayer

are exposed: those which have undergone ion-assisted inversion, or place-exchange (↓), and those which have not (↑).

For random deposition, the qualitative situation is summarized in Figure 8-6a, which represents a one-dimensional view of an electrode surface from which an anion has just become desorbed (which, in two dimensions, could free perhaps 10 or 12 lattice sites for continued growth of oxide). The dipole interactions (local repulsive effects) would clearly favor continued deposition around the place-exchanged oxide labelled A in Figure 8-6a rather than in the vicinity of B, perhaps to form a ring of surrounding oxide as depicted in a crude two-dimensional representation in Figure 8-6b, and a locally stabilized oxide network. This single surrounding ring of oxide would not fill up all the freshly exposed lattice sites but oxide deposition on the remaining peripheral free sites (and adjacent to single B sites, ↑) would be expected to be much more difficult. In this way, the act of ion desorption would create no real (effective) free space on the electrode, from the point of view of kinetic rate formulations.

After this type of oxide growth has exhausted OAu sites (↓) of type A in Figure 8-6b, continued deposition and growth may become dependent on non-ion-assisted place-exchange, depicted in Figure 8-6c. After such an event, continued peripheral growth of oxide would be facilitated, ultimately encompassing any single AuO (↑) species or sections of locally stabilized oxide. Thus, oxide growth in this manner would continue in an inherently different way from that immediately following anion desorption since (in part) anions have been removed and can no longer assist in promoting place-exchange. This suggests that Stage II represents a period of oxide growth during which O species become deposited in the vicinity of (ion-assisted) place-exchanged material, perhaps at a rate controlled by

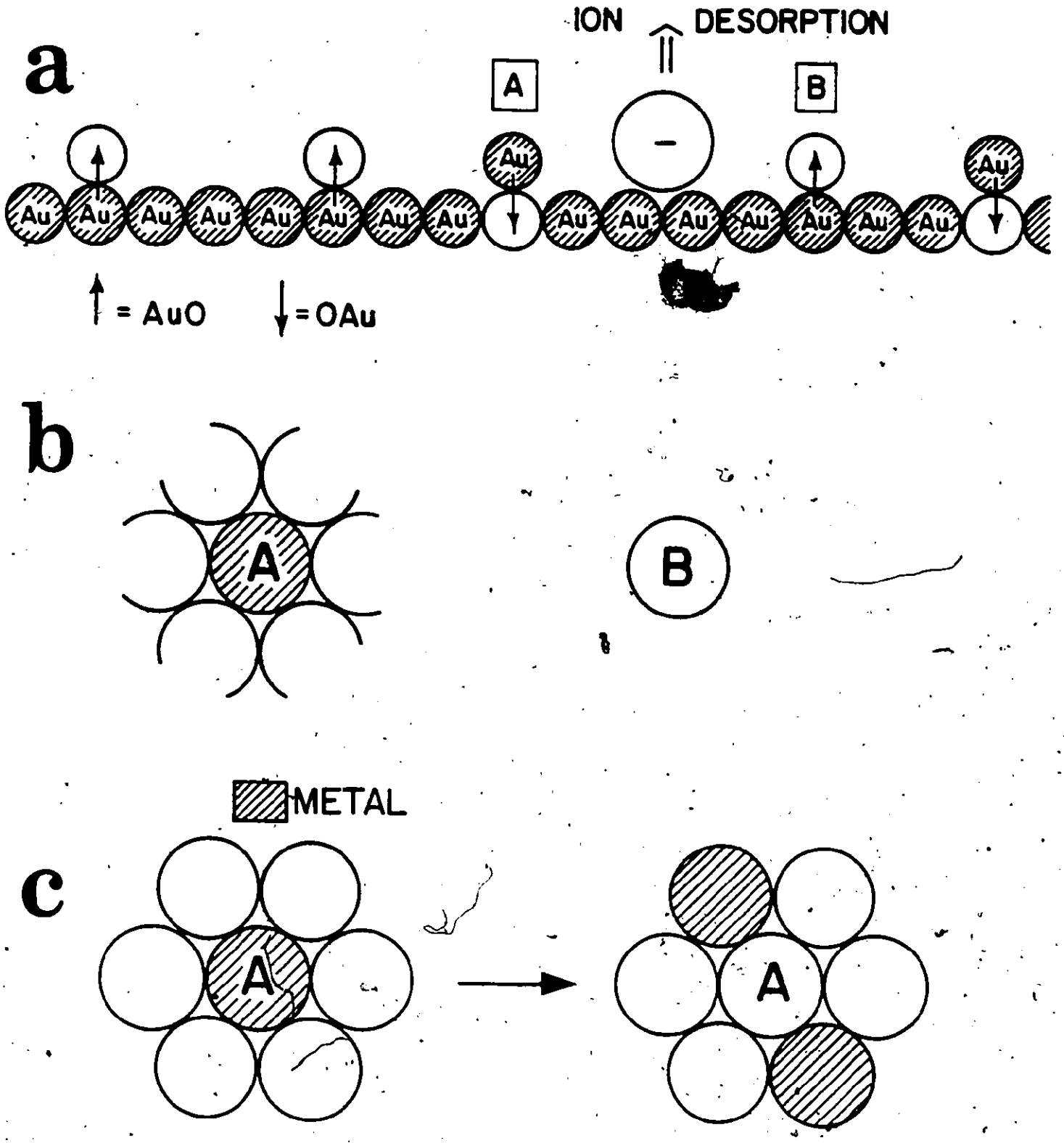

Figure 8-6 Model of processes of oxide deposition at Au: (a) ion desorption creates "free space" on electrode for continued deposition; (b) this deposition occurs preferentially in vicinity of ion-assisted place-exchanged sites and (c) continued deposition and growth of oxide requires non-ion-assisted place-exchange.